

UNIVERSITY OF NAPLES FEDERICO II

*Department of Structures
for Engineering and Architecture*

PH.D. PROGRAMME IN
SEISMIC RISK
COORDINATOR PROF. ALDO ZOLLO
XXVI CYCLE



MARIANNA ERCOLINO

PH.D. THESIS

**SEISMIC BEHAVIOR OF ONE-STORY PRECAST
BUILDINGS**

TUTOR: PROF. DR. GENNARO MAGLIULO

2014

ABSTRACT

The seismic behavior of RC one-story precast buildings is investigated in this thesis. Precast structures (mainly one-story) constitute the most widespread solution that accommodates industrial buildings in Europe. Recently, precast structures have been also increasingly used for buildings where many people are gathering together (i.e. most shopping centers, sports stadiums and apartment buildings), causing an increase of the risk related to these structures. Moreover, the safety of industrial precast buildings is a complex problem, that is related not only to the usual structural performance demand of the ordinary buildings but that is also related to functionality and production issues. The recent severe earthquakes demonstrated all these crucial features. The 20th and 29th May Emilia earthquakes, for example, hit several industrial precast structures, causing a huge economic loss (about 1 billion euros), injuries and fatalities. Moreover, the consequences become more serious if the functionality interruption (production interruption, job missing) as well as the loss of the contents (equipment, provisions, plants) are also taken into account.

The exhibited vulnerability and the central role of this structural typology motivate the development of this work. The first part of this thesis deals with the global response of precast structures. This study focuses on both the evaluation of the main structural features (geometrical and dynamic) and the design code evolution. The experience of the earthquake (Emilia, 2012) is also described. Benchmark structures and existing buildings are investigated by means of nonlinear analyses in order to justify the recorded damages and to evaluate the effect of the most common deficiencies, observed in these buildings. These results are achieved by means of detailed structural models, proposed and validated in this work. These models are efficient tools, capable to take into account the most crucial aspects (connection systems and nonstructural elements influence) in the seismic response of this construction typology. The topic of the seismic safety of industrial bindings is of great interest at regional and national level. It should be managed with a systematic procedure, especially for those

economically developed areas, where the late seismic classification caused a significant vulnerability of these structures. As a consequence of above, the described research provided the collaboration in the redaction of two important emergency documents for the retrofitting actions and for the damage assessment of industrial structures after a seismic event.

The local response of the connection systems is investigated in the second part of this thesis. The dowel connections between the precast beams and the columns and the connections between the panels and the main structure are selected due to their evidenced vulnerability and their key role in the global response. Concerning the beam-to-column connections, the results of an experimental campaign are presented and discussed in order to evaluate the behavior of the system. The experimental results are also used to develop a FEM model of the connection that allows to evaluate the influence of some geometrical and design parameters. The behavior of the connection between the structural elements and the cladding panels systems is also studied. A novel model is proposed in order to take into account the possible interaction between the panels and the structure under seismic action. The results of the performed nonlinear dynamic analyses demonstrate the high influence of these nonstructural components in the response of the whole structure, as well as the inadequacy of the typical approach, used for the connections design. The influence of the cladding systems is also investigated by means of a seismic risk study that confirms their strong influence on the global behavior of precast structures. In the last part of the work, the model with cladding panels is further developed in order to record the progressive collapse of the panels during an earthquake; this model could be an interesting tool to evaluate the actual response of a one-story precast structure interacting with the cladding panel system.

Keywords: industrial buildings, seismic performance, cladding panels, dowel connections, nonlinear analyses

Contents

ABSTRACT	I
1 INTRODUCTION	1
1.1 Research purposes and outline	3
References	6
2 GLOBAL SEISMIC BEHAVIOR	7
2.1 Seismic response of buildings during the Emilia Earthquakes.....	8
2.1.1 Precast structures description and design considerations.....	8
2.1.2 Precast structures damage observation in Emilia region.....	14
2.1.3 Seismic action and considerations concerning loss of support	18
2.1.4 Considerations concerning use of friction connections.....	23
2.1.5 Case study	25
2.1.6 Conclusions	45
2.2 Guidelines on local and global retrofitting systems of precast structures	47
2.2.1 Contents and purposes of the document.....	47
2.2.2 Existing precast buildings: typologies and recorded damages.....	48
2.2.3 Retrofitting principles and criteria	49
2.2.4 Outline of the retrofitting systems.....	51
2.2.5 Conclusions	59
2.3 GL-AeDES: form for usability judgment of precast structures	61
2.3.1 The form of usability judgment.....	61
2.3.2 Identification of the building complex (Section 0)	62
2.3.3 General characteristics of the single structure (Section 1)	64
2.3.4 Geometrical features of the structure (Section 2).....	66
2.3.5 Structural elements and behavior of the structure (Section 3)	68
2.3.6 Damage in structural elements (Section 4)	74
2.3.7 Damage in nonstructural elements (Section 5)	78
2.3.8 External dangers (Section 6)	79
2.3.9 Soil and foundation system (Section 7)	79
2.3.10 Usability judgment and emergency actions (Section 8).....	80
2.3.11 Notes (Section 9).....	83
2.3.12 Conclusions	83

2.4	Dynamic characteristics of precast buildings with and without cladding panels	85
2.4.1	State of art	86
2.4.2	One-story precast buildings and panel-to-structure connection	89
2.4.3	First period of one-story precast buildings	91
2.4.4	Bare structure model	93
2.4.5	Model of the structure with cladding system	94
2.4.6	Linear modal analyses of the case studies	96
2.4.7	Modal analysis results of the bare case studies	96
2.4.8	Modal analysis results with cladding system	99
2.4.9	Seismic zones	101
2.4.10	Closing remarks	107
	Reference	110
3	LOCAL SEISMIC BEHAVIOR	115
3.1	Beam-to-column connection	116
3.1.1	Monotonic experimental test	119
3.1.2	Cyclic test on dowel beam-to-column connection	127
3.1.3	Conclusions	140
3.2	Numerical modeling of the tested dowel connection	142
3.2.1	Concrete elements	142
3.2.2	Steel elements	145
3.2.3	Interaction	146
3.2.4	Loads	148
3.2.5	Comparison between numerical analysis and experimental test	148
3.2.6	Shear strength of the dowel connection	151
3.2.7	Evaluation of the dowel connection shear strength	151
3.2.8	Conclusions	164
3.3	Panel-to-structure connection	166
3.3.1	State of art	166
3.3.2	Benchmark structure	169
3.3.3	Nonlinear model	171
3.3.4	Seismic input	173
3.3.5	Bare structure: nonlinear analyses results	174
3.3.6	Structure with cladding panels: nonlinear analyses results	176

3.3.7 Connection safety evaluation178

3.3.8 Seismic collapse risk180

3.3.9 Progressive collapse185

3.3.10 Concluding remarks187

References189

4 CONCLUSIONS.....193

List of figures

Figure 1.1 RC precast industrial buildings.....	1
Figure 1.2 One-story RC precast industrial buildings: columns damage.....	2
Figure 1.3 (a) Collapse of roof elements form the beams and (b) collapse of the beam from the columns in one-story precast buildings.....	3
Figure 1.4 (a) Collapse of horizontal precast panels and of (b) vertical precast panels in one-story precast buildings.....	3
Figure 1.5 Shake map in terms of peak ground acceleration (May 20 2012 02:03:52 AM GMT).....	4
Figure 1.6 Elastic response spectra recorded on 20 May 2012 in Mirandola compared to elastic response spectra (DM 14/01/2008) for damping ratio equal to 5% is assumed.	4
Figure 1.7 Beam-to-column dowel connection	5
Figure 1.8 (a) Vertical cladding panels in a precast one-story building. (b) Collapse of vertical cladding panels in a precast structure (Emilia, 2012).....	6
Figure 2.1. Examples of (a) single-story and (b) multi-story precast buildings.....	9
Figure 2.2. (a) Double slope roof with corrugated tiles and (b) continuous plane roof (Bonfanti et al., 2008).	9
Figure 2.3. (a) Discontinuous plane roof and (b) shed roof (Bonfanti et al., 2008).	9
Figure 2.4. Examples of connections in precast structures: (a) pin roof element-to-beam connection; (b) dowel beam-to-column connection; (c) socket column-to-foundation connection; (d) vertical panel-to-beam connection	11
Figure 2.5. (a) Roof elements collapse due to the loss of support from main beam. (b) Loss of support of beam from column	14
Figure 2.6. (a) Loss of support of beam from column. (b) Collapse of main beam due to the loss of support on column	15
Figure 2.7. (a) Pinned beam-to-column connection failure and (b) consequent loss of support of the beam from column.....	15
Figure 2.8. Damage in columns: (a) column loss of verticality due to rotation in the foundation element; (b) cracking of the base section in a column; (c) plastic hinge at the bottom of the column and buckling of a longitudinal bar at the base.....	16
Figure 2.9. Shear collapse of column due to the interaction with infill masonry panel.....	17
Figure 2.10 (a) Collapse of horizontal precast panels. (b) Collapse of vertical precast panels	17
Figure 2.11. Details of a connection device at the top of horizontal panel: (a) anchor channel embedded in the column, (b) steel angle plate and (c) hammer head screw out of the anchor channel.....	18
Figure 2.12. Collapse of vertical precast panel connection: (a) the anchor channel embedded in the panel and the failed hammer head element; (b) profile located in the beam which the hammer head elements are welded to	18

<i>Figure 2.13. Seismic zone classification in Italy (a) in 1984 and (b) in 2003; the black dot indicates the Emilia earthquake epicentral zone (INGV, 2012).....</i>	<i>19</i>
<i>Figure 2.14. Accelerograms recorded in the station of Mirandola (Modena, Italy) (the origin of time is set at 20-05-2012 02:03:24 UTC).....</i>	<i>20</i>
<i>Figure 2.15. Elastic response spectra recorded on 20 May 2012 in Mirandola NS (green) and EW component (blue) compared to elastic response spectra for return period equal to 475y (black) and 2475y (dashed black) provided by Italian building code (DM 14/01/2008) for soil class C. A damping ratio equal to 5% is assumed.....</i>	<i>21</i>
<i>Figure 2.16. (a) Acceleration spectral ordinates recorded in Mirandola compared to the friction coefficient upper and lower bounds evaluated by Magliulo et al. (2011); (b) loss of support safety factor plotted versus fundamental periods for the recorded accelerograms, assuming $\mu=0.13$.....</i>	<i>22</i>
<i>Figure 2.17. Elastic response spectra recorded on 29 May 2012 in Cento (CNT), Finale Emilia (FIN0), Moglia (MOG0), Mirandola (MRN), San Felice sul Panaro (SAN0) and San Martino Spino (SMS0) compared to elastic response spectra for Mirandola for return period equal to 475y (black) and 2475y (dashed black) provided by Italian building code (DM 14/01/2008) for soil class C.....</i>	<i>23</i>
<i>Figure 2.18. Ratios between the design shear demand F_v in beam-to-column connection induced by wind, evaluated according to CNR 1967 (CNR67) and DM 1996 (DM96), and the connection friction strength F_f, evaluated according friction coefficient c equal to 0.35, 0.13 and 0.09, for the different case studies.....</i>	<i>24</i>
<i>Figure 2.19 Plan view of the case study.....</i>	<i>25</i>
<i>Figure 2.20 Frontal view (X direction).....</i>	<i>25</i>
<i>Figure 2.21 Lateral view (Y direction).....</i>	<i>26</i>
<i>Figure 2.22 Cross sections of column for (a) columns B,D and E and for (b) columns A and C.....</i>	<i>26</i>
<i>Figure 2.23 Detail of the beam-to-column connection.....</i>	<i>27</i>
<i>Figure 2.24 Detail of the girder-to-column connection.....</i>	<i>28</i>
<i>Figure 2.25 Detail of the roof element-to-beam connection.....</i>	<i>28</i>
<i>Figure 2.26 Columns damage in X direction after the 29th May event.....</i>	<i>29</i>
<i>Figure 2.27 Dislocation in the beam-to-column connections after the 29th May event.....</i>	<i>29</i>
<i>Figure 2.28 Dislocation in the roof-to-beam connections after the 29th May event.....</i>	<i>29</i>
<i>Figure 2.29 Moment-rotation envelope of the column A around (a) the X direction and (b) the Y direction.....</i>	<i>31</i>
<i>Figure 2.30 Moment-rotation envelope of the column C around (a) the X direction and (b) the Y direction.....</i>	<i>32</i>
<i>Figure 2.31 Moment-rotation envelope of (a) the column B and of (b) the column D and E.....</i>	<i>32</i>
<i>Figure 2.32 Structural elements layout and connection position.....</i>	<i>33</i>
<i>Figure 2.33 Flat bearing element.....</i>	<i>34</i>
<i>Figure 2.34 Accelerograms recorded in the station of Mirandola (Modena, Italy): (a) W-E component and (b) N-S component. The origin of the time is set at 20-05-2012 02:03:24 UTC.....</i>	<i>35</i>

<i>Figure 2.35 Accelerograms recorded in the station of Mirandola (Modena, Italy): (a) W-E component and (b) N-S component. The origin of the time is set at 29-05-2012 07:00:03 UTC</i>	35
<i>Figure 2.36 Elastic response spectra: (a) recorded on 20 May 2012 and (b) recorded on 29 May 2012 in Mirandola (Modena, Italy)</i>	36
<i>Figure 2.37 Vertical component of the accelerograms recorded in the station of Mirandola (Modena, Italy): (a) at 20-05-2012 02:03:24 UTC and (b) at 29-05-2012 07:00:03 UTC</i>	36
<i>Figure 2.38 Elastic response spectra of the accelerograms vertical component: (a) recorded on 20th May 2012 and (b) recorded on 29th May 2012 in Mirandola</i>	36
<i>Figure 2.39 Moment-rotation envelope around the Y direction: (a) column A and (b) column B</i>	37
<i>Figure 2.40 Moment-rotation envelope around the Y direction: (a) column C and (b) column D</i>	37
<i>Figure 2.41 Shear forces in beam-to-column connections in X direction under the horizontal components of the 29th May event</i>	39
<i>Figure 2.42 Force-deformation envelopes of the frictional elements (beam-to-column connections) for the representative columns of the structure under the horizontal components of the 29th earthquake</i>	40
<i>Figure 2.43 Force-deformation envelopes of the frictional elements (roof-to-beam connections) for the central roof element in the 4th transversal bay under the horizontal components of the 29th earthquake</i>	41
<i>Figure 2.44 Force-deformation envelopes of the frictional elements (beam-to-column connections) for the representative columns of the structure under the three components of the 29th earthquake</i>	42
<i>Figure 2.45 Force-deformation envelopes of the frictional elements (roof-to-beam connections) for the central roof element in the 4th transversal bay under the three components of the 29th earthquake</i>	43
<i>Figure 2.46 Force-deformation envelope of the frictional elements (beam-to-column connections) for the representative columns of the structure under the three components of the 20th earthquake</i>	44
<i>Figure 2.47 Force-deformation behavior of the most damaged roof-to-beam connection under the three components of the 20th earthquake</i>	45
<i>Figure 2.48 Single degree of freedom scheme</i>	50
<i>Figure 2.49 Elastic response spectrum of Mirandola (MO) – Soil type C</i>	51
<i>Figure 2.50 1 second pseudo-acceleration (%g) - Mirandola (20th May 2012)</i>	51
<i>Figure 2.51 Retrofitting solution for beam-to-column connections</i>	54
<i>Figure 2.52 Retrofitting solution for roof-to-beam connections</i>	54
<i>Figure 2.53 System to prevent the overturning of the cladding panels</i>	56
<i>Figure 2.54 Connection between the industrial floor and the column</i>	57
<i>Figure 2.55 Characteristic points for storage racks seismic safety</i>	59
<i>Figure 2.56 Section 0 of GL-AeDES: identification of the structural complex</i>	63
<i>Figure 2.57 Section 1 of GL-AeDES: identification of the single structure</i>	64

Figure 2.58 Section 2a of GL-AeDES: description of the single structure	66
Figure 2.59 Section 2b of GL-AeDES: added and connected blocks	67
Figure 2.60 Blocks in a structure: (a) integrated and (b) added case	67
Figure 2.61 Section 3a of GL-AeDES: materials and structural system	68
Figure 2.62 Section 3b of GL-AeDES: roof elements and behavior under seismic actions ...	69
Figure 2.63 Section 3c of GL-AeDES: regularity criteria	69
Figure 2.64 Section 3d of GL-AeDES: connection systems, special load and non-structural elements	71
Figure 2.65 Column-to-foundation connection with steel plate and anchors	71
Figure 2.66 Socket foundation in precast RC structures.....	71
Figure 2.67 Cladding panels: (a) horizontal and (b) vertical layout.....	73
Figure 2.68 Cast in situ concrete panels.....	74
Figure 2.69 Masonry panels	74
Figure 2.70 Steel panels.....	74
Figure 2.71 Sandwich panels.....	74
Figure 2.72 Section 4 of GL-AeDES: damage in structural elements and emergency actions	75
Figure 2.73 Cracking at the base of a precast column in a one-story industrial building: damage level D1 (Emilia, 2012)	76
Figure 2.74 Plastic hinge formation at the base of a precast column in a one-story industrial building: damage level D2 (Emilia, 2012).....	76
Figure 2.75 Plastic hinge formation at the base of a precast column in a one-story industrial building: damage level D4 (Emilia, 2012).....	77
Figure 2.76 High strain in columns due to the irregular distribution of the infill panels in a one-story industrial building that cause the global collapse: damage level D5 (Emilia, 2012).....	77
Figure 2.77 Relative displacement between the vertical panels in a one-story industrial building: damage level D2 (Emilia, 2012).....	77
Figure 2.78 Dislocation of the horizontal panels in a one-story industrial building: damage level D3 (Emilia, 2012).....	77
Figure 2.79 Damage in the column forks that constraints the beam in a one-story industrial building: damage level D4 (Emilia, 2012).....	77
Figure 2.80 Collapse of a roof element with frictional connection in a one-story industrial building: damage level D5 (Emilia, 2012).....	77
Figure 2.81 Section 5 of GL-AeDES: damage in no structural elements and emergency actions.....	78
Figure 2.82 Cracking and damage in masonry infill panels in one-story precast building (Emilia, 2012)	78
Figure 2.83 Section 6 of GL-AeDES: external dangers	79
Figure 2.84 Section 7 of GL-AeDES: soil and foundation system	80
Figure 2.85 Section 6 of GL-AeDES: usability judgment	80
Figure 2.86. Collapse of horizontal precast cladding panels in a one-story precast structure during the Emilia earthquake (2012).....	86

Figure 2.87 Collapse of vertical precast cladding panels in a one-story precast structure during the Emilia earthquake (2012).....	86
Figure 2.88 Mechanism of drift accommodation in cladding design (Wang, 1987)	87
Figure 2.89 Geometrical configuration of a typical European one-story precast industrial building (Posada and Wood, 2002)	90
Figure 2.90 Typical vertical concrete panels arrangement in a precast one-story building .	90
Figure 2.91 (a) Investigated connection between vertical precast panel and resistant structure: (b) channel bar, (c) interlock and (d) connector	91
Figure 2.92 Benchmark one-story precast building: a plan view, b transversal bays and c longitudinal bays.....	92
Figure 2.93 Linear elastic model of the bare structure in SAP2000.....	94
Figure 2.94 Linear elastic model of the structure with cladding system: a model of two vertical panels with the bi-dimensional frame and b 3D model with shell elements in SAP2000 program.....	95
Figure 2.95 Values of the first period, T , obtained by modal analyses (black circles), versus the EC8 formula (1) (gray line) for bare structures.....	97
Figure 2.96 Values of the first period, T , obtained by modal analyses (black circles), versus the height of the structure, H , for bare buildings, along with the best fit curves (solid lines) from the linear regression analyses, and the 16 th percentile curves (dash-dot lines)	99
Figure 2.97 Values of the first periods, T , obtained by modal analyses (black circles), versus the EC8 formula (1) for one-story precast buildings with cladding system (gray line)	99
Figure 2.98 Values of the first periods, T , obtained by modal analyses (black circles), versus the height of the structure, H , for buildings with cladding panels, along with the best fit curves (solid lines) from the linear regression analyses, and the 16 th percentile curves (dash-dot lines).....	100
Figure 2.99 Values of the first periods, T , obtained by modal analyses (black circles), versus the F1 function (6) for buildings with cladding system, along with the best fit curve (solid black line) from the linear regression analysis, and the 16th percentile curve (dash-dot gray line).....	101
Figure 2.100 Values of the first periods, T , obtained by modal analyses (circles), versus the EC8 formula (2.12) for bare one-story precast buildings (gray line) in all the assumed seismic zones.....	103
Figure 2.101 Regression analyses results for bare structures in all the considered seismic zones: first periods, T , obtained by the modal analyses (black circles), versus the height of the structure, H , along with the best fit curve (dash-dot black line) from the linear regression analysis and the 16 th percentile curve (dash-dot gray line)	104
Figure 2.102 First periods, T , obtained by modal analyses (black circles), versus the height of the structure, H ; along with the proposed formula (black line), obtained from the regression analysis on the bare buildings designed for all the seismic zones	104
Figure 2.103 Table 2.15 α values (black circles) versus the corresponding PGA and their regression curve (black solid line).....	105

Figure 2.104 First periods, T , obtained by modal analyses (black circles), versus the proposed formula (2.18) for one-story precast bare buildings (black solid line)	106
Figure 2.105 Values of the first periods, T , obtained by modal analyses (circles), versus the EC8 formula (1) for one-story precast buildings with cladding system (gray line) in all the assumed seismic zones	106
Figure 2.106 First periods, T , obtained by modal analyses (black circles), versus the F_1 factor (6), along with the best fit curve (solid black line) from the linear regression analysis, the 16 th percentile curve (solid gray line) and the proposed formula (9) (dash-dot red line).....	107
Figure 3.1 Beam-to-column dowel connection	117
Figure 3.2 Typical hysteretic loops for fully reverse transverse displacement	118
Figure 3.3. Experimental setup of a monotonic shear test on a beam-to-column dowel connection.....	120
Figure 3.4 Column reinforcement details	120
Figure 3.5 Beam reinforcement details.....	121
Figure 3.6 Construction phases of the tested specimen: (a) columns and dowels position; (b) beam addition	121
Figure 3.7. Cast of grout in the beam holes.....	121
Figure 3.8. Dowels restrained at the top of the beam by means of steel plate, nut and washer	121
Figure 3.9 Stress-strain relationships for steel dowel: experimental curve (blue curve) and effective curve (red curve).....	123
Figure 3.10 Experimental stress-strain relationships for steel reinforcement ($\phi=8\text{mm}$).....	123
Figure 3.11 Force-displacement curve of the monotonic test (dashed blue line) and “elaborated” curve (solid red line)	124
Figure 3.12 Loading conditions	125
Figure 3.13 Frontal cover and lateral cover.....	125
Figure 3.14 Phases of connection collapse: (a) first crack during the test and (b) final step of the test.....	125
Figure 3.15 Instrumentations records. From the top: force of the actuator, deformations of the concrete and deformations of the upper stirrup in the column	126
Figure 3.16 Geometrical layout of the column instrumentations.....	126
Figure 3.17 Experimental setup of the monotonic shear test on a beam-to-column dowel connection: (a) frontal view and (b) bottom view	127
Figure 3.18 Layout of stain gauges placed on steel elements: (a) column stirrups and (b) left dowel bar	128
Figure 3.19 Layout of strain gauges placed on concrete elements: (a) column and (b) beam	129
Figure 3.20 Layout of LVDT to record relative displacements between the beam and the column.....	129
Figure 3.21 Loading direction: (a) negative and (b) positive direction.....	130
Figure 3.22 Load history recorded by LVDT at the end of beam.....	130
Figure 3.23 First crack in the column side cover.....	131

<i>Figure 3.24 Splitting of the column side cover.....</i>	<i>131</i>
<i>Figure 3.25 Records of strain gauges on the column top surface (blue curve) along with the limit tensile strain of concrete (black line)</i>	<i>131</i>
<i>Figure 3.26 Records of strain gages on the stirrups in the column along with the yielding strain (black line).....</i>	<i>131</i>
<i>Figure 3.27 Crack opening in the column frontal cover.....</i>	<i>132</i>
<i>Figure 3.28 Splitting of the cover at the end of the test.....</i>	<i>132</i>
<i>Figure 3.29 Crack opening in the beam frontal cover</i>	<i>132</i>
<i>Figure 3.30 Crack in the beam at the end of the test.....</i>	<i>132</i>
<i>Figure 3.31 Final state of the specimen at the end of the cyclic test: (a) Frontal view and (b) bottom view.....</i>	<i>133</i>
<i>Figure 3.32 Plastic hinge in the steel dowel in the column.....</i>	<i>133</i>
<i>Figure 3.33 Records of strain gauges on the steel dowels in the beam (red curve) and in the column (blue curve) along with the yielding steel strain of the dowel (black line)...</i>	<i>133</i>
<i>Figure 3.34 Force- displacement curve of the whole cyclic test.....</i>	<i>134</i>
<i>Figure 3.35 Force- displacement curve (blue curve) and frictional resistance (gray line) up to 6th step: the red point indicates the first crack formation in the later concrete cover</i>	<i>135</i>
<i>Figure 3.36 Force-displacement curve (gray curve) and envelope at each step (circle marker) for 1st cycle (red line), 2nd cycle (blue line) and 3rd cycle (green line).....</i>	<i>136</i>
<i>Figure 3.37 Dissipated energy during the cyclic shear test, for each positive and negative semi-cycle up to 6th step</i>	<i>136</i>
<i>Figure 3.38. Experimental setup of a monotonic shear test on a beam-to-column dowel connection.....</i>	<i>137</i>
<i>Figure 3.39 Final step of the monotonic test: splitting of the concrete.....</i>	<i>137</i>
<i>Figure 3.40 Comparison between force-displacement curves of the monotonic test (red solid line) and of the cyclic test (blue solid line)</i>	<i>138</i>
<i>Figure 3.41 FEM model of the dowel connection by ABAQUS (Corp., 2010).....</i>	<i>142</i>
<i>Figure 3.42 Mechanical behavior of the smeared crack concrete model for uniaxial compressive load (Systèmes, 2008).....</i>	<i>143</i>
<i>Figure 3.43 Concrete stress-strain relationships.....</i>	<i>145</i>
<i>Figure 3.44 Stress-strain relationships for steel dowel: experimental curve (blue curve) and effective curve (red curve).....</i>	<i>146</i>
<i>Figure 3.45 Experimental stress-strain relationships for steel reinforcement ($\phi=8\text{mm}$).....</i>	<i>146</i>
<i>Figure 3.46 Adopted analytical model for cohesive interface elements.....</i>	<i>148</i>
<i>Figure 3.47 Bond-stress versus slip relationship for the deformed bar – confined concrete contact behavior according to the Eligehausen model (Eligehausen et al., 1986) ...</i>	<i>148</i>
<i>Figure 3.48 Comparison numerical analysis (blue line) vs experimental test (red line) in terms of force-displacement curve</i>	<i>149</i>
<i>Figure 3.49 Column stress distribution at the failure step resulting from the numerical model</i>	<i>149</i>
<i>Figure 3.50 Deformation of the dowel at the failure step versus the beam and column depth</i>	<i>150</i>

<i>Figure 3.51 Steel dowel and (b) measurement of the plastic hinge depth in the steel dowel after the monotonic test.....</i>	<i>150</i>
<i>Figure 3.52 Layout of the strain gauges on the column top surface</i>	<i>150</i>
<i>Figure 3.53 Eccentricity of the shear force.....</i>	<i>152</i>
<i>Figure 3.54 Shear force against the concrete core: force-displacement curves varying the dowels diameter</i>	<i>154</i>
<i>Figure 3.55 Shear force against the concrete cover: force-displacement curves varying the dowels diameter</i>	<i>155</i>
<i>Figure 3.56 Comparison between the shear strength obtained by the numerical model and the shear strength obtained by formulations available in technical literature, for different values of dowel diameter</i>	<i>156</i>
<i>Figure 3.57 Stresses in the concrete around the dowel: (a) in the cross section and (b) along the dowel (Vintzeleou and Tassios, 1986).....</i>	<i>157</i>
<i>Figure 3.58 Stresses in the concrete near the dowel at the failure step by the ABAQUS model</i>	<i>158</i>
<i>Figure 3.59 Stress distribution evaluation according to the Hetenyi theory (Hetenyi, 1946)</i>	<i>158</i>
<i>Figure 3.60 Stresses in the concrete near the dowel at the failure step by the ABAQUS model</i>	<i>158</i>
<i>Figure 3.61 Tangential stresses distribution in the concrete near the dowel at the failure step by the ABAQUS model.....</i>	<i>158</i>
<i>Figure 3.62 Shear force against the concrete core: force-displacement curves varying the frontal cover.....</i>	<i>160</i>
<i>Figure 3.63 Shear force against the concrete cover: force-displacement curves varying the frontal cover.....</i>	<i>161</i>
<i>Figure 3.64 Comparison between the shear strength obtained by the numerical model and the shear strength obtained by formulations available in technical literature, for different values of frontal cover</i>	<i>161</i>
<i>Figure 3.65 Shear force against the concrete core: force-displacement curves varying the lateral cover.....</i>	<i>163</i>
<i>Figure 3.66 Shear force against the concrete cover: force-displacement curves varying the lateral cover.....</i>	<i>163</i>
<i>Figure 3.67 Comparison between the shear strength obtained by the numerical model and the shear strength obtained by formulations available in technical literature, for different values of lateral cover</i>	<i>164</i>
<i>Figure 3.68 Benchmark one-story precast building: a plan view, b transversal bays and c longitudinal bays.....</i>	<i>170</i>
<i>Figure 3.69 (a) Investigated connection between vertical precast panel and resistant structure: (b) channel bar, (c) interlock and (d) connector.....</i>	<i>171</i>
<i>Figure 3.70 Moment-rotation envelopes</i>	<i>172</i>
<i>Figure 3.71 Linear elastic model of the structure with cladding system: a model of two vertical panels with the bi-dimensional frame</i>	<i>173</i>

<i>Figure 3.72 Spectrum of the record comparison between their mean spectrum (black solid line) to the code design spectrum (red solid line)</i>	<i>174</i>
<i>Figure 3.73 Results of the dynamic analyses on the bare model in the X direction of the structures: displacement-time curve (left plot in the first row), force-time curve (right plot in the first row) and force-displacement curve (plot in the second row).</i>	<i>175</i>
<i>Figure 3.74 Results of the dynamic analyses on the bare model in the Z direction of the structures: displacement-time curve (left plot in the first row), force-time curve (right plot in the first row) and force-displacement curve (plot in the second row).</i>	<i>175</i>
<i>Figure 3.75 Results of the dynamic analyses on the model with cladding panels in the X direction of the structures: displacement-time curve (left plot in the first row), force-time curve (right plot in the first row) and force-displacement curve (plot in the second row).</i>	<i>177</i>
<i>Figure 3.76 Results of the dynamic analyses on the model with cladding panels in the Z direction of the structures: displacement-time curve (left plot in the first row), force-time curve (right plot in the first row) and force-displacement curve (plot in the second row).</i>	<i>177</i>
<i>Figure 3.77 (a) Section of the steel profile in the beam and in the panel; (b) length and height of the steel profile.....</i>	<i>179</i>
<i>Figure 3.78 Forces in panels connections in Z direction: the first row shows the panels distribution and the second row shows the comparison between the seismic forces for the considered records (circles) and the shear strength of the connector (red dash-dot line)</i>	<i>179</i>
<i>Figure 3.79 Forces in panels connections in X direction: the first row shows the panels distribution and the second row shows the comparison between the seismic forces for the considered records (circles) and the shear strength of the connector (red dash-dot line)</i>	<i>180</i>
<i>Figure 3.80 Hazard curve for peak ground accelerations in logarithm scale</i>	<i>183</i>
<i>Figure 3.81 Hazard curve for spectral accelerations ($T=1.5\text{sec} - \xi=5\%$) in logarithm scale</i>	<i>183</i>
<i>Figure 3.82 IDA curve and PDF in terms of peak ground acceleration</i>	<i>184</i>
<i>Figure 3.83 IDA curve and PDF in terms of spectral acceleration</i>	<i>184</i>
<i>Figure 3.84 IDA curve and PDF in terms of peak ground acceleration</i>	<i>185</i>
<i>Figure 3.85 Display of the progressive collapse during one dynamic nonlinear analysis direction: (a) step of the first collapsed panel; (b) last step of the analysis</i>	<i>186</i>
<i>Figure 3.86 Displacement-time curve in X direction</i>	<i>187</i>
<i>Figure 3.87 Displacement-time curve in Z direction</i>	<i>187</i>
<i>Figure 3.88 Force-time curve in X direction.....</i>	<i>187</i>
<i>Figure 3.89 Force-time curve in Z direction.....</i>	<i>187</i>

List of tables

<i>Table 2.1. Italian building code evolution: title, acronym, presence of requirements on precast structures and on connections between structural elements, compulsoriness and relationships between the most important codes for precast structures</i>	<i>13</i>
<i>Table 2.2. Evaluation of the wind equivalent forces according to past Italian building codes (CNR-UNI 1967 and DM 1996).....</i>	<i>24</i>
<i>Table 2.3 Geometrical characteristic and reinforcement details of columns.....</i>	<i>27</i>
<i>Table 2.4 Fixed degree of freedom in the connection between the structural elements.....</i>	<i>33</i>
<i>Table 2.5 Parameters used in the evaluation of the frictional strength of the beam-to-column connections</i>	<i>38</i>
<i>Table 2.6 Compiling rules for the GL-AeDES form</i>	<i>62</i>
<i>Table 2.7 Codes of the structures for public service</i>	<i>65</i>
<i>Table 2.8 Columns cross sections reported as a function of the height of the structure (H) and of the number of the longitudinal bays ($N_{bay,x}$). Each diagram refers to one of the two values of transversal bays number ($N_{bay,z}$) and to one of the three values of transversal bays length ($L_{bay,z}$).</i>	<i>93</i>
<i>Table 2.9 First three periods of 2D and 3D bare models of a case study implemented in OpenSees and SAP2000.....</i>	<i>94</i>
<i>Table 2.10 Modal analysis results of a case study with cladding panels modeled either as two-dimensional frames (OpenSees) or by shell elements (Shell - SAP2000)</i>	<i>96</i>
<i>Table 2.11 Results of the three regression analyses for the bare precast buildings in terms of: proposed formula to predict the period (1st row), correlation factor (2nd row), standard error (3rd row), proposed formula for which the 16% of the measured periods would fall below the corresponding curve (4th row)</i>	<i>98</i>
<i>Table 2.12 Results of the regression analyses for buildings with cladding system in terms of: proposed formulas to predict the first period (1st row), correlation factor (2nd row), standard error (3rd row) and proposed formulas for which the 16% of the measured periods falls below the corresponding curve (4th row)</i>	<i>100</i>
<i>Table 2.13 Assumed seismic zones: peak ground acceleration on rock soil for a return period equal to 50yy (2nd column) and 475yy (3rd column), and peak ground acceleration for EC8 with type B soil (4th column)</i>	<i>102</i>
<i>Table 2.14 Results of the regression analyses of the bare one-story precast buildings in the four seismic zones in terms of: proposed formulas to predict the first period (1st row), correlation factor (2nd row), standard error (3rd row) and proposed formulas for which the 16% of the measured periods falls below the corresponding curve (4th row)</i>	<i>103</i>
<i>Table 2.15 α, β and R2 values from regression analysis for each seismic zone</i>	<i>105</i>
<i>Table 3.1 Unconfined concrete mechanical properties.....</i>	<i>122</i>
<i>Table 3.2 Confined concrete mechanical properties.....</i>	<i>122</i>
<i>Table 3.3 Mechanical characteristics of steel used in the prototypes.....</i>	<i>123</i>
<i>Table 3.4 Comparison between the cyclic experimental strength of the dowel connection ($V_{Rd,cyclic}$) and the literature formulas.....</i>	<i>140</i>

<i>Table 3.5 Unconfined concrete mechanical properties.....</i>	<i>145</i>
<i>Table 3.6 Confined concrete mechanical properties.....</i>	<i>145</i>
<i>Table 3.7 Comparison between numerical and experimental strains of the column frontal and lateral cover (Figure 3.52).....</i>	<i>150</i>
<i>Table 3.8 Comparison between numerical and experimental strains of the column top surface (Figure 3.52).....</i>	<i>150</i>
<i>Table 3.9 Damage percentage at the connection failure for each collapse mechanism, when the force is applied against the concrete core.....</i>	<i>154</i>
<i>Table 3.10 Damage percentage at the connection failure for each collapse mechanism, when the force is applied against the concrete cover.....</i>	<i>155</i>
<i>Table 3.11 Damage percentage at the connection failure for each collapse mechanism, when the force is applied against the concrete core.....</i>	<i>159</i>
<i>Table 3.12 Damage percentage at the connection failure for each collapse mechanism, when the force is applied against the concrete cover.....</i>	<i>160</i>
<i>Table 3.13 Damage percentage at the connection failure for each collapse mechanism, when the force is applied against the concrete core.....</i>	<i>162</i>
<i>Table 3.14 Damage percentage at the connection failure for each collapse mechanism, when the force is applied against the concrete cover.....</i>	<i>163</i>
<i>Table 3.15 Main parameters of accelerograms in the performed dynamic analyses.....</i>	<i>174</i>
<i>Table 3.16 Geometrical characteristics of the steel profiles.....</i>	<i>179</i>
<i>Table 3.17 Ground acceleration values at different probabilities of exceedance in 50 year.....</i>	<i>182</i>
<i>Table 3.18 Spectral acceleration ($T=1.50\text{sec}$ and damping value of 5%) values at different probabilities of exceedance in 50 years.....</i>	<i>183</i>
<i>Table 3.19 Seismic risk study summary with peak ground acceleration.....</i>	<i>184</i>
<i>Table 3.20 Seismic risk study summary with spectral acceleration at the first mode period.....</i>	<i>184</i>
<i>Table 3.21 Seismic risk study summary with peak ground acceleration.....</i>	<i>185</i>

Chapter 1

INTRODUCTION

Since the end of the Second World War, precast structures have been widely used in Italy and in Europe due to the several advantages of serial production of structural elements. In Italy and in Europe, precast (one-story) structures are mainly used in the industrial or commercial field (Figure 1.1a), where buildings require wide space, i.e. large bays, and very regular plants, e.g. square or rectangular shape. The widespread use and the specific function make the seismic safety of these structural typology an important issue both for the human safety and for the social and economic activities of entire region. The typical European industrial building configuration (Figure 1.1b) consists of columns, restrained at the base by socket foundations, assumed as monolithic connections (Osanai et al., 1996), and at the top by hinged prestressed beams, that support different typologies of roof elements. Precast concrete panels are typically employed as perimeter cladding elements.



(a)



(b)

Figure 1.1 RC precast industrial buildings

However, during some recent seismic events (Emilia, 2012; Turkey, 2011; L'Aquila, 2009), the high number of failures and recorded damages demonstrated the main deficiencies in the seismic response of this structural system (Magliulo et al., 2013).

Hence, some common deficiencies can be defined, despite the high variability in the used structural elements and in the geometrical parameters. Two main groups of deficiencies can be identified in the damaged precast structures. The first source of vulnerability is related to the poor seismic capacity of the structural elements: many structures showed significant damage to the structural columns (Figure 1.2), i.e. cracking, yielding, loss of verticality, and to the foundation systems, i.e. damage of the isolated socket foundations.



Figure 1.2 One-story RC precast industrial buildings: columns damage

The second order of deficiencies in existing precast structures is related to the low strength of the connection systems between the structural elements and between the structural and nonstructural components. Most of the structures in the epicentral areas of the mentioned earthquakes showed several damages to the connections; in many cases these damages were the cause of the most severe and disastrous structural collapse. Among the others, the most critical systems proved to be the connection between the horizontal elements (Figure 1.3a) and between these elements and the vertical ones (Figure 1.3b). For these connections, the late hazard evolution of some zones in Italy and the past code provisions caused the diffusion of connections relying only upon the frictional strength. Such connections typically failed due to the seismic actions, causing the loss of the support phenomena and, consequently, the structural collapse.

The earthquake experience also demonstrated another vulnerability source in the seismic response of the industrial buildings: many structures suffered the collapse of the external cladding panels due to the failure of the connection systems (Figure 1.4). The panels are RC precast elements with large dimensions that are usually considered

as nonstructural elements non-interacting with the structure during the design phase. During a seismic event, however, the panel-to-structure connection typology can cause the interaction of the panel with the structure. This can be the justification of the many failures of the connection and the modified structural response due to the unexpected interaction.



Figure 1.3 (a) Collapse of roof elements from the beams and (b) collapse of the beam from the columns in one-story precast buildings



Figure 1.4 (a) Collapse of horizontal precast panels and of (b) vertical precast panels in one-story precast buildings

1.1 Research purposes and outline

The main purpose of this work is the study of the seismic response of industrial buildings, taking into account all the most important features, components and vulnerability sources. The layout of the work follows a logical process in order to present all the results and the increasing detailing level on specific issues.

The thesis consists of two main Chapters, that divide the research activities in two parts, concerning the global and the local response of the structure, respectively.

Concerning the structural global response, detailed in **Chapter 2**, some general considerations on the earthquake experience in Emilia (2012) are discussed;

furthermore, the definition of nonlinear detailed models and to the proposal of new design formulas are included.

The behavior exhibited by the precast structures in the Emilia region (Northern Italy), hit by the two earthquakes on 20th and 29th May 2012 (Figure 1.5), is described in **Section 2.1**. According to some simple considerations on the seismic codes, on the hazard evolution and on the recorded accelerograms (Figure 1.6), the main causes of the damage are identified, supported by an exhaustive photographic report of the structures in the epicentral area. In this Section the study of an existing case study is also presented. A one-story precast industrial building is investigated, due to the recorded damage after the two Emilia earthquakes and the specific characteristics of structures and connections. In this work the actual structural behavior under seismic actions is investigated and the usual modeling approach and assumptions are tested.

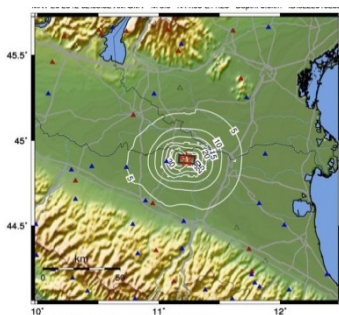


Figure 1.5 Shake map in terms of peak ground acceleration (May 20 2012 02:03:52 AM GMT)

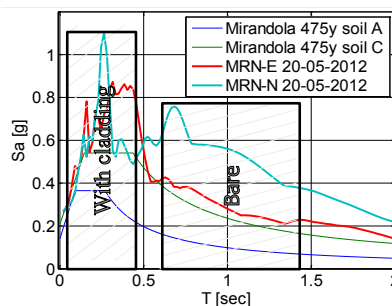


Figure 1.6 Elastic response spectra recorded on 20 May 2012 in Mirandola compared to elastic response spectra (DM 14/01/2008) for damping ratio equal to 5% is assumed.

The Emilia earthquakes hit a huge number of structures with an high indirect economic loss. This event caused the double requirement to protect the life and to early restart the economic and productive activities, highly related to the industrial construction estate. In this context the Italian scientific community compiled the “Guidelines on local and global retrofitting systems of precast structures” (**Section 2.2**), i.e. an useful reference document for professional engineers, involved in the post-earthquake assessment and retrofitting of industrial buildings.

A form for usability judgment of precast structures (GL-AeDES) is introduced in **Section 2.3**. The study of a specific form for the industrial buildings was already declared before the Emilia events by the Italian scientific community, that started the work some months before the first earthquake. The events confirmed the need of a more detailed document in order to achieve a more specific and right judgment of the residual safety of precast structures based on the experienced damages.

Finally, the global response of the structure is also investigated in terms of the dynamic characteristics, with and without the cladding panel systems interaction. In **Section 2.4** the vertical cladding panel influence on the dynamic behavior of one-story precast concrete buildings in terms of first vibrational period is investigated. In this study the definition of a linear model that includes cladding panels is described.

The specific features of the precast structures do not allow to neglect the local behavior of the connections, that are investigated in the **Chapter 3** of this thesis. The most crucial connection systems for the seismic safety of the analyzed structural typology are investigated, i.e. the beam-to-column connections and the connection between the structure and the external cladding panels.

The investigated beam-to-column connection is the dowel connection (Figure 1.7), that is the typical system in the precast European structures. A shear monotonic and cyclic test campaign on a dowel connection specimen is described in **Section 3.1** and the results are presented in terms of mechanical characteristics (strength, stiffness and ductility) and failure mechanisms. In this Section some considerations on the design formula for the connection are also provided, comparing the tests results with the literature and code provisions. On the basis of the experimental results, a FEM numerical model (**Section 3.2**) by means of the ABAQUS software (Corp., 2010) is validated in order to investigate the seismic behavior of the connection through a numerical approach.

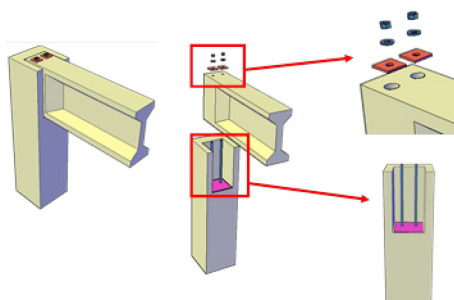


Figure 1.7 Beam-to-column dowel connection

The seismic performance of the panel-to-structure connection is investigated (Figure 1.8a) in **Section 3.3** by means of nonlinear dynamic analyses. Since the collapse of these nonstructural elements (Figure 1.8b) caused several fatalities, the global collapse of the structure is then assumed as the collapse of their connections in a seismic risk study. Moreover, a novel model is proposed, able to take into account the progressive collapse of the panels (i.e. of the connections with the structure).



(a)



(b)

Figure 1.8 (a) Vertical cladding panels in a precast one-story building. (b) Collapse of vertical cladding panels in a precast structure (Emilia, 2012)

References

- Corp., D.S.S. (2010), *Abaqus/CAE 6.10-1*, Providence.
- Magliulo, G., Ercolino, M., Petrone, C., Coppola, O. and Manfredi, G. (2013), *Emilia Earthquake: the Seismic Performance of Precast RC Buildings* Earthq Spectra.
- Osanaï, Y., Watanabe, F. and Okamoto, S. (1996), *Stress transfer mechanism of socket base connections with precast concrete columns*, *Aci Struct J.* **93**(3), 266-276.

Chapter 2

GLOBAL SEISMIC BEHAVIOR

This Chapter focuses on the global behavior of one-story precast structures under seismic actions.

The first presented work deals with the exhibited response in the municipalities hit by the two earthquakes occurred in Emilia region (Northern Italy). A description of the typical Italian precast structures is provided, as well as an account of the evolution of Italian building code for precast buildings. A photographic documentation, collected in the first days after the main-shocks, is presented in order to describe the damage and the seismic performance of the precast structural typology. Furthermore an attempt to identify the main causes of the damage is provided through the analysis of the recorded accelerograms. The last work is the study of a real case study, i.e. a precast one-story industrial building, located in Emilia and damaged by the two events of 2012. The damage observation during a direct survey is justified by means of nonlinear dynamic analyses with a detailed structural model. An effort is made in order to implement all the structural elements in the numerical model with their specific features and the actual connection characteristics and strengths.

The third and fourth Sections describes two emergency documents, that have the aim to improve the knowledge on the precast structures and reduce the uncertainties during the emergency operations, among which the usability judgment on the structure and the immediate retrofitting actions on damaged buildings.

The last Section describe the analysis on the dynamic properties of one-story precast structures, taking into account also the interaction with the external cladding panels. A parametric study is conducted in order to evaluate the dynamic response of typical precast industrial buildings by means of modal analyses. New predictive formulas are also proposed in order to evaluate the fundamental period of one story precast buildings both in the case of bare and with panels system.

2.1 Seismic response of buildings during the Emilia Earthquakes

On 20th May 2012 at 02:03:52 a.m. UTC, a 5.9 moment magnitude M_w earthquake occurred in Emilia region (Northern Italy), causing 7 casualties, about 50 injured and 5000 homeless people. The epicenter of the earthquake was located at Finale Emilia (Modena, Northern Italy). A series of after-shocks occurred in the area on the following days until a second main shock of 5.8 moment magnitude struck the same zones on 29th May, 2012, with an epicenter located at Medolla (Modena, Northern Italy), 20 km west from Finale Emilia. It occurred at 09:00:03 a.m. (local time), when the daily activities were starting again, and caused further 20 casualties, about 350 injured and raised the number of homeless from 5000 to 15000. Besides the loss in human lives, significant damage was mainly recorded in buildings and non-structural systems.

One of the main damaged system was the estate of industrial precast structures, that involved a huge economic loss due to the direct economic damage amounts (about 1 billion euros) and indirect losses, as the industrial production interruption (about 5 billion euros). The large economic loss compared to the intensity of the event is basically due to the conjunction of two factors:

- the high percentage of industrial precast buildings in the struck area;
- the vulnerability of the mentioned precast buildings.

2.1.1 Precast structures description and design considerations

In Italy, precast structures are mainly used in the industrial field, where buildings require wide space, i.e. large bays, and very regular plants, e.g. square or rectangular shape. Precast buildings can be classified according to different variables: the structural typology, the number of stories and the roof type. Three main structural typologies can be distinguished: panel structures, column structures and mixed structures. Depending on the number of stories, precast structures can be single-story “industrial” buildings (Figure 2.1a) and multi-story buildings (Figure 2.1b). Referring to the roof type, roof elements supported by beams with variable section (Figure 2.2a), continuous plane roof (Figure 2.2b), discontinuous plane roof (Figure 2.3a) and shed roof (Figure 2.3b) can be found.

In Italy the most common precast buildings are column structures: they consist of socket footing foundations in which precast columns are placed and fixed in-situ by cement mortar; the columns support pre-stressed precast beams that can have different shapes. The most frequent beam cross sections are “T” or “I” section for beams with variable section, and “Y”, “H”, “L” or rectangular section for plane beams. Reticular beams are also used, especially for very large spans. The main beams support roof elements: in multi-story buildings a cast in-situ slab is provided to cover corrugated

elements of intermediate decks; in single-story buildings, instead, a concrete slab is rarely used. Continuous or discontinuous roof elements solutions can be defined: in the first case, tiles are put side by side (Figure 2.2), in the second case tiles are spaced and alternated by light elements like translucent sheets (Figure 2.3a) or sandwich panels. An alternative solution is represented by a shed roof: it can be built using reticular beams or discontinuous beams, known in Italy as “knee beams” (Figure 2.3b), or using inclined beams supported at two different levels. Precast structures are generally completed by precast panels placed along the perimeter that can be inserted between columns or placed externally to the main structure. Infill systems can provide different solutions: horizontal precast panels connected to columns, vertical precast panels attached to horizontal beams and mixed solution including horizontal and vertical panels are all used. A more detailed list of precast structures typologies is provided by Bonfanti et al. (2008).



Figure 2.1. Examples of (a) single-story and (b) multi-story precast buildings.

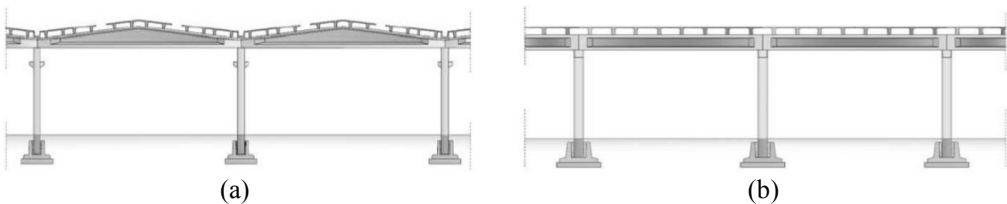


Figure 2.2. (a) Double slope roof with corrugated tiles and (b) continuous plane roof (Bonfanti et al., 2008).

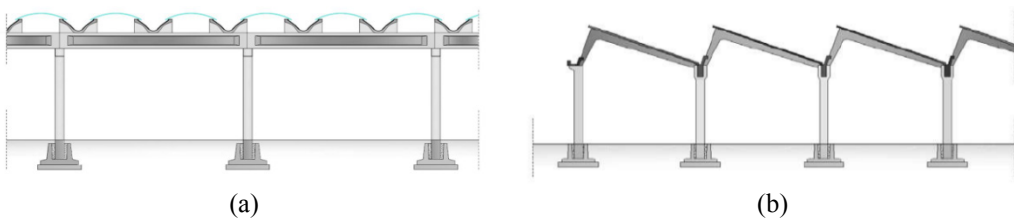


Figure 2.3. (a) Discontinuous plane roof and (b) shed roof (Bonfanti et al., 2008).

The most crucial aspect of precast structures regards the connections between structural elements. The connections are made in-situ and executed in order to reflect the calculation model assumed in the design phase. Typical connections include:

1. floor or roof adjacent elements connection;
2. roof element-to-beam connection;
3. beam-to-column connection;
4. column-to-foundation connection;
5. cladding panel-to-structural element connection.

The roof adjacent elements connections are generally made of steel angles and plates welded or bolted in order to ensure the slab continuity (Figure 2.2b).

The roof element-to-beam connections can be provided in different ways. The most common connection type provides a neoprene pad at the interface between the beam and the roof element, resulting in a friction connection. Another solution consists of steel angles bolted both to the roof element and to the beam defining a fixed connection (Figure 2.4a). A fixed connection is also given by the presence of a dowel, inserted in the roof element and in the beam.

A beam-to-column connection can be a friction connection or a dowel connection. The former type is very common in existing precast structures and generally consists of neoprene pad at the beam-to-column interface without providing any mechanical connectivity. It relies on friction for absorbing resisting forces. In the latter type a steel dowel is inserted inside the column and anchored in predefined vertical holes in the beam (Figure 2.4b); the connection requires a final grout casting. This solution defines a hinged support in the longitudinal direction of the beam.

The most common column-to-foundation connection is the socket foundation (Figure 2.4c). This typology is characterized by a RC hollow core body in which the column is inserted. Concrete or special mortar is poured to fill the gap between the column and the hollow core body of the socket foundation. The socket foundation is generally modeled as a rigid connection, due to the study performed by Osanai et al. (1996), in which it is concluded that the connection is rigid if the column embedment depth is larger than 1.5 times the depth of the column cross section.

Connections between cladding panels and structural elements (Figure 2.4d) can provide different solutions, based on steel connectors such as channel bars, fasteners, angles, brackets, etc.

A detailed list of connections in precast structures used both in Italy and Europe is provided by Mandelli et al. (2007).

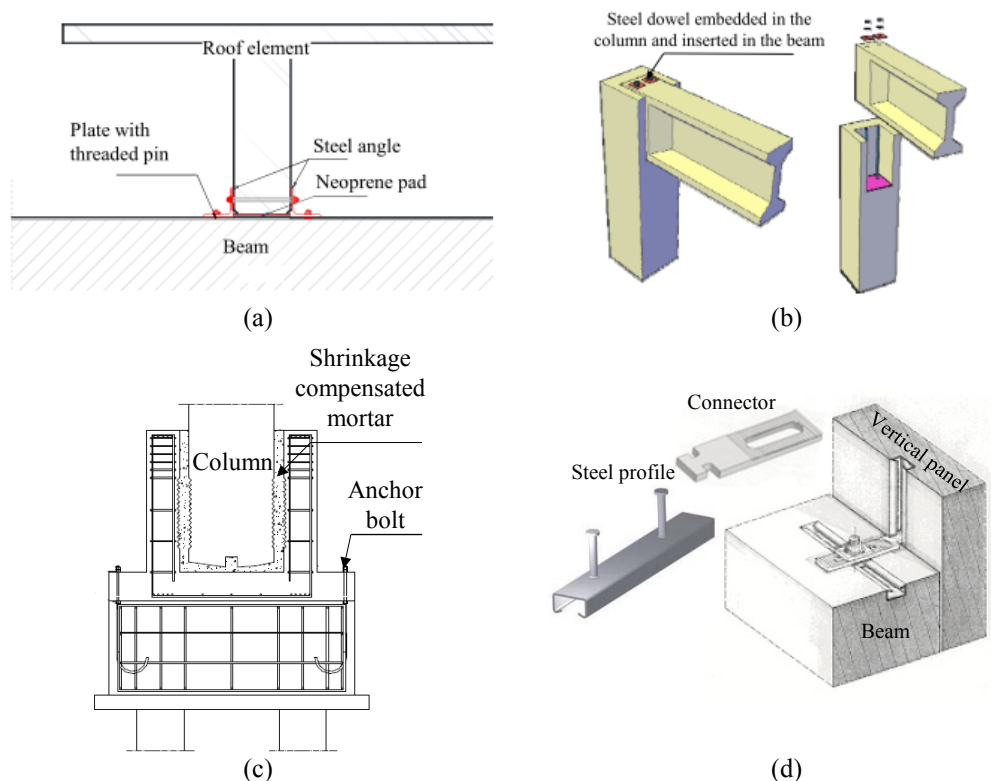


Figure 2.4. Examples of connections in precast structures: (a) pin roof element-to-beam connection; (b) dowel beam-to-column connection; (c) socket column-to-foundation connection; (d) vertical panel-to-beam connection

2.1.1.1 National seismic code evolution

In order to give an idea of the vulnerability of precast concrete buildings, a brief overview of the code evolution is given in the following, focusing the attention on the code provisions regulating the design of elements and connections in precast structures (Table 2.1).

Legge n. 1684 (1962) and its integration (Legge n. 1224, 1964) only specify the horizontal actions to consider in seismic zones in Italy without any particular requirement for precast structures. A noteworthy code is published in 1965 (Circolare del Ministero dei Lavori Pubblici n.1422, 1965), that forbids the use of horizontal joints without mechanical devices if the ratio T/N was larger than 0.35, where T is the maximum value of the shear force, N is the expected axial compression force and, implicitly, 0.35 is the friction coefficient of the connection.

In 1974, the code (Legge n. 64, 1974) introduces specific indications for the seismic design of structures. However, concerning precast structures, the code gives only a few general indications and these are for load-bearing precast panels structures.

The first specific regulations for precast structures are in the Decreto Ministeriale 3/12/1987 (1987), that already point out the role of the connections, considering also the transition phases of the construction. The requirements for the structural elements and for the connections design are still limited; it is forbidden in seismic zones to use beam-column connections that transfer horizontal forces by friction alone. The only prescriptive provision is given for the width of the beam-to-column support: “For the beams, the end support must be not smaller than the quantity $8cm + l/300$, where l is the clear beam span in centimeters”.

More detailed suggestions on precast structures are given in OPCM 3274 (2003). According to the Italian government, the application of this code is compulsory only in the case of infrastructure and strategic buildings. Multi-story framed structures and single-story structures with isostatic columns are taken into consideration, according to the number of stories and the capability of the connections in transferring bending moments. A specific behavior factor, i.e. 5.0 and 3.75 respectively, is assigned to the two structural typologies. Moreover it is recognized the significant influence of the connections on the static and dynamic behavior of the whole structure. In the case of framed structures, the codes distinguished three possible conditions:

- a. connections located well outside critical regions not affecting the energy dissipation capacity of the structure;
- b. connections located within critical regions but adequately over-designed with respect to the rest of the structure, so that in the seismic design situation they remain elastic while inelastic response occurs in other critical regions;
- c. connections located within critical regions properly designed in terms of strength, ductility and quantity of energy to dissipate.

For single-story structures with isostatic columns, the beam-column connections may be fixed or free to slide horizontally. The connections must transfer the seismic design horizontal forces, without taking into account the friction strength. For the fixed connection the capacity design approach is considered, i.e. its strength must be larger than the horizontal force that produces the ultimate resistant bending moment at the base of the column.

In Europe the precast concrete structures are regulated by the Eurocode 8 (CEN, 2005), which underlines the importance of the connections. It is required that friction resistance should be neglected in evaluating the resistance of a connection both for the beam-to-column connections and for the primary seismic elements-to-diaphragm horizontal joints. However, it should be underlined that the EC8 is not compulsory in Italy. Concerning the structural typologies, the following systems are considered for precast concrete structure: (a) frame structures, (b) wall structures, (c) dual structures (mixed precast frames and precast or monolithic walls), (d) wall panel structures (cross wall structures) and (e) cell structures (precast monolithic room cell systems). The

behavior factor for one-story framed systems ranges from a maximum of 4.95 to a minimum of 1.65 that corresponds to connections not regulated by the code.

The current Italian code (D. M. 14/01/2008, 2008) gives more attention to precast structures than do the past Italian codes. It takes the main framework of OPCM 3431, adopting some provisions of EC8. Concerning the precast column systems, the two structural categories defined in OPCM 3431 are provided, i.e. framed structures and isostatic column structures: the former include structures with continuous or hinged joints, the latter concern one-story buildings with beams hinged at one side and with a sliding support at the other one. Furthermore, the connections have to transfer the horizontal forces under the design seismic load without taking into account the friction strength; this last rule also applies to roof-to-beam connections. The code forces a reduction of 50% of the behavior factor, if some of the specific requirements concerning the connections are not followed.

Table 2.1. Italian building code evolution: title, acronym, presence of requirements on precast structures and on connections between structural elements, compulsoriness and relationships between the most important codes for precast structures

Code	Acronym	Precast structures requirements	Friction connection forbidden	Compulsoriness
Legge 25 novembre 1962, n. 1684	Legge 1684	No	-	Yes
Legge 5 novembre 1964, n. 1224	Legge 1224	No	-	Yes, integrates Legge 1684
Circolare del Ministero dei Lavori Pubblici n.1422 del 6 febbraio 1965	Circ. M. LL.PP. n.1422	No	Yes, if $T/N > 0.35$	Yes, integrates Legge 1224
Legge 2 febbraio 1974, n. 64	Legge 64	Yes	-	Yes, replaces previous codes
Decreto Ministeriale del 3/12/1987	DM 3/12/1987	Yes	In seismic zone	Yes, integrates Legge 64
Ordinanza del Presidente del Consiglio dei Ministri n. 3274 del 30/3/2003	OPCM 3274	Yes	Yes	Yes, only for infrastructures and strategic buildings
Eurocode 8	EC8	Yes	Yes	No
Decreto Ministeriale del 14/01/2008	DM 14/01/2008	Yes	Yes	Yes, integrates Legge 64 and replaces previous integrations

2.1.2 Precast structures damage observation in Emilia region

The commercial and industrial precast structures are the structural typology that suffered the most damage during the Emilia seismic events. Indeed, a direct inspection of the epicentral industrial zones in the days after the two mainshocks highlighted that more than a half of the existing precast structures exhibited significant damage.

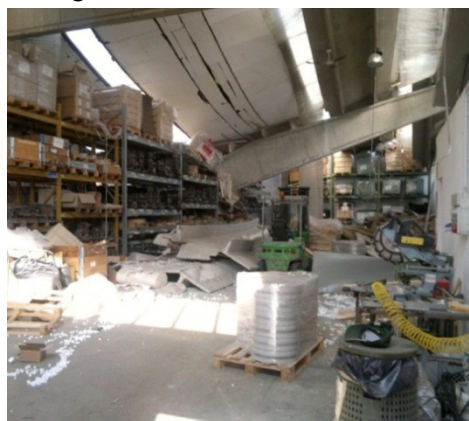
In this section the structural and non-structural damages, that occurred in precast structures during the Emilia earthquakes, are presented by a photographic documentation (Ercolino et al., 2012a; Ercolino et al., 2012b).

2.1.2.1 Damage to connections between structural components

Most of the damaged precast buildings provides friction connections between horizontal elements (beams and roof elements) or between horizontal (beam) and vertical (columns) members. The lack of connection devices is the main cause of damage in precast structures, in which the low strength given by friction mechanism causes the loss of support of both roof elements from beams and beams from columns. The consequences are disastrous: Figure 2.5a shows the loss of support of the roof elements from the main beam due to the use of friction connections and a very limited support width. Figure 2.5b shows the loss of support of a beam from the column and the consequent collapse of the roof elements, causing the failure of the whole structure.



(a)



(b)

Figure 2.5. (a) Roof elements collapse due to the loss of support from main beam. (b) Loss of support of beam from column

The lack of mechanical devices causes the loss of support of the beams from the columns also in Figure 2.6a. In other cases the loss of support causes the change of the beam restraints, that let the beam act as a cantilever, and make it collapse under the weight of the roof elements (Figure 2.6b). The vulnerability recorded in precast structures is certainly larger than the vulnerability exhibited by similar precast structures in Turkey after 1999 Kocaeli earthquake (Saatcioglu et al., 2001) the main

reason is the common presence of connections relying on friction in Emilia region, contrasting with the doweled connections used in Turkey.



Figure 2.6. (a) Loss of support of beam from column. (b) Collapse of main beam due to the loss of support on column

Some precast structures show the failure of the connections even in cases in which pin beam-to-column connections are used, due to the inadequacy of the connection design. Figure 2.7 represents a significant example of unsuitable design of the connection. The strength of the pin connection is evaluated in correspondence to the failure of the dowel; instead in Figure 2.7a, the spalling of concrete cover occurs before the yielding of the dowel, due to the small size of the cover and to the lack of dense stirrups close to the supporting zones. Consequently, it causes the collapse of the beam and roof elements which are supported by the beam (Figure 2.7b).



Figure 2.7. (a) Pinned beam-to-column connection failure and (b) consequent loss of support of the beam from column

The above presented damage highlights the low robustness of the investigated precast structures under seismic actions: in most cases the collapse of only few (even one)

connections can cause the collapse of the whole structure and, consequently, the loss of both life and inventory.

2.1.2.2 Columns damage

In Italian precast existing structures, columns are generally precast elements connected at the bottom to a socket foundation and at the top by a horizontally sliding or fixed support to the beams. Therefore the columns can be assumed to act as cantilevers fixed at the base. In presence of strong earthquakes, precast columns show:

- loss of verticality due to a rotation in the foundation element (Figure 2.8a) caused by a possible inadequate column-to-foundation connection, even if this cause is not easily ascertainable unless a direct inspection of foundation is made;
- plastic hinge development at the column base: Figure 2.8b shows an incipient plastic hinge evidenced by extensive cracks at the base, and Figure 2.8c indicates a case of longitudinal bar buckling due to the visible lack of a proper stirrup spacing in the critical zone of the column.
- shear failure due to the interaction with traditional masonry infill systems (Figure 2.9).



(a)



(b)



(c)

Figure 2.8. Damage in columns: (a) column loss of verticality due to rotation in the foundation element; (b) cracking of the base section in a column; (c) plastic hinge at the bottom of the column and buckling of a longitudinal bar at the base



Figure 2.9. Shear collapse of column due to the interaction with infill masonry panel

2.1.2.3 Infill precast panel collapse

Precast buildings infill systems in Emilia region are mostly constituted by precast cladding panels. Horizontal (Figure 2.10a) and vertical (Figure 2.10b) panels collapse is the most frequent damage in precast buildings.

The causes of collapse can be attributed to:

- a) the lack of seismic design in cladding panel-to-structural element connection devices;
- b) the pounding of roof elements, columns or other precast panels;
- c) the panel-to-structure interaction that causes additional lateral forces in the connection devices, not considered during the design process.



(a)



(b)

Figure 2.10 (a) Collapse of horizontal precast panels. (b) Collapse of vertical precast panels

Figure 2.11 shows the collapse of a horizontal panel-to-column connection due to the failure of the anchor channel embedded in the column (Figure 2.11a) and the shear failure of the steel angle plate that joints the panel to the structure (Figure 2.11b); details of the hammer head screw can be observed in Figure 2.11c. Figure 2.12 shows the collapse of a vertical panel-to-beam connection: in this case a particular connection

device is used, i.e. a steel profile is embedded in the beam (highlighted in Figure 2.12b) and some hammer head elements are welded to the profile and inserted into the anchor channel of the vertical precast panels (Figure 2.12a). Under the seismic action the screw-to-profile welding fails and causes the collapse of the panels.

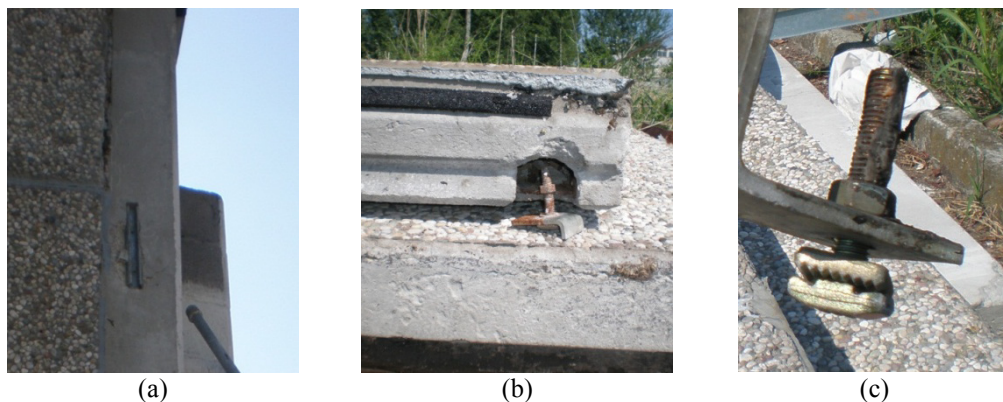


Figure 2.11. Details of a connection device at the top of horizontal panel: (a) anchor channel embedded in the column, (b) steel angle plate and (c) hammer head screw out of the anchor channel



Figure 2.12. Collapse of vertical precast panel connection: (a) the anchor channel embedded in the panel and the failed hammer head element; (b) profile located in the beam which the hammer head elements are welded to

2.1.3 Seismic action and considerations concerning loss of support

In order to understand the damage recorded after the Emilia earthquakes, a description of the Italian seismic zones is presented.

The definition of seismic zones in Italy started in 1909 following the Reggio Calabria and Messina Earthquake in 1908 that causes about 80.000 casualties. The regions in Southern Italy that suffered from this earthquake were defined seismic zones. Since then, the map has been refreshed enlarging the zones defined as “seismic” after each

significant Italian earthquake. The Emilia region that was struck by the recent earthquakes (black dot in Figure 2.13) was still out of the seismic zones in the 1984 map (Figure 2.13a). Finally, in 2003 the whole Italian territory was classified as seismic (Figure 2.13b), distinguishing four seismic zones: zone 1, 2, 3 and 4, corresponding to design peak ground acceleration at the bedrock equal to 0.35g, 0.25g, 0.15g and 0.05g, respectively. The region close to the epicenter of Emilia earthquakes was inserted in the 3rd zone.

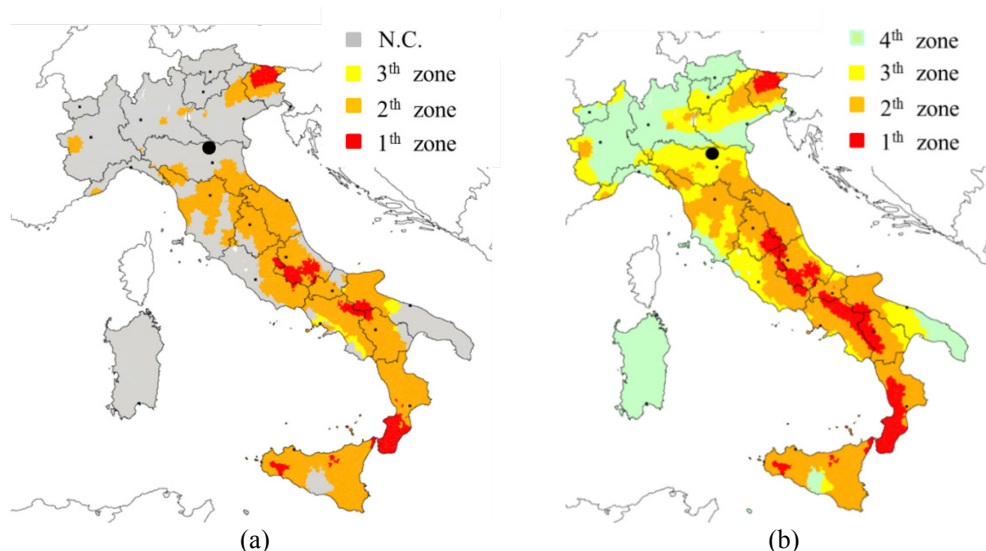


Figure 2.13. Seismic zone classification in Italy (a) in 1984 and (b) in 2003; the black dot indicates the Emilia earthquake epicentral zone (INGV, 2012)

Hence, it is expected that all structural typologies in Emilia region, designed up to 2003, do not take into account seismic design at all, increasing the seismic vulnerability of structures built in that region. In particular, precast structures built up to 2003 typically provide beam-to-column friction connections because friction connections were forbidden only in seismic zones since 1987 (Table 2.1).

Lastly, the current Italian code (DM 14/01/2008) defines hazard parameters continuously for the whole national territory, without distinguishing different seismic zones. In particular, for Mirandola (Modena, Italy) the PGA with a 10% probability of exceedance in 50 years is equal to 0.140g.

The acceleration time histories recorded (Figure 2.14) by the station MRN of the Italian National Accelerometric Network yields a maximum acceleration equal to 0.264g and 0.261g for the N-S and E-W components, respectively; the spectral ordinates reach values up to 1g (Figure 2.15). It should be noted that the recorded accelerograms include seismic site effects; indeed, MRN station is placed on a “C” class soil site (shear wave velocity ranging from 180m/s to 360m/s), based on

geological data, and T1 category according to EC8 (flat surface), as reported in the *Italian Accelerometric Archive* (Luzi et al., 2008).

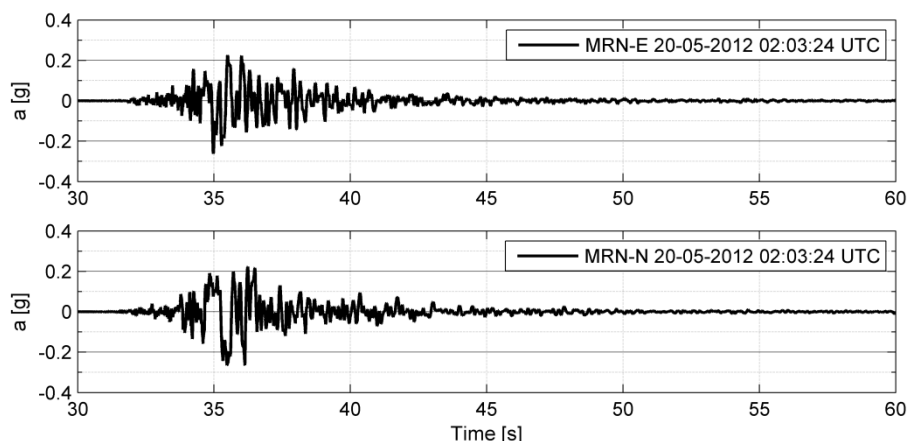


Figure 2.14. Accelerograms recorded in the station of Mirandola (Modena, Italy) (the origin of time is set at 20-05-2012 02:03:24 UTC)

In Figure 2.15 the recorded spectra are compared with the design spectra in the epicentral zone for return periods equal to 475 and 2475 years (C soil and T1 surface). The comparison demonstrates the rarity of the event, according to the actual Italian seismic hazard maps and the historical data they are based on; the NS component spectrum is generally included between the two considered design spectra for low period range, i.e. before 0.6sec, and it exceeds the spectrum with the higher return period for high period range, i.e. beyond 0.6sec.

In order to establish the spectral accelerations in the precast structures during the investigated Emilia seismic events, two period ranges can be distinguished in the spectrum of Figure 2.15, according to the extensive parametric study provided by (Magliulo et al., 2014b) on single-story precast structures designed according to the current Italian code in low-to-high seismic zones. The bare precast structures exhibit an elastic fundamental period ranging from 0.54sec to 1.45sec, while infilled precast structures range from 0.09sec to 0.40sec, due to the presence of cladding panels. No significant difference between the spectral ordinates for bare and infilled structures for NS-component is evidenced; on the contrary, in the case of EW component, the 0.09sec-0.40sec range provides larger spectral ordinates.

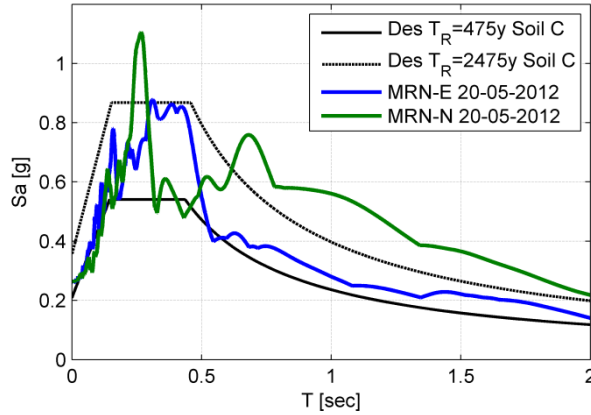


Figure 2.15. Elastic response spectra recorded on 20 May 2012 in Mirandola NS (green) and EW component (blue) compared to elastic response spectra for return period equal to 475y (black) and 2475y (dashed black) provided by Italian building code (DM 14/01/2008) for soil class C. A damping ratio equal to 5% is assumed

In the previous section it has been highlighted that loss of support has been the main cause of collapse in precast structures in Emilia region. This can be deduced also upon simple considerations on the recorded spectra (Figure 2.15). Assuming that the rigid diaphragm is not ensured, as commonly found in Emilia region precast buildings, the total seismic force F_{tot} is divided among the columns using a criterion based on influence area, i.e. proportionally to the ratio between the dead loads W_i acting on the column and the total weight of the structure W_{tot} . Considering that the participating mass ratio is 100% for the translational modes, the seismic force V_{Ed} acting on a connection can be evaluated as follows:

$$V_{Ed} = F_{tot} \cdot \frac{W_i}{W_{tot}} = W_i \cdot S_a(T_1) / g \quad (2.1)$$

The strength of a friction connection V_{Rd} can be evaluated multiplying the vertical force acting on the connection and the friction coefficient μ (2.2). Based on these considerations, the loss of support mechanism is immediately checked comparing the friction coefficient with the acceleration spectral ordinates in g, as shown in Figure 2.16. Indeed, a safety factor SF can be evaluated and plotted (Figure 2.16b) versus the fundamental period for the recorded spectra.

$$V_{Rd} = \mu \cdot W_i \Rightarrow SF = V_{Rd} / V_{Ed} = \frac{\mu}{S_a(T_1) / g} \quad (2.2)$$

According to the experimental studies conducted by (Magliulo et al., 2011) on neoprene-to-concrete connections, the friction coefficient varies in the range $0.09 \div 0.13$ for compressive stress varying between 1.7 MPa and 5.3 MPa. In Figure 2.16a these limits are compared to the recorded spectral ordinates. Figure 2.16b shows the safety factor SF , evaluated considering μ equal to 0.13. The safety factor SF is much

below 1 for a wide range of periods and confirms the vulnerability recorded in friction connection of precast structures in Emilia region.

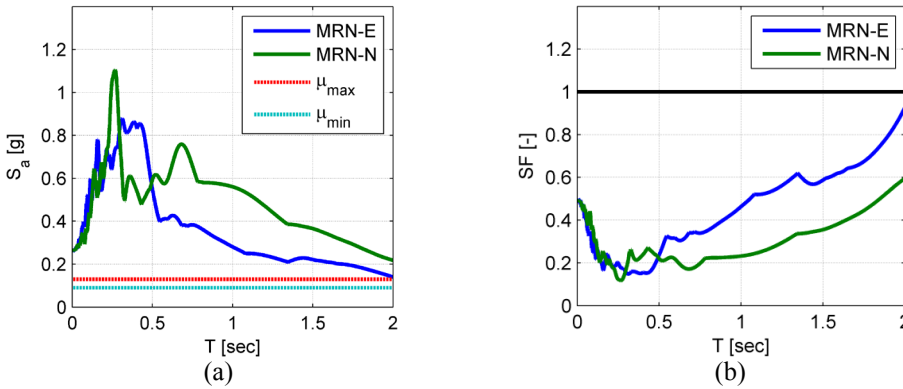


Figure 2.16. (a) Acceleration spectral ordinates recorded in Mirandola compared to the friction coefficient upper and lower bounds evaluated by Magliulo et al. (2011); (b) loss of support safety factor plotted versus fundamental periods for the recorded accelerograms, assuming $\mu=0.13$

It should be noted that the simple considerations above presented neglect both the vertical component of the seismic action and the bi-directionality of the input motion. Obviously, if the two phenomena had been taken into account, lower safety factors would have been found. Even in case larger friction coefficients had been considered, e.g. Caltrans (1994) suggests a coefficient ranging from 0.2 to 0.4 in case of neoprene/concrete interface for bridge applications, the loss of support would not have been avoided for a wide range of structural periods.

The use of an unreduced elastic spectrum for the evaluation of the force acting on beam-to-column friction connections may be questioned, since precast structures may inelastically dissipate energy. However, inelastic action in the concrete elements will not occur if the frictional strength of the connection is lower than the plastic shear, i.e. the force that causes the formation of the plastic hinge at the column base. Indeed, in this case no plastic sources are exploited and, hence, the unreduced elastic spectrum must be used for the evaluation of the seismic actions.

It is concluded that, if the shear failure of the connection comes before the flexural hinging in the column, precast structures with neoprene-concrete friction connections will exhibit a loss of support of their horizontal elements under the recorded seismic excitation. (Magliulo et al., 2008) anticipated this evidence, demonstrating that precast structures with friction connections suffer from loss of support due to the sliding of the beam from the column. This statement is based on nonlinear dynamic analyses, performed on space models subjected to the three components of an earthquake typical of an Italian medium seismicity zone.

The mainshock occurred on the 29th May 2012 is well recorded, due to the installation of temporary seismic stations around the epicentral area. The considerations above presented for the 20th May mainshock can be extended to the 29th May mainshock as well, based upon the horizontal acceleration spectra recorded in the area close to the epicenter (Figure 2.17).

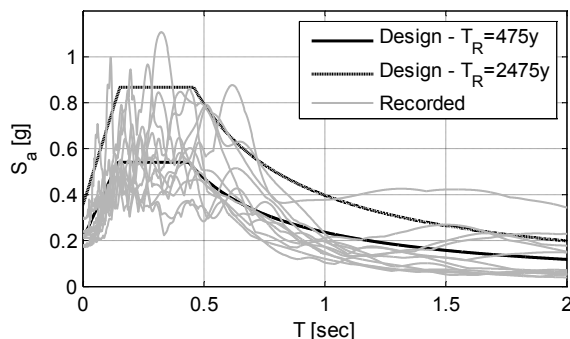


Figure 2.17. Elastic response spectra recorded on 29 May 2012 in Cento (CNT), Finale Emilia (FIN0), Moglia (MOG0), Mirandola (MRN), San Felice sul Panaro (SAN0) and San Martino Spino (SMS0) compared to elastic response spectra for Mirandola for return period equal to 475y (black) and 2475y (dashed black) provided by Italian building code (DM 14/01/2008) for soil class C.

2.1.4 Considerations concerning use of friction connections

Precast structures hit by the Emilia earthquake were designed according to different codes, depending on the construction time. Most of the precast structures in Emilia were designed without taking into account seismic forces, based on the above mentioned considerations on the seismic hazard map evolution in Italy; however, horizontal forces, i.e. wind and crane actions, were also considered.

Since the wind horizontal forces imply lateral loads on the connections, the use of friction connections may be questioned. For this reason, a parametric study is carried out in order to justify a similar widespread design choice. The study assumes a one-story precast building located close to the epicenter as a benchmark structure. Some geometrical parameters are considered, resulting in 48 case-studies, i.e. the column height H (7m, 9m, 11m, 15m), the number of the longitudinal bays (4, 6, 8, 10), the width of the two transverse bays B (15m, 19m, 25m).

In the parametric study, the horizontal shear demand in the connections caused by the wind actions is evaluated according to different past Italian codes and compared to the friction strength. In particular, the wind action is evaluated according to CNR Instructions (CNR-UNI 10012, 1967) and to DM 16/1/1996 (Decreto Ministeriale del 16/01/1996), as shown in Table 2.2. The NTC 2008 (DM 14/01/2008) is not taken into account because Emilia region has been a seismic zone since 2003 and, according to the current code, friction connections are forbidden in seismic areas.

Table 2.2. Evaluation of the wind equivalent forces according to past Italian building codes (CNR-UNI 1967 and DM 1996).

CNR 1967	p	N/m ²	wind velocity pressure	$p = c \cdot k \cdot q$
	c	[-]	external exposure and shape coefficient	0.8
	k	[-]	slenderness coefficient	$f(H/(2 \cdot B))$
	q	N/m ²	wind kinetic pressure	600
D.M.1996	p	N/m ²	wind velocity pressure	$p = q_{ref} \cdot c_e \cdot c_p \cdot c_d$
	q_{ref}	N/m ²	kinetic pressure	$q_{ref} = v_{ref}^2 / 1.6$
	v_{ref}	m/sec	wind speed	25
	c_e	[-]	external exposure coefficient	$f(H)$
	c_p	[-]	shape factor (upstream facades)	0.8
	c_d	[-]	dynamic factor	1.0

The ratios between the design shear demand in beam-to-column connection induced by wind and the connection friction strength is evaluated for the different case studies (Figure 2.18). In particular, the shear demand is evaluated according to CNR Instructions and DM 16/1/1996 and the shear strength is calculated according to friction coefficient equal to 0.35, 0.13 and 0.09. It is found that, if the friction coefficient $c = 0.35$, recommended by the mentioned Italian code (Circolare del Ministero dei Lavori Pubblici n.1422, 1965), is used, the shear demand will be always much smaller than the capacity. This outcome justifies the use of friction connections in existing structures. Vice versa, if the experimental coefficients proposed by (Magliulo et al., 2011) are considered ($c = 0.13 \div 0.09$), the capacity decreases and, in 25% cases, it can be exceeded by the shear demand.

It can be concluded that an unrealistic high friction coefficient for the evaluation of the shear capacity of the connections in the past Italian codes allowed the use of friction connections.

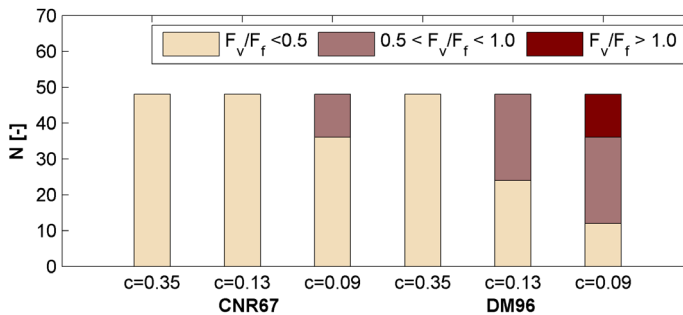


Figure 2.18. Ratios between the design shear demand F_v in beam-to-column connection induced by wind, evaluated according to CNR 1967 (CNR67) and DM 1996 (DM96), and the connection friction strength F_f , evaluated according friction coefficient c equal to 0.35, 0.13 and 0.09, for the different case studies.

2.1.5 Case study

The investigated case study is an existing one-story precast RC building, located in Mirandola (Modena, Italy) and hit by the two recent earthquakes of Emilia (20th and 29th May 2012). The structure was designed and built in 1990 and the main geometrical characteristics were given by the designers.

Figure 2.19 shows the plan view of the structure, that consists of 6 bays of 20m in X direction (transversal direction) and 5 bays of 10m in Y direction (longitudinal direction). In this figure the labels of the vertical structural elements are reported (columns) and they are explained in details in the following section. The total height of the columns is equal to 7.3 m. In the X direction the columns are connected by beams and in Y direction by secondary girders. The structure is closed with vertical precast panels along the perimeter with a height of 8.9 m (Figure 2.20 and Figure 2.21).

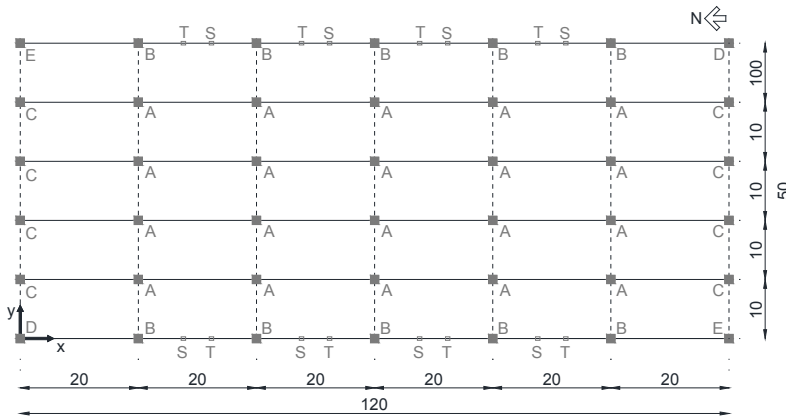


Figure 2.19 Plan view of the case study

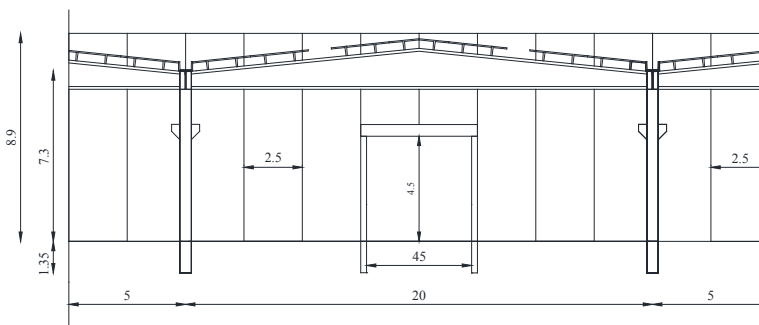


Figure 2.20 Frontal view (X direction)

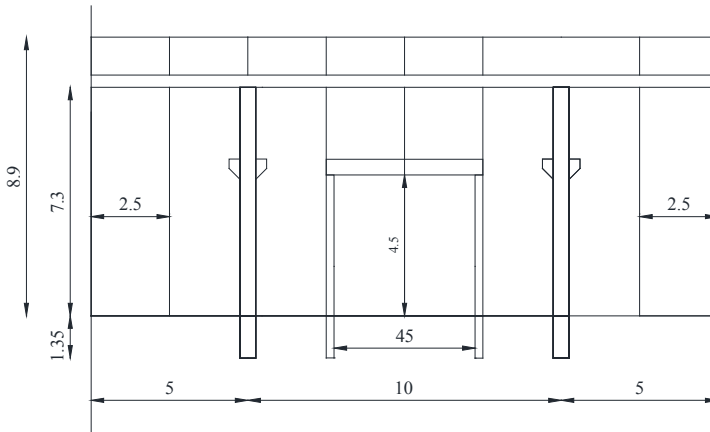


Figure 2.21 Lateral view (Y direction)

2.1.5.1 Structure and damage

The investigated industrial building consists of an assemblage of precast RC columns, fixed at the base with socket foundations. The cross section of the columns are reported in Figure 2.22 and their geometrical characteristics as well as the reinforcement percentage are reported in Table 2.3 for the typologies individuated in Figure 2.19. The concrete has a characteristic cubic compressive strength of 50MPa and the reinforcement steel has a characteristic yielding strength of 440MPa. The seismic weight of the structure is calculated considering the real dimensions and numbers of all the structural and non-structural elements (cladding panels). In the transversal direction (X direction) the columns are connected at the top by means of precast and prestressed beams with variable section. In the longitudinal direction (Y direction) the columns are connected by girders with a U cross-section.

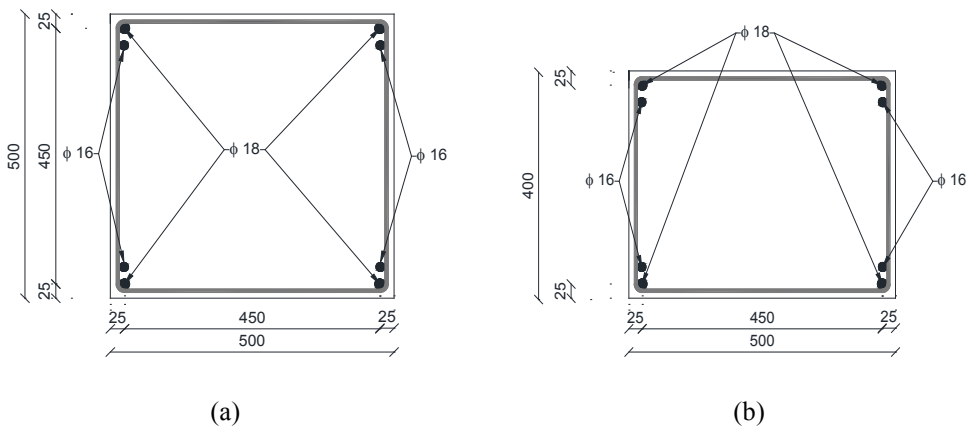


Figure 2.22 Cross sections of column for (a) columns B,D and E and for (b) columns A and C

Table 2.3 Geometrical characteristic and reinforcement details of columns

Column	Section	ρ	Stirrups
[-]	[cm x cm]	[%]	[ϕ /cm]
A	40x50	0.91	$\phi 6/20$
B	50x50	0.73	
C	40x50	0.91	
D	50x50	0.73	
E	50x50	0.73	

In order to study the seismic behavior of the structure, the connection systems are investigated.

- The connection between the transversal beams and the columns provides only a neoprene pad between the two concrete elements, without any mechanical devices (Figure 2.23). The contact surface has a length of 23cm in the X direction.
- The connection between the girder and the columns provides bolted steel angles (Figure 2.24).
- The connection between the roof elements and the beams provides only a neoprene pad between the two concrete elements, without any mechanical devices (Figure 2.25). The contact surface has a length of 13 cm in the Y direction.

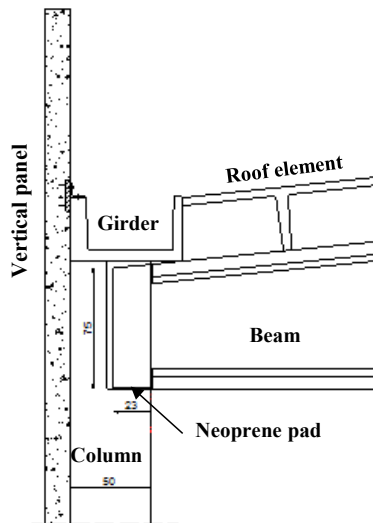


Figure 2.23 Detail of the beam-to-column connection

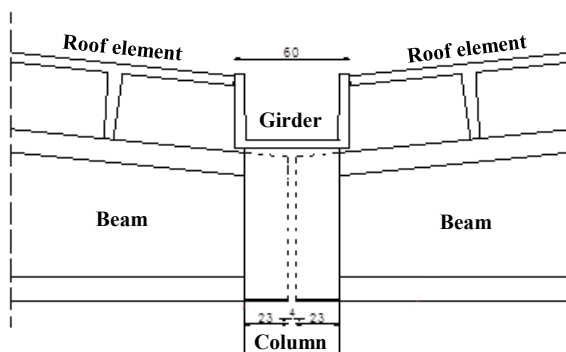


Figure 2.24 Detail of the girder-to-column connection

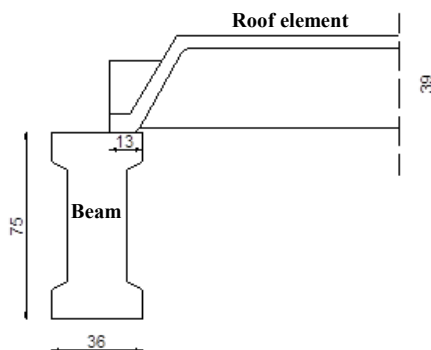


Figure 2.25 Detail of the roof element-to-beam connection

The damage observation in the case study was performed after the 29th May event before any kinds of retrofitting actions on the elements. According to this direct survey, the main recorded damages were found in the structural vertical elements, in the beam-to-column connections and in the roof-to-beam connections.

The structural columns showed cracking (Figure 2.27a) and yielding (Figure 2.27b) at the base as well as significant rotations (Figure 2.27c) in X direction.

Concerning the connections between the structural elements, significant relative displacements were recorded between the beams and the supporting columns (Figure 2.29) and between the roof elements and the beams (Figure 2.28).



Figure 2.26 Columns damage in X direction after the 29th May event



Figure 2.27 Dislocation in the beam-to-column connections after the 29th May event



Figure 2.28 Dislocation in the roof-to-beam connections after the 29th May event

2.1.5.2 Nonlinear model

A lumped plasticity model is implemented in the OpenSees program (McKenna and Fenves, 2013) in order to introduce the inelastic behavior of the structural elements, i.e. at the base of the precast columns. All the horizontal structural elements (beams, girders and roof elements) are introduced in the model as beam elastic elements. The material mechanical characteristics are assumed equal to the mean values.

The moment-rotation envelope consists of three characteristic points: the cracking, the yielding and the ultimate points. The yielding moment is assumed equal to the yielding moment of the moment-curvature curve and the ultimate moment is defined considered a low hardening (1%) value, assumed for numerical issues.

The yielding rotation is evaluated according to Fardis and Biskinis (2003):

$$\theta_y = \varphi_y \cdot \frac{L_s}{3} + 0.00275 + a_{sl} \cdot \frac{\varepsilon_y}{(d - d')} \cdot \frac{0.2d_b f_y}{8 \cdot \sqrt{f_c}} \quad (2.3)$$

In equation (2.3):

- ϕ_y is the yield curvature (evaluated as the yielding point of the moment-curvature curve);
- a_{sl} is a zero-one variable indicating the slip of the longitudinal bars from their anchorage (1-slip, 0-no slip);
- $(d - d')$ is the distance between the tension and compression reinforcement;
- ε_y is the yield strain of the tension reinforcement;
- f_y and f_c are the yield stress of the tension reinforcement and the compressive strength of the concrete (both in *MPa*), respectively.

The ultimate rotation capacity of the moment-rotation curve is calculated as:

$$\theta_u = 0.6 \cdot a_{st} \cdot (1 - 0.5a_{sl}) \cdot (0.3)^\nu \cdot \left[\frac{\max(0.01; \omega_2)}{\max(0.01; \omega_1)} \cdot f'_c \right]^{0.175} \cdot \left(\frac{L_s}{h} \right)^{0.4} \cdot 25^{\left[\frac{a \rho_w f_{yw}}{f_c} \right]} \quad (2.4)$$

In equation (2.4):

- a_{st} is a coefficient relating to the type of steel, equal to 0.0194 for ductile hot-rolled steel;
- a_{sl} is a zero-one variable indicating the slip of the longitudinal bars from their anchorage (1-slip, 0-no slip);
- ν is the axial loading ratio;
- ω and ω' are the mechanical ratios of the tension and compression reinforcement normalized to the concrete section;

- $\frac{L_s}{h}$ is the shear span ratio of the section of maximum moment;
- f_c is the uniaxial (cylindrical) concrete strength (in MPa);
- f_{yw} is the yield strength of the transverse steel;
- α is the confinement effectiveness ratio according to Eurocode 8;
- ρ_w is the ratio of the transverse steel parallel to the direction of loading.

The hysteretic rule following the indications given in Ibarra et al. (2005).

According to the described assumptions, the moment-rotation backbone curves are obtained for the columns of the case study; in the following figures (Figure 2.29, Figure 2.30 and Figure 2.31) the curves of the representative columns are reported along both the two horizontal direction.

All the masses are distributed along the structural elements and the panels weight is introduced as a distributed mass on the supporting beams or girders.

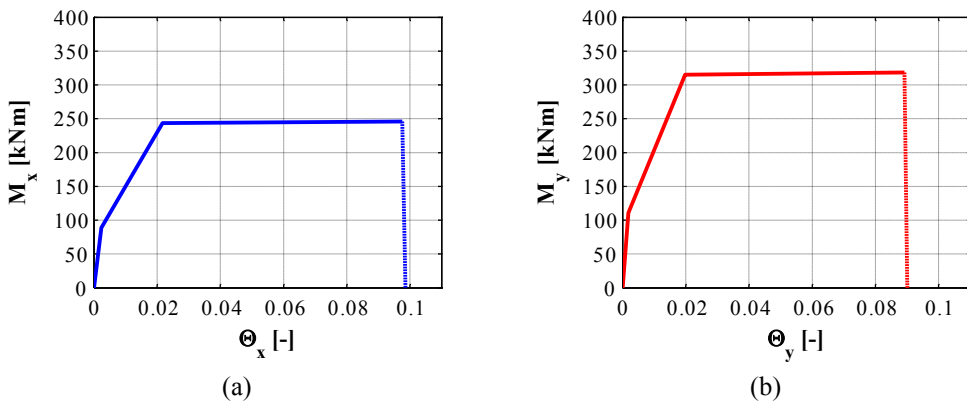


Figure 2.29 Moment-rotation envelope of the column A around (a) the X direction and (b) the Y direction

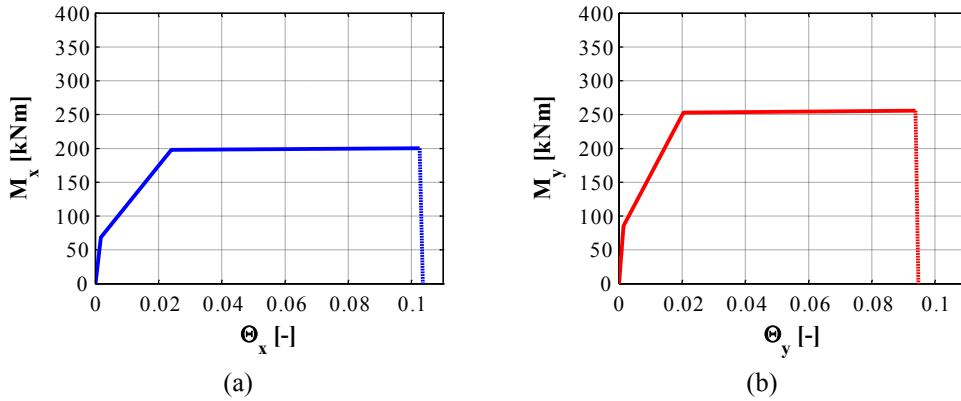


Figure 2.30 Moment-rotation envelope of the column C around (a) the X direction and (b) the Y direction

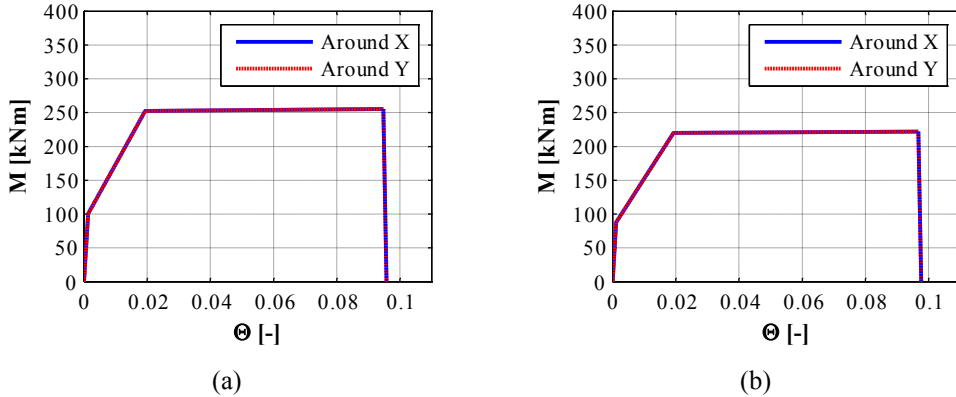


Figure 2.31 Moment-rotation envelope of (a) the column B and of (b) the column D and E

2.1.5.3 Connections modeling

The model includes all the structural elements of the buildings: the beams in both the directions, the roof elements and the columns. In order to take into account the real dynamic properties of the structures, all the elements are implemented in the model with their position in the whole structure, i.e. all the eccentricities between the connections and the elements are considered. Figure 2.32 shows the considered eccentricities in the X direction of the structure. With regards to the beam-to-column connection, two eccentricities are defined as rigid links, simulating the distances between the connection (blue circle) of the beam (the center of the neoprene pad) from the barycenter line of the column (green horizontal link) and from the barycenter line of the beam (green vertical link). With regards to the roof-to-beam connections, two eccentricities are inserted as rigid links, simulating the distances between the connection (red circle) from the beam (yellow lower vertical link) and from the

barycenter of the TT element (yellow upper vertical link). Finally, the girders are connected to the columns (black circle), considering the height of the forks (magenta link).

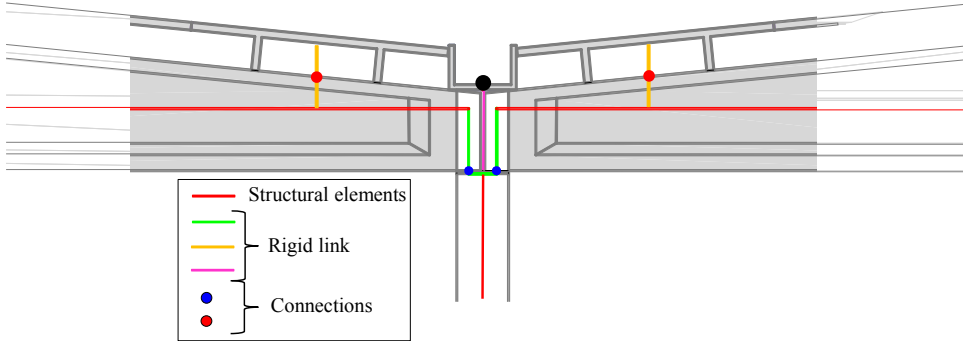


Figure 2.32 Structural elements layout and connection position

All the connections are defined with the “equalDOF” command between the two linked elements and the assumed degrees of freedom are reported in Table 2.4. The degree of freedom U_x between the beam and the column is not fixed since in X direction a frictional connection model is implemented in order to evaluate its behavior during the seismic records. Since also the frictional elements between the roof elements and the beams are introduced in the model, the degree of freedom U_y is not fixed for these connections. In all the frictional connections the degree of freedom U_z is not fixed in order to evaluate the influence of the vertical components of the considered earthquakes on the global and local response.

Table 2.4 Fixed degree of freedom in the connection between the structural elements

Connection	Fixed degree of freedom					
	U_x	U_y	U_z	R_x	R_y	R_z
Beam – column	NO	YES	NO	YES	NO	NO
Girder – column	YES	YES	YES	NO	YES	NO
Roof – beam	YES	NO	NO	NO	YES	NO

2.1.5.4 Frictional elements

In order to model the frictional connections in the nonlinear model of the case study, the “Flat slider bearing” element of the OpenSees library is introduced between the two linked structural elements. The command line for a three-dimensional problem is:

element flatSliderBearing \$eleTag \$iNode \$jNode \$frnMdlTag \$kInit -P \$matTag -Mz \$matTag <-orient \$x1 \$x2 \$x3 \$y1 \$y2 \$y3>

In this command the element (recognized by the $\$eleTag$) is defined as an object between two nodes: the $\$iNode$, that represents the flat sliding surface, and the $\$jNode$, that represents the slider. The frictional properties are defined with the $\$frnMdlTag$, that assigns a previously-defined frictional model, assumed as a Columb model in this study. The initial elastic stiffness ($\$kInit$) is defined as the shear stiffness of the neoprene pad. The force-deformation behaviors are defined for all the directions with different elastic “UniaxialMaterials”: in the P direction (vertical in this study) the compressive neoprene stiffness ($-P \$matTag$) is assigned while in the other directions a very flexible material is defined. To capture the uplift behavior of the bearing, the user-specified UniaxialMaterial in the axial direction is modified for no-tension behavior. The element orientation is defined with the orient command ($<-orient \$x1 \$x2 \$x3 \$y1 \$y2 \$y3>$), that represents the vector components in the global coordinates, defining local x-axis and local y-axis (Figure 2.33).

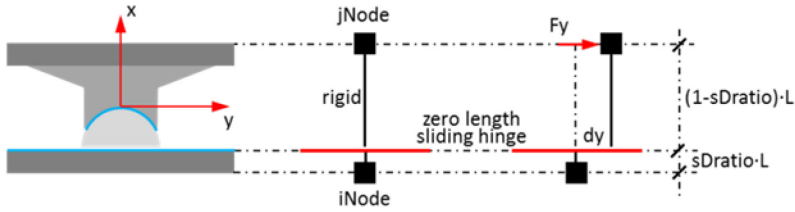


Figure 2.33 Flat bearing element

2.1.5.5 Input motion records

The dynamic analyses are performed with the accelerations-time histories recorded by the station MRN of the Italian National Accelerometric Network during the two main events of the 20th May and 29th May 2012. Some of these records have been presented in the previous paragraphs, but they are also reported in the following in order to simplify the overall understanding.

Figure 2.34 shows the N-S and E-W components of the 20th May event, that yield a maximum acceleration equal to 0.264g and 0.261g, respectively. Figure 2.35 shows the N-S and E-W components of the 29th May event, that yield a maximum acceleration equal to 0.295g and 0.224g, respectively.

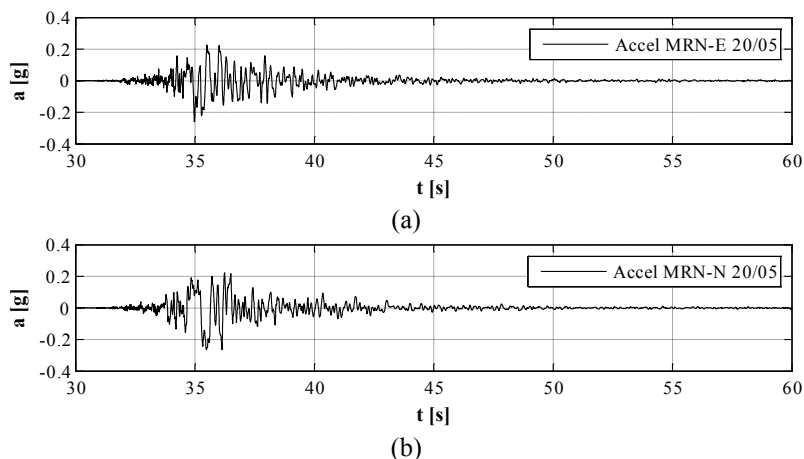


Figure 2.34 Accelerograms recorded in the station of Mirandola (Modena, Italy): (a) W-E component and (b) N-S component. The origin of the time is set at 20-05-2012 02:03:24 UTC

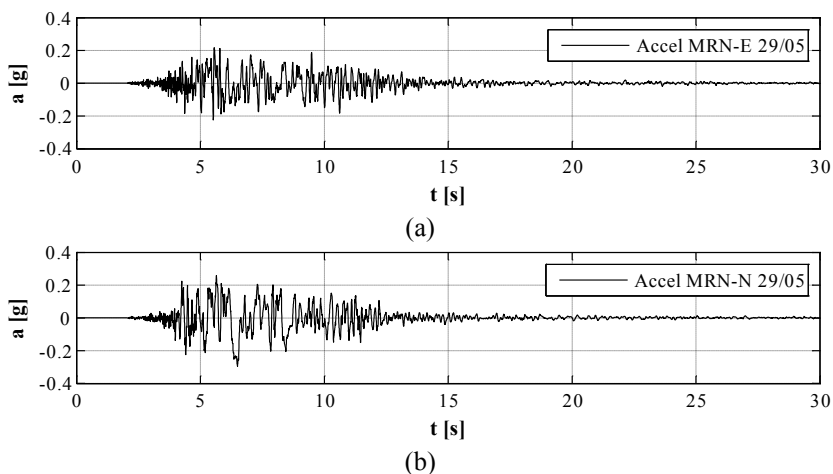


Figure 2.35 Accelerograms recorded in the station of Mirandola (Modena, Italy): (a) W-E component and (b) N-S component. The origin of the time is set at 29-05-2012 07:00:03 UTC

The spectral ordinates of the horizontal components of the two events are reported in Figure 2.36. It should be noted that the recorded accelerograms include seismic site effects; indeed, MRN station is placed on a “C” class soil site (shear wave velocity ranging from 180m/s to 360m/s), based on geological data, and T1 category according to EC8 (flat surface), as reported in the *Italian Accelerometric Archive* (Luzi et al., 2008).

In the assessment of the case study also the vertical component of the two earthquakes is considered, reported in terms of accelerograms and spectra in Figure 2.37 and in Figure 2.38.

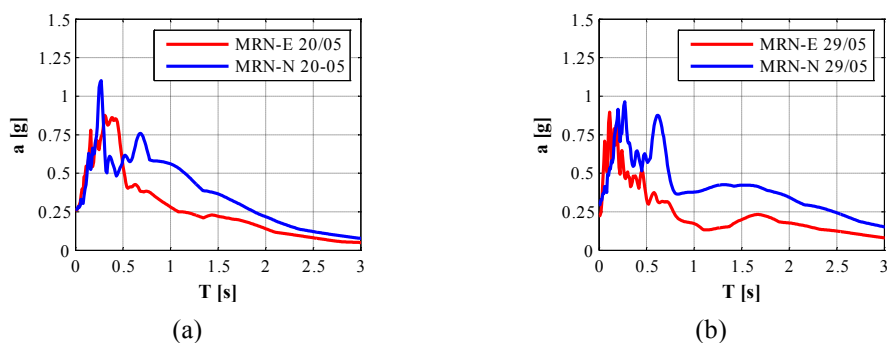


Figure 2.36 Elastic response spectra: (a) recorded on 20 May 2012 and (b) recorded on 29 May 2012 in Mirandola (Modena, Italy)

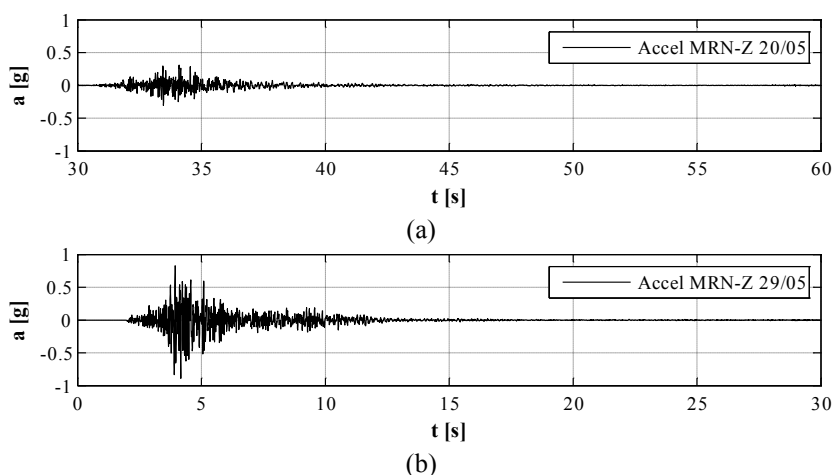


Figure 2.37 Vertical component of the accelerograms recorded in the station of Mirandola (Modena, Italy): (a) at 20-05-2012 02:03:24 UTC and (b) at 29-05-2012 07:00:03 UTC

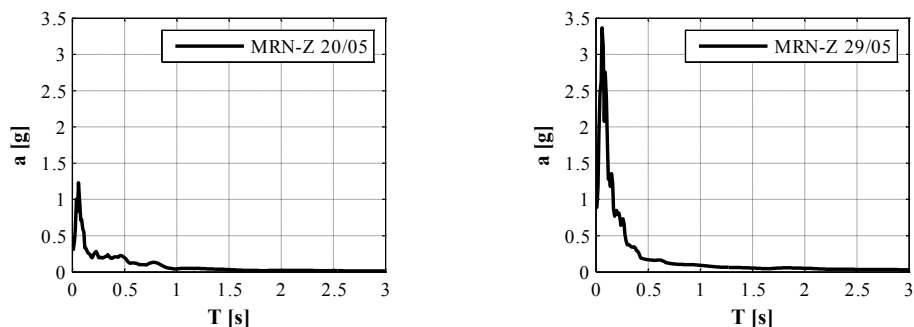


Figure 2.38 Elastic response spectra of the accelerograms vertical component: (a) recorded on 20th May 2012 and (b) recorded on 29th May 2012 in Mirandola

2.1.5.6 Results of dynamic analyses

In the following sections the results of the performed nonlinear analyses are described and discussed.

As described in the previous paragraph, the nonlinear behavior of the investigated one-story precast building is modeled with a lumped plasticity approach. A first conclusion on the seismic response of the considered case study can be drawn in terms of moment-rotation curves, recorded in the analyses with the three components of the 29th May event (Figure 2.39 and Figure 2.40). The results demonstrate that important inelastic rotations are experienced in the columns in the X direction after the second event (29th May 2012). For the sake of brevity, the moment-rotation envelope, recorded considering both the two events are not reported, since the results does not significantly change.

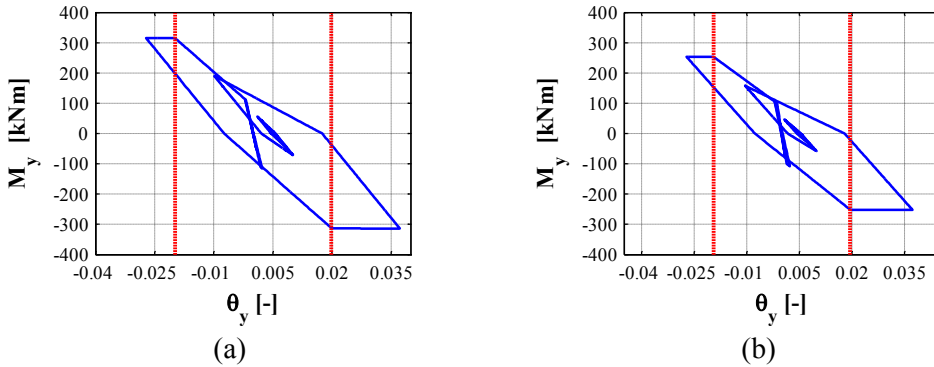


Figure 2.39 Moment-rotation envelope around the Y direction: (a) column A and (b) column B

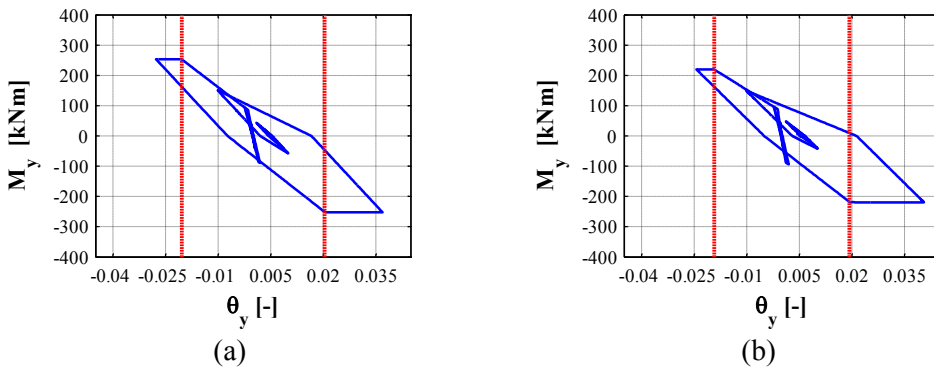


Figure 2.40 Moment-rotation envelope around the Y direction: (a) column C and (b) column D

With regards to the connection systems, a first assessment can be performed by comparing the frictional strength with the shear forces in the columns. In the following the evaluation of the frictional strength of the beam-to-column connections is reported. In order to evaluate the axial force (N) and the vertical stress (σ_v) in the connection, the following quantities are determined (Table 2.5):

- the area of the neoprene pad (A_n);
- the influencing area of the column (A_{inf});

The axial force (N) and the normal stress (σ_v) are then evaluated as:

$$N = A_{inf} \cdot w \quad (2.5)$$

$$\sigma_v = \frac{N}{A_n} \quad (2.6)$$

In this equation w is the seismic weight of the structure for unit area.

The maximum strength of the frictional connections can be evaluated according to the equation (2.7); where N is the axial force on the connection and μ is the neoprene-concrete friction coefficient.

$$R_{fr} = \mu \cdot N \quad (2.7)$$

The friction coefficient (μ) can be evaluated with the equations (2.8) and (2.9). The coefficients β and c are experimentally evaluated (Magliulo et al., 2011) and equal to 0.055 and 0.1, respectively.

$$\mu = 0.49 \quad \text{if } \sigma_v < 0.14 \text{ MPa} \quad (2.8)$$

$$\mu = c + \frac{\beta}{\sigma_v} \quad \text{if } 0.14 \leq \sigma_v \leq 5 \text{ MPa} \quad (2.9)$$

In Table 2.5 the frictional coefficient and the strength (R_{frict}) of the beam-to-column connections are reported.

Table 2.5 Parameters used in the evaluation of the frictional strength of the beam-to-column connections

Column [-]	A_{inf} [m ²]	A_n [m ²]	N [kN]	σ_v [MPa]	μ [-]	R_{frict} [kN]
A	200	0.092	306	3.33	0.12	35.7
B	100	0.115	153	1.33	0.14	21.6
C	100	0.092	306	3.33	0.12	35.7
D	50	0.115	153	1.33	0.14	21.6
E	50	0.115	153	1.33	0.14	21.6

Results with the horizontal components of 29th event

The first result is reported in terms of shear forces in the beam-to-column connections (Figure 2.41), evaluated as the columns forces in X direction. In this comparison the

shear forces in the columns A and B are divided by two since these columns support two beams in the X direction. Figure 2.41 shows the comparison of these forces with the frictional strength of the connections, S_{static} , reported in Table 2.5 as R_{frict} . Among the four typologies of columns, only for the corner columns (D) the shear forces overcome the frictional strength.

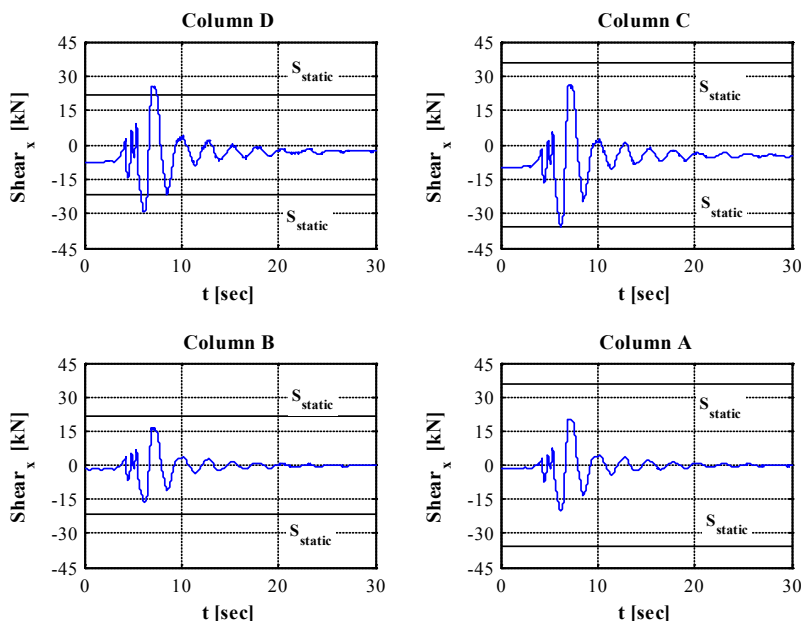


Figure 2.41 Shear forces in beam-to-column connections in X direction under the horizontal components of the 29th May event

The assessment of the beam-to-column connection behavior is also performed by investigating the frictional element response under the seismic excitations.

The frictional element envelopes are reported for some typical connections (Figure 2.42) of the structure in terms of deformation-force curve. The deformation of the element corresponds to the relative displacement between the beam and the column and the force is the shear force in the connection in X direction. The figure show that only the corner connections experience significant dislocation of the horizontal element from the column, confirming the results of the above used simplified approach, based on the shear forces of the columns.

The described results on the beam-to-column connections do not correspond to the recorded damages, since many beams in the structure showed significant relative displacements with respect to columns after the 29th event.

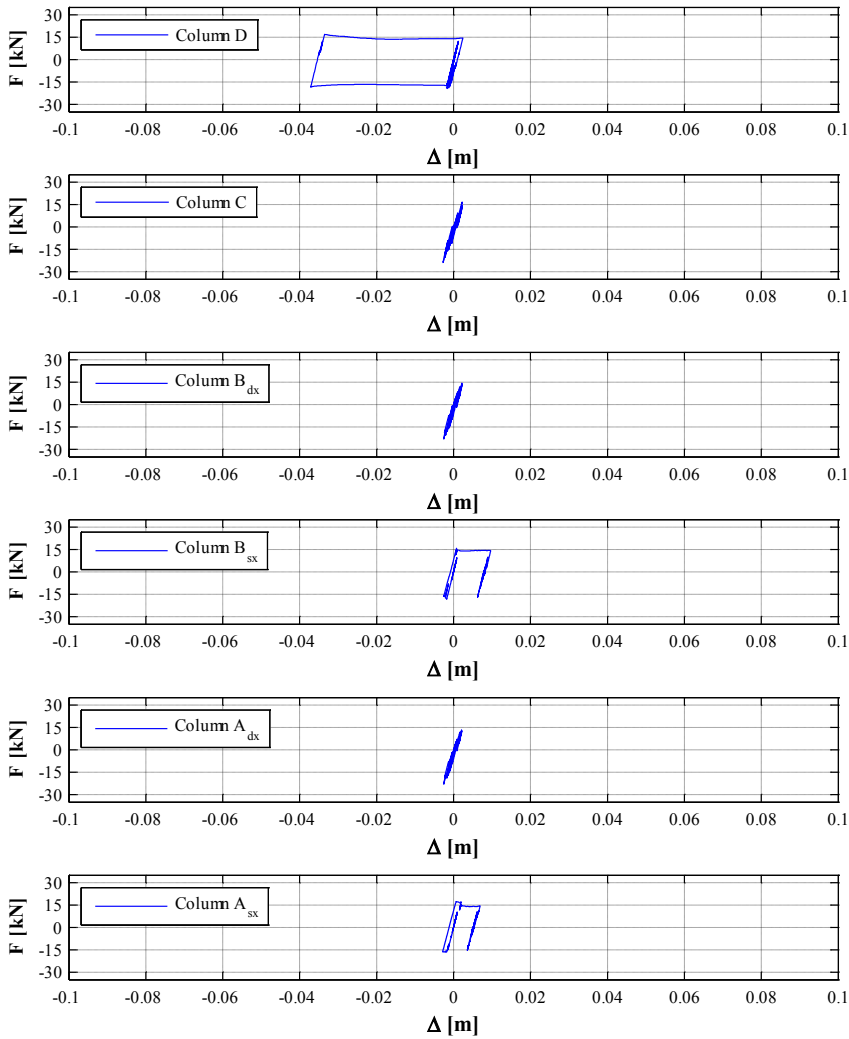


Figure 2.42 Force-deformation envelopes of the frictional elements (beam-to-column connections) for the representative columns of the structure under the horizontal components of the 29th earthquake

Cornering the behavior of the roof elements connections, Figure 2.43 shows the force-deformation envelopes of the central roof element for all the longitudinal Y bays in the 4th transversal bay. All the reported elements does not experience any relative displacements. Also these results do not correspond with the recorded damages: most of the roof elements had significant relative displacements with respect to the supporting beams and some of them lost the support, failing during the excitation.

In order to justify the damage the vertical component of the 29th earthquake is also considered in the nonlinear dynamic analysis on the same structural model. The results are reported in the following section.

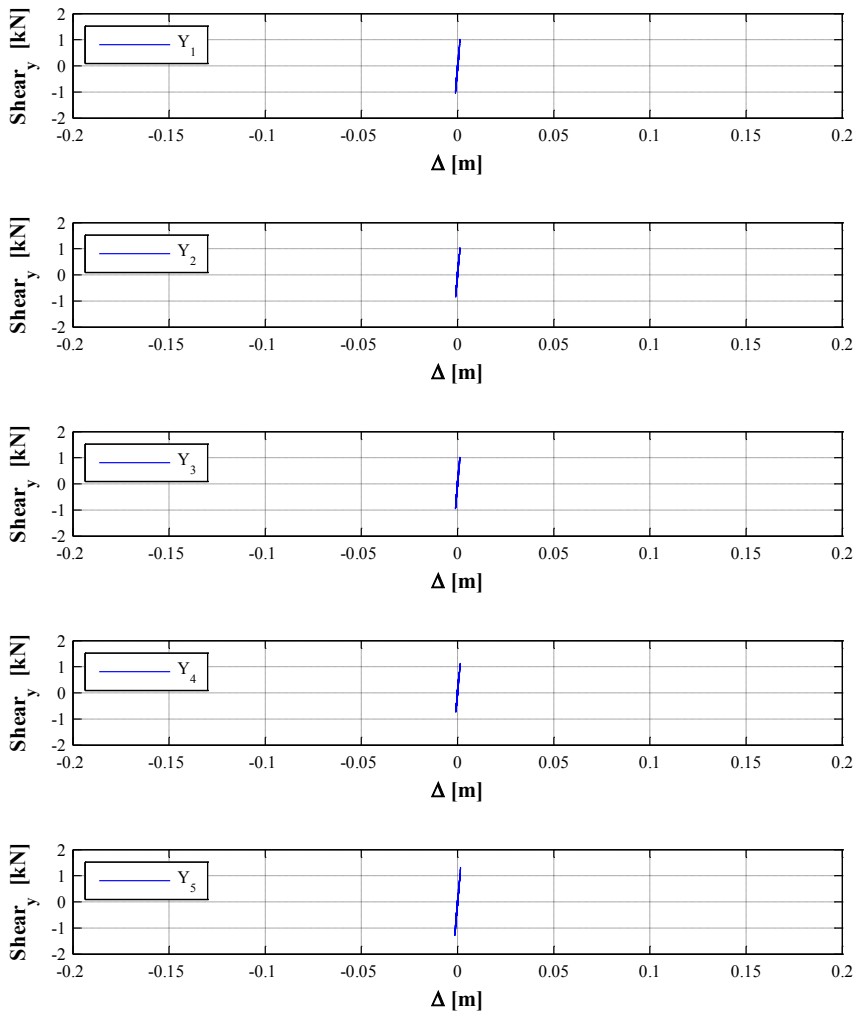


Figure 2.43 Force-deformation envelopes of the frictional elements (roof-to-beam connections) for the central roof element in the 4th transversal bay under the horizontal components of the 29th earthquake

Results with the three components of 29th event

Figure 2.44 and Figure 2.45 report the force-deformation envelopes of the frictional elements for the beam-to-column and the roof-to-beam connections, respectively. These results can justify the recorded damages in the connection systems: most of the beams and roof elements experiences important relative displacements.

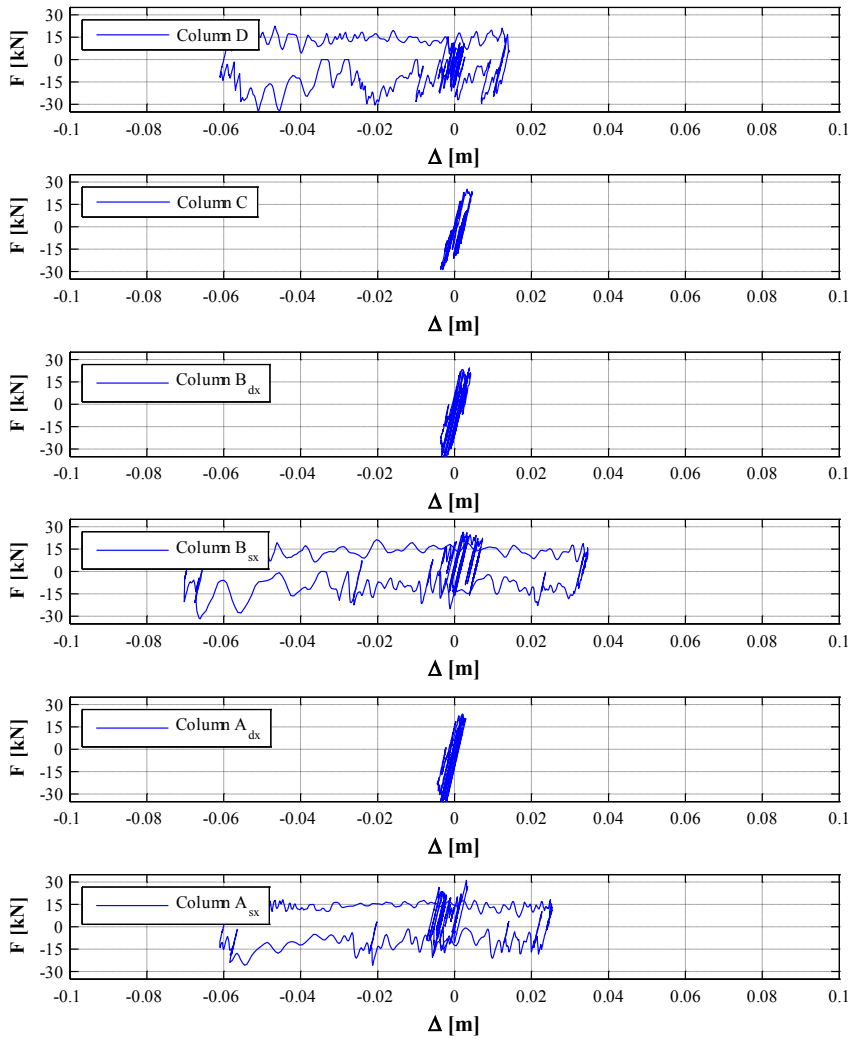


Figure 2.44 Force-deformation envelopes of the frictional elements (beam-to-column connections) for the representative columns of the structure under the three components of the 29th earthquake

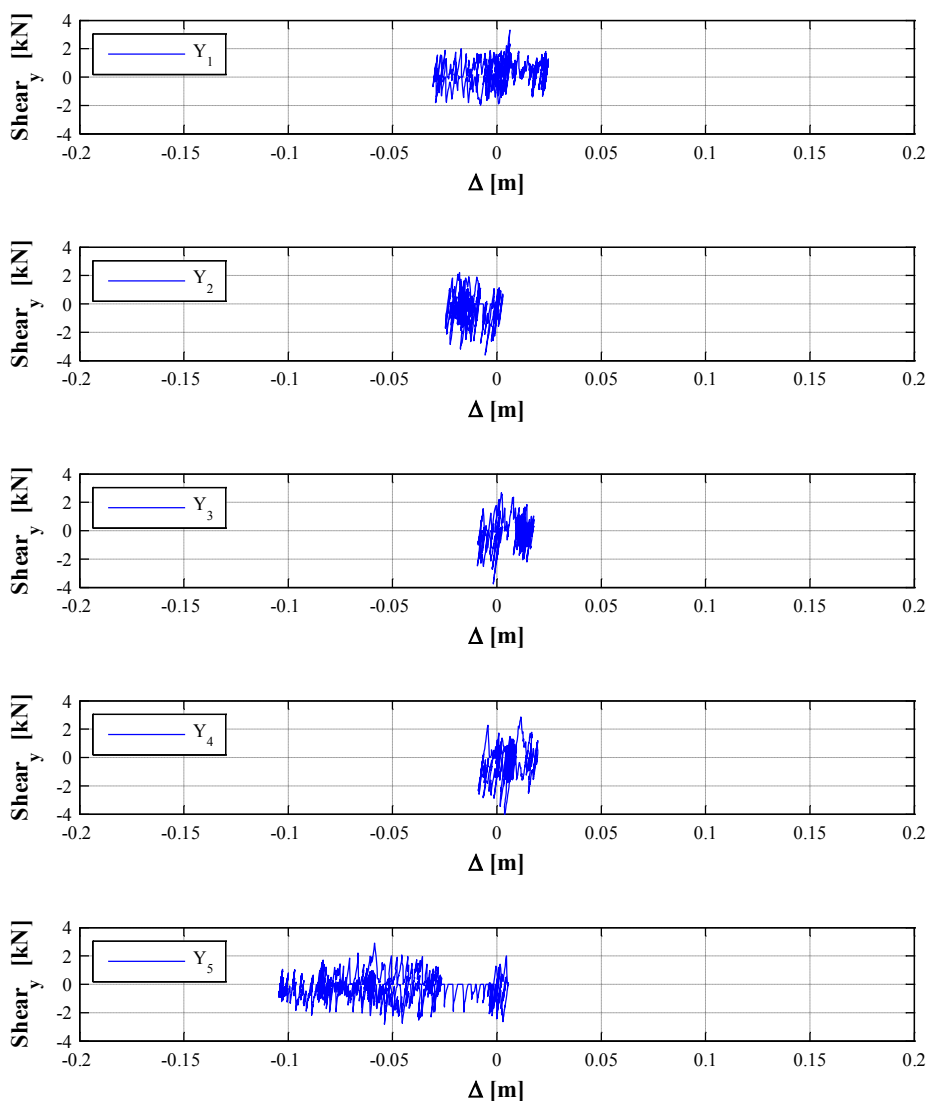


Figure 2.45 Force-deformation envelopes of the frictional elements (roof-to-beam connections) for the central roof element in the 4th transversal bay under the three components of the 29th earthquake

In the described evaluations the damages due to the first event on 20th May 2012 are not considered. However, in order to completely define the seismic behavior of the structure, the deformation of the frictional elements are also evaluated with the three components of this first earthquake. Figure 2.46 and Figure 2.47 report the friction element envelopes in the beam connections and in the most damaged roof connection, among the previously presented elements, respectively. According to this result: i) the beams do not fail due to the loss of the support since the sum of the displacement due

to the two events is smaller than the support width (23cm); whereas the collapse of some roof elements is justified since the sum of the displacements in the two analyses is larger or very close to the support width (13cm).

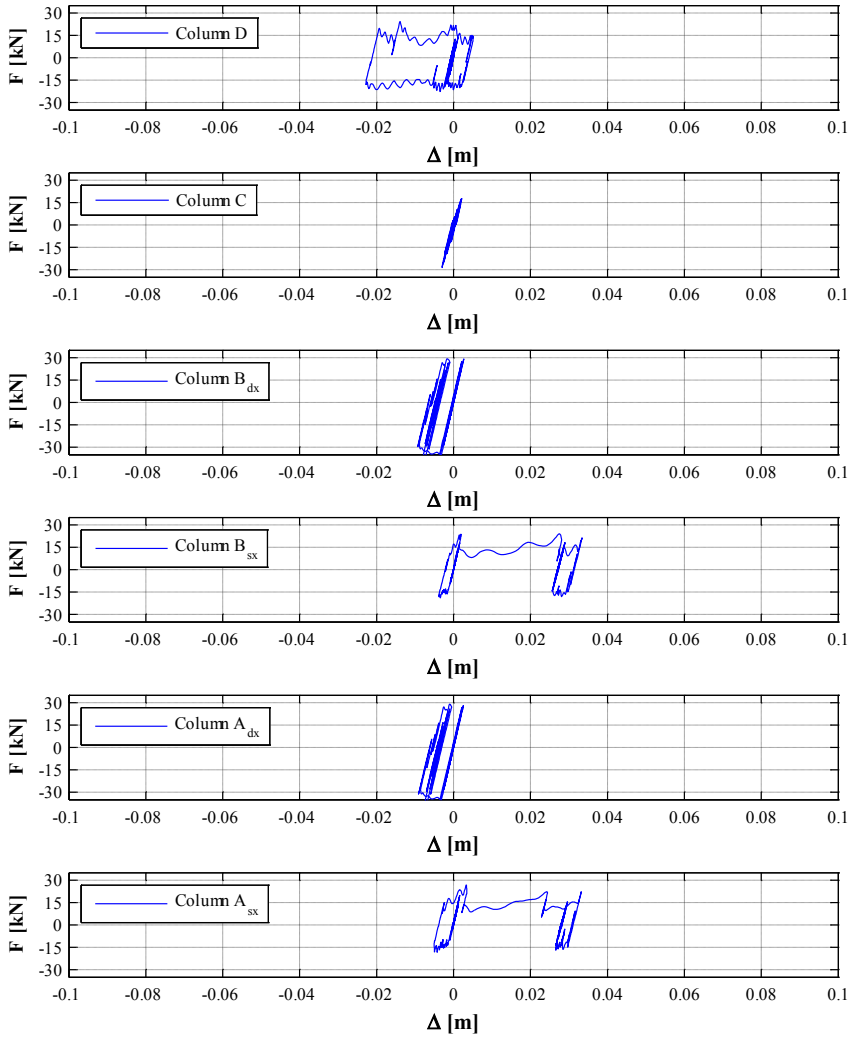


Figure 2.46 Force-deformation envelope of the frictional elements (beam-to-column connections) for the representative columns of the structure under the three components of the 20th earthquake

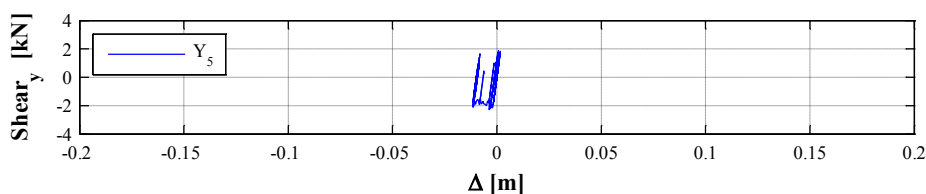


Figure 2.47 Force-deformation behavior of the most damaged roof-to-beam connection under the three components of the 20th earthquake

2.1.6 Conclusions

The 20th and 29th May Emilia earthquakes caused damage mainly to industrial precast structures with a huge economic loss, because of both the high percentage and the vulnerability of the precast buildings in the area. From the study of the precast structures, the review of the past code design provisions and the recorded structural damage, the following conclusions can be drawn.

- A direct inspection of the industrial zones shows that at least half of the industrial precast structures exhibits significant damage and a large number of people suffered death, injury and loss of property. If the first main shock had occurred during the workday, the overall balance would have been even more disastrous.
- The damage to precast structures were caused mainly by inadequate connection systems: the main recorded failures are the loss of support of structural horizontal elements due to the sliding of friction connections and the collapse of the cladding panels due to the failure of the panel-to-structure connections.

The damage can be explained by two main reasons: (a) the rarity of the event and (b) the exclusion of the epicentral region from the code-recognized seismic areas, which implied that friction connections were acceptable up to 2003.

The poor performance exhibited by the precast structures with friction connections reinforces the belief that connections relying on gravity-only load paths are not acceptable in seismic areas.

- Based on simple considerations on the recorded spectra, it is confirmed that precast structures providing neoprene-concrete friction connections should be expected to suffer from loss of support of their horizontal elements under the recorded seismic excitation.
- The vulnerability of friction beam-to-column connections is also due to the high friction coefficient ($c = 0.35$) suggested by past Italian codes for the evaluation of the friction strength. If experimental values (Magliulo et al.,

2011) had been taken into account ($c = 0.13 - 0.09$), the use of friction connections would have been limited.

The seismic behavior of an existing one-story precast industrial building is also investigated. The considered structure is located in the epicentral area of the Emilia earthquakes. According to the results of nonlinear dynamic analyses, the following conclusions can be drawn.

- A direct inspection after the 29th May event showed that the most serious damages hit the columns and the connections in the structure: high rotations and yielding at the base of the vertical structural elements were recorded and significant dislocations of the horizontal elements were also experienced.
- The defined frictional element is able to simulate the behavior of the beam-to-column connections and the roof-to-beam connections under horizontal actions.
- The nonlinear dynamic analyses have demonstrated the structural damages in the columns.
- The vertical component of the 29th May earthquake can justify the damages in the connection systems, i.e. the relative displacements and the cases of failure due to the loss of support phenomena.

2.2 Guidelines on local and global retrofitting systems of precast structures

The exhibited vulnerability of the industrial buildings during the Emilia earthquakes (2012) makes the seismic safety of this building typology a key issue. Hence, in the last years several scientific projects have been developed in order to improve the knowledge on the seismic response of RC precast structures. The interest is also demonstrated by the redaction of two important documents for the emergency management after an earthquake event and related to the seismic vulnerability of the precast structural system.

In this Section the “Guidelines on local and global retrofitting systems of precast structures” (Gruppo di Lavoro Agibilità Sismica dei Capannoni Industriali, 2012) are presented. This document was edited under the supervision of the Italian Department of Civil Protection and with the collaboration of other institutions, among which the ReLUIS consortium.

The presented document arose from the request of experts and the specialists, who operated in the struck area in Emilia region. It gives the most advanced knowledge on structural seismic safety and indicates the operational process in order to obtain the seismic usability¹, according to the actual Italian buildings codes (D. M. 14/01/2008, 2008; Circolare 02/02/2009 n. 617, 2009) and to the specifically issued law (Legge 01/08/2012 n. 122, 2012). The document gives also important recommendations on the retrofitting of the structures. In the following the summary of the document contents is reported in order to describe the general approach and the main indications.

2.2.1 Contents and purposes of the document

The two earthquakes in Emilia region on May 2012 hit an area with a high percentage of precast industrial buildings. Most of these structures were characterized by important structural deficiencies, as extensively described and justified in the previous section. As a consequence of above, the widespread damages make the emergency management difficult, because of the high number of structures to repair and the limited period of time available for the retrofitting actions.

In order to manage such a difficulty, the decree (Decreto-Legge n. 74 del 6 giugno 2012, 2012) and its law (Legge 01/08/2012 n. 122, 2012), give to the professional community a guide in the design of the actions. Concerning the investigated precast buildings, the law establishes some specific conditions, identifying these buildings as a peculiar structural typology. At this aim, the paragraph 8 of Article 3 of the law

¹ The seismic usability concept will be clearly defined in the following Section on the GL-AeDES: form for usability judgment of precast structures.

provides a summary of the main deficiencies of industrial buildings. From a technical point of view, the process, outlined by the reference law, requires a coordinated procedure, consisting of two phases:

- A the removal of the most significant structural deficiencies, in the following reported as first phase;
- B extensive and systematic actions in order to achieve the required seismic performance (Paragraph 10 of Article.3), in the following reported as second phase.

The document consists of four Chapters, that are briefly described in the following Sections:

- 1) report of the recorded damages in the precast structures after the Emilia earthquakes;
- 2) description of the widespread structural typologies of industrial buildings, not designed for seismic actions;
- 3) requirements and systems in order to obtain the seismic usability and the seismic safety;
- 4) technical forms for the design and the verification of the suggested retrofitting systems.

The first two Sections of the document describe the main characteristics and damages of precast industrial buildings. Both the topics are reported in details in the previous section of this thesis; hence, in the following a brief summary is reported.

A complete description is given for the requirements and systems, suggested by the document in order to obtain the immediate seismic usability and the seismic safety of the structure.

2.2.2 Existing precast buildings: typologies and recorded damages

Precast structures are widely used in Italy for industrial and commercial use since the second half of the XX century, causing the development of big industrial centers, consisting of buildings or complexes of buildings, with different construction age. Despite the expected high variability, it is possible to identify some common deficiencies, highlighted during the last severe earthquakes, such as L'Aquila earthquake and the two earthquakes in Emilia Romagna region. During these events, the connections represented the crucial elements in the seismic performance of both old and new buildings, causing the most of the serious and disastrous collapses.

The most common deficiency in the connection systems is the absence of mechanical devices between structural elements. In these cases, the transfer of the horizontal forces relies only upon the frictional strength between the contact surfaces. The use of similar

connections is justified by both the evolution of the seismic zonation in Italy and the past building codes provision, as extensively described in Section 2.1.

Another important source of vulnerability is related to the cladding system of precast buildings, consisting of precast RC panels, connected to the horizontal or to the vertical structural elements by means of different kinds of metallic systems. The collapse of these nonstructural element is caused by the failure of the connections and not by inadequate design and/or construction of the panels themselves. Hence, in the design of precast buildings the structural analysis under horizontal actions is performed on a frame model, consisting of columns, beams and roof elements. The external panels are taken into account only in terms of mass, neglecting their contribution to the lateral stiffness of the structure. However, under dynamic actions the cladding panels can interact with the structure, influencing the global seismic response, which does not behave as a flexible frame, but as a stiffer braced system. The resulting forces in the connection are much higher than the design ones and also differently oriented, causing the collapse of the connection system and so the failure of the panel.

Another deficiency is related to the storage rack, typically enclosed in the industrial buildings. These systems collapsed or caused damages to the structures due to the absence of any bracing systems or due to the their heavy contents.

Other noteworthy deficiencies are related to the vertical resisting elements (columns) and to their foundation systems. The precast columns and the foundation systems, (usually isolated socket foundations) exhibited some deficiencies in terms of flexural or shear strength and ductility due to the obsolete or no seismic based design approach.

2.2.3 *Retrofitting principles and criteria*

In this Section the main provisions of the document are reported for both the phases identified in the reference law (Legge 01/08/2012 n. 122, 2012).

2.2.3.1 Immediate seismic usability of the structure

The quick emergency actions (first phase) can be executed only when the damage on the main structural elements is absent or very low. In order to obtain the positive usability judgment, the following deficiencies must adequately be resolved:

- lack of connections between structural elements;
- infill precast elements not properly anchored to the main structure;
- not braced storage rack, loaded with heavy materials, that can involve in their collapse the main structure.

The most of the precast industrial structures consist of one-story buildings with slender columns, connected with socket foundations at the base, and with simply supported beams at the top. For this typology, the seismic action can be simply evaluated considering a scheme consisting of cantilever columns, connected with pendulums

(beams) and with the mass concentrated at the top. The structure can be modeled as a single degree of freedom system (Figure 2.48), characterized by a stiffness (k_{Tot}) equal to the sum of the columns stiffness (k_i), as reported in the equation (2.10), and by a mass (m_i) equal to the total structural seismic mass. In (2.10) L is the column height, I is the inertia of the column concrete section and E is the Young elasticity modulus of the concrete.

$$k_i = 3 \cdot \frac{EI}{L^3} \quad (2.10)$$

According to these assumptions, the period of the structure is known and the total seismic force can be evaluated as:

$$F_{Tot} = W_{Tot} \cdot \frac{S_a(T_1)}{g} \quad (2.11)$$

In (2.11) the spectral acceleration (S_a) can be calculated from the design spectra of the considered site with a low value of the behavior factor ($q=1.5$), given the low expected ductile response of the investigate structural system.

The evaluated force can be used to evaluate the forces in the columns and in the connections between the beams and the columns, according to the influencing area or to the stiffness of the vertical elements if the rigid diaphragm hypothesis is ensured or not, respectively.

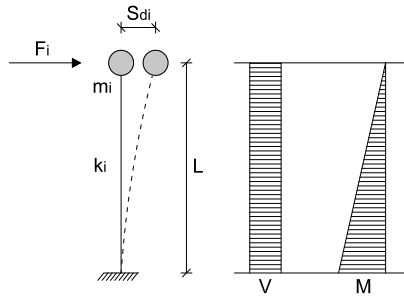


Figure 2.48 Single degree of freedom scheme

2.2.3.2 Retrofitting system for the seismic safety of one-story precast structure

The seismic retrofitting of the structures (second phase) requires the assessment of the structural seismic safety, according to the building code in force, and the actions to obtain a fixed performance level.

The law provides different options for the assessment of the structure:

- i) if the spectral acceleration experienced by the construction during the ground motion exceeded the 70% of the elastic spectral acceleration, indicated by the code for a new building with similar characteristics and on the same soil type, the structure is safe;

- ii) if the spectral acceleration was lower than the 70% of the above described spectral acceleration, the seismic assessment (Chapter 8.3 of NTC 2008) is needed within 6 months from the decree (Decreto-Legge n. 74 del 6 giugno 2012, 2012);
- iii) if the seismic safety level is lower than the 60% of the required level in a new building, the seismic retrofitting is needed (from 4 to 8 years from the seismic assessment).

An application of these criteria is reported for the structures near to the epicenter of the first main shock on 20th May 2012, i.e. Mirandola (MO): Figure 2.49 shows the elastic spectrum on soil C for Mirandola (D. M. 14/01/2008, 2008). In this diagram the gray area represents the typical period range of precast one-story structures (Magliulo et al., 2014b) and the two reported values are the limit spectral values for the considered range. Figure 2.50 shows the shaking map of the first event in Emilia region (INGV, 2012) in terms of 1 second pseudo-acceleration (in g), in which the rows indicate the Mirandola location. According to these two data, many industrial buildings may satisfy the requirement i) of the decree.

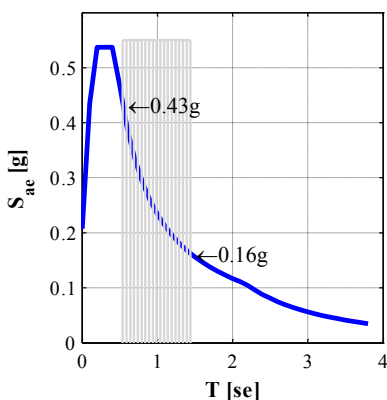


Figure 2.49 Elastic response spectrum of Mirandola (MO) – Soil type C

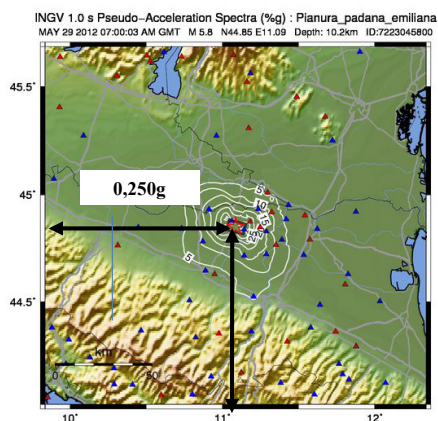


Figure 2.50 1 second pseudo-acceleration (%g) - Mirandola (20th May 2012)

2.2.4 Outline of the retrofitting systems

This section describes the proposed retrofitting systems for both the phases, reporting the document approach for each damage or structural lack. For each kind of damage or lack the document describes:

- the deficiencies and how they can be discovered during a survey;
- the required performance;
- the proposed retrofitting systems.

2.2.4.1 Actions to prevent the loss of support of the horizontal elements

Deficiencies and inspection

- A Simple support with no mechanical devices. This evidence can be revealed by a visual survey, a check of the available drawings and a visual survey of the relative displacements between the beam and the column or between the roof element and the beam.
- B Inadequate shear strength of the connection with metallic systems, revealed by a visual inspection and/or a check of the available drawings. The demand can be simply evaluated as $a_g \cdot S / g \cdot N$, where N is the vertical load on the connection, a_g is the peak ground acceleration and S is the soil coefficient.
- C Inadequate shear strength of the column forks, revealed by a visual inspection and/or the examination of the available drawings. The demand can be simply evaluated as $a_g \cdot S / g \cdot N$, where N is the vertical load, a_g is the peak ground acceleration and S is the soil coefficient.
- D Inadequate shear strength of the precast beam, demonstrated by shear cracks and/or examination of the available drawings. The demand can be simply evaluated as $\left(1 + 2.5 \cdot \frac{a_{gv}}{g}\right) \cdot N$, where N is the vertical load on the column, a_g is the peak ground acceleration and S is the soil coefficient.
- E Inadequate shear strength of the cast in situ beam, demonstrated by shear cracks and/or by the examination of the available design drawings. The demand can be simply evaluated as $\left(1 + 2.5 \cdot \frac{a_{gv}}{g}\right) \cdot N$, where N is the vertical load on the column and a_g is the peak ground acceleration.
- F Inadequate flexural strength of the beam, demonstrated by flexural cracks and/or by the examination of the available design. The demand can be simply evaluated as $\left(1 + 2.5 \cdot \frac{a_{gv}}{g}\right) \cdot N \cdot L / 2$, where N is the vertical load on the column, L is the length of the beam, N is the vertical load on the beam and a_g is the peak ground acceleration.
- G Inadequate shear strength of the cast in situ roof, revealed by a visual inspection of cracks. If the damage is present, the demand can be simply evaluated as

$\left(1 + 2.5 \cdot \frac{a_{gv}}{g}\right) \cdot N$, where N is the vertical load on the connection and a_g is the peak ground acceleration.

Requirements of the connection system

The retrofitting actions should guarantee the following requirements:

- do not allow the loss of support of the horizontal element;
- do not change the existing static scheme;
- to prevent the torsional rotation of the elements;
- to prevent or limit the relative displacements between the elements;
- do not interfere with the elements reinforcement (high concrete cover).

Retrofitting systems

- 1 Increase of the beam base on the column.

The loss of support collapse should be prevented by increasing the base of the beam, not modifying the initial resistant scheme. This action provides the difficult estimation of the relative horizontal displacement under seismic actions, with a particular attention to the vertical component of the earthquake. This system should be integrated by properly designed restraints.

- 2 New mechanical devices between the two elements.

New elements and devices (Figure 2.51) can be used in order to ensure the beam-to-column connection, as bolted metallic plates or connecting cables. Concerning the roof-to-beam connection, an example is the use of metallic devices between the TT elements and the beams (Figure 2.52). For these systems some crucial aspects are to be taken into account, as the possible interference with the existing reinforcement in the connected elements and the strength of the fork in which the beam is usually inserted.

- 3 Reducing the load.

It is possible to provide some actions in order to reduce the permanent loads on the roof.

- 4 Dissipating system.

It is also possible to use dissipative devices in order to reduce the forces and the damages due to the seismic action in the columns and in the beams.

5 Connection of the columns at the top.

The relative displacements between two columns can be reduced through their connection with metallic profiles or metallic plates. This system does not prevent either the loss of the support of the horizontal elements due to the inertia force related to their masses or their overturning. For this reason, this system should be integrated with other devices between the elements.

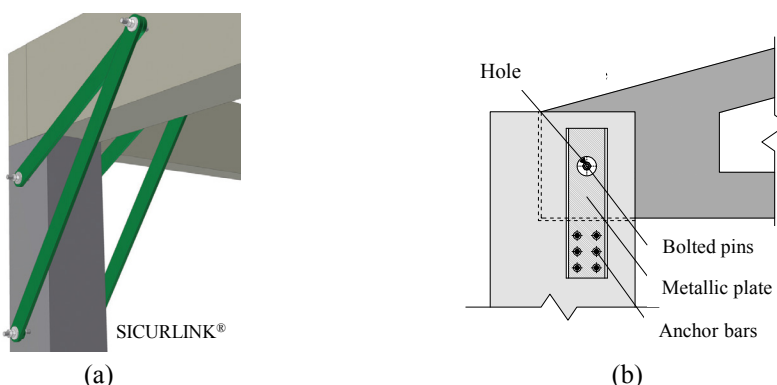


Figure 2.51 Retrofitting solution for beam-to-column connections

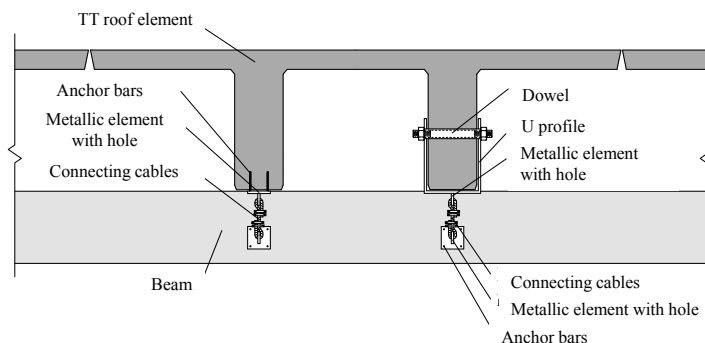


Figure 2.52 Retrofitting solution for roof-to-beam connections

2.2.4.2 Actions to prevent the collapse of the cladding panels

Deficiencies and inspection

- A Inadequate strength of the connection to prevent the out of plane collapse of the panel, assessed by a visual inspection and/or examination of the available design drawings.
- B Inadequate shear strength of the connection with respect to the demand due to the panel-to-structure interaction in the plane of the panel, assessed by a close visual inspection and/or examination of the available design drawings.

- C Inadequate flexural strength of the panel: in presence of damage it is possible to assess the geometry and the existing reinforcement.
- D Inadequate flexural strength of the masonry panels: if the damage is observed, a survey of the geometry (in particular, the ratio between height and width) and of the possible presence of reinforcing elements is required.
- E Not suitable arrangement of openings, revealed by a visual inspection of the actual shear length of the columns.

Requirements of the connection system

The retrofitting systems should guarantee the following requirements:

- to avoid the overturning of the panels;
- to allow the relative displacement between the panel and the structures in order to reduce or remove the interaction under seismic actions.

Systems

- 1 Systems to prevent the overturning failure.
In the case of horizontal panels, their overturning can be prevented through the use of steel angles bolted to the panel and to the columns and cables, fixed in the elements edges. In the case of vertical panels, the overturning can be prevented through the use of metallic devices and cables fixed to the beam and to the two upper panel edges (Figure 2.53).
- 2 Increase of the panel flexural strength.
Use of external devices and integrative elements both in the case of concrete and masonry panels.
- 3 Check of the openings arrangement.
It can be possible to remove the openings that could cause the shear failure in the columns.

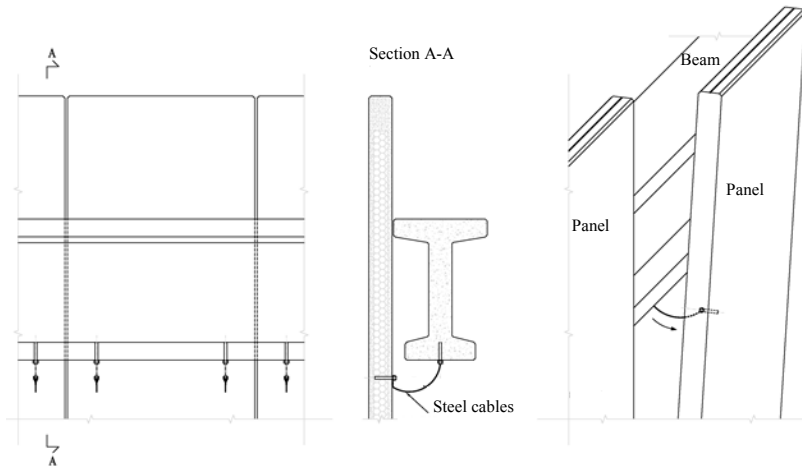


Figure 2.53 System to prevent the overturning of the cladding panels

2.2.4.3 Actions on the foundation systems

Deficiencies and inspection

- A Possible rotation of the socket foundation. If the damage is observed the ratio demand/capacity must be evaluated.
- B Insufficient flexural strength of the socket foundation.
- C Insufficient or absent foundation connections.

Requirements of the connection system

The retrofitting systems should guarantee the following requirements:

- to increase the rotational stiffness in order to ensure the connection at the base of the columns;
- to increase the strength to the lateral forces, according to a capacity design approach.

Systems

- 1 Connection of the foundation with the industrial floor (Figure 2.54).
Since the industrial buildings often provide an industrial floor with a minimum thickness of 15-20 cm, the floor can be usefully connected the isolated socket foundation in order to limit the relative displacements at the base of the columns.

- 2 Strengthening of the surrounding soil at the foundation level.
By the injection of cement mixtures at low pressure it is possible to increase the rotational stiffness and to improve the shear strength.
- 3 Strengthening of the connection between the socket foundation.
- 4 Strengthening of the walls of the socket foundation.
- 5 Strengthening of the connections between the isolated systems.

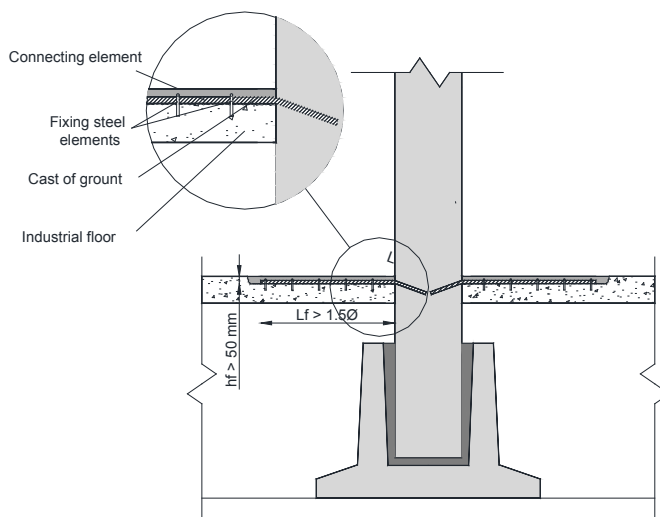


Figure 2.54 Connection between the industrial floor and the column

2.2.4.4 Actions on the vertical structural elements

Deficiencies and inspection

- A Insufficient flexural strength at the base, revealed by a visual inspection and/or an examination of the available design drawings.
- B Insufficient shear strength, due also to the arrangement of the openings and the infill panels.

Requirements of the connection system

The retrofitting actions should guarantee the following requirements:

- to increase the stiffness;
- to increase the strength;
- to increase the ductility.

Systems

1 Increase of column section.

This retrofitting technique provides an increase of the RC cross section. This measure allows to increase the shear strength, the flexural strength (by means of additional longitudinal and transversal reinforcement) and the stiffness (by the increase of the section of the column) of the element. The use of transverse reinforcement also increases the ductility of the element. This action can be used only for some sides of the perimeter columns due to the presence of the masonry infills or the cladding panels.

2 Fibre reinforcement.

A possible retrofitting technique with fibres is the use of high performance fibre-reinforced concrete (HPFRC). It is a material with high compressive strength, self-levelling, and which does not need further traditional rebars. Also other kinds of fibres can be used.

3 Jacketing.

Strengthening of the columns with steel reinforcement rebars and stirrups bolted to the structural element and connected to the foundation system.

2.2.4.5 Actions on storage rack

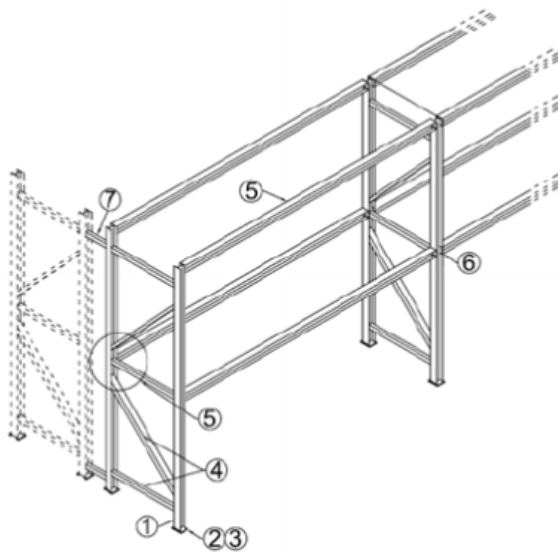
Deficiencies and inspection

- A The rotation of the element is greater than 1/100 of its height.
- B The loading units are rotated or shifted.
- C The element presents damages in the characteristic points, shown schematically in Figure 2.55.

Requirements of the connection system

The retrofitting systems should guarantee the following requirements:

- to remove any connections between the racks and the main structure, unless the connection is verified and the structure is safe under the transmitted forces;
- to realize flexible connection with the structure;
- to reinforce all the levels with system and devices in order to support the load and to prevent the contents fall.



Point	Description
1	Uprights
2	Base plate
3	Dowels
4	Bracing
5	Stringers
6	Connection between stringers and uprights
7	Spacer

Figure 2.55 Characteristic points for storage racks seismic safety

2.2.5 Conclusions

The high vulnerability of precast one-story structures was highlighted by several collapses after the Emilia earthquakes (May 2012). The topic is very significant for both the protection of human life and the social and economic impact. Legge 01/08/2012 n. 122 (2012), related to the earthquake emergency in Emilia region, outlines the regulatory framework for the retrofitting of the existing structures. It tries to accomplish both the need to protect the human life and the need to reduce the economic and social impact, especially considering the loss related to the downtime. According to the requirements of this decree and according to the most recent scientific results, the described document was developed in order to guide the professional engineers in the retrofitting actions on precast industrial buildings.

The document indications allow to find the crucial deficiencies and the best actions in order to obtain the seismic safety and a given performance level, according to the design code in force.

2.3 GL-AeDES: form for usability judgment of precast structures

The form of usability judgment of precast buildings, in the following GL-AeDES, is an emergency document, aimed at the detection of the main characteristics and damages of industrial buildings after a seismic event. The main purpose of this form is the usability judgment of the investigated structure. The GL-AeDES form is based on the already gained experience of the AeDES (Agibilità e Danno nell’Emergenza Sismica) form (Department of Civil Protection, 2008), used for the survey of the damage and for the usability judgment on RC and masonry buildings during the post-earthquake phase. The described form can be used for high-span buildings, among which the precast, masonry, steel and wood structures, that accommodate industries, shopping centers and parking. The form allows to make a speed survey, which includes geometrical, typological and design characteristics as well as the information on the damages. The established configuration optimizes the different structural and damage parameters in order to provide the most efficient path from the survey to the final decision (related to the usability or to the economic evaluation of the damage), avoiding the collection of useless data.

2.3.1 *The form of usability judgment*




As in the ordinary AeDES form, the typological classification of the different structural components is based on a behavioral approach rather than on a descriptive one. The descriptive approach generally allows to obtain an objective picture of the building characteristics, with no personal judgment and interpretation of the surveyor. This kind of approach has the obvious limitation to describe and catalog numerous and useless typological varieties of the same structural element. On the contrary, the behavioral approach provides a classification on the base of an interpretation of the behavior, involving the judgment of the surveyor. This type of approach leads to a good reliability of the data, provided that the decision requested to the operator is properly guided.

A correct use of the form depends on the surveyor knowledge about the seismic behavior of the different structural and nonstructural components, since he should be able to autonomously associate the typology to the behavior. The judgment on the single structural element, associated with the judgment of the damage, leads to build an overall assessment of the vulnerability of the building, arriving to a well-defined judgment of usability.

The form consists of nine sections that describe the general organization of the structures complex (Section 0) and of the single building (Section 1), the geometrical characteristics of the whole structure (Section 2), the detailed features of structural and nonstructural components (Section 3), the damage description (Section 4-5-6-7), and

the final usability judgment (Section 8-9). In order to simplify the interpretation and the compiling of the form, some general rules are defined (Table 2.6). Moreover, different color are used for the table background: in addition to the white background, two gray levels are used, corresponding to a higher vulnerability to the seismic actions.

Table 2.6 Compiling rules for the GL-AeDES form

Element	Compiling rule
	Capital letters in the space of the line.
	<ol style="list-style-type: none"> 1) Text: alphanumeric characters must be written in capital letters in the spaces from the left side. 2) Numbers: characters must be written in the spaces from the right side.
	The presence of these round boxes in the lists and in the rows of the form tables indicates the possibility of indicating only one option among those referred to.
	The presence of these square boxes in the lists and the rows of the form tables indicates the possibility to specify more options to those listed.

2.3.2 Identification of the building complex (Section 0)

The preliminary identification of the complex is an essential step in order to individuate the single structure to judge. The structural aggregate is defined as a complex of one or more added or integrated structures, that have to be investigate with a single form.

The result of this first step is reported in the Section 0 of the GL-AeDES form (Figure 2.56), composed of two main parts: the first one allows to univocally identify the complex, reporting different numerical codes related to national regions and municipalities; the latter reports a blank space, titled “map of the structural complex with the numerical identification of the buildings”, where the surveyor applies the reference map, given by the administration (in the following reference map), that describes the investigated structural complex. On this reference map several important information are reported and other ones have to be integrated by the surveyor:

- all the buildings in the area (black rectangles in Figure 2.56) with the corresponding labels;
- the investigated complex (red rectangles in Figure 2.56), divided by the surveyor in the constituting buildings with the corresponding labels;
- the modifications of the reported structures, defined by the surveyor changing the last two digits of the corresponding label: it is changed with a number from 1 to 50 if the aggregates is a unique aggregate on the map but it is composed by two different aggregates (blue rectangles in Figure 2.56);

- the new aggregated, not reported on the map and recognized by the surveyor assigning to it a number from 51 (green rectangles in Figure 2.56);
- the presence of significant functional elements and/or plant system (e.g. pipelines), for example if the inspection is carried out on an entire industrial complex;
- the removal of aggregates that are not in the reference map even if they are indicated on the reference map (gray rectangles in Figure 2.56).
- the position of the two points (Point 1 and Point 2 in Figure 2.56), used to identify the position of the single investigated structure.

SEZIONE 0 - IDENTIFICAZIONE AGGREGATO STRUTTURALE			
Provincia: _____		Identificativo sopralluogo	
Comune: _____		Squadra _____ Scheda n. _____ Data _____	
Frazione/Località: _____ (denominazione Istat)		IDENTIFICATIVO AGGREGATO STRUTTURALE	
		Istat Reg. _____ Istat Prov. _____ Istat Comune _____	
		N° aggregato _____	
		N° edif. componenti l'aggregato _____	
Strade delimitanti l'aggregato (Via, Corso, Vicolo, Piazza):		Cod. di Località Istat _____	
1 <input type="checkbox"/> _____		Sez. di censimento Istat _____	
2 <input type="checkbox"/> _____		Tipo di carta _____	
3 <input type="checkbox"/> _____		N° carta _____	
4 <input type="checkbox"/> _____		Dati Catastali:	
5 <input type="checkbox"/> altro _____ (Indicare: Contrada, Località, Traversa, Salta, etc.)		Foglio _____ Allegato _____	
		Foglio _____ Allegato _____	
Coordinate (punti contrapposti delimitanti l'aggregato) <input type="radio"/> piano UTM (metri) <input type="radio"/> geografiche (gradi) <input type="radio"/> altro _____			
Fuso (32-33-34) _____	Datum <input type="radio"/> ED50 <input type="radio"/> WGS84	Punto 1: Lat./Nord _____ Long./Est _____	
		Punto 2: Lat./Nord _____ Long./Est _____	
Denominazione _____			
Mappa dell'aggregato strutturale con identificazione numerica degli edifici (evidenziare eventuali collegamenti con altri aggregati mediante significativi elementi funzionali e/o impiantistici)			
<p>The map shows a structural complex on a grid. It includes several buildings: Building 01 (pink), Building 02 (pink), Building 03 (pink), and a New aggregate (green). There are also Pipelines (green lines), a Footpath (black line), and a Conveyor belt (green line). Point 1 and Point 2 are marked with red dots. Aggregates to be divided are shown in blue, and No existing aggregates are shown in gray. Numerical identifiers are provided for each building and aggregate: 08-036-022-00001-00 for Building 01, 08-036-022-00002-00 for Building 02, 08-036-022-00003-01 for Building 03, 08-036-022-00003-02 for Building 03, 08-036-022-00005-00 for the New aggregate, and 08-036-022-00006-00 for the Footpath.</p>			

Figure 2.56 Section 0 of GL-AeDES: identification of the structural complex

2.3.3 General characteristics of the single structure (Section 1)

Once the structural aggregate is identified on the reference map, the survey continues with the identification of the single building. For each aggregate form (Section 0) the number of forms for a single building is equal to the numbers of structures that make up the aggregate itself. The structure is defined as a building, usually one-story, with bays and heights larger than those ones of the ordinary buildings (e.g. residential).

In the first part of the Section 1 some general information are reported (red area in Figure 2.57), as the address and the administrative code of the structures (see Section 0).

In the blank area (blue rectangle in Figure 2.57) a schematic sketch of the structure has to be reported, indicating the eventual connected structures and one point (pink circle) on the structure in order to individuate the position (reported in the violet rectangle in Figure 2.57). The investigated building (filled areas in Figure 2.57) can be an isolated building (Case I and I option in the violet rectangle of Figure 2.57) or part of a connected structure complex (Case II in Figure 2.57). In the latter case the position of the building is indicated as internal, end or corner building (last three options in the violet rectangle of Figure 2.57, respectively).

In the field of the identification of the building (first column of the green rectangle in Figure 2.57) a reference name is reported, and it can be assumed equal to the function or to the activities in case of strategic or public structures, or equal to the owners/managers name in the case of ordinary or industrial buildings.

SEZIONE 1 Identificazione edificio

Provincia: _____

Comune: _____

Frazione/Località: (denominazione nota) _____

1 ☐ via _____

2 ☐ corso _____

3 ☐ vicolo _____ Numeri Civici _____

4 ☐ piazza _____

5 ☐ altro (Indicare Contrada, Località, Traversa, Salita, etc.) _____

IDENTIFICATIVO SOPRALLUOGO giorno mese anno _____

Squadra: _____ Scheda n. _____ Data _____

IDENTIFICATIVO EDIFICIO

N° aggregato _____ N° edificio _____

Dati catastali - Particella _____

Coordinate ☐ plane UTM (metri) ☐ geografiche (gradi) ☐ altro _____

Fuso (32-33-34) _____ Datum _____ Lat./Nord _____

☐ ED50 _____ ☐ WGS84 _____ Long./Est _____

Posizione edificio 1 ☐ isolato 2 ☐ interno 3 ☐ frontembalco 4 ☐ angolo

Denominazione edificio o proprietario _____ Codice Uso _____

Classe d'uso edificio 1 ☐ Classe I 2 ☐ Classe II 3 ☐ Classe III 4 ☐ Classe IV

Rappresentazione schematica dell'edificio con i suoi blocchi aggiunti o integrati numerati

CASE I 08-036-022-00004-00

CASE II 08-036-022-00001-00

Building 001 (Isolated) Building 002 (Internal) Building 003 (Internal) Building 004 (Internal) Building 005 (Internal) Building 006 (Corner)

Figure 2.57 Section 1 of GL-AeDES: identification of the single structure

The function (Table 2.7) is reported in the second column of the green rectangle in Figure 2.57, only if the investigate structure is used for public services. The destination use is reported in the black rectangle in Figure 2.57, indicating the classification of buildings according to the NTC/08 and taking into account the consequences of an interruption of operations or of a possible collapse during a seismic event.

Table 2.7 Codes of the structures for public service

CODE	USE	CODE	USE
S00	Education structures	S50	Military academy
S01	Nursery school	S51	Armed forces
S02	Preschool	S52	Public security
S03	Primary school	S53	Fire department
S04	Secondary school - Compulsory	S54	Italian finance police
S05	Secondary school - Optional	S55	Forest ranger
S06	High school	S60	Religious activities
S07	Professional institute	S61	Parish
S08	Technical institute	S62	Centre of prayer
S09	University (Humanities Faculty)	S70	Technological service
S10	University (scientific faculty)	S71	Water
S11	Academy and conservatory	S72	Drainage system
S12	School board offices	S73	Electricity
S20	Hospital structures	S74	Gas
S21	Hospital	S75	Telephone
S22	Nursing home	S76	Telecommunications
S23	Clinic	S80	Transportation service
S24	Heath national agency	S81	Railroad station
S25	Public service	S82	Bus station
S30	Civil and public activities	S83	Airport
S31	Government (technical offices)	S84	Naval station
S32	Government (administration)		
S33	Region		
S34	Province		
S35	Alpine association		
S36	City hall		
S37	Decentralized centre		
S38	Prefecture		
S39	Postal service		
S40	Meeting centre		
S41	Museum and library		
S42	Prison		

2.3.4 Geometrical features of the structure (Section 2)

The Section 2 consists of two main parts, shown in Figure 2.58 and in Figure 2.59.

In the first part (Section 2a) three kinds of information are reported:

- geometrical data: total number of levels, number of underground stories, mean height of the levels and of the columns and mean area of roof;
- age: construction and repairing time;
- use and exposure: destination; numbers of units and percentage of use; mean number of people in the structure and type of property (public or private).

SEZIONE 2a Descrizione edificio							
Dati metrici			Età	Uso - esposizione			
N° Piani totali con interrati	Altezza media di piano [m]	Superficie media di piano [m ²]	Costruzione e ristrutturaz. [max 4]	Uso	N° unità d'uso	Utilizzazione	Occupanti
<input type="radio"/> 1	1 <input type="radio"/> 2.7+3.5	A <input type="radio"/> ≤ 200 M <input type="radio"/> 2000 + 2500	1 <input type="checkbox"/> ≤ 1950	A <input type="checkbox"/> Residenziale	<input type="text"/>	A <input type="radio"/> > 65%	<input type="text"/>
<input type="radio"/> 2	2 <input type="radio"/> 3.5+5.0	B <input type="radio"/> 200 + 250 N <input type="radio"/> 2500 + 3000	2 <input type="checkbox"/> 51+ 61	B <input type="checkbox"/> Produttivo	<input type="text"/>	B <input type="radio"/> 30+65%	<input type="text"/>
<input type="radio"/> 3	3 <input type="radio"/> 5.0+7.0	C <input type="radio"/> 250 + 300 O <input type="radio"/> 3000 + 3500	3 <input type="checkbox"/> 62 + 75	C <input type="checkbox"/> Commercio	<input type="text"/>	C <input type="radio"/> < 30%	<input type="text"/>
<input type="radio"/> 4	4 <input type="radio"/> 7.0+10.0	D <input type="radio"/> 300 + 400 P <input type="radio"/> 3500 + 4000	4 <input type="checkbox"/> 75 + 81	D <input type="checkbox"/> Uffici	<input type="text"/>	D <input type="radio"/> Non utilizz.	<input type="text"/>
<input type="radio"/> ≥ 5	5 <input type="radio"/> 10.0+14.0	E <input type="radio"/> 400 + 500 Q <input type="radio"/> 4000 + 4500	5 <input type="checkbox"/> 82 + 86	E <input type="checkbox"/> Serv. Pubbl.	<input type="text"/>	E <input type="radio"/> In costruz.	<input type="text"/>
Piani interr.	6 <input type="radio"/> > 14.0	F <input type="radio"/> 500 + 650 R <input type="radio"/> 4500 + 5000	6 <input type="checkbox"/> 87 + 95	F <input type="checkbox"/> Deposito	<input type="text"/>	F <input type="radio"/> Non finito	<input type="text"/>
A <input type="radio"/> 0	Altezza media libera pilastri	G <input type="radio"/> 650 + 900 S <input type="radio"/> 5500 + 6000	7 <input type="checkbox"/> 96 + 02	G <input type="checkbox"/> Parcheggio	<input type="text"/>	G <input type="radio"/> Abbandonato	<input type="text"/>
B <input type="radio"/> 1		H <input type="radio"/> 900 + 1200 T <input type="radio"/> 6000 + 7000	8 <input type="checkbox"/> 03 + 07	H <input type="checkbox"/> Att. sportive	<input type="text"/>	Proprietà: A <input type="radio"/> Pubblica B <input type="radio"/> Privata	
C <input type="radio"/> 2		I <input type="radio"/> 1200 +1600 U <input type="radio"/> 7000 +10000	9 <input type="checkbox"/> ≥ 2008	I <input type="checkbox"/> Turist. ricett.	<input type="text"/>		
D <input type="radio"/> ≥ 3	7 <input type="radio"/> Valore [m]: <input type="text"/>	L <input type="radio"/> 1600 +2000 V <input type="radio"/> > 10000					

Figure 2.58 Section 2a of GL-AeDES: description of the single structure

The Section 2b detects the presence and the characteristics of blocks, added or integrated to the main structure, internally or externally placed, that can significantly influence the structural behavior under seismic action. The first main difference is related to the structure of this block: they can be distinguished in integrated or added blocks. In the first case (Figure 2.60a) the block uses some structural elements of the main building while in the latter case (Figure 2.60b) the block has a proper structural system. For each block the surveyor indicates: the materials of the vertical (S.V.) and horizontal elements (S.O); the numbers of stories, the total height, the mean area of the roof, the level height and the function. Only in the case of an added or integrated block with significant size or with specific issues, more detailed are needed, for example with a new AeDES form for ordinary structures.



2.3.5 Structural elements and behavior of the structure (Section 3)

The Section 3 of the form consists of four parts and aims to give a deep understanding of the behavior of the building, highlighting the vulnerable elements and characteristics to the seismic actions.

2.3.5.1 Section 3a: structural typology

The first part (Section 3a) is shown in Figure 2.61 and gives the following information:

- materials of the vertical, horizontal and roof elements (red table in Figure 2.61);
- foundation system (green table in Figure 2.61);
- main structural resistant system and typology of the roof level in terms of stiffness in its own plane (black table in Figure 2.61).

As anticipated, the compiling phase gives a guided path up to the usability judgment with a behavioral approach. In the Section 3a some initial behavioral indications are given, supported also by the different background colors. An example is the definition of the floor level stiffness: if the roof can be assumed as a rigid diaphragm and the vertical resistant systems provides a good behavior under horizontal action (braced frames) the box is white (C4 in second row table); if the roof is flexible in its own plane and the structure doesn't provide braced elements the box is gray (B3 in the second row table).

SEZIONE 3a Tipologia edificio (risposta multipla)				Modalità di approfondimento							
Materiale	Elementi verticali	Elementi orizzontali	Copertura	Tipologia di fondazione	Non identificata	Presunta	Da interviste	Da elaborato	Ispezione diretta	Fondazione diretta	Fondazione indiretta
	A	B	C		A	B	C	D	E	F	G
1 C.A. prefabbricato	<input type="checkbox"/>	<input type="checkbox"/>	<input type="checkbox"/>	1 Non identificata	<input type="radio"/>	<input type="checkbox"/>	<input type="checkbox"/>	<input type="checkbox"/>	<input type="checkbox"/>	<input type="checkbox"/>	<input type="checkbox"/>
2 C.A. in opera	<input type="checkbox"/>	<input type="checkbox"/>	<input type="checkbox"/>	2 Plinti isolati	<input type="checkbox"/>	<input type="checkbox"/>	<input type="checkbox"/>	<input type="checkbox"/>	<input type="checkbox"/>	<input type="checkbox"/>	<input type="checkbox"/>
3 Acciaio	<input type="checkbox"/>	<input type="checkbox"/>	<input type="checkbox"/>	3 Plinti collegati	<input type="checkbox"/>	<input type="checkbox"/>	<input type="checkbox"/>	<input type="checkbox"/>	<input type="checkbox"/>	<input type="checkbox"/>	<input type="checkbox"/>
4 Legno	<input type="checkbox"/>	<input type="checkbox"/>	<input type="checkbox"/>	4 Travi rovesce	<input type="checkbox"/>	<input type="checkbox"/>	<input type="checkbox"/>	<input type="checkbox"/>	<input type="checkbox"/>	<input type="checkbox"/>	<input type="checkbox"/>
5 Muratura	<input type="checkbox"/>	<input type="checkbox"/>	<input type="checkbox"/>	5 Platea	<input type="checkbox"/>	<input type="checkbox"/>	<input type="checkbox"/>	<input type="checkbox"/>	<input type="checkbox"/>	<input type="checkbox"/>	<input type="checkbox"/>
6 Misto acciaio - cls	<input type="checkbox"/>	<input type="checkbox"/>	<input type="checkbox"/>								
7 Altri materiali (specificare)											

Strutture - Risposta multipla - indicare al massimo 4 tipologie di combinazioni fra orizzontamento e strutture in elevazione									
Struttura verticale Impalcato intermedio	Non identificata	Sistema sismo-resistente					Sistema ibrido	Sistema duale	Dispositivi antisismici
		Strutture a pilastri		Strutture a parete					
		senza sistema controventante	con sistema controventante	a pareti portanti	a celle tridimensionali				
	A	B	C	D	E	F	G	H	
1 Assente	<input type="radio"/>	<input type="checkbox"/>	<input type="checkbox"/>	<input type="checkbox"/>	<input type="checkbox"/>	SI <input type="radio"/>	SI <input type="radio"/>	SI <input type="radio"/>	
2 Non identificato	<input type="radio"/>	<input type="checkbox"/>	<input type="checkbox"/>	<input type="checkbox"/>	<input type="checkbox"/>	SI <input type="radio"/>	SI <input type="radio"/>	SI <input type="radio"/>	
3 Impalcato deformabile nel proprio piano (e.g. gran parte dei tegoli prefabbricati binervati senza getto integrativo)	<input type="checkbox"/>	<input type="checkbox"/>	<input type="checkbox"/>	<input type="checkbox"/>	<input type="checkbox"/>	NO <input type="radio"/>	NO <input type="radio"/>	NO <input type="radio"/>	
4 Impalcato rigido nel proprio piano (e.g. soletta in c.a., solaio alveolare, tegoli con getto integrativo)	<input type="checkbox"/>	<input type="checkbox"/>	<input type="checkbox"/>	<input type="checkbox"/>	<input type="checkbox"/>	NO <input type="radio"/>	NO <input type="radio"/>	NO <input type="radio"/>	

Figure 2.61 Section 3a of GL-AeDES: materials and structural system

2.3.5.2 Section 3a: roof elements

In the Section 3b (Figure 2.62) the elements and the seismic behavior of the roof are described. In the first row of the main table the compiler has to indicate the width of the roof elements span, as well as the framework, that is single kind if there is only one frame of beams and it is double if there is a double or more frame of beams. In the same row the number of frameworks at the roof level is also required; for example, a roof that provides beams, girder and roof elements consists of three frameworks. The rows of the main table report the beam typologies, while the column indicates the closing elements at the roof level. In the smaller tables the surveyor indicates the presence of chains and the deformed characteristics of the roof.

SEZIONE 3b Copertura (risposta multipla)								
Luce max: L > 10 m		SI <input type="radio"/> NO <input type="radio"/>		Orditura: singola <input type="radio"/> doppia <input type="radio"/>		N° ordini copertura:		
Elementi di chiusura		Non identificata	Solaio piano	A doppia pendenza	A shed	Con tegoli affiancati	Con tegoli distanziati	Volta
Elementi primari								
1 Non identificati	<input checked="" type="radio"/>	<input type="radio"/>	<input type="radio"/>	<input type="radio"/>	<input type="radio"/>	<input type="radio"/>	<input type="radio"/>	<input type="radio"/>
2 Membratura a parete piena	<input type="radio"/>	<input type="radio"/>	<input type="radio"/>	<input type="radio"/>	<input type="radio"/>	<input type="radio"/>	<input type="radio"/>	<input type="radio"/>
3 Cassoni o scatolari	<input type="radio"/>	<input type="radio"/>	<input type="radio"/>	<input type="radio"/>	<input type="radio"/>	<input type="radio"/>	<input type="radio"/>	<input type="radio"/>
4 Sistemi reticolari	<input type="radio"/>	<input type="radio"/>	<input type="radio"/>	<input type="radio"/>	<input type="radio"/>	<input type="radio"/>	<input type="radio"/>	<input type="radio"/>
5 A doppia pendenza	<input type="radio"/>	<input type="radio"/>	<input type="radio"/>	<input type="radio"/>	<input type="radio"/>	<input type="radio"/>	<input type="radio"/>	<input type="radio"/>
6 Altro (specificare)								

Presenza di catene		Elementi spingenti
SI	H	I
<input type="radio"/>	<input type="radio"/>	<input type="radio"/>
NO	<input type="radio"/>	<input type="radio"/>

Caratteristiche deformative	
Non identificata	<input type="radio"/>
Deformabile	<input type="radio"/>
Rigida	<input type="radio"/>

Figure 2.62 Section 3b of GL-AeDES: roof elements and behavior under seismic actions

2.3.5.3 Section 3a: Regularity criteria

In the Section 3c (Figure 2.63) the surveyor judges the regularity of the structure according to some of the criteria, reported in NTC 2008, that may affect the vulnerability. In the case of a negative response (i.e. when the of regularity criteria is not satisfied) the check box is gray as in the case of non-regular structure the behavior is more vulnerable.

SEZIONE 3c Regolarità									
Regolarità in pianta			SI	NO	Regolarità in elevazione			SI	NO
1	Pianta compatta e simmetrica (e.g. non regolari forme in pianta a L, T, U, E, P, etc.)	<input type="radio"/>	<input checked="" type="radio"/>	1	Tutti i sistemi resistenti alle azioni orizzontali si estendono per tutta l'altezza della costruzione	<input type="radio"/>	<input checked="" type="radio"/>		
2	Rapporto tra lato maggiore e lato minore in pianta < 4	<input type="radio"/>	<input checked="" type="radio"/>	2	Tamponatura esterna (pannelli) uniformemente distribuita in altezza e assenza di finestre a nastro	<input type="radio"/>	<input checked="" type="radio"/>		
3	Rientranze in pianta che non superano il 5% dell'area totale	<input type="radio"/>	<input checked="" type="radio"/>	Regolarità in elevazione solo per strutture pluripiano					
4	Tamponatura esterna uniformemente e simmetricamente distribuita	<input type="radio"/>	<input checked="" type="radio"/>	3	Massa uniforme tra i livelli (e.g. assenza di variazione oltre il 50% tra la massa di un livello rispetto a quello adiacente)	<input type="radio"/>	<input checked="" type="radio"/>		
5	Assenza di nuclei o blocchi eccentrici	<input type="radio"/>	<input checked="" type="radio"/>	4	Rientri sezioni orizzontali non maggiori del 10% rispetto all'orizzontamento sottostante	<input type="radio"/>	<input checked="" type="radio"/>		
6	Disposizione simmetrica di pareti di taglio continue (setti) o reticolari (controventi verticali).	<input type="radio"/>	<input checked="" type="radio"/>	5	Rientro sezione orizzontale di ogni orizzontamento non maggiore del 30% del primo orizzontamento	<input type="radio"/>	<input checked="" type="radio"/>		

Figure 2.63 Section 3c of GL-AeDES: regularity criteria

2.3.5.4 Section 3a: connections, panels, loads and no structural elements

The Section 3d consists of four main parts, as indicated in Figure 2.64. The first part consists of an extensive table that aims to define all the connection systems in the

structure: column-to-foundation, beam-to-column, roof-to-beam, column-to-column and panels-to-structure. For each kind of connection the compiler has to individuate the corresponding system (row in the table) and declare the way acquisition of knowledge, i.e. how the system is individuated during the survey, since this aspect is an important information that influences the reliability of the survey. For each kind of connection systems some examples are reported in order to simplify the understanding as well as to demonstrate the capability of the proposed form to detect the characteristics of the main structural element.

Connections systems

Column/wall-to-foundation

- a. Hinge: this case can be associated at the connections with metal plate of reduced thickness anchored to the column by means of threaded bolts.
- b. Semi-fixed joint: this is the case of steel plates and bolts connection (Figure 2.65), in which the thickness of the plates and the distance between the anchor bolts are greater than in the previously described case.
- c. Fixed joint: this type can be chosen, for example, in the case of the socket foundation in the precast structures, provided by inserting the column in an isolated foundation by means of grout (Figure 2.66).

Beam-to column/wall

- a. Support: if the beam is simply supported on the column or on a bracket, usually with the interposition of a neoprene pad or a steel plate, without the addition of any mechanical devices, such as steel dowels.
- b. Hinge: if the beam is connected to the column by means of proper mechanical devices that prevent only the relative displacements, usually with the interposition of a neoprene pad or a steel plate. This case includes devices with high rotational flexibility, as in the case of the steel dowels.
- c. Semi-fixed joint: if the beam is constrained to the column with special mechanical devices that prevent the relative displacements and partially also the relative rotations.
- d. Fixed joint: if the beam is constrained to the column by means of specific mechanical devices that prevent the relative displacements and the relative rotations, as the joints in the cast in situ RC structures.
- e. Contiguous connected beams: if there is a link between two adjacent beams; this option does not preclude the options a-b-c-d.

SEZIONE 3d Tipologia connessioni, pannelli, carichi speciali, altri elementi non strutturali

Connessioni		Modalità di approfondimento				
Tipologia di connessione		Non identificata	Presunta	Da interviste	Da elaborato	Ispezione diretta
		A	B	C	D	E
1	Pilastro/parete - fondazione	<input checked="" type="checkbox"/>	<input checked="" type="checkbox"/>	<input checked="" type="checkbox"/>	<input checked="" type="checkbox"/>	<input checked="" type="checkbox"/>
1a	Cerniera	<input type="checkbox"/>	<input type="checkbox"/>	<input type="checkbox"/>	<input type="checkbox"/>	<input type="checkbox"/>
1b	Semi-incastro	<input type="checkbox"/>	<input type="checkbox"/>	<input type="checkbox"/>	<input type="checkbox"/>	<input type="checkbox"/>
1c	Incastro (e.g. plinti a bicchiere, pozzetti)	<input type="checkbox"/>	<input type="checkbox"/>	<input type="checkbox"/>	<input type="checkbox"/>	<input type="checkbox"/>
1e	Altro (specificare)	<input type="checkbox"/>	<input type="checkbox"/>	<input type="checkbox"/>	<input type="checkbox"/>	<input type="checkbox"/>
2	Trave – pilastro/parete	<input checked="" type="checkbox"/>	<input checked="" type="checkbox"/>	<input checked="" type="checkbox"/>	<input checked="" type="checkbox"/>	<input checked="" type="checkbox"/>
2a	Appoggio	<input type="checkbox"/>	<input type="checkbox"/>	<input type="checkbox"/>	<input type="checkbox"/>	<input type="checkbox"/>
2b	Cerniera (ad es. barre verticali su mensola)	<input type="checkbox"/>	<input type="checkbox"/>	<input type="checkbox"/>	<input type="checkbox"/>	<input type="checkbox"/>
2c	Semi-incastro (ad es. parz. resistenti a flessione)	<input type="checkbox"/>	<input type="checkbox"/>	<input type="checkbox"/>	<input type="checkbox"/>	<input type="checkbox"/>
2d	Incastro (ad es. emulazione c.a. in opera)	<input type="checkbox"/>	<input type="checkbox"/>	<input type="checkbox"/>	<input type="checkbox"/>	<input type="checkbox"/>
2e	A travi contigue collegate	<input type="checkbox"/>	<input type="checkbox"/>	<input type="checkbox"/>	<input type="checkbox"/>	<input type="checkbox"/>
3	Impalcato - trave	<input checked="" type="checkbox"/>	<input checked="" type="checkbox"/>	<input checked="" type="checkbox"/>	<input checked="" type="checkbox"/>	<input checked="" type="checkbox"/>
3a	Appoggio	<input type="checkbox"/>	<input type="checkbox"/>	<input type="checkbox"/>	<input type="checkbox"/>	<input type="checkbox"/>
3b	Cerniera (ad es. inserti metallici a secco)	<input type="checkbox"/>	<input type="checkbox"/>	<input type="checkbox"/>	<input type="checkbox"/>	<input type="checkbox"/>
3c	Semi-incastro (ad es. parz. resistenti a flessione)	<input type="checkbox"/>	<input type="checkbox"/>	<input type="checkbox"/>	<input type="checkbox"/>	<input type="checkbox"/>
3d	Incastro (ad es. emulazione c.a. in opera)	<input type="checkbox"/>	<input type="checkbox"/>	<input type="checkbox"/>	<input type="checkbox"/>	<input type="checkbox"/>
4	Copertura - trave	<input checked="" type="checkbox"/>	<input checked="" type="checkbox"/>	<input checked="" type="checkbox"/>	<input checked="" type="checkbox"/>	<input checked="" type="checkbox"/>
4a	Appoggio	<input type="checkbox"/>	<input type="checkbox"/>	<input type="checkbox"/>	<input type="checkbox"/>	<input type="checkbox"/>
4b	Cerniera (ad es. inserti metallici a secco)	<input type="checkbox"/>	<input type="checkbox"/>	<input type="checkbox"/>	<input type="checkbox"/>	<input type="checkbox"/>
4c	Semi-incastro (ad es. parz. resistenti a flessione)	<input type="checkbox"/>	<input type="checkbox"/>	<input type="checkbox"/>	<input type="checkbox"/>	<input type="checkbox"/>
4d	Incastro (ad es. emulazione c.a. in opera)	<input type="checkbox"/>	<input type="checkbox"/>	<input type="checkbox"/>	<input type="checkbox"/>	<input type="checkbox"/>
5	Pilastro/parete – pilastro/parete	<input checked="" type="checkbox"/>	<input checked="" type="checkbox"/>	<input checked="" type="checkbox"/>	<input checked="" type="checkbox"/>	<input checked="" type="checkbox"/>
5a	Connessioni metalliche	<input type="checkbox"/>	<input type="checkbox"/>	<input type="checkbox"/>	<input type="checkbox"/>	<input type="checkbox"/>
5b	Emulazione c.a. in opera	<input type="checkbox"/>	<input type="checkbox"/>	<input type="checkbox"/>	<input type="checkbox"/>	<input type="checkbox"/>
5c	Altro	<input type="checkbox"/>	<input type="checkbox"/>	<input type="checkbox"/>	<input type="checkbox"/>	<input type="checkbox"/>
6	Pannello - struttura	<input checked="" type="checkbox"/>	<input checked="" type="checkbox"/>	<input checked="" type="checkbox"/>	<input checked="" type="checkbox"/>	<input checked="" type="checkbox"/>
6a	Sistema isostatico	<input type="checkbox"/>	<input type="checkbox"/>	<input type="checkbox"/>	<input type="checkbox"/>	<input type="checkbox"/>
6b	Sistema integrato	<input type="checkbox"/>	<input type="checkbox"/>	<input type="checkbox"/>	<input type="checkbox"/>	<input type="checkbox"/>
6c	Sistema dissipativo	<input type="checkbox"/>	<input type="checkbox"/>	<input type="checkbox"/>	<input type="checkbox"/>	<input type="checkbox"/>

Pannelli di tamponatura	
1	<input type="radio"/> Assenti
2	<input type="checkbox"/> Prefabbricati orizzontali appesi esterni al filo pilastri
3	<input type="checkbox"/> Prefabbricati orizzontali appesi interni al filo pilastri
4	<input type="checkbox"/> Prefabbricati orizzontali infilati
5	<input type="checkbox"/> Prefabbricati verticali con chiave di taglio alla base
6	<input type="checkbox"/> Prefabbricati verticali senza chiave di taglio alla base
7	<input type="checkbox"/> Prefabbricati verticali infilati
8	<input type="checkbox"/> Prefabbricati impilati
9	<input type="checkbox"/> In c.a. gettati in opera
10	<input type="checkbox"/> Muratura
11	<input type="checkbox"/> Sandwich
12	<input type="checkbox"/> Lamiere grecate semplici
13	<input type="checkbox"/> Pareti stratificate a secco
14	<input type="checkbox"/> A base di legno
A	<input type="checkbox"/> Presenza pilastri reggi-pannello
B	<input type="checkbox"/> Presenza dispositivi di ritenuta

Carichi speciali	
1	<input type="checkbox"/> Carroponte
2	<input type="checkbox"/> Gru a sbalzo
3	<input type="checkbox"/> Soppalchi caricati
4	<input type="checkbox"/> Scaffalature vincolate alla struttura
5	<input type="checkbox"/> Scaffalature NON vincolate alla struttura
6	<input type="checkbox"/> Presenza macchinari su impalcati o su copertura
7	<input type="checkbox"/> Altro (specificare)

Altri elementi non strutturali	
1	<input type="checkbox"/> Serbatoi
2	<input type="checkbox"/> Tubazioni
3	<input type="checkbox"/> Silos
4	<input type="checkbox"/> Presenza materiali pericolosi
5	<input type="checkbox"/> Passerelle di collegam. impianti
6	<input type="checkbox"/> Altro (specificare)

Figure 2.64 Section 3d of GL-AeDES: connection systems, special load and non-structural elements

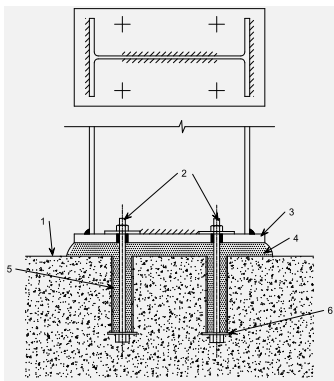


Figure 2.65 Column-to-foundation connection with steel plate and anchors

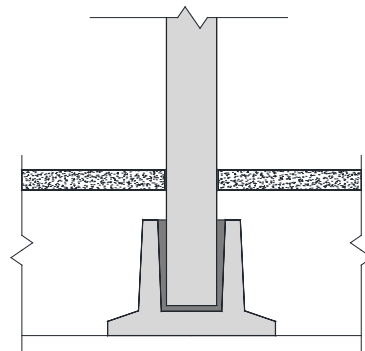


Figure 2.66 Socket foundation in precast RC structures

Intermediate deck-beam and roof-beam

- a. Support: if the roof element is simply supported on the beam, usually with the interposition of a neoprene pad or a steel plate, without the addition of mechanical devices, such as steel dowels.
- b. Hinge: if the roof element is connected to the beam by means of proper mechanical devices that prevent only the relative displacements, usually with the interposition of a neoprene pad or a steel plate. This case includes devices with high rotational flexibility, as in the case of the steel dowels.
- c. Semi-fixed joint: if the roof element is constrained to the beam with special mechanical devices that prevent the relative displacements and partially also the relative rotations.
- d. Fixed joint: if the roof element is constrained to the beam by means of specific mechanical devices that prevent the relative displacements and the relative rotations, as the joints in the cast in situ RC structures.

Column/wall-column/wall

- a. Metallic connections: if the vertical elements are connected by means of metallic devices (including welding, bolting and screws) that ensure the to shear and flexural strength.
- b. Emulation of RC structures joints: if the connection is made by overlapping parts of the vertical elements with bar outgoing, combined into a cast of concrete.

Panel-to-structure

- a. Isostatic system: if the connection system allows an interaction between the structure and the panels without causing forces in the connecting devices, or with limited forces, mainly associated to the weight of the panels. This case is represented by all the systems that, under the action of the earthquake, involve a rigid motion of the panels, allowing relative displacements between the structure and the panels, such as in the case of sliding connections.
- b. Integrated system: if the connection system causes an interaction between the structure and the panels, generating forces in the devices that depend on the intensity of the seismic. Not ductile, or with limited ductility, systems belong to this category, such as steel channel profiles, rigidly arranged in the connected elements.
- c. Dissipative system: if the connection system involves an interaction between the structure and the panels, generating forces in the connection devices, whose intensity depends on the seismic action until the attainment of a threshold

strength above which the connection behavior becomes dissipative with a high ductility. Also the dissipative connections between panels and/or between the panel and the foundation system could belong to this category.

Cladding panels

In this table (Figure 2.64) the surveyor describes the main panels typologies in the investigated structure. This nonstructural element is investigated with a specific table in the form, since it could highly influence the stiffness and the dynamic characteristics of the structure, depending on its material and its connections (see Section 3d on the connection systems).

The typologies of cladding panels are individuated according to the material they are composed of:

- vertical and horizontal precast reinforced concrete (Figure 2.67) with different types of connection with the main structure, corresponding to row from 1 to 7 of the form table;
- cast in situ concrete panels (Figure 2.68), corresponding to the 8th row of the form table;
- masonry (Figure 2.69), corresponding to the 9th row of the form table;
- steel (Figure 2.70), corresponding to the 10th row of the form table;
- composite, such as sandwich panels (Figure 2.71) and layer panels, corresponding to the 11th and 12th row of the form table.

In the same table the presence of columns used only to support the panels (13th row in the form table) and of systems to avoid the overturning (14th row in the form table) can be reported, since they could reduce the vulnerability of these nonstructural elements and of the whole structure.

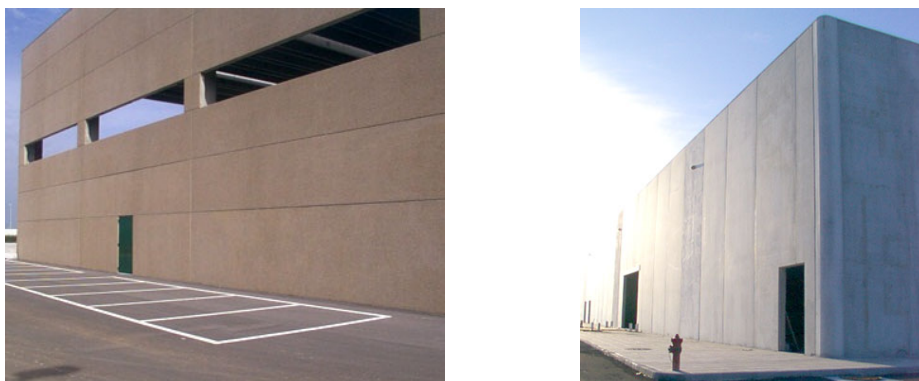


Figure 2.67 Cladding panels: (a) horizontal and (b) vertical layout



Figure 2.68 Cast in situ concrete panels



Figure 2.69 Masonry panels



Figure 2.70 Steel panels



Figure 2.71 Sandwich panels

Special loads and other no structural components

The most of the buildings with great span, e.g. the precast one-story structure, host industrial and/or commercial activities. These functions determine some peculiar aspects, that go beyond the structural characteristics of the building, but that may affect the usability of the building after a seismic event and the safety of human life. Among these aspects, in these buildings an important role is related to special loads and to the nonstructural components.

Examples of special loads in industrial buildings are: cranes, storage racks, machineries and systems. Examples of nonstructural components in industrial buildings are: silos, tanks and pipelines.

2.3.6 Damage in structural elements (Section 4)

In this Section (Figure 2.72) the results of the damage survey is reported. The form provides a detailed and extended table: the rows represent the structural components (column, beams, braces, stairs, roof elements; connection systems and added or integrated blocks); the columns represent the damage level and the kind of possible emergency action, already existing during the survey. The damage is assigned for each element or system, selecting its magnitude as well as its extension in the whole structure.

In order to enable a more effective and immediate evaluation, according to the European macro seismic scale (EMS98) (Grünthal, 1998), the damage magnitude is expressed through the well-known levels of damage, that allow comparable assessments and a standardize the language, without requirements of detailed and difficult measurements. In the described form the chosen damage levels are three: D1 (light damage) with a low structural damage; D2-D3 (medium-heavy damage) with a medium damage and D4-D5 (high damage and failure) with a very important structural damage and global collapse of the building. The extension of the damage, given a defined level, indicates the percentage of elements and system affected of that level of damage with respect to the total number of equal elements in the structure. Moreover, the sum of the percentage at the same row cannot be larger than one (for each element), vice versa the sum can be smaller than one since some elements can be not damaged.

SEZIONE 4 Danni ai COMPONENTI STRUTTURALI e provvedimenti di pronto intervento (P.I.) eseguiti																
Estensione del Livello di danno Componente strutturale e Danno pre-esistente		DANNO ⁽¹⁾									PROVVEDIMENTI DI PRONTO INTERVENTO ESEGUITI					
		D4 – D5 Gravissimo			D2 – D3 medio grave			D1 Leggero								
		> 2/3	1/3 – 2/3	< 1/3	> 2/3	1/3 – 2/3	< 1/3	> 2/3	1/3 – 2/3	< 1/3	Nullo	Nessuno	Demolizioni	Legature	Riparazioni	Puntellature
		A	B	C	D	E	F	G	H	I	L	A	B	C	D	E
Elementi strutturali	1 Pilastri	<input type="checkbox"/>	<input type="checkbox"/>	<input type="checkbox"/>	<input type="checkbox"/>	<input type="checkbox"/>	<input type="checkbox"/>	<input type="checkbox"/>	<input type="checkbox"/>	<input type="checkbox"/>	<input type="checkbox"/>	<input type="checkbox"/>	<input type="checkbox"/>	<input type="checkbox"/>	<input type="checkbox"/>	<input type="checkbox"/>
	2 Travi	<input type="checkbox"/>	<input type="checkbox"/>	<input type="checkbox"/>	<input type="checkbox"/>	<input type="checkbox"/>	<input type="checkbox"/>	<input type="checkbox"/>	<input type="checkbox"/>	<input type="checkbox"/>	<input type="checkbox"/>	<input type="checkbox"/>	<input type="checkbox"/>	<input type="checkbox"/>	<input type="checkbox"/>	<input type="checkbox"/>
	3 Pareti portanti	<input type="checkbox"/>	<input type="checkbox"/>	<input type="checkbox"/>	<input type="checkbox"/>	<input type="checkbox"/>	<input type="checkbox"/>	<input type="checkbox"/>	<input type="checkbox"/>	<input type="checkbox"/>	<input type="checkbox"/>	<input type="checkbox"/>	<input type="checkbox"/>	<input type="checkbox"/>	<input type="checkbox"/>	<input type="checkbox"/>
	4 Controventi	<input type="checkbox"/>	<input type="checkbox"/>	<input type="checkbox"/>	<input type="checkbox"/>	<input type="checkbox"/>	<input type="checkbox"/>	<input type="checkbox"/>	<input type="checkbox"/>	<input type="checkbox"/>	<input type="checkbox"/>	<input type="checkbox"/>	<input type="checkbox"/>	<input type="checkbox"/>	<input type="checkbox"/>	<input type="checkbox"/>
	5 Impalcati	<input type="checkbox"/>	<input type="checkbox"/>	<input type="checkbox"/>	<input type="checkbox"/>	<input type="checkbox"/>	<input type="checkbox"/>	<input type="checkbox"/>	<input type="checkbox"/>	<input type="checkbox"/>	<input type="checkbox"/>	<input type="checkbox"/>	<input type="checkbox"/>	<input type="checkbox"/>	<input type="checkbox"/>	<input type="checkbox"/>
	6 Scale	<input type="checkbox"/>	<input type="checkbox"/>	<input type="checkbox"/>	<input type="checkbox"/>	<input type="checkbox"/>	<input type="checkbox"/>	<input type="checkbox"/>	<input type="checkbox"/>	<input type="checkbox"/>	<input type="checkbox"/>	<input type="checkbox"/>	<input type="checkbox"/>	<input type="checkbox"/>	<input type="checkbox"/>	<input type="checkbox"/>
	7 Copertura	<input type="checkbox"/>	<input type="checkbox"/>	<input type="checkbox"/>	<input type="checkbox"/>	<input type="checkbox"/>	<input type="checkbox"/>	<input type="checkbox"/>	<input type="checkbox"/>	<input type="checkbox"/>	<input type="checkbox"/>	<input type="checkbox"/>	<input type="checkbox"/>	<input type="checkbox"/>	<input type="checkbox"/>	<input type="checkbox"/>
	8 Danno pre-esistente	<input type="checkbox"/>	<input type="checkbox"/>	<input type="checkbox"/>	<input type="checkbox"/>	<input type="checkbox"/>	<input type="checkbox"/>	<input type="checkbox"/>	<input type="checkbox"/>	<input type="checkbox"/>	<input type="checkbox"/>	<input type="checkbox"/>	<input type="checkbox"/>	<input type="checkbox"/>	<input type="checkbox"/>	<input type="checkbox"/>
Connessioni	9 Pilastro/Parete – Fondazione	<input type="checkbox"/>	<input type="checkbox"/>	<input type="checkbox"/>	<input type="checkbox"/>	<input type="checkbox"/>	<input type="checkbox"/>	<input type="checkbox"/>	<input type="checkbox"/>	<input type="checkbox"/>	<input type="checkbox"/>	<input type="checkbox"/>	<input type="checkbox"/>	<input type="checkbox"/>	<input type="checkbox"/>	<input type="checkbox"/>
	10 Trave – Pilastro/Parete	<input type="checkbox"/>	<input type="checkbox"/>	<input type="checkbox"/>	<input type="checkbox"/>	<input type="checkbox"/>	<input type="checkbox"/>	<input type="checkbox"/>	<input type="checkbox"/>	<input type="checkbox"/>	<input type="checkbox"/>	<input type="checkbox"/>	<input type="checkbox"/>	<input type="checkbox"/>	<input type="checkbox"/>	<input type="checkbox"/>
	11 Impalcato – Trave	<input type="checkbox"/>	<input type="checkbox"/>	<input type="checkbox"/>	<input type="checkbox"/>	<input type="checkbox"/>	<input type="checkbox"/>	<input type="checkbox"/>	<input type="checkbox"/>	<input type="checkbox"/>	<input type="checkbox"/>	<input type="checkbox"/>	<input type="checkbox"/>	<input type="checkbox"/>	<input type="checkbox"/>	<input type="checkbox"/>
	12 Copertura – Trave	<input type="checkbox"/>	<input type="checkbox"/>	<input type="checkbox"/>	<input type="checkbox"/>	<input type="checkbox"/>	<input type="checkbox"/>	<input type="checkbox"/>	<input type="checkbox"/>	<input type="checkbox"/>	<input type="checkbox"/>	<input type="checkbox"/>	<input type="checkbox"/>	<input type="checkbox"/>	<input type="checkbox"/>	<input type="checkbox"/>
	13 Pilastro/Parete – Pilastro/Parete	<input type="checkbox"/>	<input type="checkbox"/>	<input type="checkbox"/>	<input type="checkbox"/>	<input type="checkbox"/>	<input type="checkbox"/>	<input type="checkbox"/>	<input type="checkbox"/>	<input type="checkbox"/>	<input type="checkbox"/>	<input type="checkbox"/>	<input type="checkbox"/>	<input type="checkbox"/>	<input type="checkbox"/>	<input type="checkbox"/>
	14 Pannello – Struttura	<input type="checkbox"/>	<input type="checkbox"/>	<input type="checkbox"/>	<input type="checkbox"/>	<input type="checkbox"/>	<input type="checkbox"/>	<input type="checkbox"/>	<input type="checkbox"/>	<input type="checkbox"/>	<input type="checkbox"/>	<input type="checkbox"/>	<input type="checkbox"/>	<input type="checkbox"/>	<input type="checkbox"/>	<input type="checkbox"/>
	15 Danno pre-esistente	<input type="checkbox"/>	<input type="checkbox"/>	<input type="checkbox"/>	<input type="checkbox"/>	<input type="checkbox"/>	<input type="checkbox"/>	<input type="checkbox"/>	<input type="checkbox"/>	<input type="checkbox"/>	<input type="checkbox"/>	<input type="checkbox"/>	<input type="checkbox"/>	<input type="checkbox"/>	<input type="checkbox"/>	<input type="checkbox"/>
Blocchi aggiunti	16 Danno complessivo del blocco aggiunto A	<input type="checkbox"/>	<input type="checkbox"/>	<input type="checkbox"/>	<input type="checkbox"/>	<input type="checkbox"/>	<input type="checkbox"/>	<input type="checkbox"/>	<input type="checkbox"/>	<input type="checkbox"/>	<input type="checkbox"/>	<input type="checkbox"/>	<input type="checkbox"/>	<input type="checkbox"/>	<input type="checkbox"/>	<input type="checkbox"/>
	17 Danno complessivo del blocco aggiunto B	<input type="checkbox"/>	<input type="checkbox"/>	<input type="checkbox"/>	<input type="checkbox"/>	<input type="checkbox"/>	<input type="checkbox"/>	<input type="checkbox"/>	<input type="checkbox"/>	<input type="checkbox"/>	<input type="checkbox"/>	<input type="checkbox"/>	<input type="checkbox"/>	<input type="checkbox"/>	<input type="checkbox"/>	<input type="checkbox"/>
	18 Danno complessivo del blocco aggiunto C	<input type="checkbox"/>	<input type="checkbox"/>	<input type="checkbox"/>	<input type="checkbox"/>	<input type="checkbox"/>	<input type="checkbox"/>	<input type="checkbox"/>	<input type="checkbox"/>	<input type="checkbox"/>	<input type="checkbox"/>	<input type="checkbox"/>	<input type="checkbox"/>	<input type="checkbox"/>	<input type="checkbox"/>	<input type="checkbox"/>
	19 Danno complessivo del blocco aggiunto D	<input type="checkbox"/>	<input type="checkbox"/>	<input type="checkbox"/>	<input type="checkbox"/>	<input type="checkbox"/>	<input type="checkbox"/>	<input type="checkbox"/>	<input type="checkbox"/>	<input type="checkbox"/>	<input type="checkbox"/>	<input type="checkbox"/>	<input type="checkbox"/>	<input type="checkbox"/>	<input type="checkbox"/>	<input type="checkbox"/>
	20 Danno complessivo del blocco aggiunto E	<input type="checkbox"/>	<input type="checkbox"/>	<input type="checkbox"/>	<input type="checkbox"/>	<input type="checkbox"/>	<input type="checkbox"/>	<input type="checkbox"/>	<input type="checkbox"/>	<input type="checkbox"/>	<input type="checkbox"/>	<input type="checkbox"/>	<input type="checkbox"/>	<input type="checkbox"/>	<input type="checkbox"/>	<input type="checkbox"/>

(1) In mancanza di danneggiamento, campire **Nullo** alla voce corrispondente

Figure 2.72 Section 4 of GL-AeDES: damage in structural elements and emergency actions

The way to establish the damage extension can be clarified by the following example. Considering a precast building with 3 levels where the damage level D2-D3 is observed in the 60% of the columns, only at the ground floor: in this case the extension related to the entire building is equal to $60\% \cdot 1/3 = 20\%$ and then $< 1/3$ (row 1, column F).

In the following, some examples are reported in order to establish the damage level of the structural elements and the connection systems in some precast one-story buildings.

D1: light damage

The D1 damage level is a damage that does not significantly change the strength of the structure and does not affect the safety of the occupants (Figure 2.86). This level can be assumed also if the possible damages during a subsequent event can be prevented by simple and rapid actions.

D2-D3: medium-high damage

This damage level can significantly change the response of the structure even if the limit condition of structural collapse is not reached (Figure 2.74). Examples of this damage to connection systems are shown in Figure 2.77 and in Figure 2.78.

D4-D5: medium-high damage

This damage level clearly changes the response of the structure, causing the collapse of the main structural elements (Figure 2.75 and Figure 2.76). This level is described by more important damages than in the previous case, as failure of the connections between structural elements and between panels and structure, that can cause the collapse of the principal and secondary elements. Examples of this damage to connection systems are shown in Figure 2.79 and in Figure 2.80.



Figure 2.73 Cracking at the base of a precast column in a one-story industrial building: damage level D1 (Emilia, 2012)



Figure 2.74 Plastic hinge formation at the base of a precast column in a one-story industrial building: damage level D2 (Emilia, 2012)



Figure 2.75 Plastic hinge formation at the base of a precast column in a one-story industrial building: damage level D4 (Emilia, 2012)



Figure 2.76 High strain in columns due to the irregular distribution of the infill panels in a one-story industrial building that cause the global collapse: damage level D5 (Emilia, 2012)

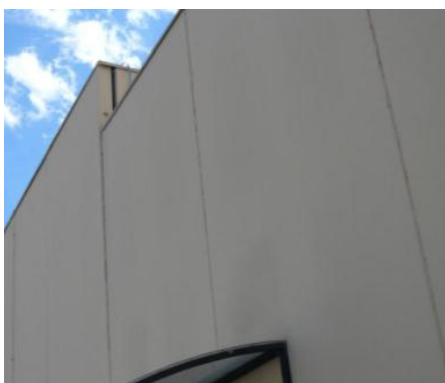


Figure 2.77 Relative displacement between the vertical panels in a one-story industrial building: damage level D2 (Emilia, 2012)



Figure 2.78 Dislocation of the horizontal panels in a one-story industrial building: damage level D3 (Emilia, 2012)



Figure 2.79 Damage in the column forks that constraints the beam in a one-story industrial building: damage level D4 (Emilia, 2012)



Figure 2.80 Collapse of a roof element with frictional connection in a one-story industrial building: damage level D5 (Emilia, 2012)

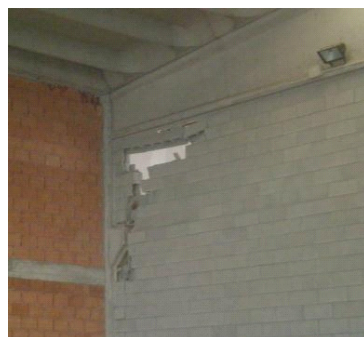
2.3.7 Damage in nonstructural elements (Section 5)

Any damage caused by the earthquake at the primary and secondary nonstructural components may influence both the classification of the structure in terms of functionality both the repairing costs estimation. In the Section 5 the information about these damage are recorded with the possible emergency actions that have already performed on the elements.

As in the previous section the form provides a specific table: the rows represent the no structural components (e.g. panels in Figure 2.82) and the columns reports the damage presence and the kind of possible emergency action, already existing during the survey. In this case the damage presence is indicated with no reference to the magnitude or to the extension in the structure.

SEZIONE 5										Danni ad ELEMENTI NON STRUTTURALI e provvedimenti di pronto intervento eseguiti						
Tipo di danno			PRESENZA DANNO	PROVVEDIMENTI DI PRONTO INTERVENTO ESEGUITI												
				Nessuno	Demolizioni	Puntelli	Riparazioni	Divieto di accesso	Barriere protettive							
			A	B	C	D	E	F	G							
Elementi primari	1	Pannelli di facciata	<input type="checkbox"/>	<input type="radio"/>	<input type="checkbox"/>	<input type="checkbox"/>	<input type="checkbox"/>	<input type="checkbox"/>	<input type="checkbox"/>							
	2	Pannelli divisori interni	<input type="checkbox"/>	<input type="radio"/>	<input type="checkbox"/>	<input type="checkbox"/>	<input type="checkbox"/>	<input type="checkbox"/>	<input type="checkbox"/>							
Elementi secondari	3	Distacco intonaci, rivestimenti, controsoffitti ...	<input type="checkbox"/>	<input type="radio"/>	<input type="checkbox"/>	<input type="checkbox"/>	<input type="checkbox"/>	<input type="checkbox"/>	<input type="checkbox"/>							
	4	Caduta tegole, comignoli, canne fumarie	<input type="checkbox"/>	<input type="radio"/>	<input type="checkbox"/>	<input type="checkbox"/>	<input type="checkbox"/>	<input type="checkbox"/>	<input type="checkbox"/>							
	5	Caduta parapetti, cornicioni	<input type="checkbox"/>	<input type="radio"/>	<input type="checkbox"/>	<input type="checkbox"/>	<input type="checkbox"/>	<input type="checkbox"/>	<input type="checkbox"/>							
	6	Danno a passerelle di collegamento	<input type="checkbox"/>	<input type="radio"/>	<input type="checkbox"/>	<input type="checkbox"/>	<input type="checkbox"/>	<input type="checkbox"/>	<input type="checkbox"/>							
	7	Danno a carroponete	<input type="checkbox"/>	<input type="radio"/>	<input type="checkbox"/>	<input type="checkbox"/>	<input type="checkbox"/>	<input type="checkbox"/>	<input type="checkbox"/>							
	8	Danno a Gru a sbalzo	<input type="checkbox"/>	<input type="radio"/>	<input type="checkbox"/>	<input type="checkbox"/>	<input type="checkbox"/>	<input type="checkbox"/>	<input type="checkbox"/>							
	9	Danni a serbatoi, silos, tubazioni	<input type="checkbox"/>	<input type="radio"/>	<input type="checkbox"/>	<input type="checkbox"/>	<input type="checkbox"/>	<input type="checkbox"/>	<input type="checkbox"/>							
	10	Danni a scaffalature	<input type="checkbox"/>	<input type="radio"/>	<input type="checkbox"/>	<input type="checkbox"/>	<input type="checkbox"/>	<input type="checkbox"/>	<input type="checkbox"/>							
	11	Danneggiamento ai serramenti	<input type="checkbox"/>	<input type="radio"/>	<input type="checkbox"/>	<input type="checkbox"/>	<input type="checkbox"/>	<input type="checkbox"/>	<input type="checkbox"/>							
	12	Danno alla rete idrica, fognaria o termoidraulica	<input type="checkbox"/>	<input type="radio"/>	<input type="checkbox"/>	<input type="checkbox"/>	<input type="checkbox"/>	<input type="checkbox"/>	<input type="checkbox"/>							
	13	Danno alla rete elettrica o del gas	<input type="checkbox"/>	<input type="radio"/>	<input type="checkbox"/>	<input type="checkbox"/>	<input type="checkbox"/>	<input type="checkbox"/>	<input type="checkbox"/>							
	14	Danno impianto di condizionamento, riscaldamento, ventilazione	<input type="checkbox"/>	<input type="radio"/>	<input type="checkbox"/>	<input type="checkbox"/>	<input type="checkbox"/>	<input type="checkbox"/>	<input type="checkbox"/>							
	15	Caduta oggetti interni o esterni non in elenco	<input type="checkbox"/>	<input type="radio"/>	<input type="checkbox"/>	<input type="checkbox"/>	<input type="checkbox"/>	<input type="checkbox"/>	<input type="checkbox"/>							

Figure 2.81 Section 5 of GL-AeDES: damage in no structural elements and emergency actions



(a)



(b)

Figure 2.82 Cracking and damage in masonry infill panels in one-story precast building (Emilia, 2012)

2.3.8 External dangers (Section 6)

In this Section (Figure 2.83) the possible external damages are reported, caused by reasons that does not belong to the investigated structure.

The causes are reported in the rows and listed in the following:

- presence of close structures with important structural and nonstructural damages, that could cause the collapse;
- pipelines damage;
- unsafe slope that can influence the safety of the structures and occupants.

In the first column the surveyor indicates if the damage is referred to the building, to the external roads used to access to the building or to the internal roads. In the second column the existing emergency actions are reported.

SEZIONE 6 Pericolo ESTERNO indotto da altre costruzioni, reti, versanti e provvedimenti di pronto intervento eseguiti							
Causa	Assente	Pericolo per:			Provvedimenti di pronto intervento eseguiti		
		edificio	vie d'accesso o di fuga	vie interne	Nessuno	Divieto di accesso	Barriere protettive
	A	B	C	D	E	F	G
1 Crolli o caduta oggetti da edifici adiacenti	<input type="radio"/>	<input type="checkbox"/>	<input type="checkbox"/>	<input type="checkbox"/>	<input type="radio"/>	<input type="checkbox"/>	<input type="checkbox"/>
2 Collasso di reti di distribuzione	<input type="radio"/>	<input type="checkbox"/>	<input type="checkbox"/>	<input type="checkbox"/>	<input type="radio"/>	<input type="checkbox"/>	<input type="checkbox"/>
3 Versanti incombenti	<input type="radio"/>	<input type="checkbox"/>	<input type="checkbox"/>	<input type="checkbox"/>	<input type="radio"/>	<input type="checkbox"/>	<input type="checkbox"/>

Figure 2.83 Section 6 of GL-AeDES: external dangers

2.3.9 Soil and foundation system (Section 7)

Section 7 (Figure 2.84) reports the information on the morphology of the site and any instability of the foundations, that may affect the geotechnical risk.

The requested analysis is qualitative and descriptive (for geotechnical risk, in fact, there are other more specific and detailed references).

Concerning the morphology, different conditions are considered:

- the structure is located on a peak, that can cause possible local amplification of the seismic excitation;
- the structure foundations are located on a strong slope or on different slope that may cause failure of the ground and of the foundations, even more when they are connected to already or going or expected instability phenomena;
- the structure is located on a level ground.

For the damage of the foundation systems is required to assess whether they are mainly caused by the seismic event or if they already exist.

SEZIONE 7 Terreno e fondazioni					
MORFOLOGIA DEL SITO				DANNI (esistenti o potenziali) ALLE FONDAZIONI	
1 <input type="radio"/> Cresta	2 <input type="radio"/> Pendio forte	3 <input type="radio"/> Pendio leggero	4 <input type="radio"/> Pianura	A <input type="radio"/> Assenti	B <input type="radio"/> Dovuti al sisma
				C <input type="radio"/> Acuiti dal sisma	D <input type="radio"/> Preesistenti

Figure 2.84 Section 7 of GL-AeDES: soil and foundation system

2.3.10 Usability judgment and emergency actions (Section 8)

In the Section 8 (Figure 2.85), the surveyor makes an assessment about the building usability according to the acquired and recorded information during the survey.

The usability judgment during the earthquake emergency is a preliminary and fast assessment that is formulated on the basis of an expert judgment and that is conducted in a limited time, on the base of a simple visual analysis and on easily available information. This judgment aims to determine whether in the presence of a seismic crisis, the damaged and hit buildings can be used with a reasonable safety of the human life.

[illegible]

Figure 2.85 Section 6 of GL-AeDES: usability judgment

Therefore, the statement of usability means that the conditions of the building before the earthquake, have not been substantially altered by the earthquake itself. This means that a following event (as an aftershock record with an intensity that does not exceed that for which the verification process is required) should not cause a significant increase of the damage level, and so a partial or total collapse of the structure. This last definition assumes that the surveyor knows the maximum intensity that can occur at the site during the seismic crisis, i.e. the reference event for the usability judgment. If this event is not explicitly quantified, it can be assumed that the reference event is the shock that has motivated the inspection.

The final Section 8 consists of five parts:

- the evaluation of the risk;
- the classification of the usability;
- the accuracy of the survey;
- possible emergency actions;
- buildings units and occupants declared not usable.

2.3.10.1 Section 8a: evaluation of the risk

The analysis of the building is summarized in the Section 8a, on the basis of the collected information and the resulting evaluations, in terms of:

- external risk, related to the possible dangerous conditions due to the close structures or to pipelines and slopes (Section 6);
- structural risk, related to the characteristics of structural elements and of the connections in the buildings (Section 3) as well as to the recorded damage after the earthquake (Section 4);
- nonstructural risk, related to the damage of the nonstructural elements (Section 5);
- geotechnical risk, related to the ground morphology as well as to the damage of the foundation system (Section 7).

For each kind of risk the team indicate the level, that can be:

- low, when no significant and dangerous damage are recorded and good structural features are found in the building;
- low with emergency actions, if the dangers can be eliminated or reduced with some fast and simple actions;
- high, if the damage can cause important dangers to the buildings and to the human life.

2.3.10.2 Section 8b: the classification of the usability

In the Section 8b, the team indicates the final usability judgment. This evaluation can be related to the previously defined risks levels, on the base of these general principles:

- if the value of each of the four types of risk can be considered "low", there are not the conditions for judging the building not usable;
- if at least one of the four types of risk is considered to be "high", the judge will provide a partial or total not usability of the building;
- if at least one of the four types of risk is considered "low with emergency actions " and the others are considered "low", the building will be considered temporarily unusable, but accessible after the actions.

The judgment consists of an intrinsic result and an external result, related to the external risk.

A – Investigate structure (potentially usable)

The building has been inspected and the visual inspection did not reveal any conditions that may justify a negative judgment. Therefore, the building could be used immediately in all its parts, without any emergency actions.

B – Temporary not usable structure (partially or totally) but usable with emergency actions

The usability judgment can be assigned to the buildings only after some emergency actions. In this case, some other information need:

- specification of the unusable parts of the structure;
- the emergency actions needed to obtain the positive judgment on the structure.

C – Partially not usable structure

The building presents a situation of risk that affects the usability of a well-defined part, that is represented in the Section 9 of the form. This part cannot affect the safety of the remaining structure.

D – Partially not usable structure with the need of deeper analysis

The judgment needs a more detailed and expert survey due to the specific characteristics of damage or of the structure.

E – Not usable structure

The building cannot be used due to the damage and the structural characteristics, recorded during the survey. This case does not means that the damage cannot be repaired but it means that all the needed actions are not simple emergency actions.

Some emergency actions can be also indicated in the form in order to reduce or remove any dangerous situation for the human safety.

F –Not usable structure for external risk

This judgment is related to the information in the Section 7 and it can be added to the intrinsic judgment. In this case the cause of the risk is reported in the Section 9 with the possible emergency actions.

2.3.10.3 Section 8c: accuracy of the survey

In this section the surveyor declares the accuracy of the performed survey, indicating the ways of inspection (partial or total), the investigated parts of the building (external) and the causes of any insufficient information and inspection (absence of owner, demolition or collapse).

2.3.10.4 Section 8d: emergency actions

In this section the team reports the description of the emergency actions, needed to obtain the usability judgment of the building.

2.3.10.5 Section 8e: unusable parts and evacuated occupants

In the box of the unusable parts, the team reports the number of units that cannot be used: this number is equal to the total number of building units only if the result of the survey is B, D or E. this number is smaller than the total number of building units when the judgment is C and it is equal to zero for the usable structure (A).

In the box the number of the evacuated occupants is reported in order to give an important information about the number of homeless after the earthquake.

2.3.11 *Notes (Section 9)*

This section reports all the note that need to clarify the judgment and the structural systems. In this section the emergency actions are also described, if necessary.

2.3.12 *Conclusions*

After a seismic event a crucial activity is the survey and assessment of the damage. In the last year this work is supported by tools and forms, that consist in checklists in order to guide the technical evaluations. One of the main advantage of this tools is the possibility to establish an homogenous survey of the damages over all of the hit estate and to obtain an immediate computerization and statistical treatment of the collected data.

Until the Emilia earthquake the survey on all kinds of structural typologies was performed by the AeDES form, i.e. the usability form for ordinary RC and masonry structures. The specific characteristics of industrial structures motivates the editing a new form, able to catch all the most important aspects that can influence the seismic performance and the safety of the structure.

In the previous sections all the form tables are described in order to show the proposed logical path that starts with the visual and behavioral characteristics investigation and arrives to the final judgment on its seismic vulnerability.

The need of a specific form is clearly demonstrated by the detailed description of the sections and tables: the contents are specifically correlated to the industrial and commercial structures as well as to their response during the last events.

2.4 Dynamic characteristics of precast buildings with and without cladding panels

Latest earthquakes, as L'Aquila (2009) and Emilia earthquakes (2012), pointed out some lacks in the design approach for precast buildings, among which the inadequacy of the panel-to-structure connection system design. Indeed, most of the numerous damaged precast buildings have showed the collapse of cladding panels, caused by the connection systems failure, even in case of a good structural response (Faggiano et al., 2009; Magliulo et al., 2013).

The experience of such a damage during past violent seismic events (Baird et al., 2011) let several research groups analyze interaction between cladding panels and supporting frame. Most of these studies refers to multi-story buildings, generally high-rise buildings in California. Much less is known about the influence that concrete panels may have on one-story precast concrete industrial buildings.

According to the design approach of the actual European and Italian codes, the precast structures are usually considered as bare systems and the cladding panels are separately designed for actions deriving by their weight and seismic or wind loads; no interaction between panels and structure is then considered. However, during a seismic event the panel-to-structure connections could let the panels collaborate with the structural system, increasing the structural stiffness and the seismic demand on the connection devices. According to Cleland and Ghosh (2007), the effect of the earthquake on precast panels comes from the inertia of the panels, that develops forces due to the restraints of their connections, and from the deformation of the frame, i.e., from the lateral drift, that can impose forces through these connections.

The poor literature and the high vulnerability of precast panels system motivate the need of an extended study on the behavior of precast panels and on their interaction with the structure. The first step of this study must be the investigation of the dynamic behavior (in particular, the vibration periods) of one-story precast structures with and without cladding panels. Such a study can also give some indications for the seismic design of structures and connection systems.

The presented work investigates the cladding panel influence on the first vibration period of typical precast industrial buildings by means of a parametric study. Both the bare model and the model with vertical panels are implemented in OpenSees (McKenna and Fenves, 2013) analysis code and modal analyses are carried out in order to record the first period of the analyzed precast structures, given the importance of such a parameter in the seismic response of structures (see D'Ambrisi et al., 2009 among the others). The inadequacy of the simplified relationship proposed by some codes to evaluate the first period for this typology of structures is also demonstrated and more suitable formulas are proposed.

2.4.1 State of art

Past earthquakes showed several damage to cladding systems in precast concrete structures, claiming the need of a renovated consideration of these non-structural elements. The current design approach aims to isolate the cladding panels from the resistant structure, by means of flexible connections, that have slots and gaps between structural and non-structural components. According to this approach, these elements are considered as non-loading bearing precast concrete panels (claddings) that are defined as “panels (structural or architectural) which resist only wind, (or seismic loads) and their own weight” (PCI, 2007).

However, during a seismic event, the panels to structure connections might be overloaded, because the gaps are too small or the slots are too short, causing the whole cladding system (panels and connections) collapse (Figure 2.86 and Figure 2.87). Furthermore, the collapse of these heavy and big precast concrete panels cannot be considered as the exceeding of a damage limit state: it should be considered not only as a serious damage to the non-structural elements but also as a high risk for the safety of human life.



Figure 2.86. Collapse of horizontal precast cladding panels in a one-story precast structure during the Emilia earthquake (2012)



Figure 2.87 Collapse of vertical precast cladding panels in a one-story precast structure during the Emilia earthquake (2012)

The high risk connected to the panels collapse and the high costs of the coatings repairing and of the structure functionality interruption move the interest of the scientific community over the last three decades. In the following, the analytical and experimental studies that investigate the influence of the precast panels on the dynamic properties of structures are reported. This state of art underlines the influence of these nonstructural elements on the dynamic properties of different structural systems. Moreover, some of the presented papers are the basis of the presented study, in defining the investigated connection typologies and a proper model for precast structures with cladding panels.

On May 18th, 1981, the National Science Foundation (NSF) of the United States and the Ministry Of Construction (MOC) of Japan under the auspices of the United States - Japan Cooperative Program on Natural Resources (UJNR) entered into an agreement to cooperate in research on the seismic behavior of steel buildings. The program consists of experimental and analytical studies carried out by investigators in the U.S. and in Japan. The centerpiece of the program is a full-scale six-story steel test structure that is constructed and tested in the Large Size Structures Laboratory of the Building Research Institute (BRI) operated by the MOC in Tsukuba, Japan. The full-scale test program is divided into four phases and the fourth phase involves installing nonstructural elements (i.e. precast concrete and glass fiber reinforced concrete panels, lightweight concrete walls, concrete block partitions, suspended ceilings, plastered and gypsum board partitions, and walls with steel doors attached and openings for large glass panels) and performing an additional series of tests. With regard to the precast panels, two general attachments are used (Roeder et al., 1987): the sway type connection, that employs a rigid bolted attachment at the floor with slotted holes at the top; and the rocking mechanism that permits three-dimensional movement at all the attachment points (Figure 2.88).

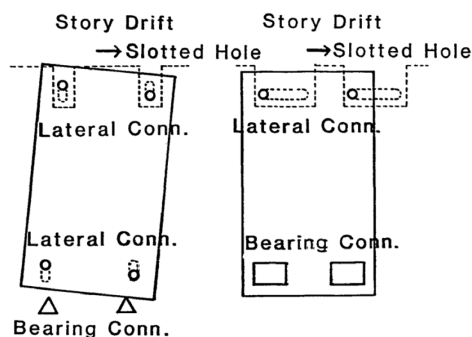


Figure 2.88 Mechanism of drift accommodation in cladding design (Wang, 1987)

In Foutch et al. (1987), the free and forced vibrations dynamic tests, performed on this full-scale six-story steel structure, are presented. These tests on the sample are conducted without and with the nonstructural elements, in order to investigate the stiffness and the period of the structure. The installation of the nonstructural elements reduces the first period of the building by 30%, which suggests that the overall structural stiffness is increased by more than 100%. Furthermore, the stiffness decreases when the elements start to damage and after 8 cycles (drift of 1/350) most of this additional stiffness is lost. Despite these important results, it is not possible to separate the particular contribution of the cladding, because the free vibration tests included either all or none of the nonstructural components.

The research team of Georgia Institute of Technology studies an existing 25-story steel-frame office structure (Palsson et al., 1984), in order to evaluate the effect of cladding panels on the free vibration properties. By comparing the ambient tests and the forced vibration test results (Goodno et al., 1983) with analytical values, it is found that the analytical periods of the bare frame structure are up to 34% and 48% greater than the measured translational and torsional periods, respectively.

Henry and Roll (1986) study the effects of the coating system on the modal properties of a nine-story and three bays reinforced concrete frame. The cladding panels are modeled using sixteen degrees of freedom shear elements, whereas the connections are considered as rigid elastic elements with fixed restraint conditions. According to a parametric study, it is found that the fundamental period is smaller than the bare frame one. However, according to Hunt and Stojadinovic (2010), the matter of this model is that the authors assume that the deformations of the cladding system occur in the panels themselves, even if the connection shear stiffness is much lower than the shear stiffness of the panel, that should be assumed as rigid block.

In different studies, Rihal (1988) and Meyyappa et al. (1981) find out that if the claddings are attached to the resistant structure the first two modal periods increase. One possible explanation, offered by Rihal, is that the effects of the added mass of the precast panels overcomes the additional stiffening offered by the panels themselves.

In a PEER (Pacific Earthquake Engineering Research Center) report, Hunt and Stojadinovic (2010) develop an extensive study on the cladding panel influence. The main result is the analytical nonlinear model used to investigate the interaction, as well as to determinate the connections demand. The investigated building is a nine-story steel building in Los Angeles. The building is modeled as a bare frame, i.e. with no cladding systems. Then, precast concrete cladding panels, modeled with finite elements, are added to the bare frame. The precast cladding panels are assumed to be rigid and are modeled with two-dimensional frames comprising rigid elastic beam elements. The behavior of frame with claddings is compared to the bare frame behavior. The results show that the fundamental period varies with a difference of only 4% between the bare frame and the frame with cladding. This means that, according to this approach, the cladding system does not significantly influence the building dynamic properties. The modal shapes were almost identical too. However, performed non-linear analyses show a significant influence of precast concrete panels on the structural behavior when strong motions occur.

During Emilia earthquake (2012) several panels systems in precast industrial buildings have collapsed due to the connection system failure. In these structures, connections between cladding panels and structural elements are provided by different solutions, based on steel connectors, such as channel bars, fasteners, angles, brackets. The

background on these specific European connections is quite limited with respect to the above mentioned connections in multistory U.S. buildings.

Colombo and Toniolo (2010) carry out an analytical study in order to find an alternative panel to structure connection system. The authors propose two models: the “isostatic” model provides panels, connected to the structure, with restraints that allow large displacements; the “collaborating” model includes wall panels connected to the main frame by fixed constraints. This last solution makes the panels integral part of the resistant system and requires a new design approach on a mixed frame-panel model. Modal analyses on a single-story industrial building are performed, providing a three-dimensional model that reproduces the structural geometry. The precast panels analytical model is represented by shell elements connected by two spherical hinges at the bottom, while at the top the panels are connected by two elements whose stiffness is taken very low or very high in order to analyze the “isostatic” or the “collaborating” model, respectively. The modal analysis results show that the first three vibration periods of the “collaborating” model are almost the one half of the corresponding periods of the “isostatic” model.

2.4.2 One-story precast buildings and panel-to-structure connection

In the previous section researches on the interaction between precast concrete panels and supporting structure are presented. Most of these studies concern steel multi-story buildings, generally typical North American office high-rise buildings. For these structural typologies, the cladding panels are different from the cladding panels used in industrial one-story precast buildings: they mainly consist of small size elements, i.e. spandrel panels and column covers, spaced by large windows.

In order to upgrade the knowledge about the specific case of industrial one-story precast buildings, this work studies the influence of vertical panels on the dynamic properties of this structural typology, in terms of first period of vibration.

The typical European industrial building configuration consists of columns, connected at the base through a monolithic connection (Osanai et al., 1996) and at the top by hinged prestressed beams, which support different typologies of roof elements (Figure 2.89). Precast concrete panels are typically employed as perimeter cladding elements. In Figure 2.90, the vertical panels arrangement is presented, i.e. the configuration studied in this study. Precast panels are made by reinforced concrete flat slabs and other materials (i.e. polystyrene), whose purposes are the weight reduction and the thermal insulation.

The precast concrete panel must be anchored with efficient connecting devices. In the case of horizontal panels, these devices connect the panel to the columns, while, in the case of vertical panels, they connect the panels to the roof horizontal beams. This study refers only to the vertical panels.

These panels are commonly considered as non-structural elements that are subjected to wind or earthquake actions, and to their own weight. If any interaction with the structure is neglected, the connection systems must ensure panel stability as well as must allow large interstory drifts, that occur during ground motions.

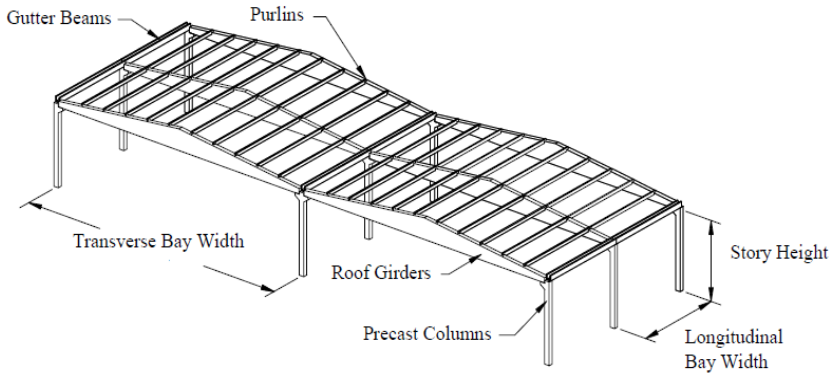


Figure 2.89 Geometrical configuration of a typical European one-story precast industrial building (Posada and Wood, 2002)

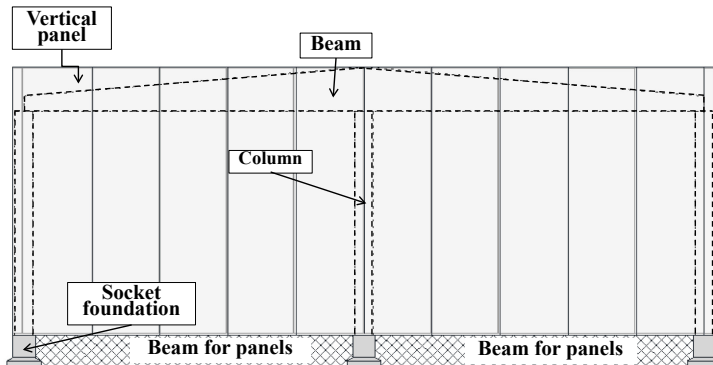


Figure 2.90 Typical vertical concrete panels arrangement in a precast one-story building

The investigated vertical panel connection system (Figure 2.91a) consists of two steel profiles, embedded in the element to be fixed (panel) and in the fixed element (horizontal element, e.g. beam). The two profiles (Figure 2.91b) are generally orthogonal in order to allow the adjustment of the panel in two directions. The connector (Figure 2.91d) is a steel plate, which may be knurled to prevent sliding; it has a hammer-end for the attachment in the connected element, and a slot for adjustment in the assembly phase. The connector links the interlock (Figure 2.91c) to the profile in the horizontal element. It follows that the connection yields three unrestrained, even though limited, translational degrees of freedom: one is ensured by the slot in the plate (typically displacement of 50 mm is allowed), and the other two are

due to the channel bars (the allowable displacement depends on the profiles length). At the bottom, the panel connection can be ensured in different ways. This connection may be achieved by clip-panel beams equipped with a fork, to which the base of the panel is rigidly connected using a mortar casting. This kind of connection is no longer in use due to the high cost of construction and to the low seismic efficiency. Welded or bolted metal anchors are today widespread.

According to the described characteristics and to the described studies, it is possible to classify the panel to structure connection and to choose the realistic model for numerical analyses. In particular, the investigated connection could be assumed as a sway-type connection. However, the seismic action is non-unidirectional load and during the ground motion the connections may be overloaded because space may be too small or the slot too short; furthermore, the sliding connections may be made ineffective by poor construction practice and lack of inspection, or the connection can deteriorate with time (Goodno and Palsson, 1986). It is simple to conclude that, if the above described connections are adopted, the panels may not be really free to slide with respect to the structure, as clearly evidenced in recent earthquakes (Magliulo et al., 2013).

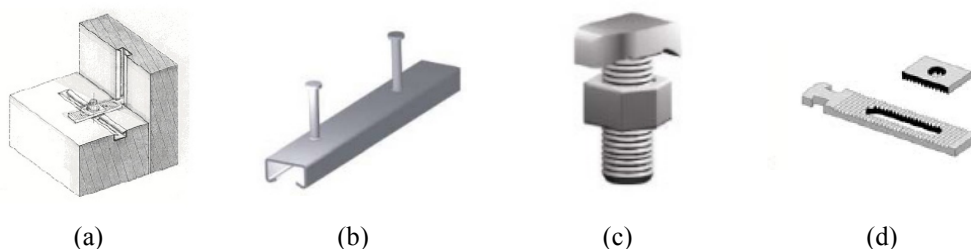


Figure 2.91 (a) Investigated connection between vertical precast panel and resistant structure: (b) channel bar, (c) interlock and (d) connector

2.4.3 First period of one-story precast buildings

The serious consequences to precast buildings during past seismic events, such as during the recent Emilia earthquake (2012), and the poor knowledge about the interaction between panels and precast structure are the motivations of this work. A parametric study is performed in order to evaluate the first period of one-story precast buildings, without and with the cladding system. In particular, the aim of the work is to compare the results of the model with cladding to the dynamic properties of the bare model, in order to evaluate the cladding system influence on the stiffness and on the first period of this structural typology.

The benchmark structure is a one-story precast structure and it is schematically described in Figure 2.92. The considered variable parameters are some geometrical characteristics: the columns height, H , (8 values), the length, $L_{bay,z}$, (3 values) and the number, $N_{bay,z}$, (2 values) of the transversal bays and, finally, the number of the

longitudinal bays, $N_{bay,x}$, (6 values). The values of these variables are shown in Table 2.8 and represent the overall range of one-story precast structure configurations. In Table 2.8 the cross sections of the columns for all the 288 case studies are reported. They are designed for a high seismicity Italian area (design peak ground acceleration at the bedrock equal to $0.27g$) according to Eurocode 8 (CEN, 2005). For each structure all the columns have the same square section, since this condition is widespread in industrial precast buildings. The concrete class is C45/55 for columns with elastic modulus equal to 36283 MPa . The seismic weights are obtained considering all structural and nonstructural elements (panels) as well as live loads on the structures; the values of the seismic weight range from 6 to 7 kN/m^2 .

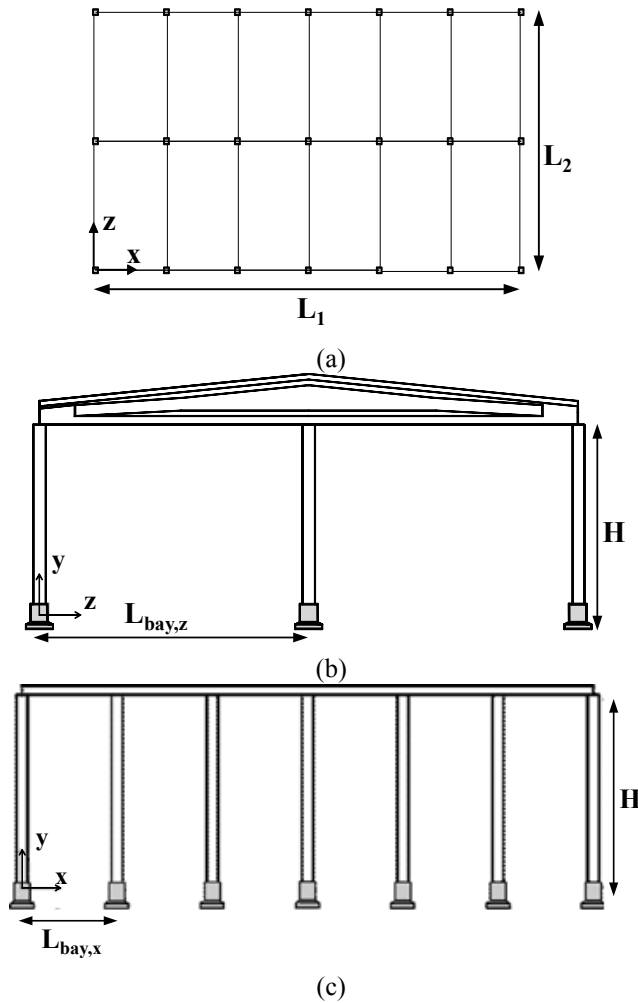


Figure 2.92 Benchmark one-story precast building: a plan view, b transversal bays and c longitudinal bays

Table 2.8 Columns cross sections reported as a function of the height of the structure (H) and of the number of the longitudinal bays ($N_{bay,x}$). Each diagram refers to one of the two values of transversal bays number ($N_{bay,z}$) and to one of the three values of transversal bays length ($L_{bay,z}$).

$N_{bay,z}$ [m]	1		2	
$L_{bay,z}$ [m]				
15m				
19m				
25m				
Symbols for columns section [cmxcm]	* 60x60		★ 80x80	
	○ 65x65		★ 85x85	
	□ 70x70		● 90x90	
	▼ 75x75		◆ 95x95	
			◀ 100x100	
			■ 105x105	
			x 110x110	
			▶ 115x115	

2.4.4 Bare structure model

The different case studies are modeled as bare three-dimensional structures in order to perform modal analyses.

Bare model consists of columns, girders (variable section beams) and secondary beams. Each of these elements is modeled as beam elastic element. For columns, halved inertia is considered due to the low values of axial loads in this type of structures. The structural model does not include roof elements, but they are considered in the mass evaluation.

The connection system of the column to the socket foundation is considered as a fixed joint (Osana et al., 1996). The beam-to-column connection is a pinned connection, that consists of a rubber support on the column and a steel dowel that connects the two

members (Magliulo et al., 2014a). This kind of connection is modeled as a hinge, not able to transfer bending forces, and hence all the beams are considered as pendulums. The roof is designed according to the code provisions in order to satisfy the rigid diaphragm hypothesis, assumed in the model. As a consequence, the total mass of the structure is concentrated in the master node at the roof level. In the 2D case the mass is assigned only in the direction of the frame while in the 3D case three degrees of freedoms are considered, i.e. the two horizontal translations and the rotation about the vertical axis.

The bare structure models are implemented in the OpenSees computer program. One of the case studies (evidenced by the red circle in Table 2) is also implemented in the SAP2000 program (CSI, 1978-2011), in order to validate the modeling process (Figure 2.94a). The comparison of the bi-dimensional and tri-dimensional case studies is shown in Table 3 in terms of first periods and demonstrates the fully matching of the two programs.

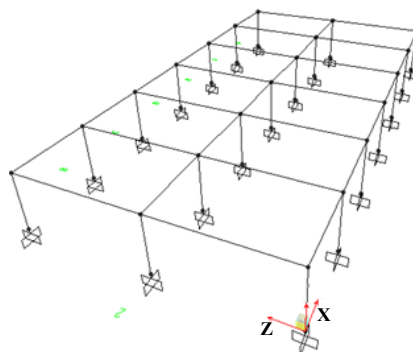


Figure 2.93 Linear elastic model of the bare structure in SAP2000

Table 2.9 First three periods of 2D and 3D bare models of a case study implemented in OpenSees and SAP2000

Period	2D – Longitudinal frame		2D – Transversal frame		3D	
	<i>SAP2000</i>	<i>OpenSees</i>	<i>SAP2000</i>	<i>OpenSees</i>	<i>SAP2000</i>	<i>OpenSees</i>
T_x [sec]	1.03	1.03	/	/	1.03	1.03
T_z [sec]	/	/	1.03	1.03	1.03	1.03
T_R [sec]	/	/	/	/	0.81	0.81

2.4.5 Model of the structure with cladding system

According to the described design approach, the panel-to-beam connections should be designed in order to allow large interstory drifts expected under dynamic actions and the vertical panels could be modeled as vertical pendulums. However, the connections adopted in the last years in Europe for panel-to-beam connections of one-story precast

industrial buildings do not actually accommodate interstory drift, causing interaction between structure and panels.

In order to take into account such an interaction the authors propose as model of the panel-to-structure connections:

- two hinge connections at the bottom of each panel;
- two constraints that allow rotations but avoid the sliding of the panel with respect to the beam, at the top of the panel.

The single panel is modeled as a two-dimensional frame (Figure 2.94a), as proposed in Hunt and Stojadinovic (2010), composed of four elastic one-dimensional elements:

- two vertical elements, characterized by area and moment of inertia equal to the half of area and moment of inertia of a single panel;
- two horizontal beams modeled as rigid bodies.

The vertical elements take into account the inertia properties of the panels and the two horizontal rigid elements give to the panel model the characteristics of a bi-dimensional element.

The seismic masses are assumed equal to the values of the bare models.

In all the models the rigid diaphragm hypothesis is used, assuming stiff and strong roof connections that allow a rigid behavior of the roof, also when the cladding panels interact with the structure.

The models with the cladding system are implemented in the OpenSees program. This proposed model is validated, comparing the modal analysis results with those obtained by a different model made by the SAP2000 program (Figure 2.94b), where the panels are implemented using shell elements.

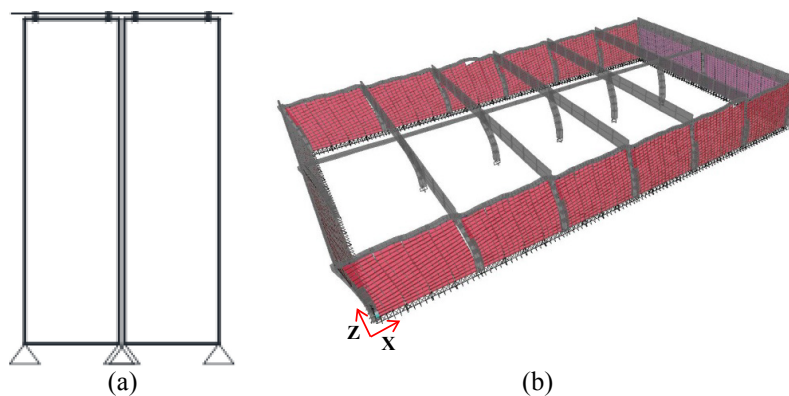


Figure 2.94 Linear elastic model of the structure with cladding system: a model of two vertical panels with the bi-dimensional frame and b 3D model with shell elements in SAP2000 program

In the following (Table 2.10), the first three periods of one of the case studies, with cladding panels modeled either as two-dimensional frames (OpenSees) or by shell elements (SAP2000), are listed. The maximum discrepancy is equal to 7% and it is justified by the different way in which the bi-dimensional elements (panels) are modeled.

Table 2.10 Modal analysis results of a case study with cladding panels modeled either as two-dimensional frames (OpenSees) or by shell elements (Shell - SAP2000)

Period	3D	
	<i>OpenSees</i>	<i>Shell - SAP2000</i>
T_z [sec]	0.166	0.174
T_x [sec]	0.120	0.130
T_R [sec]	0.0888	0.0933

The model of the cladding system (Figure 2.94a) with two-dimensional frames is proposed by the authors because of some advantages: it is easy to implement in computer programs and it can also be used to perform non-linear analyses, considering the panel-to-structure interaction in dynamic conditions. Moreover, the proposed cladding panel model gives the possibility to introduce the panel-to-panel interaction in non-linear analyses.

2.4.6 Linear modal analyses of the case studies

The performed parametric study provides the implementation of the 288 case studies, both bare and with cladding system. By comparing the results of Table 2.9 and Table 2.10, it is found that the first period may be reduced by about the 80% if the cladding system is considered in the models.

Starting from this result, the linear modal analyses of the 288 case studies are performed in order to generalize the results and to find a way to predict the modal properties of RC precast one-story buildings.

2.4.7 Modal analysis results of the bare case studies

In the following the results of the modal analyses for the bare structures are reported in terms of first period (Günaydın and Topkaya, 2013).

In Figure 2.95 the first vibrational periods are plotted versus the EC8 (CEN, 2005) and Italian code (D. M. 14/01/2008 2008) relationship (2.12). This formula is proposed to simply evaluate the first period of structures in linear analyses and it is equal to:

$$T_1 = C_1 \cdot H^{3/4} \quad (2.12)$$

where H is the total height of the structure in meters and C_1 is a coefficient that depends on the structural system: for precast structures C_1 is assumed equal to the value used for concrete framed structures, that is equal to 0.075.

In Figure 2.95 the gray line denotes the period values obtained by the code formula (2.12) and the black circles are the first periods from the performed linear modal analyses. The trend shows that the code relationship always returns lower values with respect to those obtained by modal analysis, considering stiffer structures.

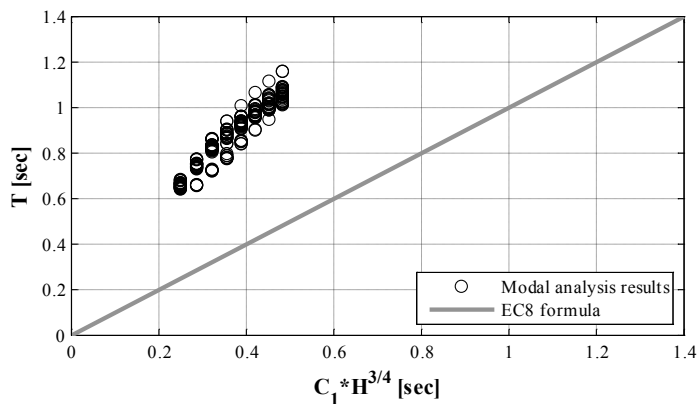


Figure 2.95 Values of the first period, T , obtained by modal analyses (black circles), versus the EC8 formula (1) (gray line) for bare structures

In order to propose a more effective formula, different regression analyses are performed on the results of the linear modal analyses, as proposed in Goel and Chopra (1997):

- unconstrained regression analysis in order to determine the values of α and β of the relationship: $T = \alpha \cdot H^\beta$, that corresponds to a linear regression problem based on the relationship:

$$\log(T) = \log(\alpha) + \beta \cdot \log(H) \quad (2.13)$$

- constrained regression analysis with the β of the previous analysis, rounded off to the nearest 0.05, e.g. $\beta = 0.51$ is rounded off to 0.50 and $\beta = 0.53$ is rounded off to 0.55;
- constrained regression analysis with the EC8 value for β , i.e. 0.75.

These procedures give different best-fit curves of the modal analysis data.

The standard error of the analysis (Goel and Chopra, 1997) is equal to:

$$s_e = \sqrt{\frac{\sum_{i=1}^n [\log(T_i) - (\log(\alpha) + \beta \cdot \log(H))]^2}{(n-2)}} \quad (2.14)$$

For a force-based design approach, the 16th percentile of the first periods could be also used (Goel and Chopra, 1997). Since the $\log(T)$ variable is assumed to be normal distributed and since s_e approaches the standard deviation for large number of samples, the 16th percentile value is found with a value of α_r equal to:

$$\log(\alpha_r) = \log(\alpha) - s_e \quad (2.15)$$

Table 2.11 shows the results of the performed regression analyses in terms of: proposed formula to predict the period (1st row), correlation factor (2nd row), standard error (3rd row), proposed formula, for which the 16% of the measured periods would fall below the corresponding curve (4th row). By comparing the analyses, it is found that: i) the error, s_e , increases when β highly deviates from its unconstrained value; ii) the correlation factor, R^2 , is quite low only in the case of β equal to the EC8 value; iii) the error and the correlation factor are insensitive to the assumed β rounding.

Table 2.11 Results of the three regression analyses for the bare precast buildings in terms of: proposed formula to predict the period (1st row), correlation factor (2nd row), standard error (3rd row), proposed formula for which the 16% of the measured periods would fall below the corresponding curve (4th row)

	Unconstrained	Rounded off β	$\beta_{EC8} = 0.75$
Period [sec] best fit	$T_L=0.28 H^{0.54}$	$T_L=0.27 H^{0.55}$	$T_L=0.18 H^{0.75}$
R^2 [-]	0.92	0.92	0.78
s_e [-]	0.0440	0.0441	0.0744
Period [sec] 16th perc.	$T_{16th}=0.27 H^{0.54}$	$T_{16th}=0.26 H^{0.55}$	$T_{16th}=0.16 H^{0.75}$

The regression formulas, predicting the first period as a function of the building height, are drawn in Figure 2.96 in terms of best fit curve (solid lines) and 16th percentile curve (dash-dot lines). In this figure the formula with the rounded off coefficient β (Table 2.11, 3rd column) and with the EC8 value (Table 2.11, 4th column) are compared. On the other hand, the formulas obtained by the constrained regression analysis with the β EC8 value (gray lines) do not fit well the modal analysis results.

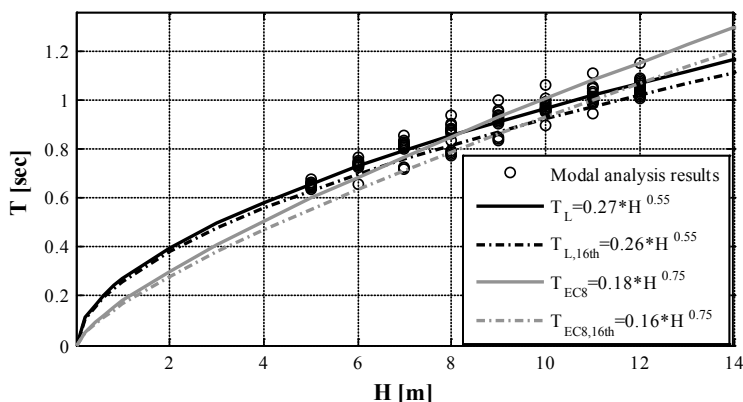


Figure 2.96 Values of the first period, T , obtained by modal analyses (black circles), versus the height of the structure, H , for bare buildings, along with the best fit curves (solid lines) from the linear regression analyses, and the 16th percentile curves (dash-dot lines)

2.4.8 Modal analysis results with cladding system

In the following the results of the modal analyses of the one-story precast buildings with cladding system are reported in terms of first periods. For all the structures with claddings the first mode is in the transversal direction (short side).

Figure 2.97 shows the first vibrational periods versus the EC8 formula (1), where C_1 is equal to 0.075. As first conclusion, it can be stated that the first vibration periods are significantly influenced by the presence of the cladding system, presenting large variations with respect to the case of bare frame (reduction up to 80%). As a consequence, the trend of the results of the modal analyses is different with respect to the results of the bare buildings: the most of the points are arranged below the bisector line. It is evident that the EC8 formula (gray line) overestimates the first period of the buildings with cladding system (black circles), considering more flexible structures.

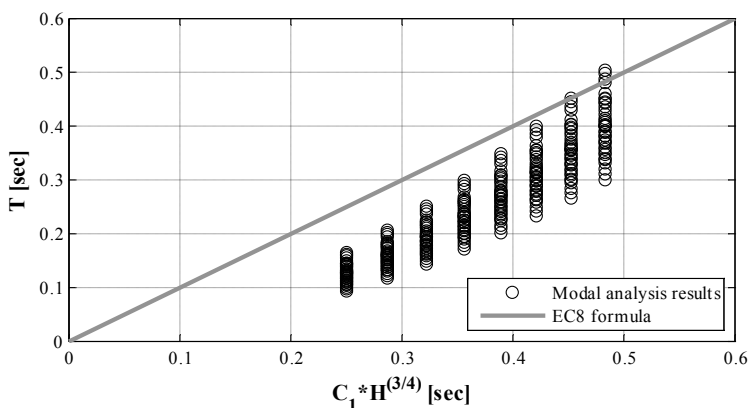


Figure 2.97 Values of the first periods, T , obtained by modal analyses (black circles), versus the EC8 formula (1) for one-story precast buildings with cladding system (gray line)

As for the bare case studies, different regression analyses are performed and the results are reported in Table 2.12 in terms of: proposed formulas to predict the first period (1st row), correlation factor (2nd row), standard error (3rd row) and proposed formulas for which the 16% of the measured periods falls below the corresponding curve (4th row). Figure 2.98 shows the best fit curve (solid lines) and 16th percentile curve (dash-dot lines) from the unconstrained regression analysis (black lines) and the constrained regression analysis with the EC8 value for β (gray lines). All the regression analyses give higher errors and lower correlation factors if compared to the bare buildings results: the relationship that includes only the height provides a worse fit of analytical results.

Table 2.12 Results of the regression analyses for buildings with cladding system in terms of: proposed formulas to predict the first period (1st row), correlation factor (2nd row), standard error (3rd row) and proposed formulas for which the 16% of the measured periods falls below the corresponding curve (4th row)

	Unconstrained	Rounded off β	$\beta_{EC8} = 0.75$
Period best fit (T_L) [sec]	$T_L=0.0149 H^{1.31}$	$T_L=0.0137 H^{1.35}$	$T_L=0.0484 H^{0.75}$
R^2 [-]	0.88	0.88	0.72
s_e [-]	0.137	0.137	0.210
Period (T_{16th}) [sec]	$T_{16th}=0.0130 H^{1.31}$	$T_{16th}=0.0119 H^{1.35}$	$T_{16th}=0.0392 H^{0.75}$

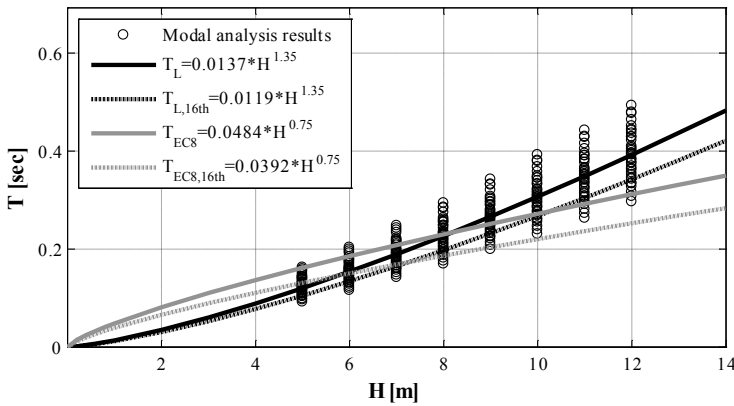


Figure 2.98 Values of the first periods, T , obtained by modal analyses (black circles), versus the height of the structure, H , for buildings with cladding panels, along with the best fit curves (solid lines) from the linear regression analyses, and the 16th percentile curves (dash-dot lines)

In order to find a better relationship, some geometrical characteristics, besides the building height, are considered (Goel and Chopra, 1998) and the following function is found to be the most suitable to fit the modal analysis results:

$$F_1 = \sqrt{L_x} \cdot H^{3/2} \quad (2.16)$$

where L_x represents the long side length (in meters) of the building and H is its total height (in meters).

In Figure 2.99 the first natural periods are reported as a function of the expression (6) along with the best fit curve from the linear regression analysis (solid black line) and the 16th percentile curve (dash-dot gray line). The experimental data are arranged according to a clear increasing linear law: the matching of the linear regression curve is very high, as proved by the correlation factor equal to 0.94.

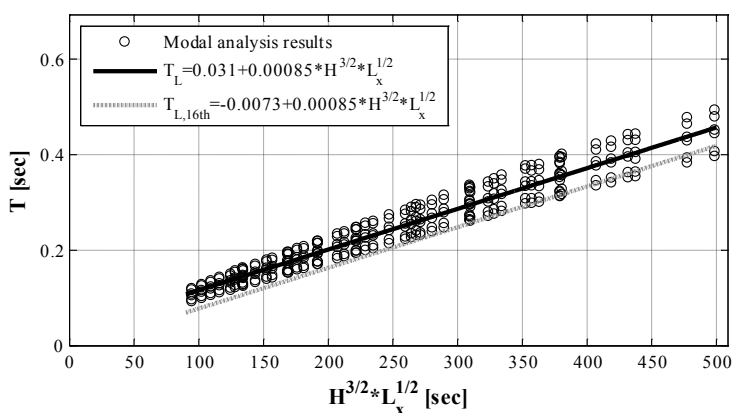


Figure 2.99 Values of the first periods, T , obtained by modal analyses (black circles), versus the $F1$ function (6) for buildings with cladding system, along with the best fit curve (solid black line) from the linear regression analysis, and the 16th percentile curve (dash-dot gray line)

2.4.9 Seismic zones

The described parametric study has been performed on buildings designed for a single high seismic zone (I in Table 2.13). In this Section this study is extended to other three seismic zones in order to cover a wider range of buildings. The same geometrical variables are considered and the same 288 case studies are implemented in OpenSees program in order to perform linear modal analyses. The design of these case studies is performed for the new seismic zones but the results in terms of section dimensions and masses are not presented in this work for sake of brevity.

Table 2.13 shows the considered seismic zones, in terms of peak ground acceleration on rock soil for a return period equal to 50 years (a_g , 2nd column) and 475 years (a_g , 3rd column), and peak ground acceleration for a return period equal to 475 years and EC8 type B soil (PGA, 4th column).

Table 2.13 Assumed seismic zones: peak ground acceleration on rock soil for a return period equal to 50yy (2nd column) and 475yy (3rd column), and peak ground acceleration for EC8 with type B soil (4th column)

<i>Seismic zone</i>	a_g ($T_R = 50yy$)	a_g ($T_R = 475yy$)	<i>PGA</i> ($T_R = 475yy$)
[-]	[g]	[g]	[g]
I	0.108	0.270	0.324
II	0.078	0.196	0.235
III	0.062	0.154	0.185
IV	0.042	0.105	0.126

Figure 2.100 shows T_1 as a function of $C_1 \cdot H^{3/4}$ for bare one-story precast buildings with floor rigid in its own plane, designed according to all the considered seismic zones. The results demonstrates again that the EC8 formula returns lower values than those obtained by modal analyses.

Table 2.14 shows the results of the regression analyses previously computed for the I seismic zone (2nd column), but extended to the II, III and IV zone (3rd, 4th and 5th column, respectively). The first row lists the regression formulas computed assuming a value of β rounded off to the nearest 0.05 with respect to the β value computed by the unconstrained regression analysis. The second and the third row list the correlation factors and the standard errors, respectively. The fourth row lists the proposed formulas for which the 16% of the measured periods would fall below the corresponding curve. According to the reported results, the regression analyses with the β values rounded off to the nearest 0.05 give very good results in terms of correlation factor and standard error for each value of PGA.

In Figure 2.101 the first periods obtained by the modal analysis (circles) of the considered bare one-story precast buildings are plotted along with the best fit curve (dash-dot black line) from the linear regression analysis and the 16th percentile (dash-dot gray line) regression formula. A plot is reported for each seismic zone.

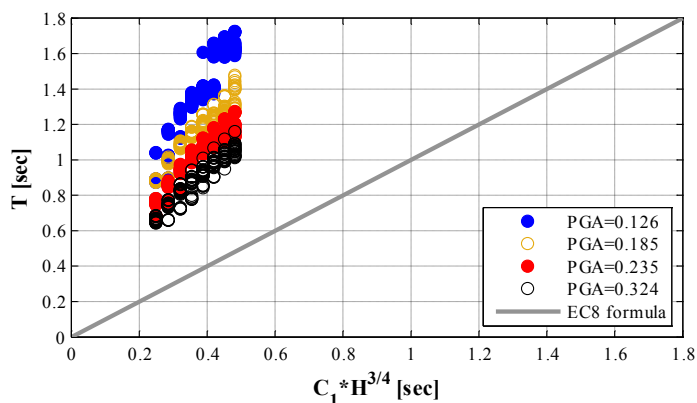


Figure 2.100 Values of the first periods, T , obtained by modal analyses (circles), versus the EC8 formula (2.12) for bare one-story precast buildings (gray line) in all the assumed seismic zones

Table 2.14 Results of the regression analyses of the bare one-story precast buildings in the four seismic zones in terms of: proposed formulas to predict the first period (1st row), correlation factor (2nd row), standard error (3rd row) and proposed formulas for which the 16% of the measured periods falls below the corresponding curve (4th row)

	Best fit (T_L)	R^2	s_e	16 percentile T_{16th}
	[sec]	[-]	[-]	[sec]
Rounded off β I zone	$0.27 \cdot H^{0.55}$	0.92	0.0441	$0.26 \cdot H^{0.55}$
Rounded off β II zone	$0.31 \cdot H^{0.55}$	0.92	0.0423	$0.30 \cdot H^{0.55}$
Rounded off β III zone	$0.31 \cdot H^{0.60}$	0.87	0.0621	$0.30 \cdot H^{0.60}$
Rounded off β IV zone	$0.27 \cdot H^{0.75}$	0.87	0.0826	$0.25 \cdot H^{0.75}$

In order to give a common formula for the first periods of bare one-story precast buildings in different seismic zones, a regression analysis is performed on all the values of first period, providing α equal to 0.30 and β equal to 0.60. As evidenced by the Figure 2.102 and by the correlation factor ($R^2 = 0.52$), the matching of the regression curve is lower than in the case of the single seismic zone (Table 2.14). Then, a new parameter (PGA) is introduced in the period formula.

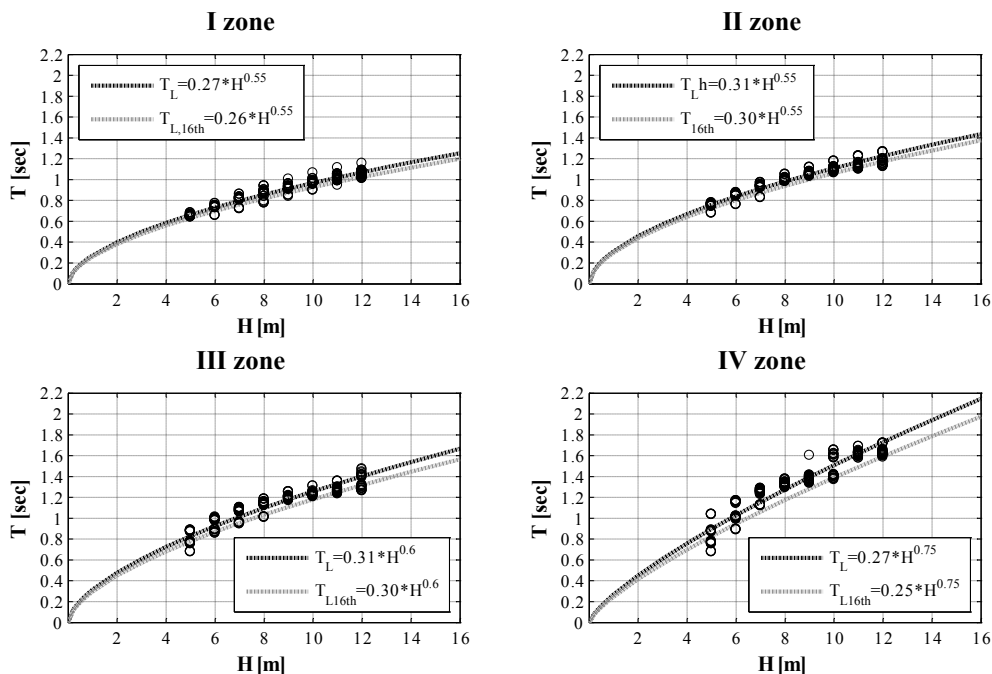


Figure 2.101 Regression analyses results for bare structures in all the considered seismic zones: first periods, T , obtained by the modal analyses (black circles), versus the height of the structure, H , along with the best fit curve (dash-dot black line) from the linear regression analysis and the 16th percentile curve (dash-dot gray line)

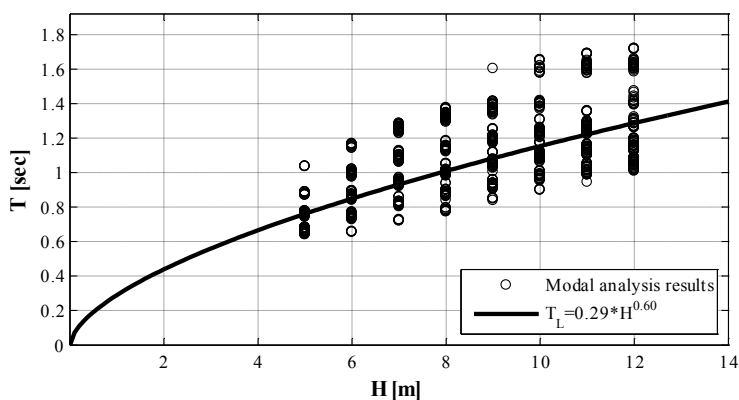


Figure 2.102 First periods, T , obtained by modal analyses (black circles), versus the height of the structure, H , along with the proposed formula (black line), obtained from the regression analysis on the bare buildings designed for all the seismic zones

This formula is evaluated according to the following procedure:

- a rounded mean value of β factor is assumed, equal to 0.60;
- a regression analysis for each seismic zone is carried out with $\beta = 0.60$ (Table 2.15);
- since a decreasing trend of α values with the seismic PGA is found, an α - PGA regression analysis is carried out and the resulting relationship (Figure 2.103) is inserted in the period formula (Figure 2.104).

In Table 2.15, for each seismic zone (1st column), the results of the constrained regression analyses ($\beta = 0.60$) on the first periods of the modal analyses, are listed in terms of α values (2nd column) and correlation factors (4th column). In Figure 2.103 the α values of Table 2.15 (the circles) are plotted as a function of PGA (expressed in g), along with their regression curve:

$$\alpha = 0.16 \cdot PGA^{-0.4} \quad (2.17)$$

In Figure 2.104 the first periods of all the bare buildings (circles) obtained by modal analyses are reported along with the proposed period formula (PGA is in g):

$$T = 0.16^2 \cdot PGA^{-0.4} \cdot H^{0.6} \quad (2.18)$$

Table 2.15 α , β and R^2 values from regression analysis for each seismic zone

Zone	α	β	R^2
I	0.25	0.6	0.91
II	0.28		0.90
III	0.31		0.87
IV	0.36		0.84

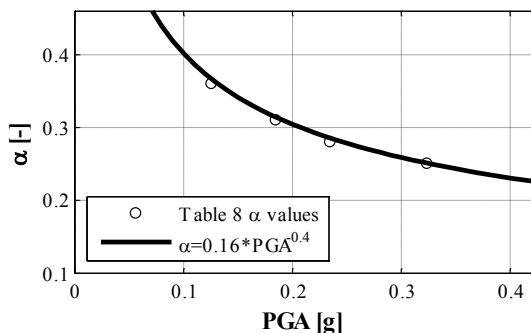


Figure 2.103 Table 2.15 α values (black circles) versus the corresponding PGA and their regression curve (black solid line)

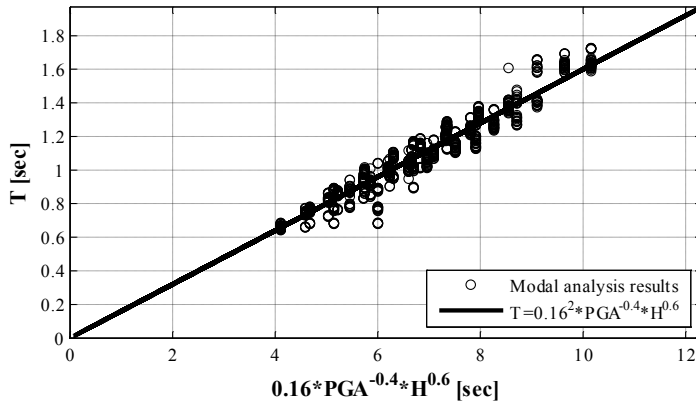


Figure 2.104 First periods, T , obtained by modal analyses (black circles), versus the proposed formula (2.18) for one-story precast bare buildings (black solid line)

The extended parametric study is then carried out for buildings that include the external cladding system. In Figure 2.105 the first periods of these buildings, obtained by the modal analysis, are plotted as a function of the EC8 first period formula, along with this formula itself.

Figure 2.105 shows again that the trend of the periods from the modal analysis (circles) is opposite to that found for bare frames: the most of the points are arranged below the EC8 formula line (gray line).

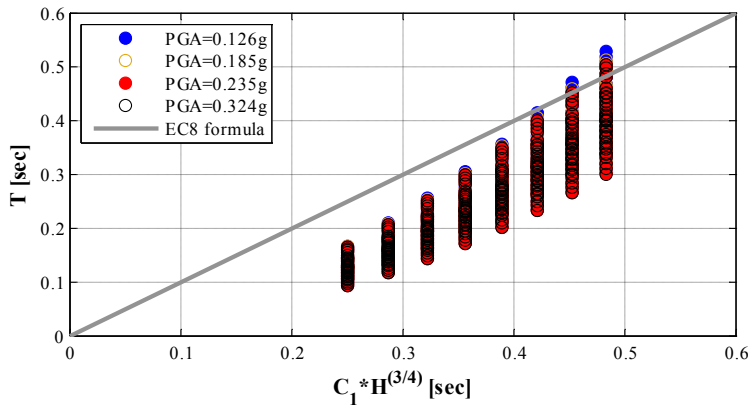


Figure 2.105 Values of the first periods, T , obtained by modal analyses (circles), versus the EC8 formula (1) for one-story precast buildings with cladding system (gray line) in all the assumed seismic zones

In order to find a better relationship for the first period of one-story precast buildings with floor rigid in its own plane and cladding system, the F_1 function (6) is considered.

In Figure 2.106 the first natural periods of the buildings with cladding system, designed for all the four considered seismic zones (black circles), are reported as a function of the F_1 parameter, along with the corresponding linear regression line (black line). The first periods are arranged according to a clear linear increasing law: the matching of the regression line is very high, as proved by the correlation factor equal to 0.93 and by a low standard error equal to 0.025 sec.

Figure 2.106 also shows the 16th percentile curve (dash-dot gray line) of the regression formula. Then, the following new formula is proposed in order to evaluate the first vibration period of one-story precast buildings with floor rigid in its own plane and cladding system:

$$T_1 = 0.00088 \cdot H^{3/2} \cdot L_x^{1/2} \quad (2.19)$$

where L_x represents the long side length in meters of the building and H is its total height in meters. In formula (2.19) the intercept value is neglected in order to have a simpler relationship, obtaining anyway lower period values (red line in Figure 2.106), which generally are on the safe side.

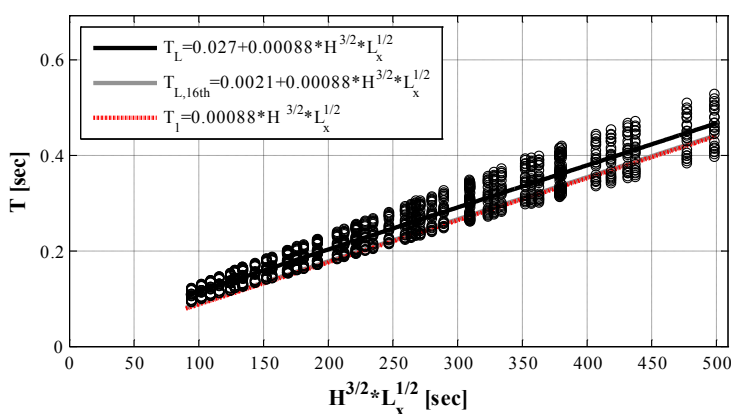


Figure 2.106 First periods, T , obtained by modal analyses (black circles), versus the F_1 factor (6), along with the best fit curve (solid black line) from the linear regression analysis, the 16th percentile curve (solid gray line) and the proposed formula (9) (dash-dot red line)

2.4.10 Closing remarks

The main purpose of the described work is the investigation of the cladding system influence on the first vibration period of one-story precast buildings with floor rigid in its own plane.

A bibliographic research shows the poor knowledge on the seismic behavior and interaction with the structure of precast concrete cladding panels, in the case of one-story precast buildings.

As a consequence, the present study starts with the definition of a linear model that includes cladding panels. The proposed model has different advantages:

- the element adopted to simulate the panel behavior is suitable to the implementation in non-linear models;
- the proposed cladding system model allows to introduce additional constraints to take into account the interaction between panels;
- the constraints between panel and main structure can be introduced easily.

A parametric study is performed in order to evaluate the dynamic properties (the first period) of 288 realistic buildings, designed according to EC8 and for different seismic zones. The considered variables are some geometrical characteristics of the structures: columns height, number and width of the bays in both the main directions of the building.

From the analysis of the first period values, the following conclusions can be drawn.

- The first vibration period is significantly influenced by the presence of the cladding system, presenting large variations with respect to the case of bare buildings (reduction up to 80%).
- The simplified EC8 formula, that evaluates the first vibration period as a function of the height of the building ($C_1 \cdot H^{\frac{3}{4}} = 0.075 \cdot H^{\frac{3}{4}}$), is not suitable either for the case of the bare building or for the case of building with cladding system. This relationship strongly underestimates the first periods of the analyzed bare one-story precast buildings, and overestimates the first periods of the same buildings with cladding system.
- With reference to the analyzed bare one-story precast buildings, a different relationship is found: $T_1 = 0.26 \cdot H^{0.55}$. This relationship is similar to the current EC8 formula and then it could be easily implemented in this seismic code.
- Extending the parametric study to four different seismic zones, the peak ground acceleration PGA is introduced as a new parameter in the period formula and a new relationship is found:

$$T_1 = 0.16^2 \cdot PGA^{-0.4} \cdot H^{0.6} \quad (2.20)$$

- In the case of one-story precast buildings with cladding system, a very good relationship is found between the first period and a proposed function, that depends on a plan dimension of the building and on its height. This relationship has a very good correlation factor and a low standard error for all the four studied seismic zones. The new formula, proposed to evaluate the first vibrational period of one-story precast buildings with cladding system, is:

$$T_1 = 0.00088 \cdot H^{3/2} \cdot L_x^{1/2} \quad (2.21)$$

where L_x represents the long side length of the building in meters and H is its total height in meters.

The formula providing the period of bare one-story precast buildings gives a realistic value of the first period and could be used in the design seismic forces evaluation when linear static analyses are performed. Moreover, a correct evaluation of periods for one-story precast buildings with cladding panels is the first step to justify the damage in these buildings under seismic actions, since it allows evaluating the demand on structural elements and connections.

It should be underlined that the above presented conclusions and results are related and limited to one-story precast buildings with vertical panels, as well as to the described panel-to-structure connections.

Reference

- Baird, A., Palermo, A. and Pampanin, S. (2011), *Facade damage assessment of multi-storey buildings in the 2011 Christchurch earthquake*, Bulletin of the New Zealand Society for Earthquake Engineering. **44**(4), 368-376.
- Bonfanti, C., Carabellese, A. and Toniolo, G. (2008), *Strutture prefabbricate: catalogo delle tipologie esistenti (in Italian)*, www.reluis.it/images/stories/Catalogo%20tipologie%20strutture%20prefabbricate.pdf, April the 13th, 2013.
- Caltrans (1994), *Bridge memo to designers. Section 7: Bridge Bearings*, California Department of Transportation.
- CEN (2005), *Eurocode 8: design of structures for earthquake resistance - Part 1: general rules, seismic actions and rules for buildings. EN 1998-1*, Brussels, Belgium.
- Circolare 02/02/2009 n. 617 (2009), *Istruzioni per l'applicazione delle "Nuove norme tecniche per le costruzioni" di cui al D.M. 14 gennaio 2008*.
- Circolare del Ministero dei Lavori Pubblici n.1422 (1965), *Istruzioni per il rilascio della dichiarazione di idoneità tecnica dei sistemi costruttivi e strutture portanti prevista negli art. 1 e 2 della Legge 5 novembre 1964, n. 1244 con particolare riferimento alle strutture prefabbricate (in Italian)*.
- Cleland, N. and Ghosh, S.K. (2007), *Seismic Design of Precast/Prestressed Concrete Structures*.
- CNR-UNI 10012 (1967), *Ipotesi di carico sulle costruzioni (in Italian)*.
- Colombo, A. and Toniolo, G. (2010), *Problemi di progettazione sismica delle connessioni dei pannelli di tamponamento ((in Italian)*, In Diciottesimo congresso del Collegio dei Tecnici della Industrializzazione Edilizia, Brescia, Italy. 799-806
- CSI (1978-2011), *SAP2000 Linear and Nonlinear Static and Dynamic Analysis and Design Of Three Dimensional Structures*, CSI Computer & Structures, Berkeley, California.
- D'Ambrisi, A., De Stefano, M. and Tanganelli, M. (2009), *Use of pushover analysis for predicting seismic response of irregular buildings: A case study*, Journal of Earthquake Engineering. **13**(8), 1089-1100.
- D. M. 14/01/2008 (2008), *Norme Tecniche per le Costruzioni (in Italian)* G.U. n. 29 4 febbraio 2008.
- Decreto-Legge n. 74 del 6 giugno 2012 (2012), *Interventi urgenti in favore delle popolazioni colpite dagli eventi sismici che hanno interessato il territorio delle province di Bologna, Modena, Ferrara, Mantova, Reggio Emilia e Rovigo, il 20 e il 29 maggio 2012*.
- Decreto Ministeriale 3/12/1987 (1987), *Norme tecniche per la progettazione, esecuzione e collaudo delle costruzioni prefabbricate (in Italian)*, G.U. n. 106 07/5/1988.
- Decreto Ministeriale del 16/01/1996 (1996), *Norme tecniche relative ai criteri generali per la verifica di sicurezza delle costruzioni e dei carichi e sovraccarichi (in Italian)*, G.U. n. 29 05/2/1996
- Department of Civil Protection (2008), *Scheda di 1° livello di rilevamento danno, pronto intervento e agibilità per edifici ordinari nell'emergenza post-sismica*.

- Ercolino, M., Coppola, O., Petrone, C. and Magliulo, G. (2012a), *Report sui danni registrati a Mirandola (MO) in seguito all'evento sismico del 29 maggio 2012 (in Italian)*, http://www.reluis.it/images/stories/2012_05_29_report%20Mirandola.pdf 28 May 2013.
- Ercolino, M., Coppola, O., Petrone, C. and Magliulo, G. (2012b), *Report sui danni registrati a San Felice sul Panaro (MO) in seguito agli eventi sismici del 20 e 29 maggio 2012* http://www.reluis.it/images/stories/report_San-Felice-sul-Panaro_20-29maggio.pdf, 28 May 2013.
- Faggiano, B., Iervolino, I., Magliulo, G., Manfredi, G. and Vanzi, I. (2009), *Post-event analysis of industrial structures behavior during L'Aquila earthquake*, *Progettazione sismica 3 English Special Edition* 203-208.
- Fardis, M.N. and Biskinis, D. (2003), *Deformation capacity of RC members, as controlled by flexure or shear*.
- Foutch, D.A., Goel, S.C. and Roeder, C.W. (1987), *Seismic Testing of Full-Scale Steel Building .I.*, *J Struct Eng-Asce.* **113**(11), 2111-2129.
- Goel, R. and Chopra, A. (1997), *Period Formulas for Moment-Resisting Frame Buildings*, *Journal of Structural Engineering.* **123**(11), 1454-1461.
- Goel, R. and Chopra, A. (1998), *Period Formulas for Concrete Shear Wall Buildings*, *Journal of Structural Engineering.* **124**(4), 426-433.
- Goodno, B.J., Craig, J.I., Meyyappa, M. and Palsson, H. (1983), *Cladding-Structure Interaction in Highrise Buildings*, CEE-7704269.
- Goodno, B.J. and Palsson, H. (1986), *Analytical Studies of Building Cladding*, *J Struct Eng-Asce.* **112**(4), 665-676.
- Grünthal, G. (1998), *European Macroseismic Scale 1998*, *Cahiers du Centre Européen de Géodynamique et de Séismologie: Volume 15*.
- Gruppo di Lavoro Agibilità Sismica dei Capannoni Industriali (2012), *Linee di indirizzo per interventi locali e globali su edifici industriali monopiano non progettati con criteri antisismici*.
- Günaydın, E. and Topkaya, C. (2013), *Fundamental periods of steel concentrically braced frames designed to Eurocode 8*, *Earthq Eng Struct Dyn.* **42**(10), 1415-1433.
- Henry, R. and Roll, F. (1986), *Cladding-Frame Interaction*, *Journal of Structural Engineering.* **112**(4), 815-834.
- Hunt, P.J. and Stojadinovic, B. (2010), *Seismic Performance Assessment and Probabilistic Repair Cost Analysis of Precast Concrete Cladding Systems for Multistory Buildings*, *Pacific Earthquake Engineering Research Center, College of Engineering, University of California, Berkeley*.
- Ibarra, L.F., Medina, R.A. and Krawinkler, H. (2005), *Hysteretic models that incorporate strength and stiffness deterioration*, *Earthq Eng Struct Dyn.* **34**(12), 1489-1511.
- INGV (2012), <http://zonesismiche.mi.ingv.it>.
- Legge 01/08/2012 n. 122 (2012), *Conversione in legge, con modificazioni, del decreto-legge 6 giugno 2012, n. 74, recante interventi urgenti in favore delle popolazioni colpite dagli eventi sismici che hanno interessato il territorio delle province di Bologna, Modena, Ferrara, Mantova, Reggio Emilia e Rovigo, il 20 e il 29 maggio 2012*.

- Legge n. 64 (1974), *Provvedimenti per le costruzioni con particolari prescrizioni per le zone sismiche (in Italian)*, G.U. n. 76 21/3/1974.
- Legge n. 1224 (1964), *Integrazioni della legge 25 novembre 1962, n. 1684, concernente provvedimenti per l'edilizia con particolari prescrizioni per le zone sismiche (in Italian)*, G.U. n. 297 01/12/1964.
- Legge n. 1684 (1962), *Provvedimenti per l'edilizia con particolari prescrizioni per le zone sismiche (in Italian)*, G.U. n. 326 22/12/1962
- Luzi, L., Hailemikaël, S., Bindi, D., Pacor, F., Mele, F. and Sabetta, F. (2008), *ITACA (ITalian ACcelerometric Archive): A web portal for the dissemination of Italian strong-motion data*, Seismol Res Lett. **79**(5), 716-722.
- Magliulo, G., Capozzi, V., Fabbrocino, G. and Manfredi, G. (2011), *Neoprene-concrete friction relationships for seismic assessment of existing precast buildings*, Eng Struct. **33**(2), 532-538.
- Magliulo, G., Ercolino, M., Cimmino, M., Capozzi, V. and Manfredi, G. (2014a), *Numerical evaluation of the strength of beam-to-column dowel connections in precast buildings under monotonic actions*, Construction and Building Materials (under review).
- Magliulo, G., Ercolino, M. and Manfredi, G. (2014b), *Influence of cladding panels on the first period of one-story precast buildings*, Bulletin of Earthquake Engineering (under review).
- Magliulo, G., Ercolino, M., Petrone, C., Coppola, O. and Manfredi, G. (2013), *Emilia Earthquake: the Seismic Performance of Precast RC Buildings Earthq Spectra*.
- Magliulo, G., Fabbrocino, G. and Manfredi, G. (2008), *Seismic assessment of existing precast industrial buildings using static and dynamic nonlinear analyses*, Eng Struct. **30**(9), 2580-2588.
- Mandelli, C., Palermo, A. and Toniolo, G. (2007), *Strutture prefabbricate: schedario dei collegamenti (in Italian)*, <http://www.reluis.it>, April the 13th, 2013.
- McKenna, F. and Fenves, G.L. (2013), *OpenSees Manual* <http://opensees.berkeley.edu>, Pacific Earthquake Engineering Research Center.
- Meyyappa, M., Palsson, H. and Craig, J., I. (1981), *Modal Parameter Estimation for a Highrise Building Using Ambient Response Data Taken During Construction*, Proc. 2nd Specialty Conf. Dyn. Resp. Struct.: Experimentation, Observation, Prediction, and Control, Atlanta, Georgia. 141-151.
- OPCM 3274 (2003), *Primi elementi in materia di criteri generali per la classificazione del territorio nazionale e di normative tecniche (in Italian)*, G.U. n. 105 del 08/05/2003.
- Osanaï, Y., Watanabe, F. and Okamoto, S. (1996), *Stress transfer mechanism of socket base connections with precast concrete columns*, Aci Structural Journal. **93**(3), 266-276.
- Palsson, H., Goodno, B.J., Craig, J.I. and Will, K.M. (1984), *Cladding influence on dynamics response of tall buildings*, Earthq Eng Struct Dyn. **12**(2), 215-228.
- PCI (2007), *Architectural Precast Concrete Manual Committee*, PCI, West Jackson Blvd, Chicago.

- Posada, M. and Wood, S.L. (2002), *Seismic Performance of Precast Industrial Buildings in Turkey*, Proceedings, 7th U.S. National Conference on Earthquake Engineering, Earthquake Engineering Research Institute, Boston, MA. 543.
- Rihal, S.S. (1988), *Earthquake resistance and behavior of heavy facades/claddings and connections in medium-rise steel-framed buildings*, Proceedings of Ninth World Conference on Earthquake Engineering, Tokyo-Kyoto, JAPAN. **6** 207-212.
- Roeder, C.W., Foutch, D.A. and Goel, S.C. (1987), *Seismic Testing of Full-Scale Steel Building* .2., J Struct Eng-Asce. **113**(11), 2130-2145.
- Saatcioglu, M., Mitchell, D., Tinawi, R., Gardner, N.J., Gillies, A.G., Ghobarah, A., Anderson, D.L. and Lau, D. (2001), *The August 17, 1999, Kocaeli (Turkey) earthquake damage to structures*, Can J Civil Eng. **28**(4), 715-737.
- Wang, M.L. (1987), *Cladding Performance on a Full Scale Test Frame*, Earthq Spectra. **3**(1), 119-173.

Chapter 3

LOCAL SEISMIC BEHAVIOR

The global structural response of RC precast buildings is largely influenced by the behavior of the connections between structural elements and between structural and non-structural components. Recent violent seismic events in Europe hit the precast structural typology and the most of the damages have been caused by the failure of the connection systems (Magliulo et al., 2013), among which the beam-to-column connections. The failure of these connections is mainly caused by two reasons: 1) the attainment of the frictional strength, if the connections do not provide mechanical devices in resisting horizontal actions (in the following, frictional connections); 2) the inadequacy of seismic details in the connected structural elements, e.g. low transversal reinforcement percentages at the ends of the RC elements, mainly related to the poor knowledge about the seismic behavior of these connections and to the lack of code design requirements. The frictional connections are typical of existing precast structures, designed only for vertical loads. In the recent structures, instead, one of the most common beam-to-column connections providing mechanical devices in resisting horizontal actions is the dowel system.

The vulnerability of the frictional connections have been already studied in Magliulo et al. (2008) and in Magliulo et al. (2011), demonstrating that the failure of precast industrial buildings due to loss of support can occur in medium seismicity zones because of the low resistance of frictional connections to horizontal forces. On the contrary, the knowledge on the dowel connection behavior is still poor and should be improved. In the first part of this Chapter the beam-to-column connection behavior is investigated by means of experimental tests and numerical investigations and by a new proposed FEM model. The mechanical characteristics of the connections are evaluated and the literature and code provisions are discusses.

During the latest earthquakes, as L'Aquila (2009) and Emilia earthquakes (2012), most of the damaged precast buildings showed the collapse of the cladding panels, due to the connection systems failure, even in case of a good structural response (Faggiano et al., 2009; Magliulo et al., 2013). The poor literature and the high vulnerability of precast panels system motivate the study of the behavior of these nonstructural components and of their interaction with the structure. The first step was described in Section 2.4, where the dynamic behavior (in particular, the vibration periods) of one-story precast structures with and without cladding panels is investigated by means of linear modal analyses. In the following the final step of this research activity is described, reporting the results of nonlinear analyses and of a seismic risk study.

3.1 Beam-to-column connection

One of the most common beam-to-column connections is the dowel system and many cases of damage have involved it during the last earthquakes. It generally consists of one or more steel dowels, embedded in the column and inserted in a beam hole, filled with mortar (Figure 3.1). The connection behavior is quite complex: it is influenced by the behavior of different materials (steel and concrete), by the established contacts between different elements (e.g. column concrete-to-dowel and mortar-to-dowel contacts) as well as by the behavior of the jointed structural elements themselves (e.g. rotational capacity of beam and column).

Numerical models of precast structures usually implement this kind of connection as a fixed hinge between the elements (Magliulo et al., 2014c), assuming the connection strong enough to avoid its failure during the ground motion. If the connection response is investigated, a more detailed model has to be implemented, as reported in Ercolino (2010). In this work the beam-to-column connections are modeled by means of a non-linear shear plastic hinge, calibrated on several experimental results. This connection macro-models result to be able to establish the failure mode of the structure, i.e. failure of the connections or flexural damage at the column base, without providing information on the connection failure mode, residual strength and damage levels of the materials. Moreover, not unique parameters are found in defining the material hysteretic behavior, due to the strict dependence on the tested specimen. In Zoubek et al. (2013) a numerical tool is presented, based on the ABAQUS FEA software (Corp., 2010), in order to model the seismic behavior of a beam-to-column connection. Although the numerical model presents a very good agreement with the results of monotonic and cyclic experimental tests, the considered connection system is a dowel connection characterized by some specific and not generalizable features: the presence of a steel tube in the beam and the very efficient concrete confinement, which highly influence the seismic behavior of the connection, are generally not provided in similar

connections made in other countries, like Italy, and are not easily modifiable in the presented numerical model.

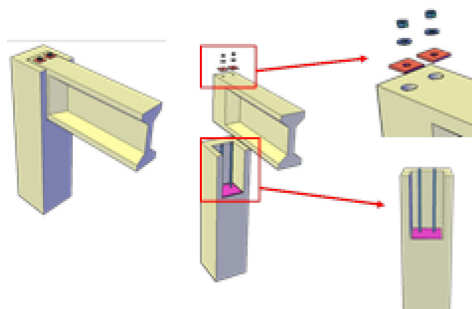


Figure 3.1 Beam-to-column dowel connection

Concerning the shear strength evaluation and failure modes definition of dowel beam-to-column connections, the first suggestions in the technical literature are given in Vintzeleou and Tassios (1986) and in Vintzeleou and Tassios (1987). In the first paper the authors assessed the formulas for the prediction of the dowel strength under monotonic loads, comparing the predicted values with some experimental results available in the literature. The main result is the evaluation of different formulas for all the possible failure mechanisms, typical of dowel connections, extensively explained in the following of this section. In the latter paper the authors present an experimental investigation of the dowel behavior under different loading histories (monotonic and cyclic) and on different specimens (3 values of concrete compressive strength, 3 bar diameters and 3 widths of dowel concrete covers). Under cyclic loads, the hysteresis loops (Figure 3.2) show an asymmetric behavior: as the width of the dowel cover decreases, the strength in the second loading direction (against the cover) becomes considerably lower than the response in the first loading direction (against the core). Moreover, important degradation effects on the strength and on the stiffness of the connection are recorded in the specimens also under low deformations, with a very pronounced pinching effect and very small cycles area (low dissipated hysteretic energy). A very important conclusion is that the response degradation due to cycling is practically independent of the concrete strength, the cover width and the bar diameter, both in terms of strength and in terms of stiffness. According to the experimental results, the authors suggest to evaluate the dowel strength under cyclic actions by multiplying the monotonic strength value (Vintzeleou and Tassios, 1986) by 0.5, if the dowel yielding occurs.

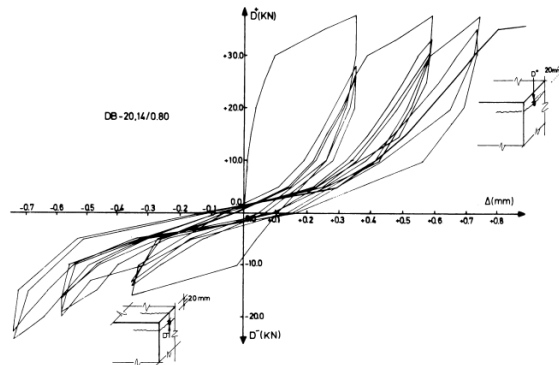


Figure 3.2 Typical hysteretic loops for fully reverse transverse displacement (Vintzeleou and Tassios, 1987)

The seismic design of dowel connections have been studied in different EU research projects, among which the most recent SAFECAS (Toniolo, 2012) project. In this project a great number of monotonic, cyclic and shaking-table tests on different connection devices are carried out, resulting in an extensive guideline for designing the connections of precast structures under seismic actions. However, the presented experiments are incomplete and the generalization of the formula to the not tested cases is complex. In Psycharis and Mouzakis (2012) the results of shaking table tests, within the SAFECAS project on different single-story frames with pinned beam-to-column connections, are reported and discussed. From the dynamic test it is found that the overall structural behavior is highly influenced by the connection response during the excitations. According to these tests, the influencing features are the cover concrete of the dowels in the direction of loading and the dowel diameter. Moreover, also in this paper the strength of the connection for cyclic response results less than the halved monotonic maximum strength. Within the SAFECAS project other experiments on the dowel connection are presented in Zoubek et al. (2013). During these experiments the behavior of the connection shows a strength degradation when cyclic loads are applied, justified by the smaller depth of the plastic hinge in the steel dowel with respect to the case of monotonic load.

In order to fill the described gap in the connections knowledge, an experimental campaign was conducted in the Laboratory of the Department of Structures for Engineering and Architecture (University of Naples). The following section focuses on the results of a monotonic and a cyclic shear test on a dowel beam-to-column connection. The tested specimen reproduces the typical features of a connection between a roof beam and an external column. In the following sections the results of the test are presented and discussed in order to evaluate the behavior of dowel connections under horizontal forces in terms of strength, stiffness, ductility and

damping properties. Moreover, a detailed description of the recorded damage pattern is reported in order to find the failure mechanisms. In the final Section, the difference between the cyclic results and the monotonic test are presented and the connection strengths are compared with the values predicted by some code and literature formulas.

3.1.1 Monotonic experimental test

An experimental campaign on beam-to-column dowel connections was performed in the Laboratory of the Department of Structures for Engineering and Architecture (University of Naples Federico II), supported by the Italian Department of Civil Protection (national project DPC-ReLUIs 2010-2013) and by ASSOBETON (Italian Association of Precast Industries). The campaign provided monotonic (Magliulo et al., 2014b) and cyclic (Magliulo et al., 2014a) tests on different connection typologies. In this section the described experimental test is a monotonic test on a dowel connection between an external column and a roof beam. The specimen (Figure 3.3) consisted of two concrete vertical lateral blocks (height: 1.0m, cross section dimensions: 60cmx60cm) and a concrete horizontal element (length: 2.10m, cross section dimensions: 60cmx60cm). The investigated dowel beam-to-column connection is provided on one side of the specimen, i.e. the left side in Figure 3.3. The setup is fixed by means of steel profiles that connect the base of the two columns at the laboratory through steel threaded bars.

The concrete structural elements (the beam and the columns) are designed according to the provisions of Eurocode 2 (CEN, 2004), Eurocode 8 (CEN, 2005) and D. M. 14/01/2008 (2008). The columns reinforcement details are reported in Figure 3.4: the reinforcement ratio for longitudinal reinforcement is the minimum request by the codes ($\rho = 1\%$) and it is assumed constant along the column height. The transversal stirrups are designed according also to the provisions of CNR 10025/98 (2000) (local loads), resulting in $\phi 8$ stirrups every 150mm (Section B-B in Figure 3.4) and in two smaller $\phi 8$ stirrups every 50mm (Section A-A in Figure 3.4). The beam reinforcement details are reported in Figure 3.5. The steel dowels (M27 - $f_{tb}=800\text{MPa}$) are placed in the column before the concrete casting (Figure 3.7a) and later they are inserted in a hole of the beam (Figure 3.7b). The connection is provided filling the beam hole with high strength grout (Figure 3.7a) and fixing the dowels at the top of the beam by steel plate, nut and washer (Figure 3.7b). For both the column and the beam, the steel dowels have frontal and lateral concrete cover equal to 150 mm and 100 mm, respectively. In order to distribute the normal stresses between the linked elements, a neoprene pad (15cmx60cmx1cm) is placed on the dowels side, designed according to CNR (10018, 1999) provisions. Since the right column only gives the support to the beam, two Teflon sheets are placed between this vertical element and the beam in order to avoid undesirable and additional frictional resistances.

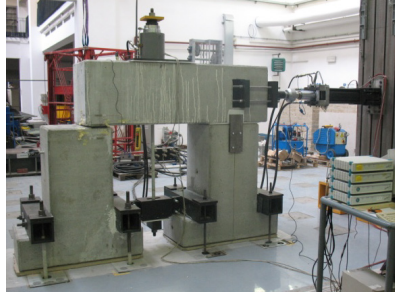


Figure 3.3. Experimental setup of a monotonic shear test on a beam-to-column dowel connection

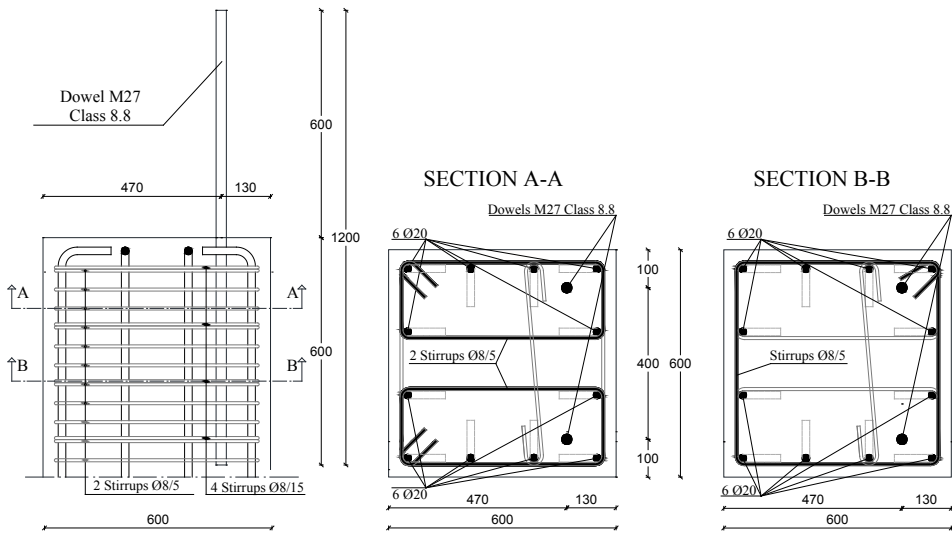


Figure 3.4 Column reinforcement details

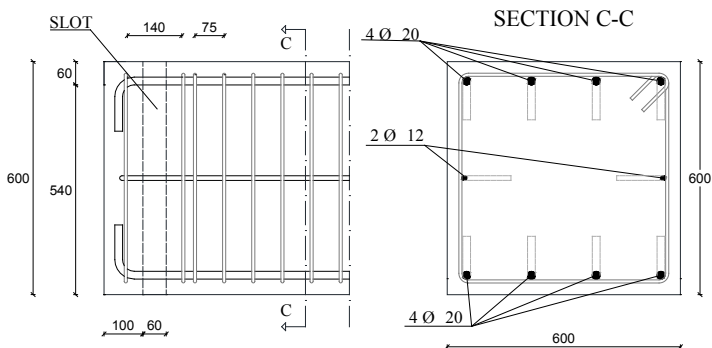


Figure 3.5 Beam reinforcement details



(a)



(b)

Figure 3.6 Construction phases of the tested specimen: (a) columns and dowels position; (b) beam addition



Figure 3.7. Cast of grout in the beam holes



Figure 3.8. Dowels restrained at the top of the beam by means of steel plate, nut and washer

3.1.1.1 Concrete material

In order to define the mechanical characteristics of the concrete material, uniaxial compression tests were performed on ten cubic specimens taken from the beam and column cast. Computed the mean cubic compressive strength ($R_{cm}=49.91\text{N/mm}^2$), the other properties of the unconfined concrete are evaluated according to the Eurocode 2 (CEN, 2004) and reported in Table 3.5 in terms of: characteristic cylinder compressive strength of the concrete at 28 days (f_{ck}), mean value of the concrete cylinder compressive strength (f_{cm}), mean value of axial tensile strength of the concrete (f_{ctm}), compressive strain in the concrete at the peak stress (ϵ_{c0}) and ultimate compressive strain in the concrete (ϵ_{cu}).

Table 3.6 shows the mechanical properties of the confined concrete for the beam and the column in terms of: confined concrete secant modulus at the peak stress, E_{sec} , confined concrete compressive strength (peak stress), f'_{cc} , and ultimate concrete compressive strain, ϵ_{ccu} .

Table 3.1 Unconfined concrete mechanical properties

R_{ck}	f_{ck}	f_{cm}	f_{ctm}	E_{cm}	ϵ_{c0}	ϵ_{cu}
[N/mm ²]	[N/mm ²]	[N/mm ²]	[N/mm ²]	[N/mm ²]	[-]	[-]
49.91	33.62	41.62	3.12	33744	0.002	0.0035

Table 3.2 Confined concrete mechanical properties

Column			Beam		
E_{sec}	f'_{cc}	ϵ_{ccu}	E_{sec}	f'_{cc}	ϵ_{ccu}
[N/mm ²]	[N/mm ²]	[-]	[N/mm ²]	[N/mm ²]	[-]
13159	48.69	0.0207	12282	50.35	0.0128

3.1.1.2 Steel material

For both the reinforcement rebars and the dowels, experimental tensile tests were performed. Concerning the reinforcement, for each diameter used in the setup a tensile test was performed on three specimens. One tensile test is also performed on a steel M27 bar, i.e. a dowel with the same geometrical and mechanical characteristics of the tested dowels. Figure 3.9 shows the experimental curve (blue curve) and the real curve for dowel (red solid curve). The effective values are the stresses and strains obtained according to the real specimen geometry, taking into account the reduction of section area and the local elongation of the steel specimen during the tests. Figure 3.10 shows the experimental curves for the reinforcement bar with the cross section diameter equal to 8mm: for the other diameters, experimental tests confirmed the same mechanical properties.

Table 3.3 Mechanical characteristics of steel used in the prototypes

Diameter	f_y	f_u	E_{cm}
[-]	[Mpa]	[Mpa]	[Mpa]
Φ8	474	701	203794
Φ12	476	624	183828
Φ20	471	704	200792

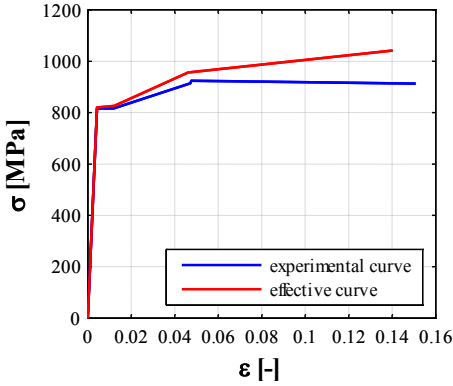


Figure 3.9 Stress-strain relationships for steel dowel: experimental curve (blue curve) and effective curve (red curve)

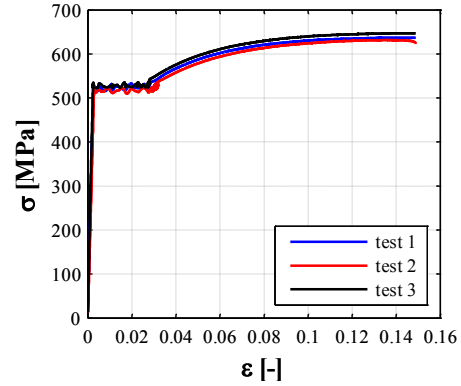


Figure 3.10 Experimental stress-strain relationships for steel reinforcement ($\phi=8\text{mm}$)

3.1.1.3 Loads

Two loads are imposed to the model: the vertical load and the seismic load. The vertical load corresponds to the constant vertical pressure imposed during the monotonic test, distributed on a portion of the beam (60cm x 50cm). The increasing horizontal displacement history is applied against the column cover.

3.1.1.4 Results of the monotonic test

The force-displacement curve (dashed blue line in Figure 3.11) of the experimental test is reported in Figure 3.11 along with the “elaborated” curve (solid red line in Figure 3.11), obtained removing the setup unwanted frictional strength (e.g. the frictional strength of the teflon sheets) (Magliulo et al., 2014a). The force is the horizontal action recorded by the horizontal actuator and the displacement is the relative displacement between the beam and the column. During the experimental test the maximum shear force reaches a value of 169.99kN when the horizontal displacement is equal to 0.83 mm. Removing the setup unwanted frictional strength from the recorded results, the maximum shear strength becomes 161.76kN. The curve shows a brittle behavior of the

dowel connection: after the achievement of the maximum strength, a very soft branch is recorded without any ductile reserve of the connection.

According to (Vintzeleou and Tassios, 1986), given the direction of the applied load (Figure 3.12) and the geometrical features of the connection system, the failure mechanism should be predicted. Since the column concrete covers (Figure 3.13) are smaller than 6-7 times the dowel diameter, a concrete failure is expected due to the tensile stresses in the cover. Moreover, since the frontal cover is larger than the lateral one, the collapse should start at the lateral cover. The described prevision corresponds to the experimental evidence: the first crack forms at the lateral cover in the column (Figure 3.14a), corresponding to the peak strength of the force-displacement curve, i.e. to the failure mechanism of the connection. After this point, increasing the horizontal displacement, the cracks also propagate in the frontal concrete cover (Figure 3.14b). The collapse mechanism of the connection is also confirmed by the records of the installed instrumentations (Figure 3.15): when the force achieves the maximum value ($t=560$ sec) a sudden increase of strains is recorded by the strain gauge on the lateral cover of the column (SV2 in Figure 3.16) and by the strain gauge on the upper stirrup in the column normal to the crack (13 in Figure 3.16).

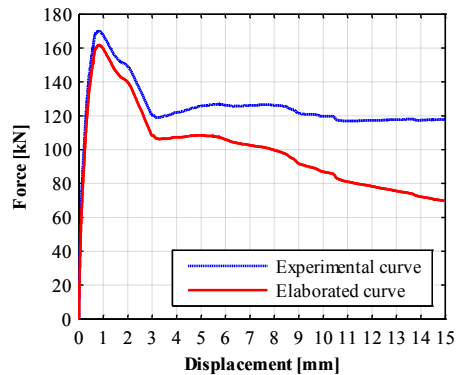


Figure 3.11 Force-displacement curve of the monotonic test (dashed blue line) and “elaborated” curve (solid red line)

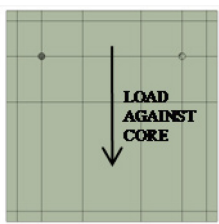


Figure 3.12 Loading conditions

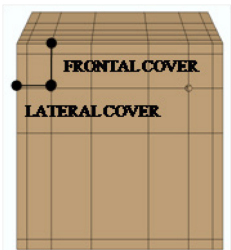
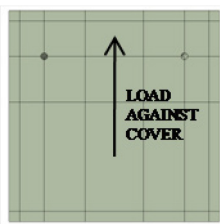


Figure 3.13 Frontal cover and lateral cover



Figure 3.14 Phases of connection collapse: (a) first crack during the test and (b) final step of the test

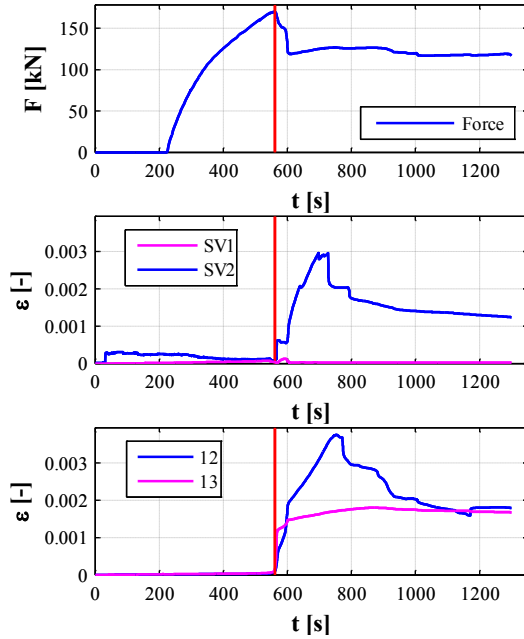


Figure 3.15 Instrumentations records. From the top: force of the actuator, deformations of the concrete and deformations of the upper stirrup in the column

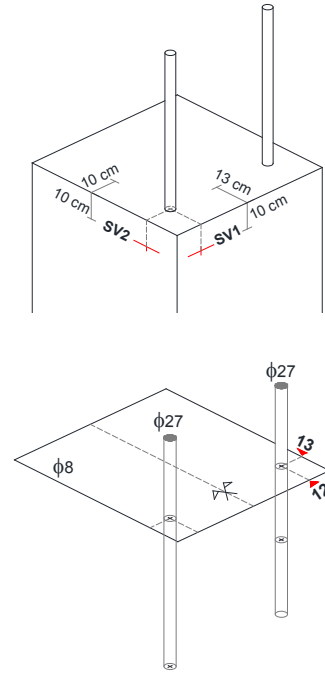


Figure 3.16 Geometrical layout of the column instrumentations

3.1.2 Cyclic test on dowel beam-to-column connection

The above cited experimental campaign on beam-to-column dowel connections, performed in the Laboratory of the Department of Structures for Engineering and Architecture (University of Naples), provides also cyclic shear tests. In the present section the described experimental test is a cyclic test on a dowel connection between an external column and a beam. The specimen (Figure 3.17) consisted of two concrete vertical lateral blocks (height: 1.0m, cross section dimensions: 60cmx60cm) and a concrete horizontal element (length: 2.10m, cross section dimensions: 60cmx60cm). The investigated dowel beam-to-column connection is provided on one side of the specimen, i.e. the left side in Figure 3.17a.

The structural elements details and the material characteristics of the materials are equal to the monotonic test setup, described in Section 3.1.1.

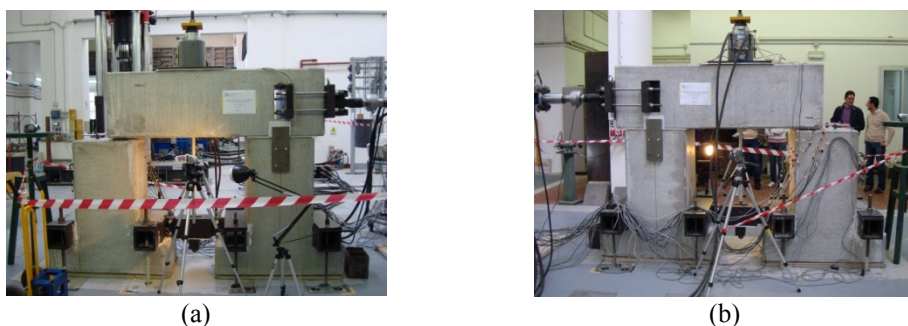


Figure 3.17 Experimental setup of the monotonic shear test on a beam-to-column dowel connection: (a) frontal view and (b) bottom view

3.1.2.1 Instrumentation

In order to record the connection behavior during the test, different instruments are installed on the specimen.

The testing loads are controlled by:

- one load cell in the vertical jack, applying the vertical loads to the specimen, that measures the axial force;
- one load cell in the horizontal actuator, applying the horizontal load, that records the imposed displacements.

The local deformation of the setup and of the structural materials are recorded by means of LVDT and strain gauges. Since the setup configuration is symmetric with respect to the column, these instruments are placed only on one side of the specimen:

- 3 strain gauges on the first three stirrups from the top in the column, parallel to the load direction (e.g. 13 in Figure 3.18a) and 3 orthogonal to the load direction (e.g. 12 in Figure 3.18a);

- 2 strain gauges on the steel dowel, one in the column (B in Figure 3.18b) and one in the beam (B1 in Figure 3.18b) at a width of 10cm from the element surface in both the cases;
- 4 biaxial strain gauges are placed on the top of the column and all around the dowel, in the direction of horizontal load (e.g. S6 in Figure 3.19a) and in the transversal one (e.g. S1 in Figure 3.19a);
- 1 uniaxial strain gauges are placed on the column lateral side in the direction of the horizontal load (SV2 in Figure 3.19a) and 1 uniaxial on the frontal side in the transversal direction (SV1 in Figure 3.19a);
- 2 biaxial strain gauges are placed on the bottom of the beam and close to the dowel in the direction of the horizontal load (e.g. T3 in Figure 3.19b) and in the transversal one (e.g. T2 in Figure 3.19b);
- 2 uniaxial strain gauges are placed on the vertical surfaces of beam lateral cover, in the direction of horizontal load (TV1 in Figure 3.19b) and of beam frontal cover in the transversal direction (TV2 in Figure 3.19b);
- 2 LVDT (C2 e C1 in Figure 3.20), with a maximum elongation of 50 mm, placed horizontally at the beam-end cross section, in order to evaluate any displacement and rotation with respect to the column.

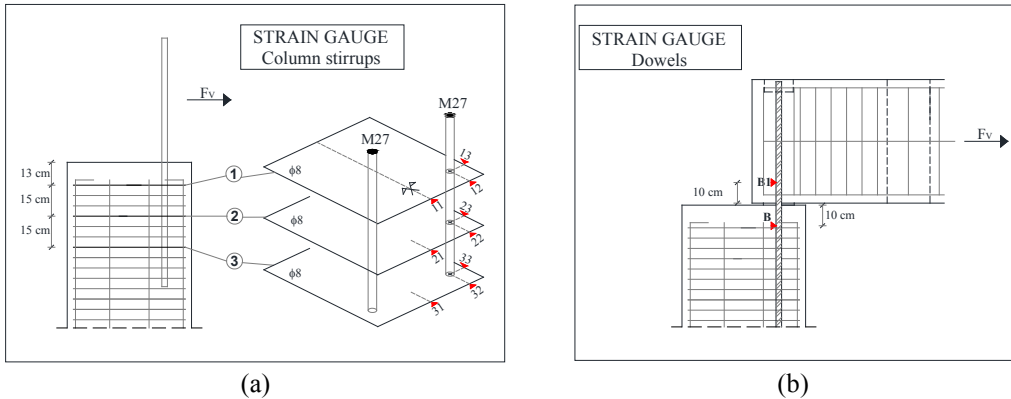


Figure 3.18 Layout of stain gauges placed on steel elements: (a) column stirrups and (b) left dowel bar

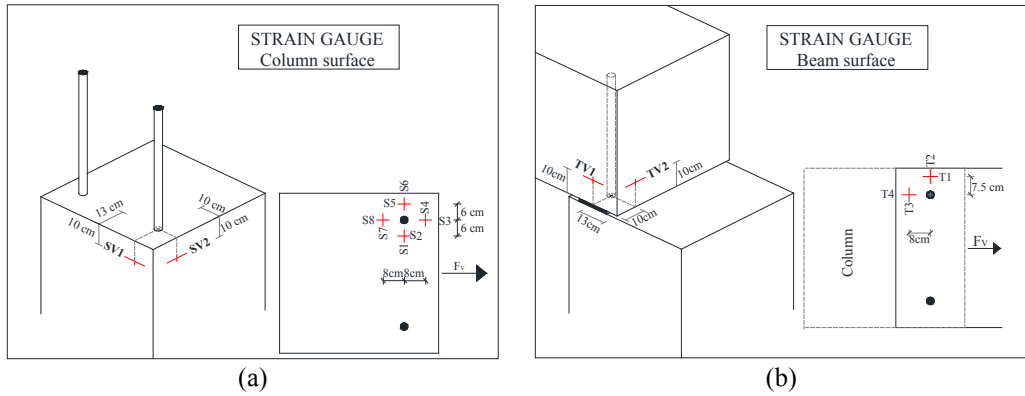


Figure 3.19 Layout of strain gauges placed on concrete elements: (a) column and (b) beam

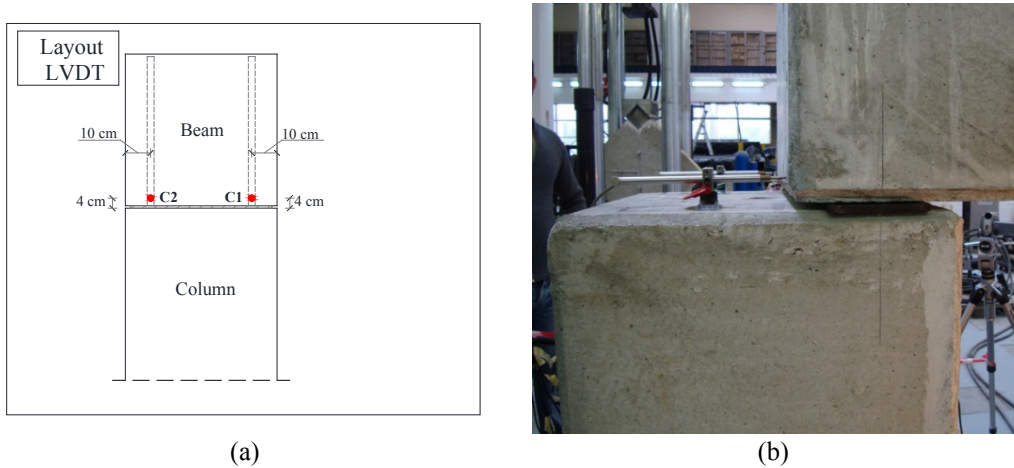


Figure 3.20 Layout of LVDT to record relative displacements between the beam and the column

3.1.2.2 Testing protocol

The cyclic test consists of two loading phases:

- the application of the vertical load, simulating the gravity load;
- the application of a cyclic horizontal load, simulating the seismic action.

The vertical load is provided by a vertical jack with a rate of 3 kN/s up to the maximum value of 450 kN. This vertical load activates the frictional contact between the concrete and the neoprene pad, which highly influences the connection strength. Before the horizontal load application, a period of 10 sec is waited in order to guarantee the stabilization of the system and of the instruments. The horizontal load is

provided by a hydraulic actuator with a displacement control method. The loading history adopted in the cyclic test is defined on the basis of the results of the monotonic test. The horizontal displacements are applied in two directions (Figure 3.21): if the load is applied against the concrete core the displacement is assumed positive and if the load is applied against the concrete cover the displacement is assumed negative. Figure 3.22 shows the loading history, composed of 16 steps, defined by three complete cycles with the same displacement amplitude. The rate is equal to 0.02mm/s up to the 12th step and with a rate of 0.04mm/s up to the end. The test stops after about 2h.



Figure 3.21 Loading direction: (a) negative and (b) positive direction

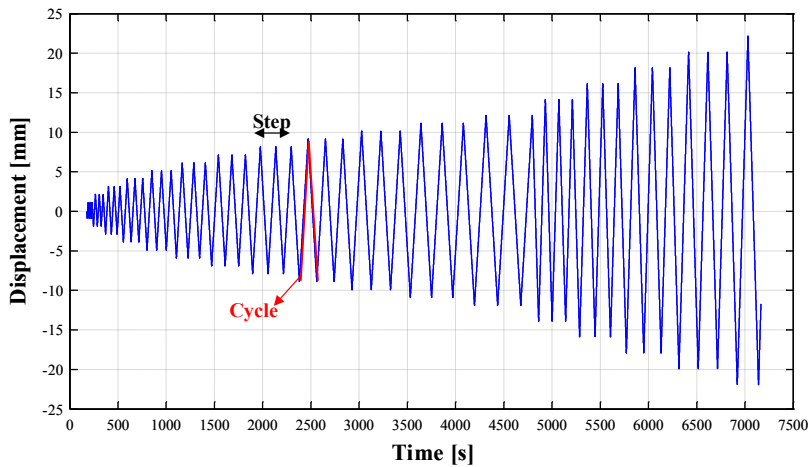


Figure 3.22 Load history recorded by LVDT

3.1.2.3 Results: damage

According to the connection system geometry and to the possible failure modes in dowel connection (Vintzeleou and Tassios, 1986), the first crack should appear at the column side cover. In the considered test, hence, the column concrete covers (lateral and frontal) are smaller than the limit value of 6-7 times the dowel diameter (M27).

Moreover, the frontal cover (130mm) is larger than the lateral one. As expected, the first crack appears at the column lateral surface, along the alignment of the two dowels, and it propagates up to column frontal surface (Figure 3.23 and Figure 3.24). The same damage pattern is observed on the two sides of connection, with a little time gap due to negligible setup asymmetries. The crack opening is confirmed by the records of the strain gauges on the column surface (Figure 3.25): at time $t=801\text{sec}$, the strain gauge on the column lateral cover (S6 in Figure 3.19(a)) reaches the strain (ϵ_{ct}) corresponding to the maximum tensile strength (blue curve in Figure 3.25). The failure mode and the time are also confirmed by the records of the strain gauges (parallel to the load) on the steel stirrups in the column (Figure 3.26): the steel strains in the second stirrups (green curve in Figure 3.26) reaches the yielding value ($\epsilon_{y,\text{reinf}}$) few seconds before the first crack formation and only after the crack propagation the same stirrup ends to work because of the instrumentation damage. Concerning the third stirrup (blue curve in Figure 3.26), it reaches the yielding value ($\epsilon_{y,\text{reinf}}$) but it continues to work since it is placed at 41 cm from the column top surface while the crack has a length of about 30cm.



Figure 3.23 First crack in the column side cover

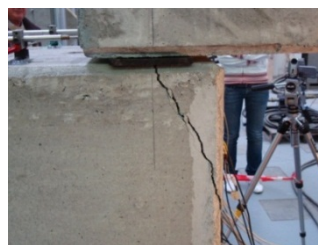


Figure 3.24 Splitting of the column side cover

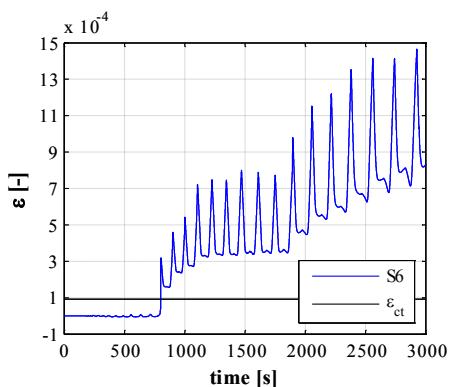


Figure 3.25 Records of strain gauges on the column top surface (blue curve) along with the limit tensile strain of concrete (black line)

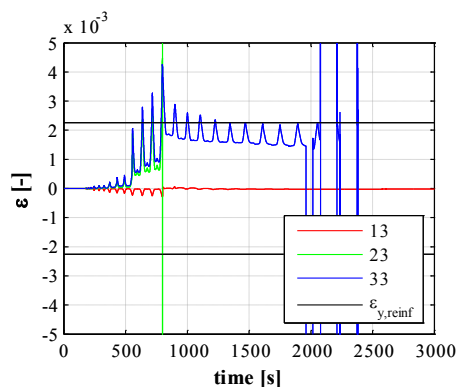


Figure 3.26 Records of strain gages on the stirrups in the column along with the yielding strain (black line)

At higher values of horizontal displacement, the lateral crack width increases and two other inclined cracks form at the column frontal surface (Figure 3.27) up to the complete concrete expulsion (Figure 3.28). An inclined crack appears also on the beam frontal surface (Figure 3.29), that increases at the end of the experiment (Figure 3.30). The cyclic test continues and other cracks open in the column: they are parallel to the first crack and provide the expulsion of other concrete portions from the column (Figure 3.31(a)-(b)). The concrete expulsion allows to check of the dowel deformation at the end of the test. In Figure 3.32 the right dowel is shown: the width of the formed plastic hinge is measured equal to 80 mm from the bottom surface of the beam. The propagation of the plastic zone in the dowels are also demonstrated by the strain gauges on these steel elements (B in Figure 3.18(b)), located at 10cm from the top column surface. The plastic hinge propagates up to the instrument depth since the strains in the steel dowels in the column (blue curve in Figure 3.33) reaches the yielding value ($\epsilon_{y,dow}$). In Figure 3.33 the records of the strain gauge on the dowel in the beam are reported with the red curve, demonstrating the development of the plastic hinge also in the horizontal element.



Figure 3.27 Crack opening in the column frontal cover



Figure 3.28 Splitting of the cover at the end of the test



Figure 3.29 Crack opening in the beam frontal cover



Figure 3.30 Crack in the beam at the end of the test



Figure 3.31 Final state of the specimen at the end of the cyclic test: (a) frontal view and (b) bottom view



Figure 3.32 Plastic hinge in the steel dowel in the column

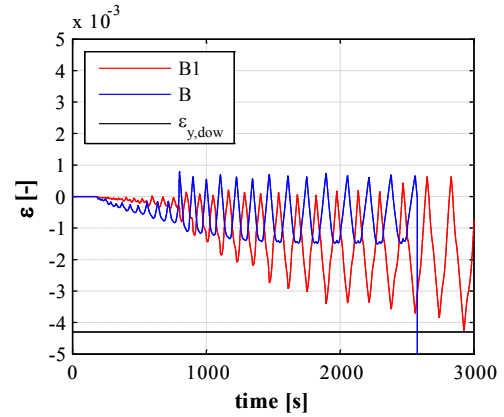


Figure 3.33 Records of strain gauges on the steel dowels in the beam (red curve) and in the column (blue curve) along with the yielding steel strain of the dowel (black line)

3.1.2.4 Force –displacement curve

The force-displacement curve of the performed cyclic test is shown in Figure 3.34. The curve shows the displacements recorded in the LVDT at beam head (C1) along with the forces recorded in the actuator load cell. As anticipated, the positive values of displacements and forces correspond to the horizontal load against the column concrete

core, while the negative results correspond to the load against the concrete cover. The behavior of the connection appears asymmetrical in the two directions, presenting higher values of strength if the load is applied against the column core (positive values). Moreover, in this direction the shear force increases as well as the horizontal displacements up to the end of the test with a limited connection stiffness degradation. On the contrary, when the horizontal load is applied against the column frontal cover (negative values), the connection exhibits a brittle behavior: as soon as the maximum shear strength is reached, the strength and the stiffness of the connection significantly decrease. The described behavior in the two investigated directions are confirmed by the failure mechanism that involves the frontal cover, reducing the stiffness and the strength of the connection in this direction.

In order to investigate the seismic response of the connection, the force-displacement curve is reported up to the 6th step of loading history, i.e. when the strength degradation is larger than the 20% (blue solid line in Figure 3.34). The forces are the actuator forces that also include the additional strengths of the setup, i.e. the frictional strength of the neoprene pad, frictional strength of the Teflon sheets and strength of the setup components. In order to evaluate these additional contributes, a cyclic test is performed on the tested specimens with the same load protocol without the connection on the left side, i.e. before connecting the two dowels into the beam with the mortar. The result of this additional test are reported with a gray solid line in Figure 3.35: up to the 6th step of the loading history, the additional strength can be mainly related to the frictional strength of the concrete-neoprene contact, evaluated by the authors according to Magliulo et al. (2011). Moreover, in Figure 3.35 the first crack formation is reported with a red circle, demonstrating the correspondence of this damage with the weaker loading condition and with the maximum strength of the connection.

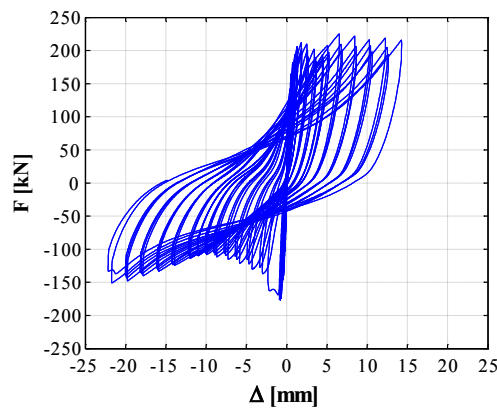


Figure 3.34 Force- displacement curve of the whole cyclic test

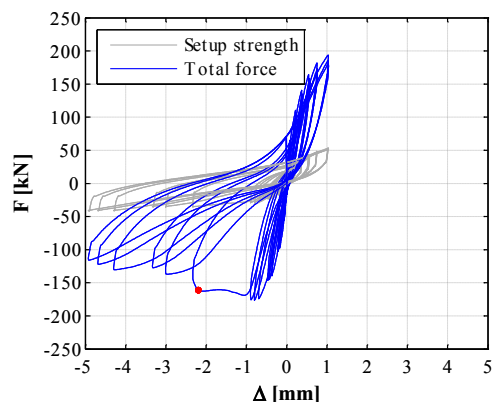


Figure 3.35 Force- displacement curve (blue curve) and frictional resistance (gray line) up to 6th step: the red point indicates the first crack development in the later concrete cover

If the maximum recorded displacements at each step are reported with the corresponding experimental force, the envelope of the cyclic behavior is obtained: Figure 3.36 shows the three envelopes, corresponding to the three cycles of each step up to the 6th step. When the horizontal load acts against the column concrete core, at the last step the first cycle force is equal to 193.8kN at an horizontal displacement of 1.94mm; this force decreases to 182.1kN and to 180.8kN at the second and third cycle, respectively. This trend is observed during the whole cycle, i.e. the maximum shear strength in the first cycle is always greater than the values achieved in the following cycles at the same displacement. Moreover, the difference between these values increases with the horizontal displacements. When the horizontal load acts against the column concrete cover, the maximum shear strength is reached at second cycle of the fourth step and it is equal to 176.57kN.

Figure 3.37 shows the dissipated energy during the cyclic test, evaluated as the area under the force-displacement curve. For each cycle of each step, white bars represent the dissipated energy when the load is applied against the column core (positive semi-cycle); gray bars represent the dissipated energy when the load is applied against the column cover (negative semi-cycle). Black bars represent the dissipated energy at the end of a complete cycle, evaluated as the sum of the positive and negative semi-cycle energies. The positive dissipated energy is quite similar to negative one up to the third step, confirmed by a symmetric response of the connection, shown in Figure 3.36. Dissipated energy of a whole cycle at each step is always greater for the first cycle due to degrading occurrence also in each step.

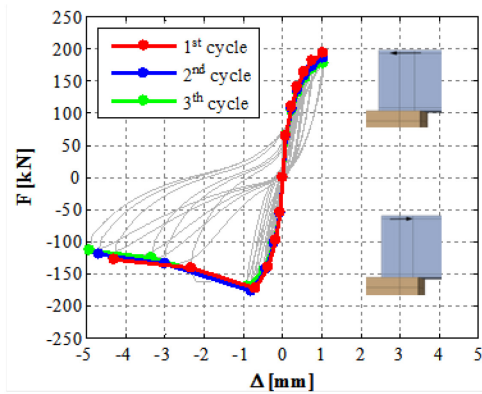


Figure 3.36 Force-displacement curve (gray curve) and envelope at each step (circle marker) for 1st cycle (red line), 2nd cycle (blue line) and 3rd cycle (green line)

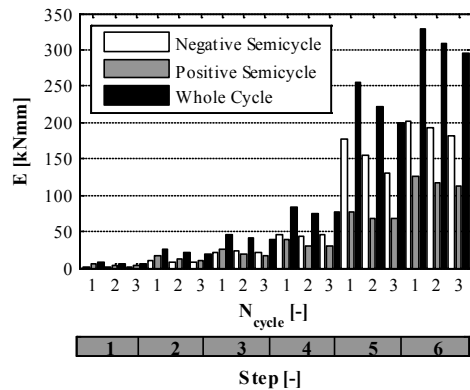


Figure 3.37 Dissipated energy during the cyclic shear test, for each positive and negative semi-cycle up to 6th step

3.1.2.5 Comparison between the monotonic and the cyclic shear test

As anticipated, the described test belongs to an experimental campaign that provides also a monotonic test on a beam-to-column connection (Figure 3.38), with the same geometrical features. The experimental evidence shows a first crack at the lateral cover in the column, that propagates in the frontal concrete cover (Figure 3.39), as in the cyclic test. The results of this test are reported in Figure 3.40 (red curve) in terms of actuator horizontal force and LVDT displacement. The curve is reported up to the ultimate displacement, assumed for the cyclic test. In this curve the peak strength of the force-displacement curve corresponds to the first crack formation in the lateral column cover; after this point a high strength degradation is recorded, demonstrating the brittle nature of the failure mechanism.

The monotonic force-displacement curve are compared with the negative semi-cycles of the cyclic test and the following conclusions can be drawn:

- the elastic stiffness of two specimens is equal;
- the values of the maximum connection strength are very close;
- the strength degradation that follows the failure mechanism is recorded in both the experimental tests.

The last two considerations demonstrate that there is not degradation when cyclic loads are applied. Such a conclusion disagrees with some literature evidences; e.g. experimental results reported in Zoubek et al. (2013) and in Vintzeleou and Tassios (1987). In these works the strength of the connection highly decreases when cyclic loads are applied to the specimen. According to the results of the monotonic and the cyclic tests, described by Zoubek, the difference is explained by the different depth of

the plastic hinge. In order to justify the results, the failure mechanisms are investigated. In the literature works the failure mechanism is related to the flexural yielding of the dowel and to the crushing of the surrounding concrete, both in the monotonic and in the cyclic experiments. In the presented tests the failure mechanisms always involve the cover concrete. So it can be stated that the brittle nature of the phenomenon can justify the same value of maximum strength in the monotonic and cyclic test.

Concerning the post-peak behavior, after the maximum strength and failure mechanism achievement, the behavior of the two tests is still similar. This results still disagrees with the literature reference reported above. After the first crack formation the dowels start bearing the load as demonstrated by the strain gauge records on the dowels (B and B1) and in this condition the dowel action should be highly influenced by the load type, as numerically and empirically demonstrated by Vintzeleou and Tassios (1987). However, the experimental evidence can be justified because the yielding strains are achieved in the dowel only at 6.99mm of displacement, that is higher than the assumed ultimate value.

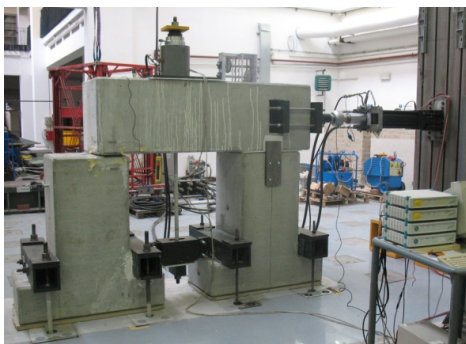


Figure 3.38. Experimental setup of a monotonic shear test on a beam-to-column dowel connection



Figure 3.39 Final step of the monotonic test: splitting of the concrete

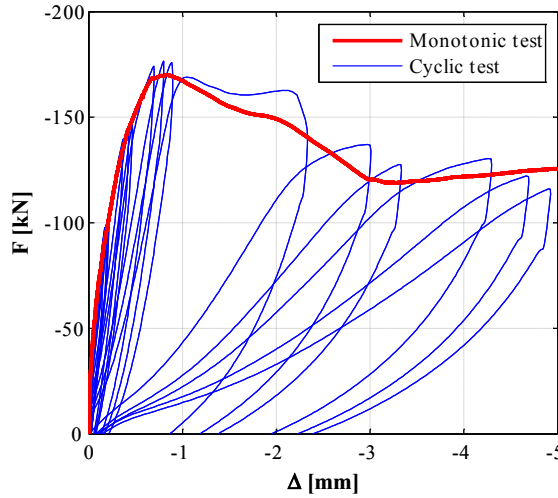


Figure 3.40 Comparison between force-displacement curves of the monotonic test (red solid line) and of the cyclic test (blue solid line)

3.1.2.6 Comparison with literature formulas

In this Section the experimental results of the cyclic tests are compared with some literature formulas, proposed to evaluate the cyclic shear strength of the dowel connections. The considered relationships are listed and presented below.

- The CNR 10025/98 (2000) formula evaluates the strength of a dowel beam-to-column connection according to equation (3.1). This formula is valid if the eccentricity of shear force is less than the halved diameter (d_b) of the dowel. Since the eccentricity is defined as the half of the thickness of the support between the beam and the column, in the analyzed case it is equal to the halved neoprene pad thickness (10mm) and then the equation (3.1) can be used for the comparison.

$$V_{Rd,CNR} = c \cdot d_b^2 \cdot \sqrt{f_{yd} \cdot f_{cd}} \quad (3.1)$$

In (3.1): c is equal to 1.2 if the confining pressure is neglected and equal to 1.6 if confining pressure is considered; f_{cd} is the design compressive strength of concrete and f_{yd} is the design yielding strength of dowel. CNR relationship does not consider the influence of concrete cover depth on the connection shear strength and the case of cyclic loads.

- According to Vintzeleou and Tassios (1986), when concrete covers are greater than 6-7 times the dowel diameter, Failure I (simultaneous dowel yielding and concrete crushing) occurs and the dowel shear strength can be evaluated with (3.2), if eccentricity is equal to zero.

$$V_{Rd,V\&T}^I = k \cdot d_b^2 \cdot \sqrt{f_{ys} \cdot f_{cc}} = 1.3 \cdot d_b^2 \cdot \sqrt{f_{ys} \cdot f_{cc}} \quad (3.2)$$

As anticipated, in (Vintzeleou and Tassios, 1987) the design dowel force under cyclic loads in case of Failure I can be obtained by multiplying the design strength values by 0.5:

$$V_{Rd,V\&T}^{I.C} = 0.5 \cdot V_{Rd,V\&T}^I \quad (3.3)$$

- If the concrete cover is lower than 6-7 times the dowel diameter, the strength of the connection is related to concrete failure rather than to dowel crisis (concrete splitting). Depending on the ratio between concrete cover depth of the frontal cover and of the lateral cover, a side splitting or a bottom splitting could occur.

If the lateral cover is smaller than the frontal one, a side splitting occurs and dowel shear strength can be calculated with (3.4).

$$V_{Rd,V\&T}^{II,L} = 2 \cdot d_b \cdot b_{ct} \cdot f_{ct} \quad (3.4)$$

In (3.4) b_{ct} is the net width of the concrete section, f_{ct} is the concrete tensile strength and d_b is the dowel diameter.

When the frontal cover is small enough in comparison with the width of the column, the bottom splitting failure occurs and the force strength is equal to:

$$V_{Rd,V\&T}^{II,B} = 5 \cdot f_{ct} \cdot c \cdot d_b \cdot \frac{c}{0.66 \cdot c + d_b} \quad (3.5)$$

In (3.5) c is the value of the frontal cover. The case of cyclic loads are not contemplate in both the equations (3.4) and (3.5).

In Table 3.4 the comparison of these literature formulas and the experimental results of the cyclic test are reported. All the strengths are evaluated with the mean value of the material strengths and with the resistant diameter of the dowel. The CNR formulas ($V_{Rd,CNR}$) give values very close to the experimental strength even if this code considers a different failure mechanism with respect to the experienced collapse. The same conclusion can be drawn in the case of the Vintzeleou and Tassios formula under

monotonic load for the case of Failure I ($V_{Rd,V\&T}^I$). Obviously, in this case the reduction factor of 0.5 in the $V_{Rd,V\&T}^{I,C}$ formula gives a too low value of the strength. If the failure mechanism is considered the comparison with experimental results should be performed with the lateral concrete splitting ($V_{Rd,V\&T}^{II}$) formula, that gives smaller value than the experimental strength.

Table 3.4 Comparison between the cyclic experimental strength of the dowel connection ($V_{Rd,cyclic}$) and the literature formulas

$V_{Rd,cyclic}$	$V_{Rd,CNR(c=1.2)}$	$V_{Rd,CNR(c=1.6)}$	$V_{Rd,V\&T}^I$	$V_{Rd,V\&T}^{I,C}$	$V_{Rd,V\&T}^{II}$	$V_{Rd,V\&T}^{II,B}$
[kN]	[kN]	[kN]	[kN]	[kN]	[kN]	[kN]
176.6	129.5	172.7	140.3	70.2	82.5	58.0

3.1.3 Conclusions

An extensive experimental campaign is performed in order to investigate the seismic behavior of dowel beam-to-column connections in precast structures. The presented section describes the results of a monotonic and a cyclic test on a dowel connection between an external column and a roof beam. The setup is designed according to the actual European and Italian building codes and it is loaded with a vertical load and with a displacement history up to the failure. During the two tests the horizontal load mainly caused damage on the column, while no relevant cracks affect the beam until the end of test. The damage pattern and the instrumentation records show that the first damage in the connection is the crack development in the column concrete lateral cover.

In both the tests, according to the force-displacement curve of the test, the lateral cover splitting occurs when the maximum strength of the connection is achieved. It can be assumed that for this loading condition the behavior has a brittle nature, showing an high degradation of stiffness and strength after the maximum strength. Concerning the cyclic test, when the horizontal load acts against the column concrete core, the force-displacement curve presents higher strength values until the end of the test, since the connection behavior is related to the steel dowels yielding.

The dissipated energy of the connection is evaluated as the area under the force-displacement curve and the recorded values are very low, demonstrating that this connection cannot influence the dissipative properties of the whole structure under dynamic actions.

The cyclic force-displacement curve, recorded when the load is applied against the column cover, is compared with the results of the monotonic shear test. By the comparison it is found that the strength of the two tested specimens are very close. Moreover, the brittle nature of the failure mechanism is confirmed in both the tests by

the highly degrading behavior after the peak strength in the force-displacement curves. In the final part of the work the experimental results of the cyclic tests are compared with some literature formulas, proposed for evaluating the shear strength of dowel connections. The comparison highlights that the best relationship is the CNR formula even if this code considers a different failure mechanism. If the failure mechanism (lateral concrete splitting) is considered and the corresponding literature formula is used (Failure II-side splitting), the predicted strength highly underestimates the response of the connection.

3.2 Numerical modeling of the tested dowel connection

This section presents this non-linear three-dimensional model of a beam-to-column dowel connection, calibrated on the results of an experimental monotonic test. The characteristics of the tested connection and of the FEM model are described in order to demonstrate the capability of the model in describing the behavior of a large range of precast structures connections. Some parametric studies are also performed, varying some geometrical characteristics of the dowel connection, in order to establish their influence on the behavior of the system as well as to evaluate the reliability of the most common formulae, available in technical literature and used to predict the dowel connections strength.

The model (Figure 3.41) consists of four main parts: the concrete elements (beam and column), the steel elements (reinforcement and dowels), the contact surface (neoprene pad) and the interactions between materials. In the following, the model, in terms of elements and materials, is described in detail.

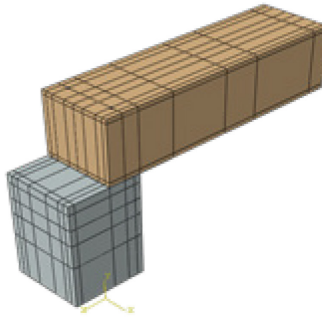


Figure 3.41 FEM model of the dowel connection by ABAQUS (Corp., 2010)

3.2.1 Concrete elements

Numerical model

The concrete elements (beam and column) are modeled as three-dimensional deformable elements, adopting the C3D8R element of the ABAQUS three-dimensional solid element library. This element is an hexahedral and linear element recommended for analysis characterized by contact problems and affected by large deformations. As reported in the name of the element, it is a 3D continuum element (C), with 8 nodes linear brick (8) and reduced integration (R).

For the column and the beam a smeared crack concrete model is assumed. This model is included in the ABAQUS/Standard library for reinforced concrete structures. It is suitable to reproduce cracking in tension and crushing in compression under monotonic deformation and low confining pressures (i.e. less than four or five times the maximum value of uniaxial compressive strength). Two reinforced concrete crack models are

introduced in the late 1960s: the discrete crack model (Ngo and Scordelis, 1967) and the smeared crack one (Rashid, 1968). The smeared crack concrete model is based on the idea that in the concrete, due to its heterogeneity and due to the presence of reinforcement, many small cracks develop and only in a later stage of the loading process they link up to form one or more dominant cracks. In (Borst et al., 2004) it is demonstrated that this model can simulate the diffuse cracking patterns that arise due to the heterogeneity of the concrete and the presence of reinforcement. The presence of cracks is taken into account thanks to constitutive laws that influence stress and stiffness of the material in each point of integration.

The described model needs the definition of the elastic and inelastic behavior under compression and tension stresses and of the breaking surface shape. In the following these input parameters are described in detail, in order to allow reproducing the model. For uniaxial compressive loads, the smeared crack concrete initially shows an elastic behavior, after that inelastic deformations occur and the stiffness starts to decrease (Figure 3.42). The stress-strain curve of the concrete can be evaluated according to several models.

When tension stresses occur, the behavior of the concrete is modeled linear elastic until the cracking point, where the cracks form: the stress at this point is assumed equal to the medium value of the concrete tensile strength (see Section 3.1.2), while the strain is assumed equal to 0.0093% (Figure 3.42).

The post-cracking behavior is defined by the “tension stiffening” model. This model depends on the density of reinforcement, on the quality of the bond between the rebar and the concrete, on the relative size of the concrete aggregate compared to the rebar diameter, and on the mesh refinement. A reasonable choice for relatively heavily reinforced concrete, modeled with a fairly detailed mesh, is to assume a linear softening post-peak behavior, according to the model of Vecchio (2000). The “strain” option of ABAQUS is used in order to assign this kind of behavior. It specifies two points of the post-cracking curve: the cracking failure point and the cracking ultimate point.

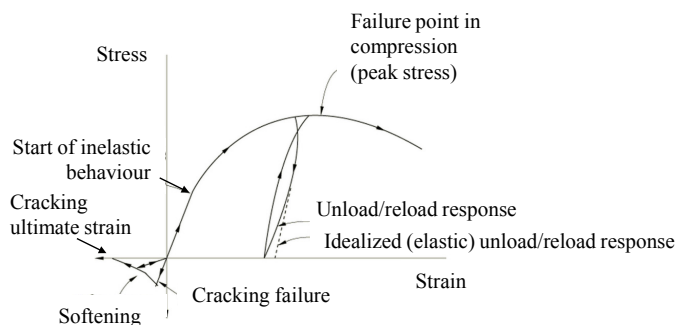


Figure 3.42 Mechanical behavior of the smeared crack concrete model for uniaxial compressive load (Systèmes, 2008)

In order to completely define the smeared crack concrete model, the failure ratios should be fixed so that the cracking surface is described. The failure surface is defined by four "failure ratios":

- the ratio between the ultimate compressive stress for biaxial tensional state and the ultimate compressive stress for uniaxial tensional state; this ratio is assumed equal to 1.16, which is the ABAQUS default value (Systèmes, 2008);
- the absolute value of the ratio between the failure tensile stress and the ultimate compressive uniaxial stress, evaluated according to the mechanical characteristics of the concrete (see Section 3.1.2);
- the ratio between one of a principal components of plastic deformation for ultimate compressive stress under biaxial state of tension and the plastic deformation for ultimate compressive stress under uniaxial state of tension; this ratio is assumed equal to 1.28, which is the ABAQUS default value (Systèmes, 2008);
- the ratio between main cracking stress for biaxial state of tension, when the other main tension reaches its maximum value in compression, and the cracking uniaxial tension; this ratio is assumed equal to 1/3, which is the ABAQUS default value (Systèmes, 2008).

Concrete material

Three different smeared crack concrete models have to be defined for the concrete elements (beam and column): i) confined concrete for the column; ii) confined concrete for the beam and iii) unconfined concrete for both column and beam. The confined behavior is differently defined for the beam and the column since the longitudinal and transversal reinforcements are differently distributed in these two elements.

In order to define the mechanical characteristics of the concrete material, uniaxial compression tests were performed on ten cubic specimens taken from the beam and column cast. Computed the mean cubic compressive strength ($R_{cm}=49.91\text{N/mm}^2$), the other properties of the unconfined concrete are evaluated according to the Eurocode 2 (CEN, 2004) and reported in Table 3.5 in terms of: characteristic cylinder compressive strength of the concrete at 28 days (f_{ck}), mean value of the concrete cylinder compressive strength (f_{cm}), mean value of axial tensile strength of the concrete (f_{ctm}), compressive strain in the concrete at the peak stress (ϵ_{c0}) and ultimate compressive strain in the concrete (ϵ_{cu}). The stress-strain law of Popovics (1973) is adopted for the unconfined concrete (red curve in Figure 3.43).

Table 3.6 shows the mechanical properties of the confined concrete for the beam and the column in terms of: confined concrete secant modulus at the peak stress, E_{sec} , confined concrete compressive strength (peak stress), f'_{cc} , and ultimate concrete

compressive strain, ε_{cu} . The constitutive law of Mander et al. (1988) is adopted for the beam and column confined concrete (green and blue curve, respectively, in Figure 3.43).

Table 3.5 Unconfined concrete mechanical properties

R_{ck}	f_{ck}	f_{cm}	f_{ctm}	E_{cm}	ε_{c0}	ε_{cu}
[N/mm ²]	[N/mm ²]	[N/mm ²]	[N/mm ²]	[N/mm ²]	[-]	[-]
49.91	33.62	41.62	3.12	33744	0.002	0.0035

Table 3.6 Confined concrete mechanical properties

Column			Beam		
E_{sec}	f'_{cc}	ε_{ccu}	E_{sec}	f'_{cc}	ε_{ccu}
[N/mm ²]	[N/mm ²]	[-]	[N/mm ²]	[N/mm ²]	[-]
13159	48.69	0.0207	12282	50.35	0.0128

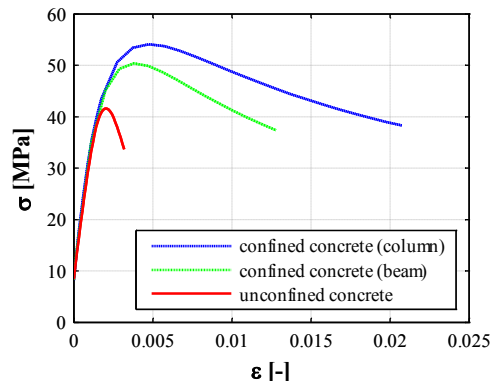


Figure 3.43 Concrete stress-strain relationships

3.2.2 Steel elements

Numerical model

The specimen contains two groups of steel elements: the reinforcement steel and the steel dowels. By the software ABAQUS (Corp., 2010), steel elements can be modeled through a discrete or a continue technique. In the former case, truss or beam elements are created and a perfect correspondence of deformations with the concrete is assumed. In the latter case, a distribution of thin layers with an equivalent thickness is included in the model and the reinforcement is linked to the concrete in order to describe the mutual interaction between the two materials.

In the model of tested beam and column, truss elements are adopted in order to introduce longitudinal and transversal reinforcement, considered embedded in the concrete. The beam web rebars ($2\phi 12$) are not introduced in the model, since they negligibly influence the structural element strength.

On the contrary, the steel dowels are modeled as three-dimensional elements and interface elements are defined in order to take into account the bond slip phenomena.

Steel material

For both the reinforcement rebars and the dowels, experimental tensile tests were performed. Concerning the reinforcement, for each diameter used in the setup a tensile test was performed on three specimens. One tensile test is also performed on a steel M27 bar, i.e. a dowel with the same geometrical and mechanical characteristics of the tested dowels. Figure 3.44 shows the experimental curve (blue curve) and the effective curve for dowel (red solid curve). The effective values are the stresses and strains obtained taking into account the reduction of section area and the local elongation of steel specimen during the tests. Figure 3.45 shows the experimental curves for the reinforcement bar with the cross section diameter equal to 8mm: for the other diameters, experimental tests confirm the same mechanical properties.

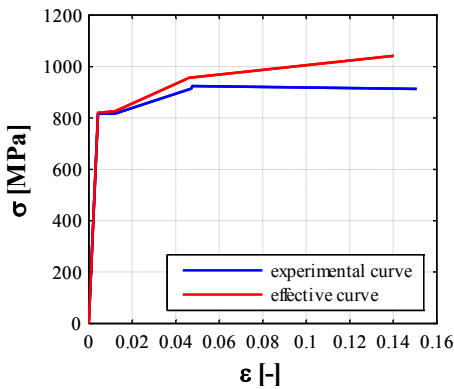


Figure 3.44 Stress-strain relationships for steel dowel: experimental curve (blue curve) and effective curve (red curve)

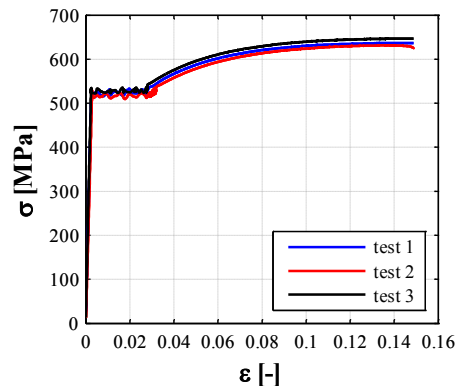


Figure 3.45 Experimental stress-strain relationships for steel reinforcement ($\phi=8\text{mm}$)

3.2.3 Interaction

The definition of the interaction and of the contact surface between elements is a key step in the implementation of the finite element model, influencing the final results and the convergence of the nonlinear analyses. Three contact surfaces are defined in the investigated dowel connection: the neoprene-concrete contact surface, the interaction between steel dowels and concrete/grout, and between steel reinforcement and concrete. This last interaction is modeled considering the perfect adhesion between concrete and reinforcement rebar.

The interaction between dowel and concrete/grout is modeled by an interface element of the ABAQUS software, called “cohesive element”. This element is used to model a

negligible (geometrically) thin layer of bond using a *traction-separation*- and its behavior is defined in terms of a “traction-separation” law, i.e. that is able to catch both the start of the delamination and its propagation. It is able to catch both the start of the delamination and its propagation, even in conditions of mixed modes. The adopted model is showed in Figure 3.46 and it derives from a simplification of the model proposed in Eligehausen et al. (1986). In this study the authors used experimental results in order to deduce an analytical model for the local bond stress-slip relationship of deformed bars valid for confined concrete under generalized excitations (Figure 3.47). The simplified model consists of two branches: a linear increasing branch and a softening branch, that starts at the damage beginning. The characteristic points of the model are obtained according to the following rules: i) the maximum stress (τ_0) and the corresponding slip displacement (s_0) are assumed equal to the coordinates of the C point of the Eligehausen model (τ_{max} , s_1) (Eligehausen et al., 1986); ii) the softening branch (i.e. the s_c value) is defined imposing that the fracture area (G_c , filled area in Figure 3.46) is equal to the values obtained from the integration of the Eligehausen formula from zero to the s_3 displacement, i.e. the residual strength (τ_r) is neglected.

As described in the Section 2.1, a neoprene pad is interposed between the beam and the column. The deriving concrete-to-neoprene interaction offers a frictional strength that is a not negligible contribution to the total connection strength. In the described finite element model the interaction between beam and neoprene and between column and neoprene (generally, concrete and neoprene) is introduced, by the ABAQUS model called “static-kinetic exponential decay”, as a purely frictional interaction, which is able to develop only tangential stresses. The neoprene-concrete friction coefficient is calculated according to the formulas reported in Magliulo et al. (2011), where this coefficient is related to the compressive stress acting on the contact surface: the obtained value is equal to 0.122.

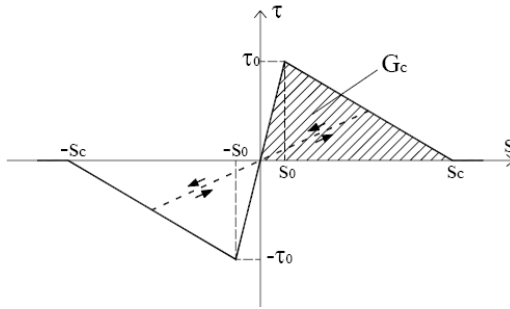


Figure 3.46 Adopted analytical model for cohesive interface elements

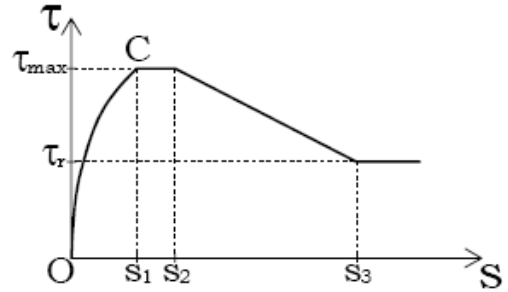


Figure 3.47 Bond-stress versus slip relationship for the deformed bar – confined concrete contact behavior according to the Eligehausen model (Eligehausen et al., 1986)

3.2.4 Loads

Two loads are imposed to the model: the vertical load and the seismic load. The vertical load corresponds to the constant vertical pressure imposed during the monotonic test, distributed on a portion of the beam (60cm x 50cm). In order to apply the horizontal forces, the increasing horizontal displacement history provided during the test is applied to the beam. The versus of the displacement is assumed equal to the experimental one, so that the load is applied against the column cover.

3.2.5 Comparison between numerical analysis and experimental test

The results of the numerical analyses are compared with those obtained from the experimental shear test. Figure 3.48 shows the force-displacement experimental curve (red line) along with the corresponding curve obtained from the FEM analysis (blue solid line). The use of the confined concrete does not significantly change the analysis results; hence, in order to reduce the numerical effort, the unconfined concrete material is used for the whole cross-section of beam and column. The experimental curve is the “elaborated curve” shown in Figure 3.11 (red line), but it is reported until the strength degradation is equal to 20%, since smaller values of forces are not significant in defining the connection behavior. The force shown by the numerical curve is the total shear in the column and the displacement is the relative displacement between the beam and the column. The comparison shows a good fitting in terms of maximum strength and initial stiffness: the maximum shear strength obtained by the numerical model is equal to 160.92kN, while the actual value obtained by the shear test is equal to 161.9kN, with a difference equal to 0.52%.

The reliability of the numerical model is also verified in terms of failure mode. The side splitting of the concrete, i.e. the failure of the lateral cover, is recorded in the

model, as evidenced in the experimental test. Figure 3.49 shows the stress distribution in the column at the failure step, evidencing that the concrete tensile strength (red color) is reached in the fibers of the lateral cover.

The post-peak behavior is not recorded during the analysis because of convergence problems. This problem does not influence the validation of the model, since the connection has a brittle behavior and the last step of the numerical analysis corresponds to the attainment of the failure mechanism in the concrete. As a consequence of above, the model can be considered suitable, since it is able to catch the two main parameters of the actual behavior: the initial stiffness and the maximum strength of the dowel connection.

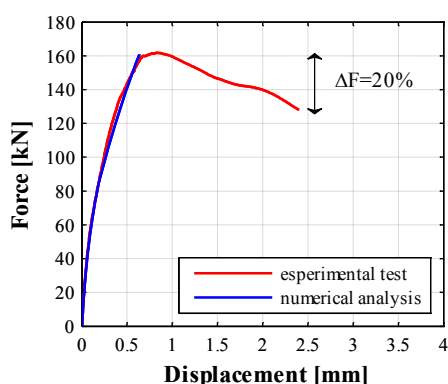


Figure 3.48 Comparison numerical analysis (blue line) vs experimental test (red line) in terms of force-displacement curve

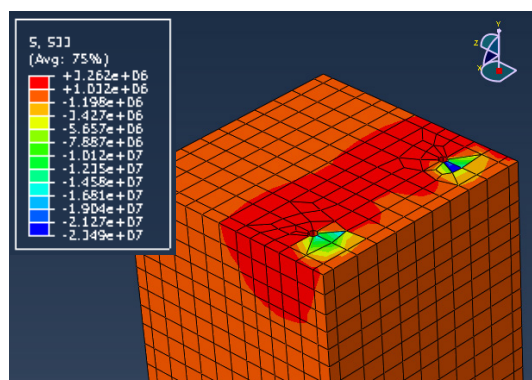


Figure 3.49 Column stress distribution at the failure step resulting from the numerical model

At the failure step, the local demand of the concrete, of the dowels and of the stirrups is also evaluated. According to several experimental tests (Zoubek et al., 2013), the plastic hinges in the dowels form at small depths in the column and in the beam (3-4cm). The deformation at the internal face of the dowel is reported along the beam and column depth in Figure 3.50; the tensile deformation is assumed positive and the compressive deformation is assumed negative. The higher deformations are recorded at a depth of 3 cm in the column and in the beam; this value of depth corresponds to the experimental evidence, i.e. to the depth at which the dowel appears deformed during the inspection of the specimen after the monotonic test (Figure 3.51). A good matching is also found in terms of concrete strains: at the failure step, corresponding to the maximum strength of the connection, the strains recorded by the installed instrumentation are very close to the values estimated by the proposed numerical model (Table 3.7 and Table 3.8).

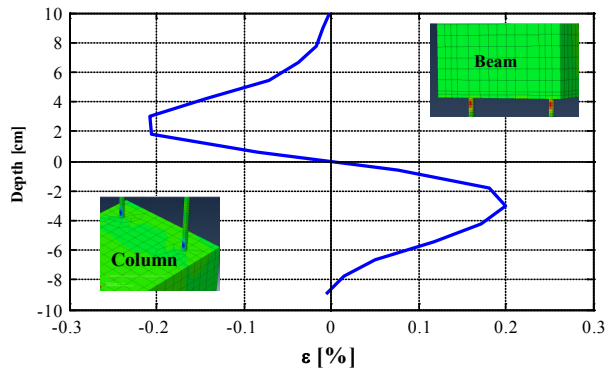


Figure 3.50 Deformation of the dowel at the failure step versus the beam and column depth



Figure 3.51 Steel dowel and (b) measurement of the plastic hinge depth in the steel dowel after the monotonic test

Table 3.7 Comparison between numerical and experimental strains of the column frontal and lateral cover (Figure 3.52)

SV1		SV2	
$\epsilon_{c,num}$	$\epsilon_{c,exp}$	$\epsilon_{c,num}$	$\epsilon_{c,exp}$
0.0033%	0.0038%	0.0099%	0.0082%

Table 3.8 Comparison between numerical and experimental strains of the column top surface (Figure 3.52)

	S1	S2	S3	S4
$\epsilon_{c,num}$	-0.016%	0.003%	0.012%	0.073%
$\epsilon_{c,exp}$	-0.011%	0.0008%	0.010%	0.097%

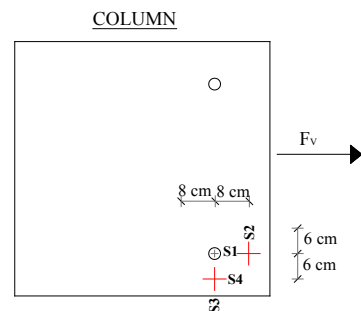


Figure 3.52 Layout of the strain gauges on the column top surface

3.2.6 Shear strength of the dowel connection

An extensive parametric study is carried out in order to investigate the main parameters which influence the shear strength of the dowel connection. The results of this investigation are used to compare the numerical results of the FEM model with the formulae of the technical literature in terms of connection strength and failure modes.

3.2.6.1 Parametric study

The case studies are defined considering three variables: the dowel diameter, the size of the frontal concrete cover and the size of the lateral concrete cover. The connection layout as well as the mechanical properties of the materials (concrete, reinforcement steel and dowels steel) are assumed equal to the properties of the tested specimen. All the connections are implemented by the ABAQUS software, according to the proposed numerical model, and horizontal loads are applied both against the column concrete core and against the column concrete cover.

The results are presented in terms of strength at the failure mechanism of the connection, that corresponds in all the cases to the last step of the nonlinear analyses. At this step the stress values of the materials are equal or very close to their limit values, as shown in the following.

3.2.7 Evaluation of the dowel connection shear strength

In this Section the reference formulae, which provide the shear strength of the dowel connection, are reported. They are compared with the results of the numerical analyses, taking into account the achieved failure mechanism. In all the considered relationships the mean values of the materials strength are used.

The CNR 10025/98 (2000) provides a formula to evaluate the shear strength of the dowel connection. According to this code, if the eccentricity of the shear force (Figure 3.53) is less than half of the dowel diameter (d_b), the connection shear strength is equal to:

$$V_{Rd} = c \cdot d_b^2 \cdot \sqrt{f_{yd} \cdot f_{cd}} \quad (3.6)$$

where c is equal to 1.2, d_b is the dowel diameter, f_{cd} is the concrete design compressive strength and f_{yd} is the dowel design yielding strength. The CNR formulation does not consider the influence of the concrete cover on the connection shear strength, because it supposes that the connection failure always occurs for simultaneous dowel yielding and concrete crushing.

In the analyzed case the shear force eccentricity is less than half of the dowel diameter, because it is equal to half of the neoprene pad thickness.

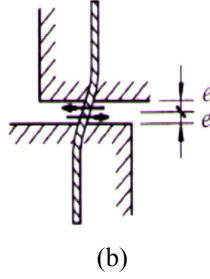


Figure 3.53 Eccentricity of the shear force

According to Vintzeleou and Tassios (1986) there are two possible failure modes of the dowel connection: the simultaneous dowel yielding and concrete crushing (failure mode I), and the concrete splitting (failure mode II). As already discussed in Section 2.2, the two mechanisms depend on the size of the concrete cover in the direction of the load (frontal cover) and in the orthogonal direction (lateral cover) with respect to the dowel diameter. When the concrete covers are greater than 6-7 times the dowel diameter, the failure mode I occurs [8] and, if the shear force eccentricity is negligible, the connection shear strength is equal to:

$$V_{Rd} = k \cdot d_b^2 \cdot \sqrt{f_{ys} \cdot f_{cc}} = 1.3 \cdot d_b^2 \cdot \sqrt{f_{ys} \cdot f_{cc}} \quad (3.7)$$

where f_{ys} is the yield stress of the steel and f_{cc} is the concrete compressive strength. If the concrete cover is lower than 6-7 times the dowel diameter, the strength of the connection is related to the concrete failure rather than to the dowel crisis (failure mode II). Depending on the ratio between the concrete cover in the load direction (frontal cover c_F) and in the orthogonal direction (lateral cover c_L), a bottom splitting (i.e. the failure of the frontal cover) or a side splitting occurs. For low values of c_L/c_F , a side splitting occurs and the connection shear strength is equal to:

$$V_{Rd} = 2 \cdot d_b \cdot b_{ct} \cdot f_{ct} \quad (3.8)$$

where b_{ct} is the net width of the concrete section, evaluated as the section width (normal to the load) minus the diameter of the dowels and f_{ct} is the concrete tensile strength.

If the strength of the connection is related to the concrete failure rather than to the dowel crisis (the concrete cover is lower than 6-7 times the dowel diameter), for low values of c_F/c_L a bottom splitting occurs and the connection shear strength is equal to:

$$V_{Rd} = 5.0 \cdot d_b \cdot c \cdot f_{ct} \cdot \frac{c}{0.66 \cdot c + d_b} \quad (3.9)$$

where c is the frontal concrete cover.

3.2.7.1 Influence of the dowel diameter

The first set of case studies investigates the influence on the connection shear strength of the dowel diameter, ranging from 14mm to 24mm. In these case studies constant values of lateral ($c_L=100\text{mm}$) and frontal cover ($c_F=130\text{mm}$) are assumed. The dowels are threaded steel bars, therefore the resistant diameters, rather than the nominal ones, are used for the strength evaluation.

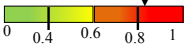
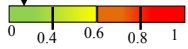
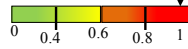
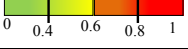
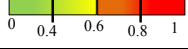
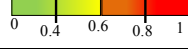
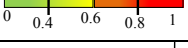
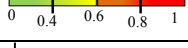
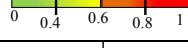
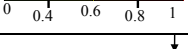
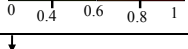
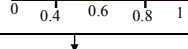
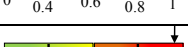
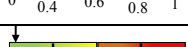

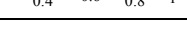
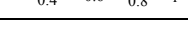
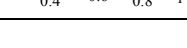
The six diameter values correspond to six numerical models, implemented in the ABAQUS software. For each model, the connection strength corresponding to the failure mechanism is evaluated.

If the force is applied against the concrete core, the failure mechanism involves the lateral concrete cover (failure mode II – side splitting) or the steel dowel and the surrounding compressed concrete (failure mode I). In order to show the failure mode of each connection, the damage percentage at the failure step related to each possible mechanism is showed in Table 3.9. The black arrow indicates the percentage of stress with respect to its limit value. For the failure mode II (side), the black arrow indicates the percentage of the concrete tensile stress with respect to the concrete tensile strength; while for the failure mode I, the black arrow indicates the mean of the percentages of the dowels stresses and of the concrete compressive stress with respect to the corresponding limit values (steel yielding and concrete crushing, respectively). For the failure mode II (bottom splitting), the frontal cover exhibits tensile stresses for small diameters and compressive stresses for higher diameters. In Table 3.9 the black arrow shows the percentage of the concrete tensile or compressive stress with respect to the corresponding strength. Failure mode I only occurs for the connection with the smallest diameter (M14). In all the other cases, the failure occurs because of the concrete splitting, according to the rule for which the concrete failure occurs if the cover is smaller than 6-7 times the dowel diameter. As the diameter increases, the stresses in the dowels and in the surrounding concrete decrease until the 45% of their limit values. The force-displacement numerical curves of the six analyzed cases are reported in Figure 3.54. The first evidence is the increasing of strength and stiffness with the dowel diameter. The major failure displacements are recorded when the connection failure is also characterized by high stresses in the dowels (for the three smallest diameters), while in the other cases the failure displacements are lower and remain almost constant (the decrement with respect to the maximum displacement is around the 30%).

If the force is applied against the concrete cover, the frontal cover always exhibits tensile stresses. In Table 3.10 the percentages of damage are reported for all the three mechanisms. The black arrow in the column of the failure mode II due to the bottom

splitting indicates the percentage of the tensile stress in the column frontal cover with respect to the tensile strength of the concrete. Since in all the analyzed cases the ratio between the lateral and the frontal cover is constant and lower than one, the connection failure is caused by the lateral cover splitting. For this loading condition, even though the trend of the force-displacement curves is more regular, the strength on average decreases of the 15% with respect to the case of load applied against the concrete core.

Table 3.9 Damage percentage at the connection failure for each collapse mechanism, when the force is applied against the concrete core

d_b [mm]	Failure mode II (side)	Failure mode II (bottom)	Failure mode I
14			
16			
18			
20			
22			
24			

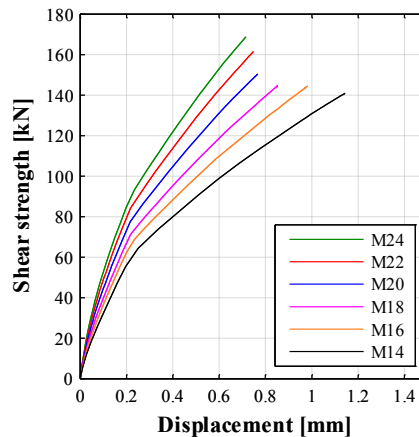
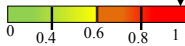
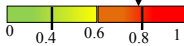
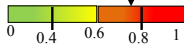
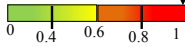
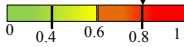

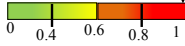
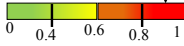
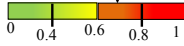
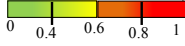
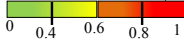
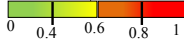
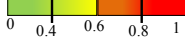
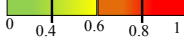
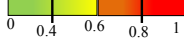
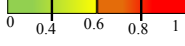
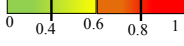
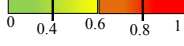


Figure 3.54 Shear force against the concrete core: force-displacement curves varying the dowels diameter

Table 3.10 Damage percentage at the connection failure for each collapse mechanism, when the force is applied against the concrete cover

d_b [mm]	Failure mode II (side)	Failure mode II (bottom)	Failure mode I
14			
16			
18			
20			
22			
24			

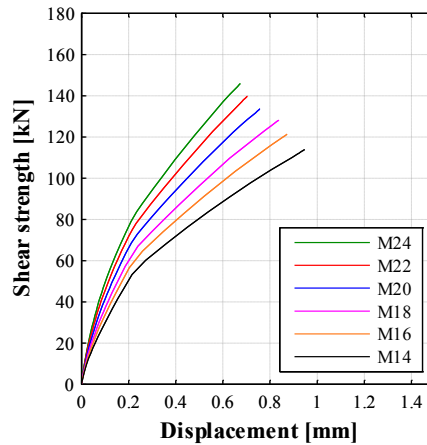


Figure 3.55 Shear force against the concrete cover: force-displacement curves varying the dowels diameter

The strength of each case study is compared (Figure 3.56) with the above presented literature formulae (see Section 5.2). The considered formulae are the CNR one (equation (3.6), black line) and the Vintzeleou and Tassios relationships (equations (3.6), (3.7), (3.8) and (3.9), green, magenta and cyan line, respectively). The failure modes are identified by different marker shapes: the diamond marker is used for the failure mode I, the circle marker is used for failure mode II with side splitting mechanism and the square marker is used for failure mode II with bottom splitting mechanism. The literature formulae provide different values with respect to the numerical results; however these differences can be justified.

For failure mode I the formulae are based on experimental tests in which the tested connections were different with respect to the investigated ones. For example, the coefficient $k=1.3$ is based on tests performed on connection systems with smooth steel bars as reinforcement.

In the case of splitting failure, the differences can be understood discussing the expression (3.8). According to Vintzeleou and Tassios (1986), in a horizontal section I-I (Figure 3.57), the compressive stresses on the concrete (σ_{cc}) are equilibrated by the tensile stresses (σ_{ct}). When these tensile stresses achieve the tensile strength of the concrete, a longitudinal crack opens and the failure starts.

According to Hetenyi (1946) and considering the bar as a beam on an elastic foundation, the compressive stress (σ_{cc}) distribution along the bar can be computed as:

$$d_b \sigma_{cc}(x) = \left[\frac{-2\beta D}{\sinh^2 \beta L - \sin^2 \beta L} \left[\sin \beta L \cosh \beta x \cos \beta(L-x) - \sinh \beta L \cos \beta x \cosh \beta(L-x) \right] \right] \quad (3.10)$$

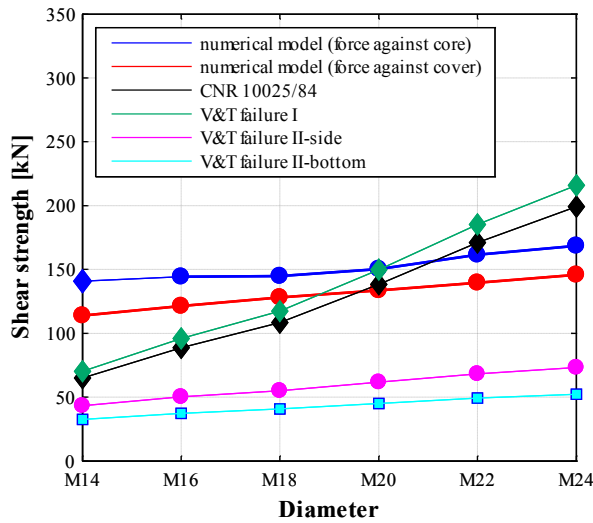


Figure 3.56 Comparison between the shear strength obtained by the numerical model and the shear strength obtained by formulations available in technical literature, for different values of dowel diameter

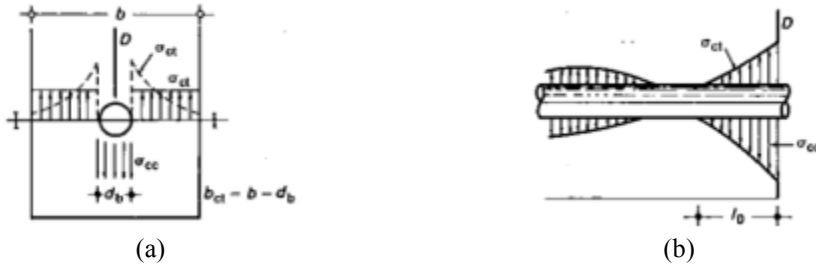


Figure 3.57 Stresses in the concrete around the dowel: (a) in the cross section and (b) along the dowel (Vintzeleou and Tassios, 1986)

In the formula (3.10) β is the foundation modulus, x is the distance from the concrete external surface, L is the dowel length embedded in the concrete and D is the shear load. According to the Vintzeleou and Tassios (1986) assumptions, the compressive stresses result equal to zero at $x=2.5d_b$, assuming $\beta L=5$ (usual concrete quality) and $L=8d_b$. The total compressive force is equal to:

$$F_{cc} = d_b \int_0^{2.5d_b} \sigma_{cc}(x) dx \approx 1.22D \quad (3.11)$$

Then the strength D_{cr} can be obtained by the equilibrium at $x=2.5d_b$:

$$F_{cc} = F_{ct} \rightarrow 1.22D_{cr} = f_{ct} \cdot b_{ct} \cdot 2.5 \cdot d_b \quad (3.12)$$

The comparison between the numerical results obtained by the ABAQUS model and those obtained by the expressions (3.10), (3.11) and (3.12) is reported in the following in the case of dowel diameter equal to M20. Figure 3.58 shows the compressive stress distribution obtained by the ABAQUS model, while Figure 3.59 shows the same distribution evaluated by the expression (3.10) and according to the investigated connection ($\beta=0.047$ and $L=600\text{mm}$). According to the analytical distribution, the length of the compressive stresses results equal to 46.2mm (x_c), i.e. 2.31 times the dowel diameter. In the FEM model this length is equal to 50mm and this result confirms the validity of the proposed model as well as the assumption of Vintzeleou and Tassios (1986). Concerning the tensile stresses, the distribution is reported in Figure 3.60 (red color) and it shows that they are equal to zero at 100mm (x_t). If in equation (3.11) and in the equation (3.12) the equilibrium is evaluated at 100mm , the resistance becomes equal to:

$$D_{cr} = \alpha \cdot b_{ct} \cdot d_b \cdot f_{ct} = 4.88 \cdot b_{ct} \cdot d_b \cdot f_{ct} \quad (3.13)$$

It is evident that the (7) is different than the (3), justifying the differences between the results obtained by the expression (3) and the ABAQUS model (see Figure 3.61). Other sources of differences between numerical analyses and literature formulae are: the neglecting of the tangential stresses, assumed equal to zero at 100mm, even though they are not negligible (Figure 3.61); the neglecting of the steel stirrups in the column in the strength evaluation.

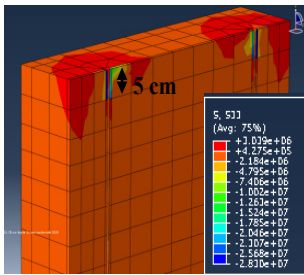


Figure 3.58 Stresses in the concrete near the dowel at the failure step by the ABAQUS model

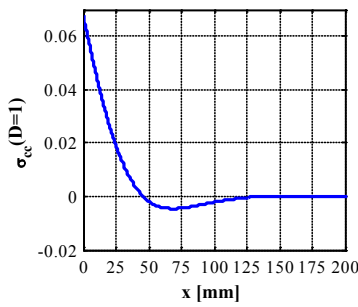


Figure 3.59 Stress distribution evaluation according to the Hetenyi theory (Hetenyi, 1946)

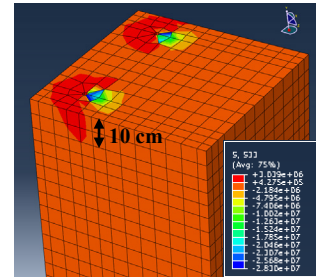


Figure 3.60 Stresses in the concrete near the dowel at the failure step by the ABAQUS model

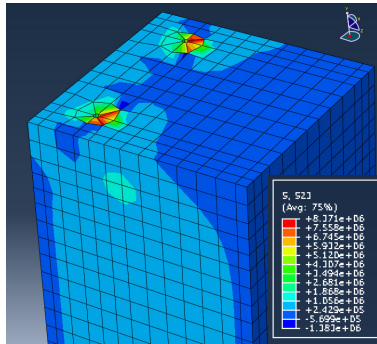


Figure 3.61 Tangential stresses distribution in the concrete near the dowel at the failure step by the ABAQUS model



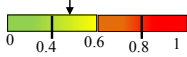
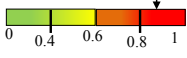
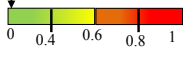
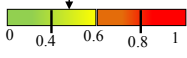
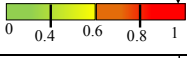
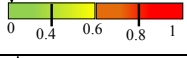
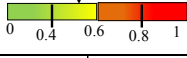
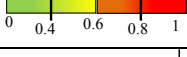
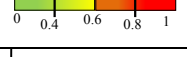
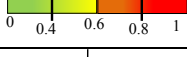
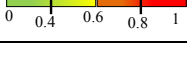
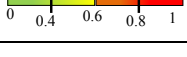
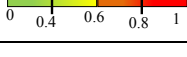
3.2.7.2 Influence of the frontal cover

The set of numerical analyses that investigates the frontal cover influence are reported in the following. The reference connection has a constant dowel diameter (M27) and a constant value of lateral cover ($c_L=100\text{mm}$).

If the horizontal force acts against the concrete core, the connection failure always occurs for side splitting of the column concrete (Table 3.11). For this loading condition, the frontal cover does not significantly influence the connection strength, that varies of the 12% (Figure 3.62). This happens because, if the horizontal force acts against the concrete core, the exhibited failure mechanisms are only the failure mode I and the failure mode II due to the concrete side splitting; this is confirmed by Table 3.11, where the frontal cover always shows very low compressive stresses. Furthermore, in the analyzed case, the ratio between the lateral cover and the dowel diameter is constant and much lower than 6.

If the horizontal force acts against the concrete cover, the connection failure always occurs when the concrete reaches the tensile strength in the lateral cover (Table 3.12), unless in the case the frontal cover c_F is equal to 50mm. In this case the bottom and the side splitting contemporaneously occur and the connection strength is very low (Figure 3.63). As expected, the tensile stresses in the frontal cover decrease at the increasing of the frontal cover (Table 3.12) and, for values of c_F larger than 100 mm, the connection strength reaches an almost constant value (Figure 3.63), which is related to the side splitting. The analyses, performed with the horizontal force acting against the concrete cover and with a constant value of the ratio between the lateral cover ($c_L=100$ mm) and the dowel diameter (M27) much lower than 6, confirm that for c_L/c_F ratio values lower than one a side splitting occurs; on the contrary, if such a ratio is larger than one, a bottom splitting occurs.

Table 3.11 Damage percentage at the connection failure for each collapse mechanism, when the force is applied against the concrete core

c_F [mm]	Failure mode II (side)	Failure mode II (bottom)	Failure mode I
50			
100			
150			
200			
250			

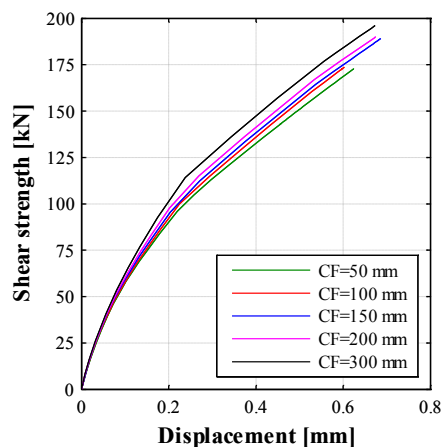
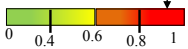
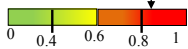




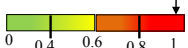
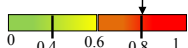
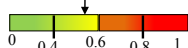
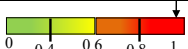
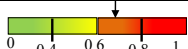

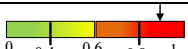
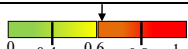
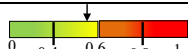


Figure 3.62 Shear force against the concrete core: force-displacement curves varying the frontal cover

Table 3.12 Damage percentage at the connection failure for each collapse mechanism, when the force is applied against the concrete cover

c_F [mm]	Failure mode II (side)	Failure mode II (bottom)	Failure mode I
50			
100			
150			
200			
250			

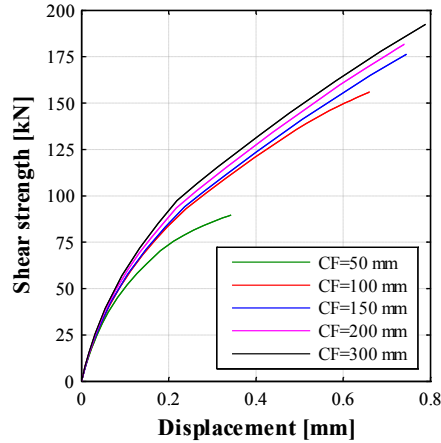


Figure 3.63 Shear force against the concrete cover: force-displacement curves varying the frontal cover

In Figure 3.64 the results of the numerical analyses obtained varying the frontal cover are compared to the results of the formulae, (3.7), (3.8) and (3.9). Even though for the most of the cases the failure is related to the side splitting, the formula (3.8) provides too low strength values, as illustrated in Section 5.3.2. Formulae and (3.7) provide results closer to those provided by the numerical analyses, unless in the case of $c_F=50\text{mm}$, when the failure involves the frontal cover.

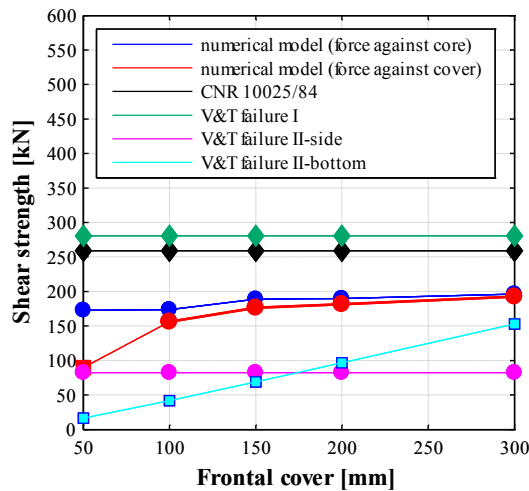


Figure 3.64 Comparison between the shear strength obtained by the numerical model and the shear strength obtained by formulations available in technical literature, for different values of frontal cover

3.2.7.3 Influence of the lateral cover

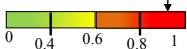

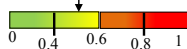
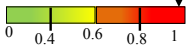

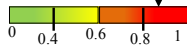

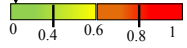
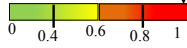
A third set of numerical analyses is performed varying the lateral cover, assigning a constant dowel diameter (M27) and a constant frontal cover ($c_F=130$ mm).

When the horizontal force acts against the concrete core, for the lateral cover $c_L= 50$ mm the connection failure is due to the side splitting (Table 3.13). For greater lateral covers, the connection failure is still due to the side splitting, but the stress in the dowel becomes closer to the yielding one (second column in Table 3.13). The increase of the lateral cover leads to a better confining effect, so that the connection shows a higher shear strength (Figure 3.65).

When the horizontal force acts against the concrete cover, the connection failure is due to the concrete side splitting for the cases with $c_L= 50$ mm and $c_L= 100$ mm; while it is strongly conditioned by the bottom splitting failure for the largest value of the lateral cover ($c_L= 200$ mm). Obviously, as the lateral cover increases, the stress of the dowel at the failure also increases (Table 3.14). For this loading condition, the shear strength as well as the failure displacement are highly influenced by the lateral cover depth (Figure 3.66).

Figure 3.67 shows the comparison between the numerical results obtained by the ABAQUS model and the results provided by the formulae, (3.7), (3.8) and (3.9), confirming the bad prediction of these relationships in evaluating the connection strength.

Table 3.13 Damage percentage at the connection failure for each collapse mechanism, when the force is applied against the concrete core

c_L [mm]	Failure mode II (side)	Failure mode II (bottom)	Failure mode I
50			
100			
200			

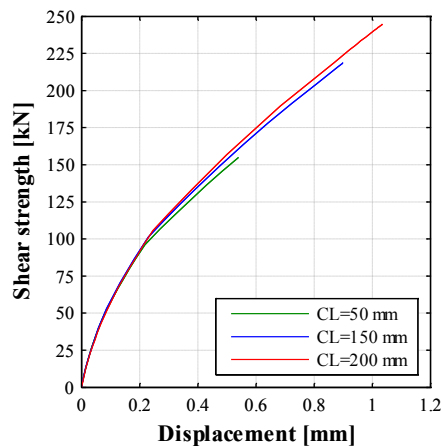


Figure 3.65 Shear force against the concrete core: force-displacement curves varying the lateral cover

Table 3.14 Damage percentage at the connection failure for each collapse mechanism, when the force is applied against the concrete cover

c_L [mm]	Failure mode II (side)	Failure mode II (bottom)	Failure mode I
50			
150			
200			

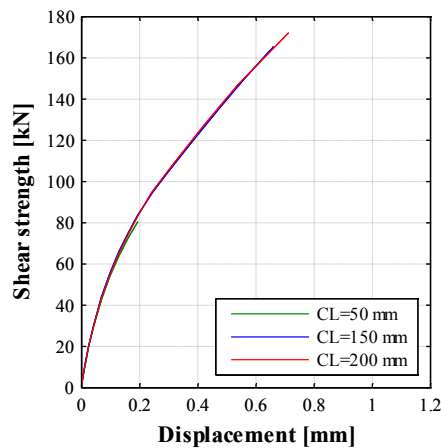


Figure 3.66 Shear force against the concrete cover: force-displacement curves varying the lateral cover

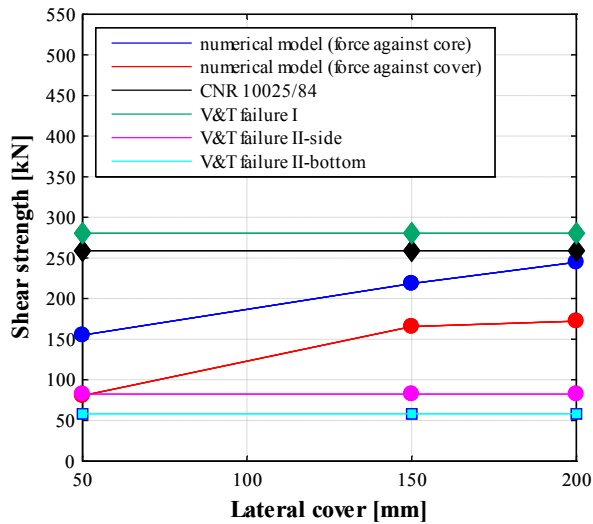


Figure 3.67 Comparison between the shear strength obtained by the numerical model and the shear strength obtained by formulations available in technical literature, for different values of lateral cover

3.2.8 Conclusions

The seismic response of concrete precast buildings is highly influenced by the response of the connection systems, among which the beam-to-column connection. The presented work investigates the response of dowel beam-to-column connections, typical of European precast industrial buildings, by means of a FEM model of this connection, validated by experimental test results. The reference test is the shear monotonic test on a dowel beam-to-column connection, described in Section 3.1.1. The results of the test confirm the expected behavior of this kind of connection under horizontal load, showing a brittle splitting failure in the concrete lateral cover of the column.

The numerical model of the connection is presented in details and compared with the results of the monotonic test, showing a good agreement in terms of maximum strength, failure mechanism and local stress.

An extensive parametric study is performed in order to discuss the influence of some geometrical characteristics of the investigated connection on its shear strength. Many case studies are implemented by varying the diameter of the dowels as well as the lateral and frontal concrete covers of the column, and nonlinear analyses are performed. The results of all the case studies show the sensitivity of the model to the parameters variation in terms of strength and of failure mechanism. It is confirmed that, if the lateral and the frontal covers are lower than 6-7 times the dowel diameter, the failure involves the concrete splitting, both in the case of force acting against the concrete core and in the case of force acting against the concrete cover. Furthermore, if

the lateral cover is equal or lower than the frontal cover, the side splitting occurs; otherwise, only in the case of force acting against the concrete cover, the failure also involves the bottom splitting.

The results of the parametric study are finally compared with some formulae proposed in technical literature: the CNR 10025/84 one and the Vintzeleou and Tassios relationships.

The CNR 10025/84 formula and the Vintzeleou and Tassios one, which takes into account the failure mechanism involving the steel dowel and the surrounding compressed concrete (failure mode I) are very similar and generally are the closest to the results of the numerical analyses, even though the FEM analyses in the most of the cases show a failure mode II (concrete splitting). The low reliability of these formulas are justified considering that they are based on experimental tests in which the tested connections were different with respect to the investigated ones.

On the other side, the Vintzeleou and Tassios relationships concerning the side and the bottom splitting provide too low strengths with respect to the numerical ones. The large differences are discussed and justified considering the assumptions made by the theoretical formulae.

3.3 Panel-to-structure connection

The presented study investigates the cladding panel influence on the seismic response of a benchmark precast industrial building, designed according to Eurocodes, by means on nonlinear dynamic analyses. Both the bare model and the model with vertical panels are implemented in the OpenSees (McKenna and Fenves, 2013) program, according to the models described and proposed in the Section 2.4. The results of the nonlinear analyses show the high influence of the panel-to-structure interaction on the seismic global response of the precast buildings: the forces distribution in the structural elements changes due to the high stiffness of the nonstructural panels. As a consequence of above, high values of forces are recorded in the connections systems between the panels and the structure, that are demonstrated to be higher than the design strength capacity.

A seismic risk assessment analysis is also performed in order to evaluate the influence of the panels on the global collapse probability of failure. Assuming that the failure of the panels corresponds to the achievement of the ultimate limit state, the incremental dynamic analyses demonstrate that the probability of failure drastically decreases if the cladding panels are introduced in the model since their collapse always forward the structural elements damage and collapse (e.g. the achievement of the ultimate rotation capacity in the precast columns).

If the panel collapse (i.e. the panel-to-structure connection failure) is not assumed as the global structural collapse but their influence on the seismic response cannot be neglected, a new model is needed in order to take into account the effective distribution of damage, failure and forces during the seismic excitation. This need motivates the implementation of an innovative model that considers the panel presence in the structure but that controls the damage state in the connections during the analysis steps, removing the failed elements when the connection strength is achieved. The results of the nonlinear dynamic analyses with this model demonstrate an important difference in the structure response if the panels collapse is simulated, justifying some recorded damages and the real behavior of the structure when the interaction cannot be neglected.

3.3.1 State of art

The panel-to-structure interaction problem is an important topic, related to the economic losses in industrial production and to the life safety of humans. The scientific community studied this problem over the last fifty years: in the Section 2.4 the studies on the dynamic characteristics of structures with panels are reported, while in the following the main results about the panels influence on the seismic response of structures are described.

The first studies that recognized the important influence of cladding panels on the structural response are the researches of Gjelsvik (1974) and Oppenheim (1973).

In the following years the research team of Georgia Institute of Technology developed a research program with the aim to study an existing 25-story steel-frame office structure (Palsson et al., 1984), developing several researches on the dynamic influence of cladding and on the seismic response of the connected structures. Since the results on the dynamic properties demonstrated the high influence of the panels (Section 2.4), the researcher group justify this influence by investigating the cladding panels as potential sources of lateral stiffness. In the framework of the study, Goodno and Palsson (1986) developed four different analytical models to represent the building precast façade, among which the interstory shear stiffness model was found to be the simplest and the most efficient one. In this model, the authors added the stiffness of the cladding panels through a constant interstory shear stiffness value, at each story. According to the results of the analyses on this model, the authors concluded that the building claddings and the other nonstructural components are largely neglected sources of lateral stiffness in high-rise buildings: the added stiffness provided by architectural elements may substantially alter the overall building response and invalidate the response predictions based on a bare frame model.

The same researcher group also tried to model the presence of cladding panels by introducing slotted connections in order to represent the case in which the interaction between the panels and the structure is avoided (Goodno et al., 1984). The results of this study demonstrated that the performance of the structure is distinctly different when cladding effects are included in the model. Moreover, in all the investigated cases, the peak interstory drift along the direction of the applied ground motion exceeded the allowable drift values in the slotted connections; demonstrating that the slot dimension should also be greater than the recorded drift if the interaction could be neglected. In Goodno and Craig (1989) a summary of this research was provided, showing that the precast cladding systems contribute to the lateral strength of multistory buildings and that the research was going to develop special connections devices between panels and structure, able to provide additional damping, i.e. dissipative systems, in order to reduce the expected drifts in case of seismic events. The basic concepts on structure ductility, connection devices and high damping panels, able to reduce the seismic response of structures, are summarized in Pinelli et al. (1995).

An interesting work on the effect of the external cladding system on the damping properties of a steel structure was carried out in Thiel et al. (1986), who conducted a series of nonlinear dynamics analyses of a benchmark 15-stories and four spans building, with uniformly distributed mass and stiffness. The cladding system was modeled as concentrated dampers at each floor, with an elastic perfectly plastic behavior and the results of the nonlinear dynamic analyses were recorded in terms of

roof displacement and total shear at the base. The main conclusion was that the efficiency of the damper, which represent the panels, increases with the assigned yielding strength level; for high levels of the yielding strength and a frame viscous damping of 2%, the response of the structure reduces by approximately 40% in terms of maximum displacement in the panels, and by 45%, in terms of base shear. However, even if the authors argued that the effective damping of a building can be increased through the activation of the lateral resistance of the cover panels and through the hysteretic behavior of the connections, the connections require very high stiffness to be effective, too high if compared to the typical designed devices.

Wolz et al. (1992) analyzed the case of a six-story building, modeled in 1:4 scale with two panels for each bay, introduced in the model as rigid truss elements, connected at the beam-to-column joint. The two connections were modeled with a bilinear force-deformation backbone curve, with an arbitrarily chosen initial stiffness. Some dynamic analyses were performed with some input records with a maximum amplitude of 0.3g and then the displacements at the top are recorded both with and without the trusses, showing that the displacements of the model with panels were 33% lower than the ones recorded on the bare frame.

In a PEER (Pacific Earthquake Engineering Research Center) report, Hunt and Stojadinovic (2010) studied a nine-story steel building in Los Angeles, modeled with and without the external cladding panels. The building is modeled as a bare frame, i.e. with no cladding systems. As anticipated in the Section 2.4.1 of this thesis, according to the modal analyses in this work, the cladding system did not significantly influence the building dynamic properties both in terms of periods and modal shapes. However, the performed non-linear analyses (static and dynamic) showed a significant influence of the precast concrete panels on the structural behavior when strong motions occur.

As indicated by previous studies, the panel-to-structure connection behavior has a significant influence on the interaction between supporting frame and cladding panels. Stiffness and strength of these connections vary widely, consequently a large effort in collecting data is needed, in order to study the influence of the cladding system on the building response. In the last years a significant research effort has been done and is ongoing in order to study precast buildings connection systems. Two main European research projects are conducted in these years on precast buildings: the SAFECAST (Toniolo, 2012) and the SAFECLADDING projects. The first project was concluded in 2012 and its main scope was the improvement of the knowledge on the seismic behavior of precast pre-stressed structures, with specific reference to connections. The latter project is ongoing and it studies the influence of cladding panels on the resisting system of precast industrial buildings. Within these projects several papers have been recently published, among them the paper of Biondini et al. (2013). This paper studies the influence of vertical panels on the seismic behavior of one-story precast structures.

The study considers the panel as pendulum, with two hinges applied one at the top and one at the bottom of each panel, and two main degrees of reciprocal connection between the panels: a) absence of connections (statically determined solution) with structural response given only by the columns, and b) perfectly rigid connections (integrated solution) with structural response almost only given by the wall panels. Since in the latter case the forces on the connections are too high and the design of proper devices is too difficult, the authors propose the use of an innovative dissipative connection between vertical panels in order to attenuate the seismic response of the integrated wall-frame system. The effectiveness of this solution is demonstrated by means of nonlinear static (pushover) analyses and nonlinear dynamic analyses under recorded and artificial earthquakes.

3.3.2 Benchmark structure

The benchmark structure is a one-story precast industrial building. The geometrical features of the structure are described in Figure 3.68. The building consists of precast columns, fixed at the base (Osanai et al., 1996), and connected at the top by hinged prestressed beams, which support the roof elements.

The structure is designed for a medium-high seismicity Italian area (design peak ground acceleration at the bedrock equal to 0.168g) according to Eurocode 8 (CEN, 2005) and for a ductility class “H”. The concrete class is C45/55 for columns with elastic modulus equal to 36283 MPa. The seismic weight is obtained considering all the structural and the nonstructural elements (panels) as well as the live loads on the structures; the values of the seismic weight is about 7kN/m².

The columns have a square cross-section (80cm x 80cm), reinforced with 28 ϕ 22 as longitudinal bars ($\rho=1.66\%$) and with stirrups ϕ 10 spaced of 12.5 cm. The horizontal elements are designed according only to the vertical loads (structural and accidental loads) and they consist of prestressed TT roof elements, variable section prestressed beams in the transversal direction (Z direction in Figure 3.68) and rectangular cross-section beams in the longitudinal direction (X direction in Figure 3.68). The assumed behavior factor is equal to 4.5, as indicated in the EC8 for RC frames.

The investigate panel system consists of vertical RC precast panels, connected to the roof horizontal beams. The investigated connection system (Figure 3.69a) consists of two steel profiles, embedded in the element to be fixed (panel) and in the fixed element (horizontal element, e.g. beam). The two profiles (Figure 3.69b) are generally orthogonal in order to allow the adjustment of the panel in two directions. The connector (Figure 3.69d) is a steel plate, which may be knurled to prevent sliding; it has a hammer-end for the attachment in the connected element, and a slot for adjustment in the assembly phase. The connector links the interlock (Figure 3.69c) to the profile in the horizontal element. It follows that the connection yields three

unrestrained, even though limited, translational degrees of freedom: one is ensured by the slot in the plate (typically displacement of 50 mm is allowed), and the other two are due to the channel bars (the allowable displacement depends on the profiles length). At the bottom, the panel connection can be ensured in different ways. This connection may be achieved by clip-panel beams equipped with a fork, to which the base of the panel is rigidly connected using a mortar casting. This kind of connection is no longer in use due to the high cost of construction and to the low seismic efficiency. Welded or bolted metal anchors are today widespread. According to the described characteristics and to the described studies, it is possible to classify the panel to structure connection and to choose the realistic model for numerical analyses. In particular, the investigated connection could be assumed as a sway-type connection.

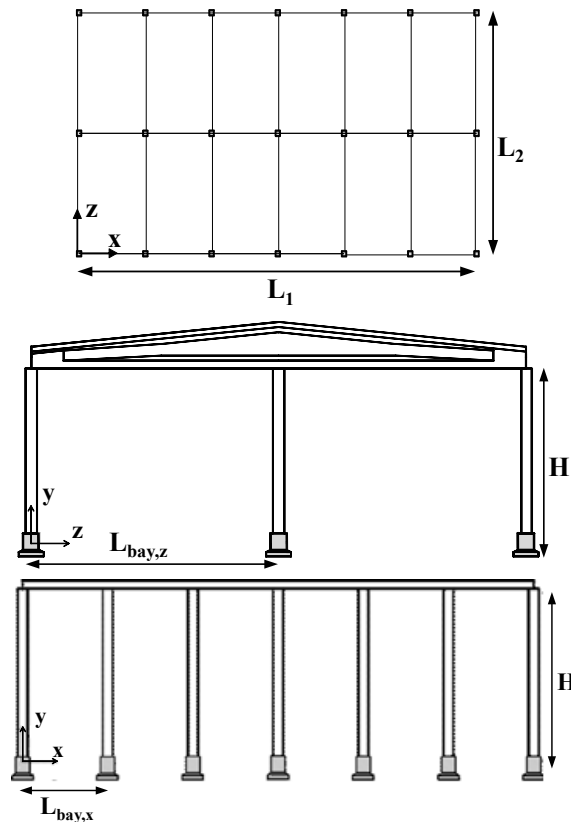


Figure 3.68 Benchmark one-story precast building: a plan view, b transversal bays and c longitudinal bays

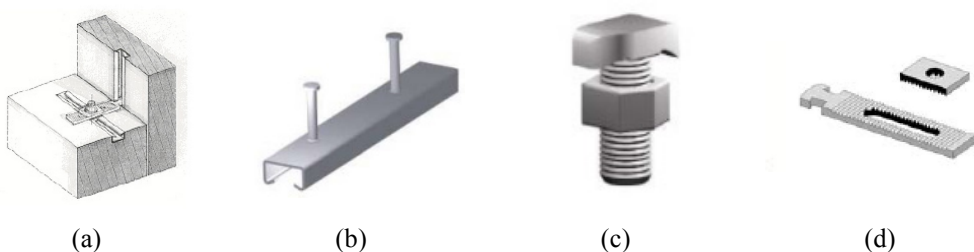


Figure 3.69 (a) Investigated connection between vertical precast panel and resistant structure: (b) channel bar, (c) interlock and (d) connector

3.3.3 Nonlinear model

This study aims at investigate the influence of the precast panels on the seismic response of one-story precast structures by means of nonlinear dynamic analyses. The analyses are performed on the bare frame as well as on the structure with cladding panels in the software OpenSees. In the bare case the panel-to-structure interaction is neglected, representing the widespread modeling approach of precast structures. The nonlinear behavior of the structure is concentrated at the column base by means of a lumped plasticity model. In the model with cladding panels the interaction is considered by modelling the cladding panels and their connection.

The moment-curvature envelope of the columns is obtained considering three types of fibers in the cross-section: the unconfined concrete fibers in the concrete cover; the concrete confined fibers (Mander et al., 1988) in the concrete core and the steel fibers of the reinforcing bars. On the results of the fiber analysis of the section, the plastic hinge behavior is evaluated in terms of moment-rotation envelope. The adopted model is a tri-linear envelope, which neglects the cracking point, defining three characteristic points: the yielding, the capping and post-capping points. The values of this points are assumed according to Fischinger et al. (2008), where the best envelope for precast columns are suggested, according to the results of some experimental tests.

The yield drift is calculated according to the formula proposed by Fardis and Biskinis (2003):

$$\theta_y = \phi_y \cdot L_s / 3 + 0.00275 + \frac{\varepsilon_y}{d - d'} \cdot \frac{0.2 \cdot d_b \cdot f_y}{\sqrt{f_c}} \quad (3.14)$$

where:

- ϕ_y is the yield curvature (evaluated as described in the previous section);
- L_s is the shear span;
- a_{s1} is a zero-one variable indicating the slip of the longitudinal bars from their anchorage (1-slip, 0-no slip);

- $(d - d')$ is the distance between the tension and compression reinforcement;
- ε_y is the yield strain of the tension reinforcement;
- f_y and f_c are the yield stress of the tension reinforcement and the compressive strength of the concrete (both in MPa), respectively.

The other points of the moment-rotation curve were calculated according to Haselton (2006):

$$\theta_{cap} = 0.12 \cdot (1 + 0.4 \cdot a_{st}) \cdot 0.2^v \cdot (0.02 + 40 \cdot \rho_{sh})^{0.52} \cdot 0.56^{0.01 f_c} \cdot 2.37^{10.0 \rho} \quad (3.15)$$

$$\theta_{pc} = 0.76 \cdot 0.031^v \cdot (0.02 + 40 \cdot \rho_{sh})^{1.02} \leq 0.1 \quad (3.16)$$

Equations (3.15) and (3.16) are the capping and the post-capping rotation capacity, respectively. In the expressions above ρ and ρ_{sh} denote the longitudinal and transverse reinforcement ratios, respectively, and v is the axial load ratio.

Whereas M_y can be calculated analytically, the capping moment (M_c) is determined from:

$$\frac{M_c}{M_y} = 1.25 \cdot 0.89^v \cdot 0.91^{0.01 \cdot f_c} \quad (3.17)$$

The energy dissipation capacity of the plastic hinge is taken into account by the factor λ (3.18). Since, it is important to realize that the envelope curve used in the Ibarra model is a monotonic one, and cannot be directly compared with the envelope of the cyclic response, a normalized energy dissipation capacity is calculated as:

$$\lambda = 127.2 \cdot 0.19^v \cdot 0.24^{s/d} \cdot 0.595^{V_p/V_n} \cdot 4.25^{\rho_{sh,eff}} \quad (3.18)$$

Where s/d is the ratio of stirrup spacing to column depth; V_p/V_n is the ratio of shear at flexural yielding to shear strength; and $\rho_{sh,eff}$ is the effective ratio of transverse reinforcement.

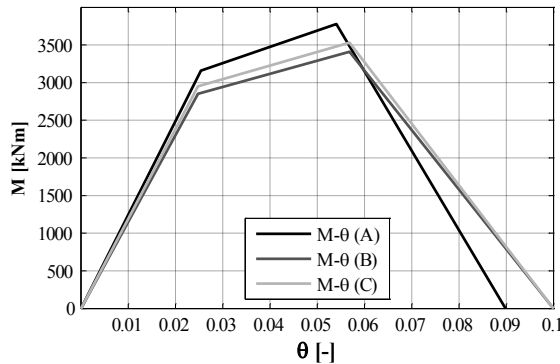


Figure 3.70 Moment-rotation envelopes

As anticipated, the adopted model for panels and connection system is assumed in order to take into account the possible interaction between the panels and the structure. As in Section 2.4, the model of the panel-to-structure connections consists of:

- two hinge connections at the bottom of each panel;
- two constraints that allow rotations but avoid the sliding of the panel with respect to the beam, at the top of the panel.

The single panel is modeled as a two-dimensional frame (Figure 3.71), as proposed in Hunt and Stojadinovic (2010), composed of four elastic one-dimensional elements:

- two vertical elements, characterized by area and moment of inertia equal to the half of area and moment of inertia of a single panel;
- two horizontal beams modeled as rigid bodies.

The vertical elements take into account the inertia properties of the panels and the two horizontal rigid elements give to the panel model the characteristics of a bi-dimensional element. The seismic masses are assumed equal to the values of the bare models. In both the bare model and the model with the cladding panels the rigid diaphragm hypothesis is used, assuming stiff and strong roof connections that allow a rigid behavior of the roof, also when the cladding panels interact with the structure.

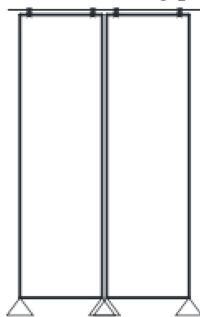


Figure 3.71 Linear elastic model of the structure with cladding panels: a model of two vertical panels with the bi-dimensional frame

3.3.4 Seismic input

The nonlinear dynamic analyses are performed with a set of 7 natural accelerograms (CEN, 2005), selected in order to match the code elastic spectrum of the considered seismic zone (Iervolino et al., 2010). The records and the verification of the spectrum compatibility are reported in Figure 3.72. In Table 3.15 the main parameters of the natural earthquakes are reported in terms of: earthquake ID (1st column), name of the real event (2nd column), date of the event (3rd column), magnitude (4th column), peak ground acceleration (5th column) and type of soil according to the EC8 categories (6th columns).

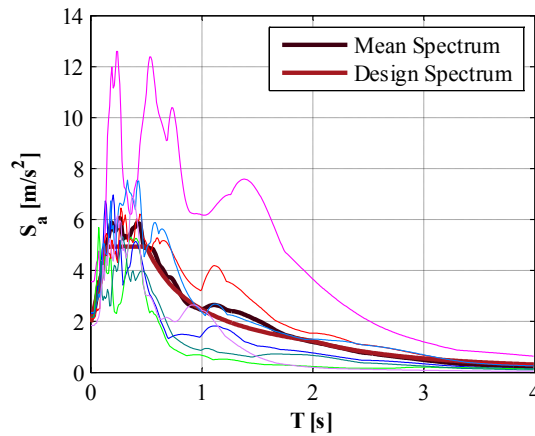


Figure 3.72 Spectrum of the record comparison between their mean spectrum (black solid line) to the code design spectrum (red solid line)

Table 3.15 Main parameters of accelerograms in the performed dynamic analyses

Earthquake ID	Earthquake Name	Date	Mw	PGA [m/s ²]	EC8 Site class
414xa	Kalamata	13/09/1986	5.9	2.3537	B
147ya	Friuli (aftershock)	15/09/1976	6.0	2.3189	
413xa	Kalamata	13/09/1986	5.9	2.1082	
1714ya	Ano Liosia	07/09/1999	6.0	2.1588	
6093ya	Kozani (aftershock)	19/05/1995	5.2	1.8431	
239xa	Dursunbey	18/07/1979	5.3	2.1314	
199ya	Montenegro	15/04/1979	6.9	3.5573	

3.3.5 Bare structure: nonlinear analyses results

The dynamic analyses are performed on both the bare and with the cladding panels models and the behavior in the two main directions (X and Z) are investigated, separately applying the records in X and Z directions of the structure.

The results of the nonlinear dynamic analyses on the bare model are reported in terms of displacement-time and force-time curves and the global response of the structure is shown in terms of the force-displacement diagram. In these diagrams the force is the sum of the shear forces in the columns in the investigated direction and the displacement is the displacement of the master joint at the roof level in the investigate direction. Figure 3.73 and Figure 3.74 show the results for the bare structure in X and Z directions, respectively.

Under all the considered set of natural accelerograms, the structure does not experience any inelastic deformation for both the directions.

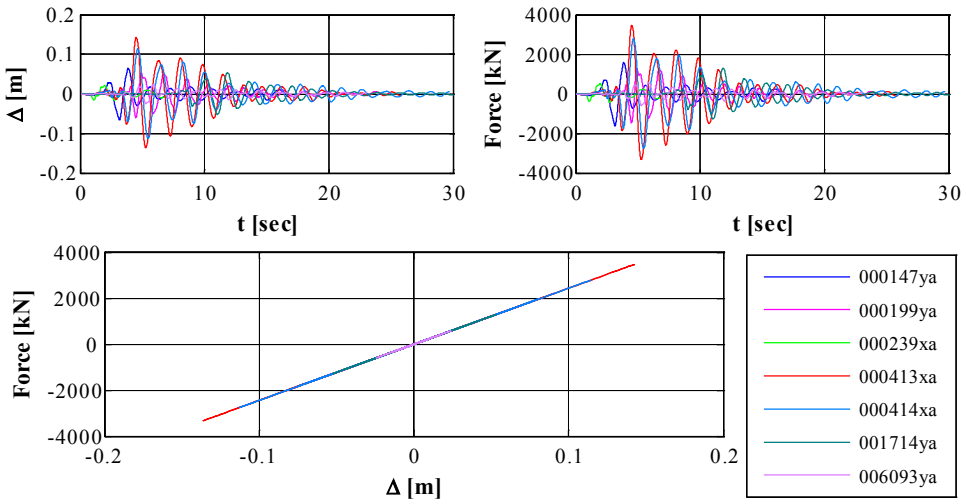


Figure 3.73 Results of the dynamic analyses on the bare model in the X direction of the structures: displacement-time curve (left plot in the first row), force-time curve (right plot in the first row) and force-displacement curve (plot in the second row).

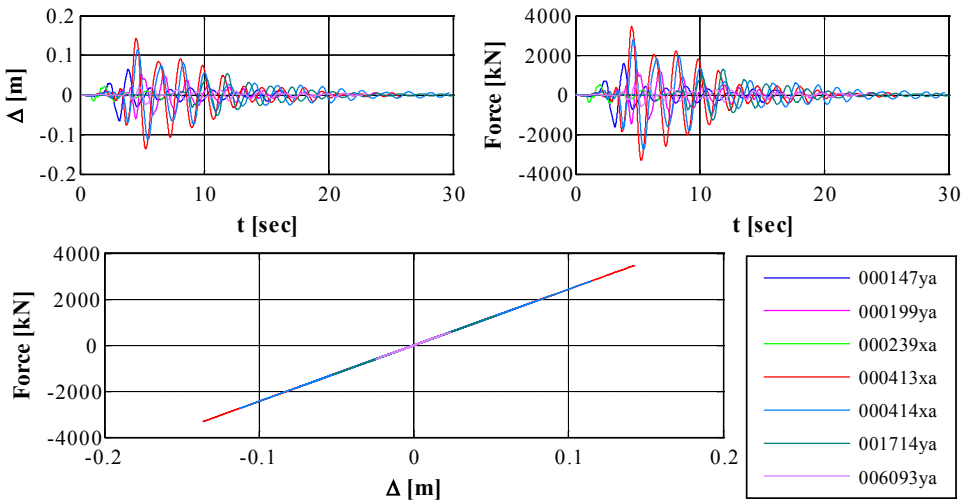


Figure 3.74 Results of the dynamic analyses on the bare model in the Z direction of the structures: displacement-time curve (left plot in the first row), force-time curve (right plot in the first row) and force-displacement curve (plot in the second row).

The elastic response of the considered benchmark structure does not seem to be logical and correct because of two main considerations: i) in the design phase a high value of the behavior factor (4.5) is assumed; ii) the longitudinal reinforcement in the column cross-section is higher than the minimum percentage required by the code (1%). Therefore, according to these two considerations, the overstrength of the structure

should not be high and under an earthquake with the maximum ground acceleration equal to the design acceleration, an inelastic behavior is expected. However, there are other sources of overstrength in the structure, listed in the following.

- a. The stiffness of the structures with columns loaded by low axial forces (typical for one story structures) is much lower than the one assumed in the design phase. The structure is designed with the cracked inertia, i.e. half of the gross inertia. Therefore the demand is considerably lower than the design one.
- b. Medium values of the material mechanical characteristics are considered in the model of the dynamic analyses.

However, one should be very careful in the interpretation of this result, which basically suggests that one-story industrial buildings will typically have very large overstrength related to very large degree of seismic safety. This deterministic point of view is not correct. If one properly takes into account the variability in the seismic action and materials (Fischinger et al., 2009) the probability of collapse of such structures could be considerably high, regardless the high level of overstrength. In addition to this, it should not be forgotten, that in this study it is assumed that the connections are strong.

3.3.6 Structure with cladding panels: nonlinear analyses results

The results of the dynamic analyses on the model with cladding panels are reported as in the previous section in terms of displacement-time curve, force-time curve and force-displacement diagram, reported in Figure 3.75 and in Figure 3.76 for the structure with panels in X and Z directions, respectively.

The investigated structure does not experience inelastic deformations under the considered set of accelerograms but the values of displacements and forces are much lower than those recorded in the dynamic analyses on the bare model.

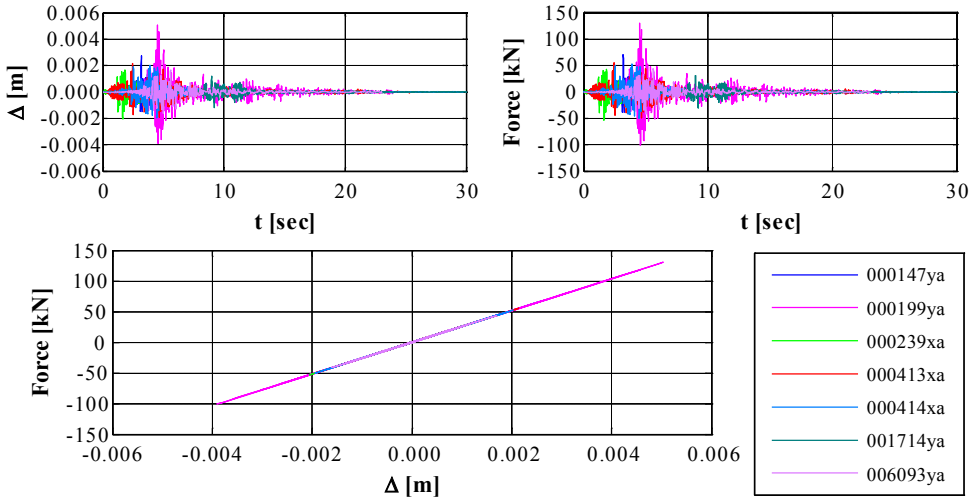


Figure 3.75 Results of the dynamic analyses on the model with cladding panels in the X direction of the structures: displacement-time curve (left plot in the first row), force-time curve (right plot in the first row) and force-displacement curve (plot in the second row).

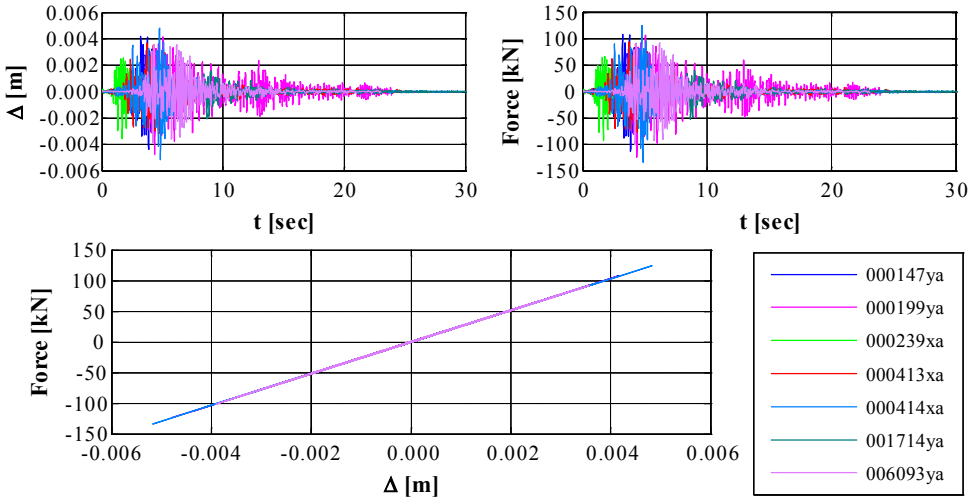


Figure 3.76 Results of the dynamic analyses on the model with cladding panels in the Z direction of the structures: displacement-time curve (left plot in the first row), force-time curve (right plot in the first row) and force-displacement curve (plot in the second row).

This result can justify the main failures recorded in the last severe earthquakes in Europe: the high stiffness of the cladding panels cause a reduction of the seismic forces in the structural elements (columns) but also high forces in the connections, directed in the plane of the panels and larger than the ones, evaluated in the design phase.

3.3.7 Connection safety evaluation

In order to calculate the ratio between the design strength of the connections and the real forces due to the earthquake, the design of a typical connection is performed and its strength is compared to the dynamic analyses results.

The widespread failure mechanisms in the panel-to-structure connections are the shear failure of the connector and the failure of the steel profile. The first failure mode is related to the shear force in the plane of the panel, while the latter one is caused by the forces in the out of plane direction.

The seismic design forces for the connection between the panel and the structure (horizontal elements in the case of vertical panels) are related only to the weight of the nonstructural component and directed in the orthogonal direction of the panel (out of plane direction). In particular, the panel is usually assumed as a doubly-supported beam (at the top and at the base), subjected to a distributed load, given by the equation (3.19).

$$F_a / L = \left(\frac{S_a \cdot W_a}{q_a} \right) / L \quad (3.19)$$

$$S_a = \alpha \cdot S \cdot \left[\frac{3 \cdot \left(1 + \frac{Z}{H} \right)}{1 + \left(1 - \frac{T_a}{T_1} \right)^2} - 0.5 \right] \geq \alpha \cdot S \quad (3.20)$$

In the equation (3.19) L is the height of the panel (length of the supported beam), W_a is the seismic weight of the panel; S_a is the spectral acceleration of the element, evaluated with the (3.20), and q_a is the behavior factor for nonstructural elements, assumed equal to 2.0. In the equation (3.20) α is the ratio between the maximum ground acceleration and the gravity acceleration (g), T_a is the fundamental period of the element (0.25sec), T_1 is the structure fundamental period, Z is the height of the barycenter and S is a coefficient that accounts for the soil and topography type.

As explained above, the design forces of the supports are directed in the out of plane direction; hence, their values (24.08kN) are used in order to design the steel profile (Figure 3.77 and Table 3.16). The connector is designed according to the steel profile dimensions and in this study it is assumed as a treated bar with a diameter of 16mm and strength class 8.8.

By comparing the strength of the connector with the dynamic results, it is found that in both the directions the shear strength of the connector is smaller than the seismic forces in the connection: Figure 3.78 and in Figure 3.79 show the recorded forces in the panel direction (Z and X direction, respectively) at the connection level (circles) for all the considered records and the shear strength of the connector (red dash-dot line).



Figure 3.77 (a) Section of the steel profile in the beam and in the panel; (b) length and height of the steel profile

Table 3.16 Geometrical characteristics of the steel profiles

a	b	t	e	d	L	i	h_{ef}
[mm]	[mm]	[mm]	[mm]	[mm]	[mm]	[mm]	[mm]
46	32	2	25	20	200	250	120

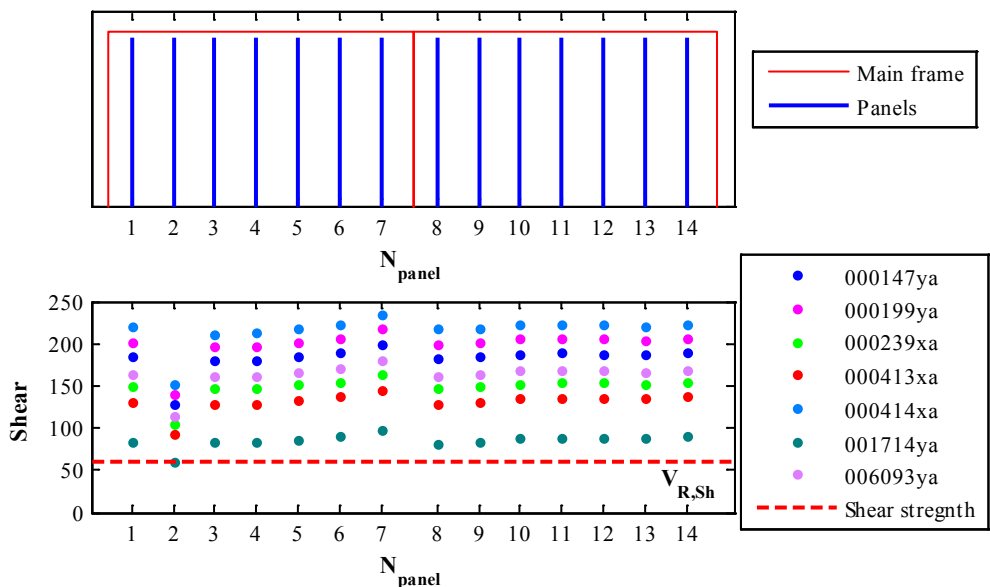


Figure 3.78 Forces in panels connections in Z direction: the first row shows the panels distribution and the second row shows the comparison between the seismic forces for the considered records (circles) and the shear strength of the connector (red dash-dot line)

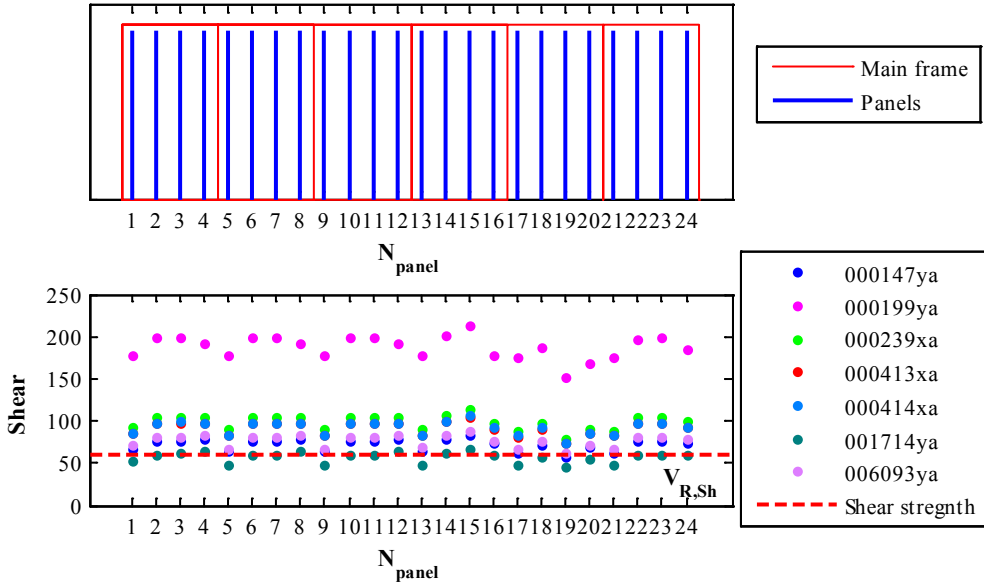


Figure 3.79 Forces in panels connections in X direction: the first row shows the panels distribution and the second row shows the comparison between the seismic forces for the considered records (circles) and the shear strength of the connector (red dash-dot line)

3.3.8 Seismic collapse risk

In this section the assessment of the seismic collapse risk of a benchmark structure with and without the cladding panels is performed according to the PEER methodology. The main purpose of this methodology is to predict the probability of exceeding a certain level of performance in the structure. In this study, the global collapse limit state of the structure is considered, i.e. the condition in which a structural system is unable to support vertical loads when subjected to seismic excitation.

3.3.8.1 Methodology

The used approach is the IM-based approach in order to evaluate the annual frequency of exceeding for the considered limit state (Cornell et al., 2002). The probability of exceeding the limit state of global collapse, that is the "probability of failure", is evaluated as:

$$P_{LS} = P[D > C] \quad (3.21)$$

where D is the demand and C is the capacity at the collapse.

As suggested by the same authors, the problem can be resolved into two parts: a seismological part and a structural engineering one, according to the Total Probability Theorem (TPT).

After mathematical steps and using an exponential hazard curve law ($H_{S_a}(x) = k_0 \cdot x^{-k}$) the following relation is obtained:

$$\overline{H}_{LS}^{1year} = H_S(m_{S_c}) \cdot \exp\left(\frac{1}{2} \cdot k^2 \cdot \beta_{TOT}^2\right) \cdot \exp\left(\frac{1}{2} \cdot \beta_{H_s}^2\right) \quad (3.22)$$

In this equation some important assumptions are considered:

- $S_{a,c}$ (median value of the limit state capacity) is a lognormal random variable;
- H_S (hazard) is a lognormal random variable with a dispersion β_{H_s} and its median approximated by a power-law relationship defined by parameters k and k_0 ;
- the total uncertainties of the collapse capacity β_{TOT}^2 is equal to the sum of the variance due to record-to-record (RTR) variability and the variance due to the uncertainty in numerical modeling (FEMA, 2008).

Incremental dynamic analyses

In order to evaluate the limit state capacity ($S_{a,C}$), incremental dynamic analyses are performed (Vamvatsikos and Cornell, 2002). An IDA study is a dynamic analysis study of a given structural model at different levels of intensity; it involves a series of dynamic nonlinear runs performed under scaled accelerograms, whose IMs are, ideally, selected to cover the whole range from elastic to nonlinear and finally to collapse of the structure. The purpose is to record damage measures DMs of the structural model at each level of IM and the resulting values are plotted versus the intensity as continuous curves, an IDA curve. This is a plot of a state variable (DM) recorded in an IDA study versus one or more IMs that characterize the applied scaled accelerogram.

The IDA curve gives the information to assess the reaching of a certain level or limit-state. The IM-based rule, which is considered in this work to assess the global collapse limit state, is needed to assess collapse capacity, i.e. to have a single point on the IDA curves defining the global collapse limit state. If $IM \geq C_{IM}$ then the limit-state is exceeded. In this work, the strategy for evaluating the global collapse point is the one proposed by FEMA (2000). According to this rule the last point on the curve with a tangent slope 20% of the elastic slope is defined to be the capacity point. This rule is justified by the fact that the flattening of the curve is an indicator of the dynamic instability, which is an indicator of collapse.

Seismic hazard function

The hazard curve provides the mean annual (or in 50 year) frequency of exceeding a particular PGA or IM for a given period and damping ratio.

The peak ground acceleration (PGA) and the spectral acceleration at the first mode, $S_a(T_1)$, are considered as IM's scalars for this seismic risk study.

The likelihood of exceeding the IM 's during a specified time range can be taken from a Probabilistic Seismic Hazard Analysis of the site. A site-specific seismic hazard analysis is performed based on the Italian seismic zonation. The hazard curves are taken from the website of INGV (<http://esse1.mi.ingv.it>). Specifically, the project of Meletti and Montaldo (2006) provides the results of site-specific seismic hazard analysis based on the Italian seismic zonation. This project has two sections: D2 gives the seismic hazard map of the peak ground acceleration at nine different probabilities of exceeding in 50 years; D3 gives the seismic hazard map of the spectral acceleration for 10 spectral periods (in the range between 0.1 and 2.0 seconds). These values have been calculated for all the points of Italian seismic zonation (a grid with a step of 0.05 degrees): for each point the 50th percentile (median values), the 16th and the 84th percentiles are available.

In this work the hazard function is derived for the considered seismic zone, having those following characteristics:

ID= 32979; Long.= 14.2837; Latitude= 40.8822; $a_g(T_r = 475\text{years}, 50^{\text{th}}\text{perc.}) = 0.167g$

In Table 3.17 a_g and $S_a(T = 1.5\text{sec})$ values for all the available probabilities P_{V_r} (and corresponding return period T_R) are presented. The value of spectral acceleration is taken at $T = 1.5\text{sec}$ since the fundamental elastic period of the analyzed structure is $T_{1,analysis} = 1.66\text{sec}$.

Table 3.17 Ground acceleration values at different probabilities of exceedance in 50 year

T_R [yy]	P_{V_r} [%]	a_g^{50th} [g]	a_g^{16th} [g]	a_g^{84th} [g]
30	81%	0.0457	0.0238	0.0489
50	63%	0.0600	0.0369	0.0667
72	50%	0.0731	0.0469	0.0813
100	39%	0.0867	0.0578	0.0968
140	30%	0.1016	0.0701	0.1132
200	22%	0.1204	0.0848	0.1328
475	10%	0.1679	0.125	0.1500
975	5%	0.2132	0.1694	0.2367
2475	2%	0.2798	0.2360	0.3148

Table 3.18 Spectral acceleration ($T=1.50\text{sec}$ and damping value of 5%) values at different probabilities of exceedance in 50 years

T_R [yy]	P_{Vr} [%]	S_a^{50th} [g]	S_a^{16th} [g]	S_a^{84th} [g]
30	81%	0.0148	0.0132	0.0234
50	63%	0.0251	0.0222	0.0388
72	50%	0.0329	0.0293	0.0515
100	39%	0.0418	0.0356	0.0633
140	30%	0.0522	0.0421	0.0762
200	22%	0.0632	0.0509	0.0914
475	10%	0.0911	0.0741	0.1310
975	5%	0.1174	0.0975	0.1700
2475	2%	0.1563	0.1342	0.2293

The hazard curve can be approximated by a power-law relationship in the region of interest (DOE, 1994):

$$H_{ag}(x) = P[a_g \geq x] = k_{0,ag} \cdot x^{-k_{ag}} ; H_{Sa}(x) = P[S_a \geq x] = k_{0,Sa} \cdot x^{-k_{Sa}} ;$$

where k_0 and k are parameters defining the shape of the hazard curve.

In order to define these parameters the method of least squares is used, applied to the three lowest probabilities (10%; 5% and 2%). The evaluated hazard curves for the two IM's are reported in Figure 3.80 and in Figure 3.81.

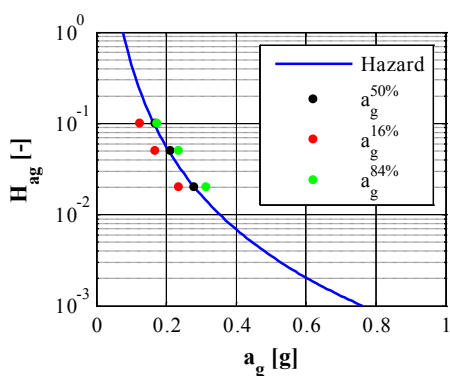


Figure 3.80 Hazard curve for peak ground accelerations in logarithm scale

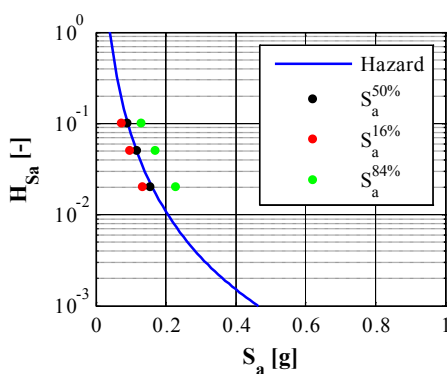


Figure 3.81 Hazard curve for spectral accelerations ($T=1.5\text{sec}$ - $\xi=5\%$) in logarithm scale

3.3.8.2 Bare structure results

The IM-based approach is used in order to estimate the probability of collapse of one-story precast structure. The IDA curves and the corresponding PDF distribution are

reported both in terms of peak ground and spectral acceleration (Figure 3.85) at the first mode period.

The limit value to assess the seismic safety is assumed from the recommendations suggested by the Joint Committee on Structural Safety (JCSS, 2001). For the analyzed industrial buildings (with moderate consequences of failure) and seismic action (a large uncertainty of loading) the target reliability is 2.5% in 50 years. According to the results of the risk seismic analysis (Table 3.19 and Table 3.20) the structure is safe in both the cases of peak ground and spectral acceleration.

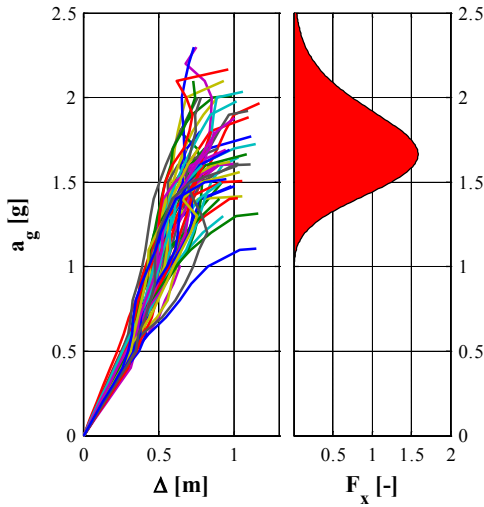


Figure 3.82 IDA curve and PDF in terms of peak ground acceleration

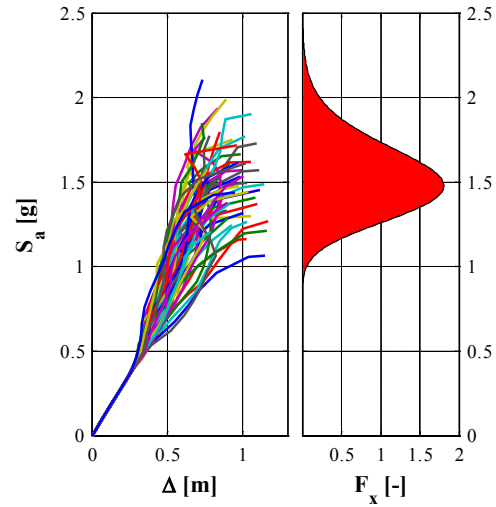


Figure 3.83 IDA curve and PDF in terms of spectral acceleration

Table 3.19 Seismic risk study summary with peak ground acceleration

m_{ag}	β_{RTR}^2	β_{TOT}^2	β_{Hs}^2	k	$H_S(m_{ag})$	$\exp(1/2 k^2 \beta_{TOT}^2)$	$\exp(1/2 k^2 \beta_{Hs}^2)$	$H_{LS,50}$
[g]	[-]	[-]	[-]	[-]	[%]	[-]	[-]	[%]
1.71	0.022	0.355	0.025	3.0	0.0088	4.94	1.01	0.044

Table 3.20 Seismic risk study summary with spectral acceleration at the first mode period

m_{Sa}	β_{RTR}^2	β_{TOT}^2	β_{Hs}^2	k	$H_S(m_{Sa})$	$\exp(1/2 k^2 \beta_{TOT}^2)$	$\exp(1/2 k^2 \beta_{Hs}^2)$	$H_{LS,50}$
[g]	[-]	[-]	[-]	[-]	[%]	[-]	[-]	[%]
1.52	0.022	0.354	0.077	2.8	0.0035	4.13	1.04	0.015

3.3.8.3 Structure with cladding results

The incremental dynamic analyses are also performed on the model with cladding panels. In the following the results are reported in the X direction in terms of IDA curve and PDF distribution (Figure 3.84). The IDA curves are reported in terms of peak ground acceleration and. The point that defines the global capacity of the structure is defined on the IDA curves as the point at which the strength in the connection system is achieved, i.e. the shear failure of the connector occurs. Such an assumption is justified by the high impact of the panels collapse on the human life safety, as broadly explained and demonstrated in the previous sections.

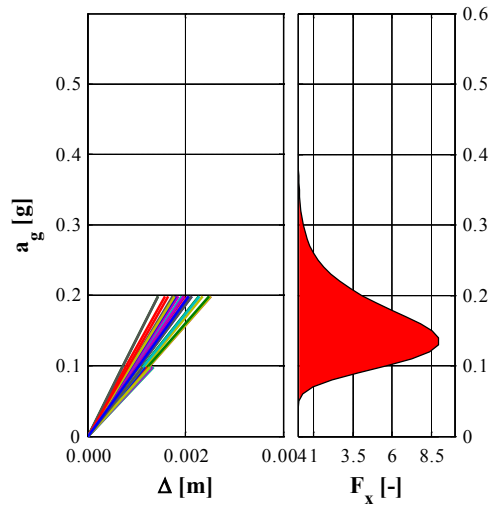


Figure 3.84 IDA curve and PDF in terms of peak ground acceleration

Table 3.21 Seismic risk study summary with peak ground acceleration

m_{ag}	β_{RTR}^2	β_{TOT}^2	β_{HS}^2	k	$H_S(m_{ag})$	$\exp(1/2 k^2 \beta_{TOT}^2)$	$\exp(1/2 k^2 \beta_{HS}^2)$	$H_{LS,50}$
[g]	[-]	[-]	[-]	[-]	[%]	[-]	[-]	[%]
0.15	0.097	0.429	0.025	3.0	13	6.90	1.01	90

3.3.9 Progressive collapse

In order to improve the knowledge on the cladding panels interaction, a novel model is implemented in the program OpenSees (McKenna and Fenves, 2013), that takes into account the achievement of the maximum strength in the panel-to-structure connection through the “Removal” command (Talaat and Mosalam, 2009).

This command allows to “remove” from the resistant structure all the cladding panels that achieve the maximum strength in the connection system during the nonlinear dynamic analysis: once the collapse of the panel is achieved, the analysis of the structure continues without the collapsed panels.

Each panel is characterized by two connections at the top with the structure and for each connection a limit domain is defined in terms of displacements. In this study, only the shear mechanism of the connector is considered; hence, for the action out of the plane a very large limit displacement is assumed. The limit displacement in the panel direction is obtained from the ratio between the shear strength of the connector and the stiffness of the panels.

During the analyses, the display function shows the progressive collapse of the panels, defined with different connection limit domains in both the investigated directions (Figure 3.85).

The progressive collapse is also demonstrated by numerical results in terms of displacement-time curve (from Figure 3.86 and Figure 3.87) and force-time (Figure 3.88 and Figure 3.89), where the force is the sum of the shear forces in the columns and the displacement is the displacement of the master joint at the roof level. For the sake of brevity, the results for one of the considered records are shown.

Such a model can be used in order to achieve two main purposes: i) the evaluation of the real forces at the base of the structural elements during an earthquake; ii) the justification of the recorded damage in the structural elements due to a seismic event after the collapse of the cover panels; iii) the evaluation of the seismic response and the collapse risk of precast one-story structure in which the achievement of the panel collapse does not correspond to the achievement of the global collapse.



Figure 3.85 Display of the progressive collapse during one dynamic nonlinear analysis direction: (a) step of the first collapsed panel; (b) last step of the analysis

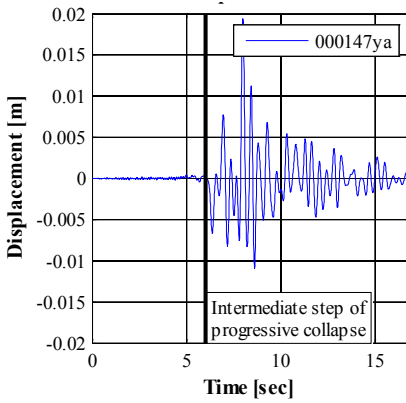


Figure 3.86 Displacement-time curve in X direction

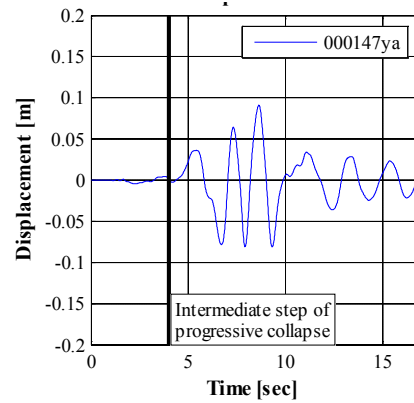


Figure 3.87 Displacement-time curve in Z direction

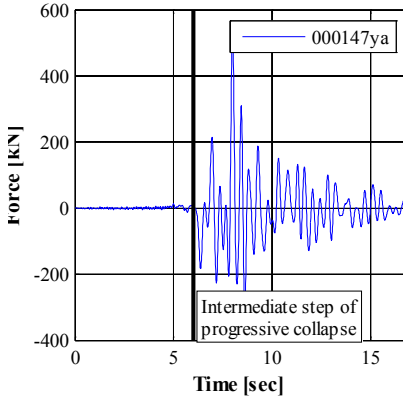


Figure 3.88 Force-time curve in X direction

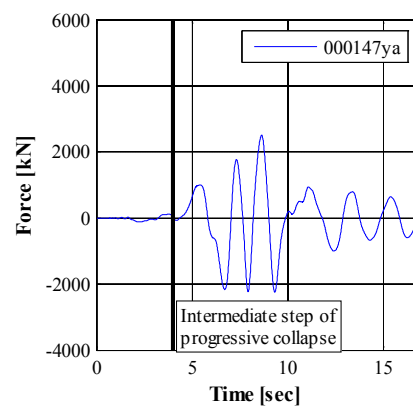


Figure 3.89 Force-time curve in Z direction

3.3.10 Concluding remarks

This work studies the influence of the cladding panels on the seismic response of one-story precast structures. Such influence is evaluated comparing the results of nonlinear analyses on two structural models: one in which the interaction between the panel and the structure is neglected (bare structure) and one in which this interaction is considered, modeling also the behavior of the panels (model with cladding panels).

The results of the analyses underline that the panels have an important influence on the global behavior of the structure. The high levels of forces in the panels motivate the study of the connections response: in order to evaluate the security factors with respect the failure of the connection components, a typical connection between vertical panels and beams is designed. By the comparison between the connection strength and the

recorded forces, it is demonstrated that under seismic action the collapse of the infill can occur due to inadequate strength of the connection system.

A seismic risk study is then performed in terms of global collapse probability, that confirms the significant influence of the precast panels on the behavior of the structure. In this study, when the cladding panels are considered in the model, the condition of collapse always corresponds to the collapse of the panel connection, taking into account the problem related to the safety of life.

In order to investigate the real behavior of the structures, a novel model is developed that simulates the progressive collapse of the panels. This model allows to monitor the redistribution of the forces during an accelerations record in all the structural elements. The first result is related to the forces in the columns, that increase as the panels fail, justifying the recorded damage, occurred in the structural elements during some seismic events, after the collapse of the panels. This model can also be used in order to study the seismic response of structures, in which the influence of the panels cannot be neglected but their collapse is not assumed as the structure collapse, e.g. when the connection with the structure achieves the maximum strength, the panel does not bear any force deriving from the earthquake but the collapse of the structure is not achieved because it is somehow preserved the safety of human life.

References

- 10018, C. (1999), *Apparecchi di appoggio per le costruzioni*.
- Biondini, F., Dal Lago, B. and Toniolo, G. (2013), *Role of wall panel connections on the seismic performance of precast structures*, B Earthq Eng. **11**(4), 1061-1081.
- Borst, R.d., Remmers, J.J.C., Needleman, A. and Abellan, M.-A. (2004), *Discrete vs smeared crack models for concrete fracture: bridging the gap*, International Journal for Numerical and Analytical Methods in Geomechanics. **28**(7-8), 583-607.
- CEN (2004), *Eurocode 2: design of concrete structures - Part 1-1: General rules and rules for buildings*, Brussels, Belgium. .
- CEN (2005), *Eurocode 8: design of structures for earthquake resistance - Part 1: general rules, seismic actions and rules for buildings*. EN 1998-1, Brussels, Belgium.
- CNR 10025/98 (2000), *Istruzioni per il progetto, l'esecuzione ed il controllo delle strutture prefabbricate in calcestruzzo (in Italian)*.
- Cornell, C., Jalayer, F., Hamburger, R. and Foutch, D. (2002), *Probabilistic Basis for 2000 SAC Federal Emergency Management Agency Steel Moment Frame Guidelines*, Journal of Structural Engineering. **128**(4), 526-533.
- Corp., D.S.S. (2010), *Abaqus/CAE 6.10-1*, Providence.
- D. M. 14/01/2008 (2008), *Norme Tecniche per le Costruzioni (in Italian)* G.U. n. 29 4 febbraio 2008.
- DOE (1994), *Natural phenomena hazards design and evaluation criteria for Department of Energy Facilities*, DOE-STD-1020-94.
- Eligehausen, R., Popov, E.P. and Bertero, V.V. (1986), *Local bond stress-slip relationships of deformed bars under generalized excitation*, University of California. 169.
- Ercolino, M. (2010), *Inelastic seismic response and risk analysis of one-storey precast buildings*, Graduation Thesis.
- Faggiano, B., Iervolino, I., Magliulo, G., Manfredi, G. and Vanzi, I. (2009), *Post-event analysis of industrial structures behavior during L'Aquila earthquake*, Progettazione sismica **3 English Special Edition** 203-208.
- Fardis, M.N. and Biskinis, D. (2003), *Deformation capacity of RC members, as controlled by flexure or shear*.
- FEMA (2000), *Recommended seismic design criteria for new steel- moment frame buildings*, Venture, S.J.
- FEMA (2008), *ATC-63 Project Report: Quantification of Building Seismic Performance Factors*.
- Fischinger, M., Kramar, M. and Isakovic, T. (2009), *Seismic safety of prefabricated reinforced-concrete halls - analytical study*, Gradev. **61**(11), 1039-1045.
- Fischinger, M., Kramar, M. and Isaković, T. (2008), *Cyclic response of slender RC columns typical of precast industrial buildings*, B Earthq Eng. **6**(3), 519-534.
- Gjelsvik, A. (1974), *Interaction Between Frames and Precast Panel Walls*, Journal of the Structural Division (ASCE). **100**(2), 405-426.
- Goodno, B.J. and Craig, J.I. (1989), *Historical Overview of Studies on the Contribution of Cladding to Lateral Resistance of Buildings*, Chicago.

- Goodno, B.J. and Palsson, H. (1986), *Analytical Studies of Building Cladding*, Journal of Structural Engineering-Asce. **112**(4), 665-676.
- Goodno, B.J., Palsson, H. and Douglas, G.P. (1984), *Localized Response and Implications for Seismic Design*, Proceedings of the Eighth World Conference on Earthquake Engineering, San Francisco. 1143-1150.
- Haselton, C. (2006), *Assessing Seismic Collapse Safety of Modern Reinforced Concrete Moment-Frame Buildings*.
- Hetenyi, M. (1946), *Beams on elastic foundation*, Ann Arbor, University of Michigan Press.
- Hunt, P.J. and Stojadinovic, B. (2010), *Seismic Performance Assessment and Probabilistic Repair Cost Analysis of Precast Concrete Cladding Systems for Multistory Buildings*, Pacific Earthquake Engineering Research Center, College of Engineering, University of California, Berkeley.
- Iervolino, I., Galasso, C. and Cosenza, E. (2010), *REXEL: computer aided record selection for code-based seismic structural analysis*, B Earthq Eng. **8**(2), 339-362.
- JCSS (2001), *Probabilistic model code, Part 1: basis of design*, 12th draft.
- Magliulo, G., Capozzi, V., Fabbrocino, G. and Manfredi, G. (2011), *Neoprene-concrete friction relationships for seismic assessment of existing precast buildings*, Eng Struct. **33**(2), 532-538.
- Magliulo, G., Ercolino, M., Cimmino, M., Capozzi, V. and Manfredi, G. (2014a), *Cyclic shear test on dowel beam-column connections*, Earthquakes and Structures (under review).
- Magliulo, G., Ercolino, M., Cimmino, M., Capozzi, V. and Manfredi, G. (2014b), *Numerical evaluation of the strength of beam-to-column dowel connections in precast buildings under monotonic actions*, Construction and Building Materials (under review).
- Magliulo, G., Ercolino, M. and Manfredi, G. (2014c), *Influence of cladding panels on the first period of one-story precast buildings*, Bulletin of Earthquake Engineering (under review).
- Magliulo, G., Ercolino, M., Petrone, C., Coppola, O. and Manfredi, G. (2013), *Emilia Earthquake: the Seismic Performance of Precast RC Buildings* Earthq Spectra.
- Magliulo, G., Fabbrocino, G. and Manfredi, G. (2008), *Seismic assessment of existing precast industrial buildings using static and dynamic nonlinear analyses*, Eng Struct. **30**(9), 2580-2588.
- Mander, J.B., Priestley, M.J.N. and Park, R. (1988), *Theoretical Stress-Strain Model for Confined Concrete*, J Struct Eng-Asce. **114**(8), 1804-1826.
- McKenna, F. and Fenves, G.L. (2013), *OpenSees Manual* <http://opensees.berkeley.edu>, Pacific Earthquake Engineering Research Center.
- Meletti, C. and Montaldo, V. (2006), *Stime di pericolosità sismica per diverse probabilità di superamento in 50 anni: valori di ag (in Italian)*, INGV.
- Ngo, D. and Scordelis, A.C. (1967), *Finite element analysis of reinforced concrete beams*, Journal of the American Concrete Institute. **64** 152-163.
- Oppenheim, I.J. (1973), *Dynamic Behavior of Tall Buildings with Cladding*, Fifth world conference on earthquake engineering, Rome.

- Osanai, Y., Watanabe, F. and Okamoto, S. (1996), *Stress transfer mechanism of socket base connections with precast concrete columns*, *Acı Structural Journal*. **93**(3), 266-276.
- Palsson, H., Goodno, B.J., Craig, J.I. and Will, K.M. (1984), *Cladding influence on dynamics response of tall buildings*, *Earthq Eng Struct Dyn*. **12**(2), 215-228.
- Pinelli, J., Craig, J. and Goodno, B. (1995), *Energy-Based Seismic Design of Ductile Cladding Systems*, *Journal of Structural Engineering*. **121**(3), 567-578.
- Popovics, S. (1973), *A numerical approach to the complete stress-strain curve of concrete*, *Cement and Concrete Research*. **3**(5), 583-599.
- Psycharis, I. and Mouzakis, H. (2012), *Assessment of the seismic design of precast frames with pinned connections from shaking table tests*, *B Earthq Eng*. **10**(6), 1795-1817.
- Rashid, Y.R. (1968), *Analysis of reinforced concrete pressure vessels*, *Nuclear Engineering and Design*. **7** 334-344.
- Systèmes, D. (2008), *Abaqus Scripting User's Manual*, Providence, RI, USA.
- Talaat, M. and Mosalam, K.M. (2009), *Modeling progressive collapse in reinforced concrete buildings using direct element removal*, *Earthq Eng Struct Dyn*. **38**(5), 609-634.
- Thiel, C.C., Elsesser, E., Lindsay, J., Kelly, T., Bertero, V.V., Filippou, F. and McCann, R. (1986), *Seismic Energy Absorbing Cladding System: A Feasibility Study*, ATC-17 Seminar and Workshop on Base Isolation and Passive Energy Dissipation, San Francisco.
- Toniolo, G. (2012), *SAFECAST project: European research on seismic behaviour of the connections of precast structures*, 15th World conference on earthquake engineering (15WCEE), Lisbon, Portugal.
- Vamvatsikos, D. and Cornell, C.A. (2002), *Incremental dynamic analysis*, *Earthq Eng Struct Dyn*. **31**(3), 491-514.
- Vecchio, F.J. (2000), *Disturbed stress field model for reinforced concrete: Formulation*, *J Struct Eng-Asce*. **126**(9), 1070-1077.
- Vintzeleou, E.N. and Tassios, T.P. (1986), *Mathematical-Models for Dowel Action under Monotonic and Cyclic Conditions*, *Mag Concrete Res*. **38**(134), 13-22.
- Vintzeleou, E.N. and Tassios, T.P. (1987), *Behavior of Dowels under Cyclic Deformations*, *ACI Struct J*. **84**(1), 18-30.
- Wolz, M.W., Hsu, C.C. and Goodno, B.J. (1992), *Nonlinear Interaction between Building Structural Systems and Nonstructural Cladding Components*, In ATC-29 Seminar and Workshop on Seismic Design and Performance of Equipment and Nonstructural Elements in Buildings and Industrial Structures.
- Zoubek, B., Isakovic, T., Fahjan, Y. and Fischinger, M. (2013), *Cyclic failure analysis of the beam-to-column dowel connections in precast industrial buildings*, *Eng Struct*. **52**(0), 179-191.

Chapter 4

CONCLUSIONS

The industrial precast buildings are a widespread typology in Europe that have a key role in the seismic safety in terms of economic losses and life protection. The present thesis concerns the seismic behavior of these structures. The main purpose is the development of the knowledge on their seismic response by means of numerical analyses, experimental tests and earthquake evidences.

In the first part of the work, the damages due to the Emilia earthquakes on May 2012 were studied and discussed in order to justify the response and to recognize the main vulnerability sources of the industrial buildings. According to this study, it is found that the damages to precast structures were mainly caused by inadequate connection systems. A more detailed study is then performed on an existing structure, located in the epicentral area and damaged after the 29th May event. A modeling effort was made in order to implement all the structural elements and the connection systems. In particular, the frictional connections between the beams and the columns and between the roof elements and the beams were modeled with their actual mechanical behavior under horizontal and vertical earthquake components. The results on the nonlinear dynamic analyses with the recorded input of the 29th May event justified the occurred damages in the structure and in the connections.

In industrial buildings, the contents safeguarding and the functionality of the structure are added to the life protection goal. Hence, the emergency management is a crucial phase that should be properly organized in order to reduce the indirect losses due to a seismic event. At this purpose two national documents were issued: the “Guidelines on local and global retrofitting systems of precast structures” and the form for usability judgment of precast structures (GL-AeDES). The first document is a guide for the retrofitting actions on precast industrial buildings; while the usability form is an useful tool for the structure survey after a seismic event, that helps the user to an aware judgment of the safety of the investigated industrial structure.

The seismic response of precast structures is highly influenced by the connections behavior as well as by the interaction with the nonstructural component, e.g. the cladding panels systems. Indeed, the most common exhibited failures are both the loss of support of structural horizontal elements due to the failure of the existing connections and the collapse of the cladding panels due to the failure of the panel-to-structure connections.

Concerning the panels influence, the dynamic properties (the first period) of 288 realistic buildings, designed according to EC8 and for different seismic zones, were evaluated taking into account the panel-to-structure interaction. The modal analyses demonstrated that the first vibration period is significantly influenced by the presence of the cladding system. Moreover it was found that the simplified EC8 formula, that evaluates the first vibration period as a function of the height of the building, is not suitable either for the case of the bare building or for the case of building with cladding system; as a consequence, new predictive formulas were proposed. The influence of the panels was also investigated by means of nonlinear dynamic analyses. The results demonstrated the high vulnerability of the panel-to-structure connections, designed for low forces that do not take into account the interaction with the structure. Moreover, a novel model is proposed in order to record both the progressive collapse of the nonstructural panels due to an earthquake and the redistribution of forces and deformation in the structural elements.

An extensive study was performed in order to investigate the seismic behavior of the dowel beam-to-column connections, typically used in precast structures. The results of an experimental campaign on a seismic designed connection, under monotonic and cyclic loads, were described. In both the tests the damage pattern showed that the first damage in the connection was the splitting of the column concrete lateral cover, that also corresponded to the failure mechanism of the connection. The force-displacement envelope demonstrated the brittle behavior of this connection, due to a significant stiffness and strength degradation after the concrete cracking. Moreover, the very low values of the dissipated energy during the cyclic test demonstrated that this connection cannot influence the dissipative properties of the whole structure under dynamic actions. Comparing the cyclic and the monotonic force-displacement curves, no degradation in the connection behavior was found both in terms of strength and in terms of stiffness. This evidence was justified by the failure mode, that involved the concrete response under tensile stresses.

The high number of influencing variables and the need of general results motivated an innovative numerical model of the tested specimen. The FEM model was firstly validated on the results of the monotonic test and then used to perform an extended

parametric study. The results of all the case studies showed the sensitivity of the model to the considered variable parameters both in terms of strength and failure mechanism. Moreover, the influence of some geometrical features on the seismic response of this connection was evaluated and discussed.